Evaluation of a Solvent-less Method for Estimating Asphalt Binder Properties of Recycled Asphalt Pavement

by

Pamela Turner

A thesis submitted to the Graduate Faculty of
Auburn University
In partial fulfillment of the
requirements for the Degree of
Master of Science

Auburn, Alabama
May 4, 2013

Approved by

Randy West, Chair, Director, National Center for Asphalt Technology
David Timm, Brasfield & Gorrie Professor of Civil Engineering
Rod Turochy, Associate Professor of Civil Engineering
James R. Willis, Assistant Research Professor, National Center for Asphalt Technology

ABSTRACT

Increasing amounts of Reclaimed Asphalt Pavement (RAP) are being used in response to the rising costs of asphalt materials. The asphalt paving industry currently lacks a method for characterizing the properties of the asphalt binder contained in the RAP which are necessary for proper design of asphalt mixtures utilizing RAP. The objective of this study was to develop a solvent-less method for determining high and intermediate-temperature properties of the asphalt binder in RAP. The candidate method chosen for evaluation was a torsional test performed on small bars of asphalt mix using the Dynamic Shear Rheometer (DSR) combined with the Hirsch model. This was believed to be a good candidate test due to the use of existing laboratory equipment, small sample size, and the fact that the test results were similar to those provided by other mixture and binder tests.

The results of this study indicated that the torsion bar test showed promise for measuring the mixture stiffness of the RAP materials. The Hirsch model calculation showed promise for estimating the asphalt binder properties of the RAP materials but could not accurately estimate the asphalt binder properties of plant- or laboratory-produced mixes. The Hirsch model calculation also could not accurately estimate changes in the asphalt binder properties of these mixes due to increasing RAP content.

Table of Contents

List of Tables

LIST OF FIGURES

INTRODUCTION

The cost of asphalt paving materials has been steadily increasing in recent years. Asphalt binder prices are currently between $500 and $600 per ton in some locations, where comparable materials were about $350 in 2005 (*1,2*). While this cost increase is tied to rising crude oil costs, petroleum costs are just one reason for the increasing costs of asphalt mixtures. New processing techniques used by oil refineries reduce the amount of asphalt binders produced. Cokers, for example, remove more light ends from the oil which allows the refiners to produce greater quantities of profitable fuels, but leaves less of the heavier materials that make up asphalt binders. High fuel prices also affect the cost of asphalt pavements by increasing the costs of getting raw materials to the plant and paving mixtures to the job site (*3*).

However, asphalt pavements are a highly recyclable material and can be completely re-used. The Federal Highway Administration (FHWA) estimates that of the approximately 100 million tons of asphalt pavement removed from roadways each year in the United States, 80-million tons are recycled, or reclaimed, as part of new hot-mix asphalt (HMA) pavements. This makes asphalt pavement the most recycled material by tonnage and is almost twice the amount of recycled paper, plastic, aluminum, and glass combined per year. The second most recycled material is scrap metal, which is recycled at a rate of 70-million tons per year. Percentage-wise this amounts to an 80%recycling rate for asphalt pavements, second only to the 93% rate for automotive batteries (*4*).

Reclaimed asphalt pavement (RAP) materials are beneficial because they contain asphalt binders and aggregates which can replace a portion of the materials

needed for pavement construction and rehabilitation projects. The asphalt binder in RAP reduces the amount of new asphalt binder required while the aggregates and fines in the RAP are used as part of the overall aggregate gradation, reducing the need for new aggregates. This is especially beneficial in areas where good quality aggregates are not available and must be imported (*5*). Despite its many benefits, RAP usage does present some challenges. When RAP materials are used in an asphalt mixture, the asphalt binder and aggregates affect the properties of the mix design and must be considered. RAP aggregates can be treated as another aggregate source and are easily characterized after using either a solvent extraction or an ignition oven to remove the asphalt binder. The RAP binder, however, is much more difficult to characterize. One challenge with RAP binders is the lack of consensus on the extent to which RAP binders blend with virgin binders during production. Current theories on blending range from the hypothesis that no blending occurs between the RAP and virgin binder to the other end of the spectrum which assumes that complete blending occurs. Many asphalt practitioners believe that the actual amount of blending most likely falls somewhere in between the two extremes. The amount of blending that occurs will affect the overall binder stiffness of the HMA. If no blending occurs between the virgin and RAP binders then there is no need to characterize the RAP binder properties. If total or even partial blending occurs, then as the amount of RAP used in a mix design increases, the effect of the RAP binder on the total binder properties will increase (*6*).

Another concern with RAP binders is the characterization of their properties. RAP binder properties are currently obtained by using solvent extraction to remove the asphalt binder from a sample of RAP. A distillation recovery procedure is then used to

remove the solvent from the RAP binder so that it can be tested using conventional methods. Solvent extraction and recoveries have many disadvantages and may not provide an accurate representation of the RAP binder. Studies have shown that exposure to the chlorinated solvents typically used for extractions can harden asphalt binders, especially if they are left in solution for long periods of time at elevated temperatures. The distillation procedures used to remove the solvent from the asphalt binder have been found to leave residual solvents behind in the binder, causing it to appear softer. Particularly stiff asphalt binders may not be completely removed from the RAP aggregates, leaving behind some stiffer portions of the binder which may also cause the recovered RAP binder to appear softer (*7*). For agencies, simply obtaining the solvents needed to perform the extraction procedure is difficult as some states have banned chlorinated solvents altogether due to their toxicity and health risks. Increased costs to buy and dispose of the solvents are also prohibitive with the price of tricholorethylene (TCE) at approximately $20 a gallon (a complete extraction can take up to one gallon of solvent) *(8).*

This inability to accurately characterize RAP binder properties becomes an issue with mixes containing large amounts of RAP materials. The more RAP materials used in a mix design, the greater the effect the RAP binder will have on the overall binder properties of the mix. AASHTO M323, *Standard Specification for Superpave Volumetric Mix Design*, currently recommends a tiered approach to HMA mixes containing RAP. Mixes with less than 15% RAP do not require adjustment of the binder properties as the small amount of RAP binder contributed will not significantly change the stiffness of the mix. Mixes with 15 – 25% RAP require adjusting the virgin binder grade one PG grade

softer to account for the stiffening effect of the RAP binder. Mixes with more than 25% RAP require the creation of blending charts to measure the effect of the RAP binder. Blending charts use the properties of the virgin binder and the recovered RAP binder to create linear plots from which the binder properties of blended materials can be estimated and are used to determine either the maximum amount of RAP that can be added without changing the virgin binder grade or the virgin binder grade necessary to achieve a specified target binder grade at a certain RAP percentage.

The lack of an accurate method for characterizing RAP binder properties and determining their effect on mixtures binder properties can lead to mixtures with inadequate stiffness levels. Without accurate methods of obtaining and testing RAP binder properties, agencies have the dilemma of either limiting RAP contents to low percentages, accepting the blending chart values knowing that they may not be accurate, or finding alternative methods of characterizing these mixes.

OBJECTIVE

The National Center for Asphalt Technology (NCAT) was tasked by the Alabama Department of Transportation (ALDOT) to develop a solvent-less method for characterizing the binder properties of RAP and mixes containing RAP that can be used in place of the traditional solvent extraction procedures. Ideally the test should be simple to perform, simple to analyze, and use existing laboratory equipment with minimal modifications. The research presented in this report covers the evaluation of one of the candidate test methods - small bars of HMA tested in the Dynamic Shear Rheometer (DSR). The data from this procedure were evaluated to determine if it can

be used to provide a reasonable estimate of binder stiffness properties when combined with a mathematical model for calculation of binder stiffness.

This project consisted of 4 tasks:

- Literature Review,
- Selection of a potential method,
- Characterization of RAP and virgin materials used in the evaluation, and
- Evaluation of potential method to characterize virgin and RAP materials.

LITERATURE REVIEW

A review of available literature was conducted on subjects related to the use of RAP in asphalt mixtures. The purpose of the literature review was to summarize the issues that occur when using RAP materials and to identify potential new test methods for characterizing RAP binders. The discussion includes current practices, issues relating to the current practices, and proposed alternatives. The literature review is organized into the following topics:

- Extraction and characterization of RAP binder using solvent extraction,
- effect of RAP on the performance properties and asphalt binder characteristics of HMA,
- research on proposed new methods for characterizing RAP binders, and summary of key findings.

Extraction and Characterization of RAP Binders

The research and development of extraction / recovery procedures through the years have typically indicated three unresolved issues with recovered asphalt binders.

1. The hardening that occurs when asphalt binders react with solvents while in solution,
2. The incomplete removal of the harder asphalt binder fractions from the aggregates, and
3. The incomplete removal of solvents from the recovered asphalt binders.

These issues are in addition to the basic concerns that arise from using chemicals (cost, storage, removal, toxicity).

The extraction and recovery of asphalt materials has been practiced since the early 1900s. Early methods developed by Dow and Abson used carbon disulfide (CS_2) as the extraction solvent and a simple distillation procedure to recover the asphalt binder. Centrifuge and reflux extraction procedures combined with vacuum distillation were developed in the 1920s. The Abson recovery method was developed by Gene Abson in the 1930's using benzene as the solvent. During this research, other available solvents were tried and rejected as replacements for the highly flammable and toxic benzene. Carbon tetrachloride, the only readily available chlorinated solvent at that time, was found unsuitable for asphalt work because the chlorine molecules affected the recovered asphalt binder the same way oxygen would in an air blowing operation, and caused the recovered asphalt to stiffen significantly. Abson and other researchers at

that time assumed that all chlorinated solvents would affect asphalt the same way and, therefore, declared them unusable (*9*).

Around 1960, chlorinated solvents began to become commercially available for use in cleaning, degreasing, and food applications. At that time, many labs began using trichloroethylene (TCE) for extractions in which recovered asphalt properties were not needed. Continued work by Abson in 1933 found that, contrary to previous conclusions, some chlorinated solvents were acceptable for determining recovered asphalt binder properties. In a study of several commercial grades of TCE, it was found that the extraction and reagent grades all gave penetration, ductility, and softening point values that were sufficiently close to those of the original binders. This work led to the replacement of benzene with the chlorinated solvents. A slight hardening of the asphalt binders was noted with the use of chlorinated solvent, but it had not been fully investigated at that time *(9)*.

In 1991, Burr performed a study that showed that all solvents used to extract asphalt binder resulted in some form of solvent hardening. It was determined that the amount of hardening was dependent on the temperature used during the extraction and the amount of time the asphalt binder was allowed to remain in solution. A relationship between the oxidative tendencies of an asphalt binder and its solvent hardening tendencies was also found. Recommendations from this work included using a room temperature extraction procedure and completing the recovery as quickly as possible *(10)*.

A study conducted by Peterson, et al. (2000) as part of NCHRP 9-12, *Incorporation of Reclaimed Asphalt in the Superpave System*, was intended to evaluate the effect of solvent extractions on asphalt binder properties. The goal was to identify the best combination of extraction and recovery procedures and to identify possible changes to the binder aging procedures used in the Superpave performance grading system for recovered RAP binders. Two extraction methods were evaluated as part of the study: ASTM D2172-95 *Test Methods for Quantitative Extraction of Bitumen from Bituminous Paving Mixtures*, Method A; and a method based on an extraction procedure developed by Texas A&M (described in AASHTO TP2-94, *Method for the Quantitative Extraction and Recovery of Asphalt Binder from Hot Mix Asphalt*). For ASTM D2172-95 Method A, both the Abson (ASTM D1856-95a, *Recovery of Asphalt from Solution by Abson Method)*, and Rotary-Evaporator (which was not yet a stand alone test procedure) recovery procedures were used. The AASHTO TP2 method was developed to be a complete system that combined the extraction vessel in-line with the Roto-Vap device, therefore only the Roto-Vap recovery was evaluated for this procedure. Three solvents commercially available at the time were also evaluated: trichloroethylene, toluene/ethanol blend, and *n*-Propyl Bromide. Multiple combinations of the extraction procedures and solvents were used to extract and recover two sources of RAP (from Florida and Kentucky). The recovered RAP binders were fully characterized according to AASHTO MP1a-98, *Performance Graded Asphalt Binder.* Three levels of aging were used: Rolling Thin Film Oven (RTFO) and Pressure Aging Vessel (PAV), RTFO only, and unaged. Comparisons were made between the different combinations of extraction and recovery procedure to determine if there was any effect

on the binder content, aggregate gradation, and PG grade of the recovered RAP binders.

The research showed that there was no change in aggregate properties between the different methods. Asphalt contents were found to differ by as much as 0.5% between methods, possibly due to differing methods of recovering the -200 material (-200 aggregate retained in the recovered binder will increase the calculated binder content). DSR tests on the recovered RAP binders showed statistically significant differences in the test results between the combinations. The asphalt binder recovered using the Centrifuge method with the Abson recovery procedure had the lowest stiffness and the highest variability. The centrifuge method with the Roto-Vap recovery procedure had the highest stiffness. It was also determined that further aging after the extraction / recovery procedure did not significantly change the RAP binder properties. The final recommendation of the project was that the SHRP extraction and recovery procedure with *n*-Propyl bromide was the best combination for extracting and recovering the RAP materials used in the study (*7*).

Effect of RAP on the Properties of Hot-Mix Asphalt

Researchers have looked for ways to quantify the effect of RAP on the properties of asphalt mixtures since before the implementation of the Superpave mix design process. In 1999, Soleymani et al. attempted, as part of a larger study, to validate the use of linear blending charts to estimate the asphalt binder properties of mixtures containing RAP and rejuvenating agents. Unlike previous work that focused on viscosity and penetration results, this research looked at the binder properties used in

the Superpave system. Complex shear modulus (G^*_{binder}), phase angle (δ_{binder}), stiffness (*S*), and relaxation (*m*-value) were studied at temperatures ranging from 90 to -12°C. Asphalt binder blends were made using a 150-200 penetration virgin binder that had been conditioned in the RTFO and PAV to simulate an aged RAP binder. The aged binder was combined with four recycling agents, characterized, and plotted against percentage of recycling agent (0 – 100%).

Statistical analyses on the results suggested that the linear blending chart relationship was valid for predicting specification parameters of blended binders. Blending charts for four parameters were recommended: high-temperature specification properties ($G^*/\sin\delta$), intermediate-temperature specification properties ($G^*\sin\delta$), low-temperature stiffness (*S*), and low-temperature relaxation (*m*-value). This work validated the use of the new Superpave binder parameters for characterizing the effect of RAP on the binder properties of a mixture. It also allowed the continued use of the simple, linear blending charts used with previous grading systems. The work was limited, however, by the use of artificially aged binders instead of actual RAP binder and the assumption that the RAP binder blended completely when mixed with virgin materials in an asphalt mixture. Since this project focused solely on “artificially” created blends of laboratory aged binders, there was no way to account for the actual interactions between RAP binder and virgin binders *(11*).

NCHRP 9-12, *Incorporation of RAP in the Superpave System* (McDaniel et al., 2000) was designed to evaluate the effect of RAP on HMA mix design and material selection. Since the Superpave mix design system in its initial form did not account for the use of RAP, the goal of this project was to make recommendations for incorporating

RAP into the mix design procedure. Factors studied included the amount of blending that occurs between RAP and virgin materials, the effect of RAP stiffness on mixture properties, and the effect of RAP content on mixture properties at high and low-temperatures. Two virgin binders (PG 52-34 and PG 64-22) and three RAP materials (chosen to represent a range of RAP stiffnesses from soft to hard) were incorporated into the testing methodology. The first question addressed in the study was the amount of blending capacity of RAP and virgin binders in an asphalt mixture. This was accomplished by creating asphalt mixture test specimens using two RAP contents (10 and 40%). The test specimens were created using three methods:

1. A “real world” case representing typical laboratory procedures for blending RAP and virgin materials,
2. A “black rock” or “zero blending” case using virgin and RAP aggregates with only virgin binder, and
3. A “total blending” case using virgin and RAP aggregates blended with pre-blended RAP and virgin binder.

The specimens were tested for Shear Stiffness at 20 and 40°C using the Superpave Shear Tester (SST) procedures described in AASHTO TP7-94, *Determining the Permanent Deformation and Fatigue Cracking of Hot Mix Asphalt (HMA) Using the Superpave Shear Tester (SST)*. Cold temperature tests were performed as described in AASHTO TP9-96, *Method for Determining the Creep Compliance and Strength of Hot Mix Asphalt Using the Indirect Tensile Test Device*. The test results for the “real world’ case were compared to the zero and total blending cases to see which case they most closely matched.

The next question addressed in the study was the effect of increasing RAP content on mixture performance characteristics. Two of the RAP materials (soft and stiff) were used in four percentages (0, 10, 20, and 40%) with mixes containing either a PG 52-34 or a PG 64-22 virgin binder. The same mixture tests as before were performed on these blends to study the effect of increasing RAP content. The last question was addressed by the binder effects study which used recovered RAP binders to create blending charts based on the Superpave asphalt binder tests. The RAP binders were blended with the virgin binders (0, 10, 20, and 40%) and characterized according to AASHTO MP1-98, *Specification for Performance Graded Asphalt Binder*. The binder test results were compared to the blending charts to evaluate the effectiveness of the Superpave binder tests for identifying changes in the asphalt binder due to the addition of RAP.

It was determined based on the testing that all three of the RAP binders blended to some extent with the virgin binder; however, the softer RAP blended more than the stiffer RAP. It was also determined that at 10% RAP content, the real-world results were statistically the same as for the total blending and zero blending cases. In other words, the addition of 10% RAP did not significantly change the performance of the mixtures. The 40% “real-world” specimens were significantly different from the zero-blending specimens and were closer to the total blending case, but not necessarily a statistical match. This would imply that some level of blending occurred between the virgin and RAP binders.

The research also confirmed that the Superpave binder tests were adequate for creating blending charts and that blending charts could be used to predict either the

virgin binder properties or the asphalt mixture properties. A recommendation was made to RTFO age the extracted RAP binder to remove any residual solvent. The research did not indicate the need for any other modifications to the existing Superpave binder tests for RAP binders. It was also found that some of the blending charts became non-linear at about 40% RAP. Because of this finding, the researchers recommended caution when using blending charts for high RAP content mixtures.

Increasing RAP content was found to increase the high-temperature and low-temperature stiffness of the mixtures, decrease the fatigue life of the mixtures at 400 and 800 microstrain, and have very little effect on the low-temperature tensile strength of the mixture. The results matched the blending recommendations already in place for mixes containing RAP as described in AASHTO M323. Mixes below 10-15% RAP did not need adjustments to the virgin binder to account for the RAP binder as their properties did not differ significantly from the mixes containing only virgin binder. Mixes containing from 15 - 25% RAP required a decrease of the virgin binder of one temperature grade softer for both high and low-temperatures. Mixes containing over 25% RAP showed significant differences from those without RAP and require blending charts to evaluate the effect of RAP on the binder properties (*6)*.

McDaniel and Shah (2003) conducted a follow up project to determine if the NCHRP 9-12 findings were applicable to other sources of RAP, particularly those from the north central United States. The project studied mixes containing up to 50% RAP to determine if such high RAP mixes were suitable for use if properly designed. Three RAP materials from the Midwest were chosen (Michigan, Missouri, and Indiana) and mixes containing 0 and 50% RAP were designed in the lab (one RAP mix could not be

designed using 50% RAP so 40% was used for that source). A medium RAP level was also used and set to match the normal contractor usage for each RAP source (15-25%). In addition to laboratory testing, plant produced mixes were studied using one of the RAP sources.

The first portion of the testing included characterization of the RAP and virgin binders as well as the extracted plant mix binder according to AASHTO MP1a-98, *Specification for Performance Graded Asphalt Binder*. The results from the binder testing were used to create plots of binder properties verses RAP content for each RAP source. In the second part of the study, mixture tests were performed on the virgin, intermediate, and high RAP percentage mixes to measure complex shear modulus and shear strain using the Superpave Shear Tester (SST) at 20 and 40°C according to AASHTO TP7-94.

In most cases, the blending chart plots were linear as found in previous studies as long as the recovered materials were considered to be RTFO aged after the extraction process and tested as such. One of the RAP sources did not show linear blending behavior during any of the testing. It was noted that this could have been due to aging issues with the plant mix or the RAP materials as this RAP was older than the other two sources used.

Results from the mixture tests showed that increased RAP contents caused increased mixture stiffness in most cases, although in some cases the higher RAP mixes showed decreased rutting resistance. It was theorized that this was due to the influence of the finer RAP aggregate gradations and reinforced the need to take RAP

aggregate structure into account when developing a mix design with high RAP content. The results of this study validated the NCHRP 9-12 findings that high RAP content mixes could be successfully designed if the RAP and virgin materials were properly characterized. Linear blending charts were found to be suitable for quantifying RAP binder properties *(12).*

Daniel et al. (2010) studied the effect of RAP on the extracted asphalt binder properties of plant-produced mixtures. A total of 28 plant-produced HMA mixes were sampled from seven mix plants. The sampled mixes had RAP contents ranging from 0 to 25% and virgin binder grades ranging from a PG 58-34 to a PG 70-22. The percentage of RAP binder replacement (the percentage of the total binder content of the mix taken up by the RAP binder) was calculated for each mix. This value was referred to as the total reused binder (TRB) and served as a way to normalize the mixes with respect to the different binder contents of the RAP sources and mixes. Extraction and recovery testing was done on the HMA mixes and RAP materials at two separate laboratories using the centrifuge extraction procedure (AASHTO T176 Method A) and Abson recovery (AASHTO T170) with TCE as the solvent. Recovered binder samples were tested to determine their performance grade (PG) according to AASHTO M320, *Specification for Superpave Performance Graded Asphalt Binder*, and critical cracking temperatures using AASHTO PP-42. The PG grades of the virgin binders were also determined.

The findings from the research showed that the high-temperature PG grade of the HMA mixes either remained the same or increased by one grade with the addition of up to 25% RAP. The low-temperature PG grades also either stayed the same or

changed only one grade. It was noted that even when the low PG grade changed, the actual continuous low-temperature grade only changed a few degrees. Some of the mixes showed improved low-temperature grades while others showed a decrease in low-temperature grade. Critical cracking temperatures indicated an improvement in thermal cracking performance with increased RAP binder. It was recommended that the TRB value be used to normalize different mixtures with respect to asphalt binder properties as this was a more accurate representation of the amount of RAP binder in the mix than the bulk RAP percentage (*13*).

Hajj et al. (2011) performed a study to evaluate the impact of high RAP content on moisture damage and thermal cracking using Marshall mixes sampled from a project in Manitoba, Canada. The mixes were designed using three RAP contents (0, 15, and 50%). A PG 58-28 binder was used for all of the mixes. An additional 50% RAP mix was made using a PG 52-34 virgin binder. All the mixes were designed to have similar gradations and binder contents and were produced at the same plant. In addition to the plant-produced mix, raw materials were collected so that differences between plant mix and laboratory compacted test specimens could be evaluated. Laboratory test specimens were aged for 4 hours at 275°C prior to compaction while the plant-produced specimens were heated and compacted without additional aging. Testing included extraction and recovery on all the mixes (plant and laboratory) using the centrifuge extraction method (AASHTO T176 Method A) and rotary evaporator recovery (ASTM D5404). The solvent used was a toluene and ethanol blend. The virgin and recovered asphalt binders were tested to determine their continuous grade temperatures and PG grades according to AASHTO M320. Compacted mix specimens were subjected to

either 0, 1, or 3 freeze-thaw cycles and then tested to determine their resistance to moisture damage using the tensile strength ratio (TSR) method described in AASHTO T283, *Resistance of Compacted Bituminous Mixture to Moisture-Induced Damage*. In addition to TSR, the conditioned samples were also tested according to AASHTO TP62 to assess changes in mixture dynamic modulus, |*E**|, due to moisture conditioning. Finally, the conditioned test specimens were tested using the Thermal Stress Restrained Specimen Test (TSRST) described in AASHTO TP10, *Method for Thermal Stress Restrained Specimen Tensile Strength*. The TSRST cools a 2 inch wide by 2 inch thick by 10 inch long restrained beam of mix at a rate of 10°C per hour and records the temperature and stress at which fracture occurs.

The researchers found that at 0 and 15% RAP, the recovered binders met the project binder grade requirement of PG 58-28. The 50% RAP met the high-temperature grade requirement but did not meet the low-temperature requirement, even with the softer virgin binder. Plant-produced test specimens were found to be stiffer in most cases than the laboratory produced specimens, although overall moisture damage trends and ranking were similar for all of the tests performed. In general, the 50% RAP mixes had acceptable resistance to moisture damage. Moisture damage resistance improved with the use of the softer virgin binder. Mix stiffness in the dynamic modulus test increased with increasing RAP content. Switching to the lower stiffness virgin binder decreased the mixture stiffness. Dynamic modulus values also decreased with increasing number of freeze-thaw cycles with the no freeze-thaw condition being the stiffest and the three freeze-thaw cycles being the least stiff. The TSRST fracture temperatures for the 0 and 15% RAP content specimens were very similar to the virgin

binder low critical temperature. The 50% RAP content specimens had TSRST fracture temperatures several degrees warmer than the virgin binder, indicating decreased thermal cracking resistance. Using a softer virgin binder improved the TSRST fracture temperature for the 50% RAP mix. The TSRST results showed no further reduction in fracture stress for the conditioned specimens with increasing RAP content. Monitoring of the project site after 13 months of service showed that there were no pavement distresses for any of the mixes evaluated at that time (*14*).

Mogawer, et al. (2012) evaluated the characteristics of plant-produced HMA containing high percentages of RAP. Eighteen mixes (9.5 and 12.5-mm nominal maximum aggregate size (NMAS)) were obtained from three contractors located in the Northeastern United States. The mixes had RAP contents ranging from 0 to 40% RAP and four virgin binder grades (PG 64-22, PG 64-28, PG 52-28, and PG 52-34). As part of the mix sampling process, production data was collected including mixing and discharge temperatures, storage time, and plant type. Test specimens were compacted at the plant and in the laboratory to study the effect of reheating the RAP mixes.

Testing included extraction and recovery of the RAP mixes using the centrifuge extraction method described in AASHTO T164 Method A and the Abson recovery method described in AASHTO T170. The recovered binders were tested to determine their PG grades according to AASHTO M320. Frequency sweep tests were run using the DSR at multiple temperatures and frequencies so that master curves of binder complex shear modulus, G^*_{binder}, could be created using the Christensen-Anderson model (CA). Data points from the master curves were used with the Hirsch model to estimate a master curve of E^*_{mix} for the mixes. This master curve was assumed to

represent a scenario where the RAP and virgin binders had completely blended as the extraction and recovery processes force total blending of the binders. The recovered asphalt binders were also tested in the bending beam rheometer (BBR) and direct tension test (DTT) to determine their low critical cracking temperature (T_{crit}) according to AASHTO R49, *Practice for Determining the Low-temperature Performance Grade of Asphalt Binders*. Finally, the recovered binders were tested before and after long term aging in the pressure aging vessel (PAV) using AASHTO TP92, *Determining the Cracking Temperature of Asphalt Binder using the Asphalt Binder Cracking Device (ABCD)*, which also gives a value of T_{crit}.

Mixture testing included dynamic modulus, E^*_{mix}, using the Asphalt Mixture Performance Tester (AMPT) at multiple temperature and frequencies to allow for the creation of master curves. The mix master curves were compared to those estimated from the recovered asphalt binder tests to evaluate the degree of blending that occurred in the RAP mixes. Cracking resistance was measured using the Overlay Tester (OT) device at 15°C with a joint opening of 0.06-cm and failure criteria of 93% reduction from the initial load or 1,200 cycles. The OT measures the ability of a mix to resist crack propagation from bottom to top due to a predetermined displacement and gives a measure of cycles to failure. Moisture and rutting susceptibility were tested using the Hamburg Wheel Tracking Device (HWTD) at 50°C. The stripping inflection point (SIP) determined by plotting rut depth versus the number of wheel passes indicates when the mix specimen begins to experience stripping due to moisture damage. Workability of the mixes was measured using a device developed by the Massachusetts Dartmouth

Highway Sustainability Research Center that measures the workability of an HMA mix using torque measurement principles.

Results from this study showed that it was important to document how RAP mixes are produced and handled as differences in the recorded production parameters were shown to have an effect on the degree of blending between RAP and virgin binders. Differences in the production parameters were also found to affect workability and mixture performance. Reheating of the mixtures was found to impact mixture stiffness compared to mixes that had test specimens compacted at the plant (i.e., not reheated). Reheated RAP mixes also showed decreased sensitivity to increasing RAP content when measured by E^*_{mix}. Comparison of the estimated and tested E^*_{mix} master curves indicated that in many cases there was a good degree of blending occurring between the RAP and virgin binders.

Both the recovered binder and mixture stiffness testing showed that stiffness increased with increasing RAP content and that changing to a softer virgin binder decreased the overall stiffness. Recovered binder testing indicated that differences in mix stiffness with increasing RAP content were more pronounced at higher temperatures than at low-temperatures. At low-temperatures, the ABCD device gave lower T_{crit} values for both the “as-extracted” and PAV aged recovered binders than the AASHTO R49 procedure. Results for both procedures indicated that the use of a softer virgin binder may improve low-temperature properties of the RAP mixes. The OT results showed decreased cracking resistance (lower number of cycles to failure) with increasing RAP content. This trend agrees with the results from both of the low-temperature tests on the recovered asphalt binder which also showed increased T_{crit}

(decreased cracking resistance) with increasing RAP content. For one of the contractors, the use of a softer PG grade virgin binder did not improve the OT results. The other contractor's mixes did show improved cracking resistance using the softer PG virgin binder. Only one of the RAP mixes (30%) failed the moisture damage test in the HWTD. It was theorized that a low plant discharge temperature for this mix may have been the cause. Workability testing showed that the addition of RAP decreased mixture workability and that the use of a softer virgin binder could improve workability to levels comparable to the control mixes (*15*).

McDaniel et al. (2012) studied the effect of RAP on the performance characteristics of plant-produced HMA mixtures. The goal of this research was to use the high and low-temperature properties of plant-produced RAP to determine if the current tiered guidelines for RAP usage given in AASHTO M323 are valid. Plant-produced mixtures were chosen as it was thought they would do a better job reflecting factors such as plant type, amount of mixing, mixing temperature, and mix handling, all of which may affect the amount of blending that occurs between RAP and virgin binders. Additional research included a comparison of two methods of extracting and recovering RAP binders and an investigation into the amount of blending that occurs during virgin and RAP binders during production.

To perform the study, four contractors were asked to supply six HMA mixes designed to be as similar as possible (volumetrics, gradation, binder content). The mixes consisted of a control PG 64-22 mix with no RAP, three PG 64-22 mixes with increasing RAP contents (15, 25, and 40%), and two PG 58-28 mixes with high RAP contents (25 and 40%). The PG 64-22 binder was chosen as it was a locally available

material and the PG 58-28 was chosen as that was the PG grade required by the current RAP usage guidelines for mixes containing 15-25% RAP.

Asphalt binder testing for this study included verification of performance grade (PG) for the virgin binders. In addition, frequency sweeps of binder complex shear modulus were conducted in the DSR at multiple temperatures and frequencies for master curve construction. A comparison was done between the centrifuge extraction method with Abson recovery and the combined extraction/recovery procedure described in AASTHO T319, *Quantitative Extraction and Recovery of Asphalt Binder from Asphalt Mixtures*. The centrifuge extractions used methylene chloride (mCl) for the solvent and the T319 procedure used an n-propyl bromide (nPB) solution. After recovery, the RAP binders were tested for PG grade and DSR frequency sweeps.

Mix testing included a verification of the volumetric properties and mixture dynamic modulus using the universal testing machine (UTM-25) and the procedure described in AASHTO TP62. At low-temperatures, indirect tensile (IDT) creep (-20, -10, and 0°C) and strength (-10°C) testing (AASHTO T322) was performed to measure the thermal cracking behavior of the mixes and a procedure developed by Christensen was used to calculate a low critical cracking temperature, T_{crit}. Finally, samples from one contractor were sent to the FHWA Turner-Fairbank Highway Research Center (TFHRC) for testing utilizing a newly developed cyclic axial pull-pull test to study the effect of RAP content and virgin binder on the fatigue life of the mixes.

The amount of blending that occurred in the mixture was estimated using a procedure developed by Bonaquist which used recovered binder properties of the RAP

mixes with the Hirsch model to estimate a mixture master curve based on the results. The master curves for the recovered RAP mixes were assumed to represent a fully blended condition (the extraction /recovery process is assumed to force total blending of the RAP and virgin binders). Master curves developed from the E^*_{mix} testing on the individual plant-produced mixes were compared to the estimated master curves from the Hirsch model. Tested E^*_{mix} master curves that closely followed the estimated total blending master curve were theorized to indicate a good degree of blending while mixtures whose master curves deviated significantly from the estimated total blending case were assumed not to be well blended.

For the binder testing, it was found that increasing RAP content increased the high-temperature stiffness of the recovered asphalt binders. The low-temperature stiffness of the recovered binders also increased with increasing RAP binder, but not as much as for the high-temperature properties. Changing to a PG 58-28 caused both the high and low-temperature grades of the recovered binders to decrease. Overall, the changes in PG grade with increasing RAP content were not as great as expected, particularly for the low-temperature grade. Using Bonaquist's master curve procedure, a significant amount of blending was found in the majority of the mixtures containing RAP. The comparison of the extraction/recovery methods did not show any clear pattern as to which might be better. The different methods appeared to affect different binder / RAP combinations differently. It was theorized that this may be due to the normal issues seen with solvent extractions.

Mixture stiffness, E^*_{mix}, increased with increasing RAP content in most cases, particularly at intermediate and high-temperatures. This increase was not always

statistically significant for the PG 64-22 mixtures, except at the 40% RAP level, where all but one of the mixtures showed evidence of being statistically different. Switching from PG 64-22 to PG 58-28 resulted in a reduction in stiffness of the mixes. Also, in many cases, the E^*_{mix} values of the PG 58-28 mixtures were significantly higher at the higher RAP percentage than the lower, which indicated that the stiffening effect of the RAP binder was more significant for the softer virgin binder grade. The addition of RAP did not significantly change the cold temperature properties for the PG 64-22 mixes containing up to 25% RAP. The 40% RAP PG 64-22 mixtures did show stiffer cold temperature properties in some cases but were still determined to be acceptable compared to the control mixture. As with the high-temperature properties, using the softer virgin binder grade significantly lowered the low-temperature stiffness of the mixes.

Fatigue properties of the RAP mixes did not meet conventional expectations. It was expected that increasing RAP content would decrease the fatigue life of the mixtures. The TFHRC testing did not show this. Mixtures with 40% RAP showed the greatest fatigue life in many cases. Changing to the softer virgin binder increased the fatigue life for the 25% RAP mixtures but did not have as great an effect on the 40% mixtures. It was speculated that since the procedure used for this analysis was fairly new that further investigation may be required (*16*).

A study by Zhao et al. (2012) used laboratory performance tests to evaluate the effect of high percentages of RAP on warm-mix asphalt (WMA) mixtures. Rutting resistance, fatigue life, and moisture susceptibility were studied. Four WMA mixtures were designed using the Marshall mix design procedure with 0, 30, 40, and 50% RAP

and a PG 64-22 virgin binder. In addition, two HMA control mixtures were designed with 0 and 30% RAP. Aggregate gradations and binder contents were kept similar for all the mixes. HMA and WMA samples were taken at the plant and the WMA test specimens compacted on site to avoid reheating and moisture loss. The HMA test specimens were compacted at a later time. Testing included rut depth in the Asphalt Pavement Analyzer (APA) at 50°C and moisture susceptibility using the Hamburg Wheel Tracking Device (HWTD) and AASHTO T283 with one freeze-thaw cycle. Fatigue cracking resistance was measured using the Indirect Tension (IDT) resilient modulus, IDT creep, and IDT tensile strength at 25°C and beam fatigue test at 7°C. The minimum dissipated creep strain energy ($DCSE_f$) from the IDT creep test and the dissipated creep strain energy threshold from the IDT strength and resilient modulus tests were used to calculate the energy ratio for each mix. Other studies at the University of Florida have related energy ratio to resistance to top-down cracking (*18*). The beam fatigue test used a strain level of 300 microstrains and a loading frequency of 10 Hz in accordance with AASHTO T321. From the beam fatigue test, a ratio of dissipated energy change and number of cycles to 50% of initial stiffness were used to evaluate the fatigue life of the mixes.

It was found that rutting resistance was improved by adding RAP to the mixes. The improvement for WMA was greater than that of the HMA mixes. $DCSE_f$ results from the IDT tests showed a slight reduction in the WMA resistance to top-down cracking with the addition of RAP, but the dissipated energy ratio from the beam fatigue test indicated an improvement in fatigue life. The number of cycles to 50% of initial stiffness in the beam fatigue device indicated that the addition of RAP increased the

fatigue life of the WMA mixes while decreasing the fatigue life of the HMA mixes. Increasing the RAP content of the HMA mix did not show a significant effect on fatigue measured by either procedure (*17*).

Research on Proposed Methods for Characterizing RAP Binders

Due to the issues with solvent extractions, much of the recent work on RAP binders has focused on finding a way to test the RAP material as a whole. A study by Zofka et al. (2004) attempted to identify an alternative low-temperature test for asphalt mixtures. Three alternative procedures to solvent extractions were evaluated for determining the low-temperature binder properties of RAP to use in blending charts. The tests evaluated included a rock strength device, an indentation tester, and the bending beam rheometer (BBR). The rock strength device and indentation tester were abandoned early due to testing limitations that were beyond the scope and budget of the project to fix. The BBR test used small beams of asphalt mixture (6.25-mm thick by 12.5-mm wide by 100-mm long) cut from Superpave gyratory compactor specimens made using two virgin binder grades: PG 58-28 and PG 58-34. RAP and millings were added at 0, 20, and 40% to the virgin materials. The BBR specimens were tested to determine their low-temperature stiffness and relaxation properties at -18 and -24°C. The mix beams were conditioned and loaded similarly to the standard BBR test for asphalt binders except that the testing load was increased from 100 to 450 grams. In addition to the BBR tests, IDT tensile strength tests were performed on the mixes at -18 and -24°C to determine the low-temperature stiffness of the mixes. The BBR mix stiffness results were used with the Hirsch model to backcalculate low-temperature binder stiffness results for the mixes. Extraction and recovery testing was performed on

the mix so that a comparison could be made between the backcalculated binder stiffness and the recovered binder stiffness.

The mix stiffness results from the BBR test were found to correlate reasonably well with the IDT stiffness results with the best correlation occurring at the warmer test temperature. In about 50% of the comparisons, the BBR stiffness was identical to the IDT stiffness. Mixture stiffness values calculated using the Hirsch model with the BBR stiffness of the recovered binders were higher than the IDT and mix BBR stiffness in almost all of the cases. Backcalculated binder data from the Hirsch model for the samples tested were under-estimated when compared to the recovered RAP binder tested at the same temperatures; however, they ranked the materials the same when different mixtures and RAP contents were compared. Further work was recommended to refine the Hirsch model to achieve a better match between the backcalculated stiffness results with the recovered binder results. Of particular concern was the unreasonable sensitivity of the mixture stiffness to changes in the binder stiffness (*19*).

In 2005, Zofka continued the work described above in another study. The results included a refinement to the Hirsch model used in the earlier paper to obtain predicted low-temperature mix stiffness values. The original Hirsch model equation was found to over-predict the mixture stiffness (both from the BBR test and from the IDT) when calculated from the BBR stiffness values obtained from testing recovered binders. To correct this, the model coefficients were modified. The modified Hirsch equation was used to backcalculate binder stiffness values using the stiffness results from the mixture BBR tests for 10 mixes used in the earlier study. The results showed that in some cases, there was a much improved correlation between recovered binder stiffness and

backcalculated binder stiffness. For other cases, the backcalculated values were still under-estimated compared to the tested values.

Discussion on this research by Don Christensen provided some insight as to why there may be such great discrepancies between the measured and backcalculated cold temperature stiffness values. Christensen agreed with the authors that the discrepancy may be partly due to differences in the aggregate properties of the mixtures, as the equation seems to be sensitive to the elastic modulus of the aggregate. He also stated that some of the discrepancy is because the Hirsch model was calibrated for a dynamic compression test instead of the flexural creep test used for this study. He proposed a relationship between creep stiffness (*S*) and the compressive modulus (*E*) as functions of time (*t*) as shown in Equation 1:

$$S(t) = 0.66E(t)^{0.994} \quad (1)$$

While the version of the Hirsch model discussed in this stage of Zofka's research showed better correlation than the previous version, it appears that more work is needed to further calibrate the model and to determine the effect of aggregate type on the test results *(20)*.

One of the concerns with Zofka's testing of mix samples in the BBR was whether or not the small size of the BBR specimens could accurately represent the mixture. The 6.25-mm thick by 12.5-mm wide by 100-mm long specimens for the BBR may not have the same volume of material as a larger sample, especially when cut from asphalt mixtures containing aggregate particles that exceed the thickness of the beam. Velasquez et al. (2010) used several methods of analysis to determine if the small BBR

specimens could be used to accurately determine mixture stiffness at cold temperatures. Ten laboratory mixes using four asphalt binder grades and two types of aggregate were chosen for the study. Samples were compacted to 4% air voids using a linear kneading compactor. Sets of three size beams were cut for each mix: 6.25 x 12.5 x 100-mm, 12.5 x 25 x 200-mm, and 18.75 x 37.5 x 300-mm. Each set of beams was tested in 3 point bending at three temperatures based on the low-temperature grade of the binder (low grade +22°C, low grade + 10°C, low grade -2°C). The two larger sets of beams were tested using an MTS 810 servo hydraulic load frame. The smaller set was tested using the BBR method described by Zofka.

Mix stiffness results at the high and intermediate-temperatures showed negligible differences due to sample size. At the lower temperature, there was a more pronounced difference in the results, especially for the smaller samples. The researchers noted that the MTS device had issues with icing at this temperature level, which could have caused error in the readings. Statistical analysis of the effects of size, time, temperature, binder type, and aggregate on the creep stiffness at high and intermediate-temperature showed that the only factor that did not have a statistical influence on the creep stiffness was sample size. Low-temperature test results were not included in the statistical analysis due to the icing issue.

Once the lack of effect of sample size was determined, the aggregate structure of the different size samples was evaluated using digital imaging analysis and finite element modeling. Based on the results of the study, it was determined that the volumetric fraction and average size distribution of the aggregates were similar between the three specimen sizes. Microstructural information was also found to be similar.

From these findings, the researchers concluded that the small-sized specimens tested in the BBR could adequately represent the asphalt mixtures *(21)*.

Bennert and Dongre (2010) evaluated the Hirsch model for backcalculating asphalt binder properties (G^*_{binder} and δ_{binder}) using E^*_{mix} data obtained from dynamic modulus testing. Samples of loose plant mix were obtained and tested for E^*_{mix} according to AASHTO TP 79-09, *Determining the Dynamic Modulus and Flow Number for Hot Mix Asphalt (HMA) Using the Simple Performance Test System*. Samples of the same plant mix were also extracted and the asphalt binder recovered. The recovered asphalt binders were then tested in the DSR to determine their stiffness (G^*_{binder}) over a range of temperatures and frequencies. The initial set of samples tested did not contain any RAP. Without RAP in the mix, the backcalculated and tested results were expected to be similar and give an indication of the validity of the method. For the backcalculations, the researchers used a generalized logistic equation to create a master curve of the E^*_{mix} data. The E^*_{mix} version of the Hirsch model was then used to estimate the binder complex shear modulus, G^*_{binder}. The Christiansen-Anderson (CA) model was used to create master curves of the backcalculated G^*_{binder} results and compare them to the binder test results from the extracted binders. The estimated G^*_{binder} data were then fit to the generalized logistic model and the constants obtained from that equation used to estimate δ_{binder}.

Once the researchers determined that a good correlation was possible between the backcalculated binder data and actual tested binder results for mixes without RAP, they explored ways to use the backcalculated results. One possibility was using the backcalculated binder properties in the Mechanistic-Empirical Pavement Design Guide

(MEPDG) level 1 analysis. An MEPDG analysis on a mix with four RAP contents (0, 15, 20, and 25%) using binder properties obtained from the backcalculation procedure showed reasonable rutting behavior with rut depth decreasing as RAP content increased. Top-down cracking results did not rank as expected. A comparison between G^*_{binder} results backcalculated from the plant mix at intermediate-temperatures and the cracking resistance based on the Overlay Tester showed a good correlation between the OT and the backcalculated G^*_{binder} resistance to reflection cracking (*22*).

A study by Tran et al. (2010) also evaluated the possibility of using the Hirsch model to backcalculate the high-temperature properties of asphalt binders using mixture dynamic modulus (E^*_{mix}) values. The researchers used HMA mixes sampled during the 2006 construction of the National Center for Asphalt Technology (NCAT) Pavement Test Track. Mix specimens were tested for E^*_{mix} over a range of temperatures and frequencies described in AASHTO TP62. The E^*_{mix} version of the Hirsch model was used to backcalculate G^*_{binder} for the mixes. CA master curves were created for the backcalculated G^*_{binder} values and the master curve parameters used to estimate $\delta_{binder.}$ Virgin binders sampled at the asphalt plant were RTFO aged and tested over a range of temperatures and frequencies in the DSR to create master curves of binder stiffness. The backcalculated G^*_{binder} values were compared to the tested G^*_{binder} values to determine if the Hirsch model backcalculation method could accurately estimate the high-temperature stiffness properties of the plant-produced mixes.

For the binders used in this study, the backcalculation procedure under-estimated G^*_{binder} at the higher test temperatures. The δ_{binder} values did not follow any particular trend compared to the tested values and varied by as much as 10° high or

low. Backcalculated critical temperatures varied from the virgin binder critical temperatures by anywhere from 0.5 to 15.1°C. The researchers recommended further calibration of the Hirsch model to determine if individual calibrations for local materials could improve the accuracy of the backcalculated data. It was suggested that different calibrations for laboratory and plant-produced mixes may also be necessary (*23*)

Swiertz et al. (2011) conducted a study to evaluate a proposed method of estimating the low-temperature properties of HMA blends containing RAP and reclaimed asphalt shingles (RAS). The proposed method consisted of testing three sets of BBR test specimens prepared as follows:

1. Virgin binder tested using standard BBR procedure as described in AASHTO T313,
2. Mortar made from RAP passing the No. 50 sieve and retained on the No. 100 sieve (designated SRAP), and
3. Mortar made from SRAP aggregate recovered using an ignition furnace, blended with RTFO aged virgin binder at a binder content equal to that of the SRAP (designated RRAP).

The two sets of mortar samples were tested at temperatures corresponding to the low-temperature grade of the virgin binder and the difference between the SRAP and RRAP properties for BBR (stiffness (*S*) and *m*-value) were calculated. Since the aggregate and binder contents were the same for both sets of specimens, the difference between the test results was theorized to be due solely to the increased stiffness of the RAP binder. This difference was used to shift the virgin binder test results to provide an

estimate of the RAP binder properties. The estimated RAP binder properties were then used along with the virgin binder properties to create blending charts for estimating the effect of adding different percentages of RAP to HMA. Additional work was done to determine if the same shifting procedure could be applied to testing low-temperature fracture energy properties using the single-edge notched beam (SENB) test. For this test, specimens were created in a similar manner as before with the addition of a 3-mm notch in the width of the BBR side mold. Materials tested included one RAP source blended with two virgin binders and one RAS source blended with one virgin binder. Samples were tested at -6, -12, and -18°C to measure stress intensity factor K_{IC} and fracture energy, with the load and displacement at failure also reported.

Artificially created RAP [virgin binder aged through two cycles of long-term aging in the pressure-aging vessel (PAV) blended with RAP aggregate recovered using the ignition oven] was used to verify the ability of the proposed method to identify the low-temperature binder properties of HMA containing RAP. The artificial RAP was blended with two virgin binders (PG 64-22 and PG 58-28) at 15 and 25%. The blends were tested using the proposed procedure and the estimated low-temperature properties were compared to BBR test results on binders created by blending the virgin and artificially aged RAP binder. It was found that the proposed procedure could estimate the low-temperature properties of the artificial RAP blends within 1°C of the tested values. When the proposed procedure was used to estimate the low-temperature properties using combinations of actual RAP materials (4 sources) and virgin binder (PG 64-22 and PG 58-28), it was shown that the interaction of RAP and virgin binder was different for different combinations of materials. This would imply that the current

tiered approach to RAP blends may not be valid for all materials. It also implied that an assumed constant rate of change for continuous grade per percent of RAP binder replacement may not be valid for every RAP and virgin binder combination. The procedure worked for RAS materials as well as RAP binders and allowed for the estimation of the low-temperature properties of blends containing both RAP and RAS materials. SENB testing could detect changes in the mixture fracture energy of the asphalt mixtures due to the addition RAP and RAS materials but more work will be needed to define what the differences mean (*24*).

Summary of Key Findings

Key findings from the literature review are listed as follows:

1. RAP binders are typically characterized using one of the available combinations of solvent extraction and recovery procedures. While these procedures provide recovered RAP binder to test, the binder properties are affected by the process. Solvents affect recovered RAP binder properties through chemical hardening, retained solvent, or both. The amount of time needed to complete the extraction / recovery process can also affect the binder as can the temperature at which the procedure is performed (*7, 9, 10*).

2. Linear blending charts created using the properties obtained from Superpave performance testing of the virgin and recovered RAP binders are the current method of choice for characterizing asphalt mixtures containing more than 25% RAP. While much work has been done to validate the use of these charts, it is noted that they have limitations (*6, 11,12*).

3. Blending charts assume full blending between RAP and virgin binders as well as linear behavior with increasing RAP content. This may not be the case and could lead to inaccurate estimation of the binder properties of RAP mixtures (*6, 11, 12*).

4. RAP mix designs with high percentages of RAP can provide acceptable performance if aggregate and binder properties are properly characterized and accounted for (*6, 12, 13, 14, 15, 17*).

5. Researchers have not achieved a clear understanding of how much blending occurs between virgin and RAP binder in HMA. Studies have determined that there is some degree of blending of the binders, but that the amount of blending varies. Factors that may influence the amount of blending include RAP content, virgin binder stiffness, and mixture handling. Lack of precision in characterizing binders recovered from RAP and RAP mixtures makes studying this topic difficult (*6, 15*).

6. The addition of RAP to HMA mixes increases the high-temperature stiffness of HMA. The amount of stiffening increases with increasing RAP content, with higher RAP content mixes being significantly stiffer than virgin mixes. Lower RAP contents may or may not be significantly stiffer at high-temperatures than virgin mixes. Research on this behavior illustrates the need to account for the RAP binder in HMA mixes containing high percentages of RAP (typically >25%) and supports the current AASHTO M323 tiered approach to accounting for RAP binder based on RAP content (*6, 12, 13, 14, 15, 16, 17*).

7. Although it was expected that the addition of RAP would decrease the fatigue life of HMA mixes, this was not always the case. Some research showed that mixes with up to 40% RAP showed an improved fatigue life. Other research showed the expected decrease in fatigue resistance for higher RAP content mixes. In cases where the fatigue life decreased with the addition of RAP, changing to a softer virgin binder grade as recommended in AASHTO T323 lessened the effect (*6, 16*).

8. As with the fatigue life, increased RAP content is expected to decrease the cold temperature cracking resistance of HMA mixes. The research shows that this does occur, but the change is usually much smaller than the effect on the high-temperature properties. Some of the research indicated that mixes containing up to 40% RAP still provided acceptable low-temperature properties compared to the virgin mixes. It was also shown that reducing the stiffness of the virgin binder improved the low-temperature properties of the RAP mixes (*6, 14, 15, 16*).

9. Use of the Hirsch model to backcalculate binder stiffness as a function of tested mixture E^*_{mix} was explored and found to be a potential method for characterizing the binder properties of asphalt mixtures. Recent research shows that the Hirsch model has a tendency to under-estimate G^*_{binder} and has difficulty estimating δ_{binder}. It is possible that further calibration of the model will improve the correlation (*22, 23*).

10. Work has been done to identify ways to test mixture stiffness in the laboratory to obtain the inputs needed for the Hirsch model. Research in this area has

primarily focused on creating a specimen to test in existing binder testing equipment such as the BBR. Success has been limited by the difficulty obtaining of representative a test specimen small enough to fit into the test equipment and by the need to calibrate the models to reflect the differences between binder and mixture testing methods (*19, 20, 21, 24)*.

EXPERIMENTAL PLAN

The mixture test chosen for evaluation in this study was a mixture torsion bar test similar to the one described in ASTM D7552-09, *Determining the Complex Shear Modulus (G^*_{mix}) of Bituminous Mixtures Using Dynamic Shear Rheometer*. The torsion bar procedure was developed by Gerry Reinke at Mathy Construction Co. This test was chosen because of its small sample size and ability to be performed on the DSR, an existing piece of binder testing equipment, with commercially available fixtures. The test provides a measure of mixture complex shear modulus (G^*_{mix}) over a range of frequencies and can easily be run at multiple temperatures, allowing for the creation of master curves of mixture stiffness. This section includes a discussion of the test materials and procedures used to evaluate the DSR torsion bar procedure.

Materials

The following is a description of the materials used to evaluate the DSR torsion bar procedure. The materials tested included mixes containing only virgin components (asphalt binder and aggregate), mixes containing only RAP materials, HMA mixes designed at multiple RAP contents, and plant-produced mixes containing RAP.

Virgin Binder

The virgin binders used in this study were locally available PG 64-22 and SBS modified PG 76-22 binders. Table 1 shows the high, intermediate, and low true grade temperatures for these asphalt binders as tested by NCAT. Both virgin materials met the requirements for their performance grade criteria.

TABLE 1 Virgin Binder Properties

	High T_{crit}, °C	Int T_{crit}, °C	Low T_{crit}, °C
PG 64-22	68.3	23.9	-23.2
PG 76-22	78.3	22.4	-24.1

Virgin Aggregate

The virgin aggregates used for this study were a combination of locally available materials including: a limestone in several different sizes from Calera, Alabama; a granite #89 from Columbus, Georgia; and a natural sand from Shorter, Alabama. Table 2 shows the aggregate gradations and bulk specific gravities (G_{sb}).

TABLE 2 Virgin Aggregate Gradation

	Percent Passing, %					
	Limestone				Granite	Shorter Sand
Sieve Size, mm	#89	#67	#7	#820	#89	
50	100	100	100	100	100	100
37.5	100	100	100	100	100	100
25	100	100	100	100	100	100
19	100	100	100	100	100	100
12.5	100	84.2	97.1	100	100	100
9.5	99.5	50.2	74.4	100	99.5	100
4.75	37.5	10.3	15.2	96.7	27.1	100
2.36	8.2	2.6	1.9	61.7	3.3	94.6
1.18	3.2	1.5	1.2	38.3	1.6	79.5
0.6	2.0	1.3	1.0	25.2	1.6	51.4
0.3	1.7	1.3	1.0	17.8	1.6	21.7
0.15	1.6	1.3	1.0	13.0	1.6	5.2
0.075	1.5	1.2	0.9	10.1	1.6	0.9
G_{sb}	2.645	2.746	2.717	2.646	2.61	2.656

RAP Materials

Five Alabama RAP sources were evaluated and designated as RAP 1 through RAP 5 for reference purposes. Table 3 shows the supplier information, designations, aggregate gradations (% passing each sieve size), asphalt contents, and specific gravities for each of the RAP sources as received. A map showing the supplier locations is included in Appendix A. Gradations and specific gravities were evaluated on aggregates recovered from the RAPs by solvent extraction (ASTM D2172, Method A) using trichloroethylene. The maximum theoretical specific gravity (G_{mm}) and aggregate bulk specific gravity (G_{sb}) were required to calculate the volumetric properties of the test specimens. G_{mm} was determined using AASHTO T209, *Theoretical Maximum Specific Gravity and Density of Hot Mix Asphalt*. The aggregate bulk specific

gravities (G_{sb}) were determined using either AASHTO T84, *Specific Gravity and Absorption of Fine Aggregate*, or AASHTO T85, *Specific Gravity and Absorption of Coarse Aggregate*.

TABLE 3 RAP Properties

	RAP				
	Wiregrass Const. Co.	**East Alabama Paving**	**McCartney Const. Co.**	**S.T. Bunn Const. Co**	**APAC**
Sieve Size, mm	**1**	**2**	**3**	**4**	**5**
25.0	100.0	100.0	100.0	100.0	100.0
19.0	100.0	100.0	100.0	97.7	100.0
12.5	99.8	95.6	99.9	90.7	97.4
9.5	95.4	85.8	95.7	84.1	88.3
4.75	71.4	65.6	62.3	65.3	62.9
2.36	58.1	53.0	38.0	47.1	40.5
1.18	46.9	42.9	23.0	35.8	23.7
0.600	32.9	32.4	14.3	28.0	12.1
0.300	20.4	21.8	8.0	17.1	5.5
0.150	12.3	14.5	4.4	9.7	3.3
0.075	8.5	9.5	2.9	7.2	2.2
% AC	5.2	4.7	4.7	4.7	4.6
Gmm	2.476	2.52	2.548	2.511	2.487
Gmb	2.573	2.647	2.748	2.61	2.719

The gradations shown in Table 3 were based on the as-received RAP materials. RAP 3 had been fractionated over a 4.75-mm sieve at the plant. RAP materials from the other sources did not indicate any processing prior to their arrival at NCAT.

Mix Designs

Mix designs were created using both the virgin and RAP materials. These blends were used to determine if the torsion bar procedure could detect changes in

mixture properties due to increasing RAP content. Plant-produced mixes were also obtained from several contractors.

RAP Mix Designs

Three of the RAP sources were used along with the virgin aggregates and binders to create mix designs containing 20, 35, and 50% RAP by weight of aggregate according to Alabama Department of Transportation (ALDOT) mix design procedures. In order to represent the aggregate sizes most commonly used in Alabama surface mixtures, a different maximum aggregate size (MAS) was used for each RAP source. The RAP 2 mix designs had MAS of 12.5-mm, RAP 3 had MAS of 19.0-mm, and RAP 5 had MAS of 25.0-mm. Tables 4-6 show the mix design gradations and volumetrics.

TABLE 4 Properties of Mix Designs Using RAP 2

	RAP 2, % Passing		
Sieve Size, mm	**20%**	**35%**	**50%**
25.0	100.0	100.0	100.0
19.0	100.0	100.0	100.0
12.5	100.0	99.9	99.9
9.5	98.8	97.4	96.4
4.75	68.0	66.6	64.3
2.36	55.3	54.4	52.6
1.18	43.7	43.0	43.2
0.600	29.3	29.5	29.2
0.300	14.3	14.4	14.3
0.150	8.1	8.5	8.1
0.075	5.1	5.6	5.1
Opt AC, %	6.3	5.9	6.2
VMA, %	16.7	15.9	16.3
VFA, %	75.9	74.2	76.4

TABLE 5 Properties of Mix Designs Using RAP 3

	RAP 3, % Passing		
Sieve Size, mm	**20%**	**35%**	**50%**
25.0	100.0	100.0	100.0
19.0	99.7	99.6	99.4
12.5	94.5	94.9	92.9
9.5	84.5	85.0	80.9
4.75	64.4	62.9	58.8
2.36	48.2	48.8	47.8
1.18	37.0	38.4	38.6
0.600	24.2	25.6	26.2
0.300	11.8	12.9	13.4
0.150	7.2	8.0	8.4
0.075	5.3	5.7	6.0
Opt AC, %	5.1	5.1	5.1
VMA, %	14.4	15.2	14.6
VFA, %	72.4	72.7	71.8

TABLE 6 Properties of Mix Designs Using RAP 5

	RAP 5, % Passing		
Sieve Size, mm	**20%**	**35%**	**50%**
25.0	100.0	100.0	100.0
19.0	99.7	96.3	94.5
12.5	90.0	87.2	87.0
9.5	73.7	76.9	78.7
4.75	51.3	51.6	60.0
2.36	37.7	36.9	48.7
1.18	28.3	27.6	37.5
0.600	18.1	18.0	24.4
0.300	8.3	8.7	11.6
0.150	5.0	5.4	7.2
0.075	3.5	3.9	5.0
Opt AC, %	4.8	4.7	4.9
VMA, %	13.8	13.5	14.4
VFA, %	71.6	70.2	71.3

Plant-Produced Mix

Samples of plant-produced mixes containing RAP were obtained from local contractors. Table 7 shows the job mix formula information for these mixes. These materials were given alphabetical designations to distinguish them from the 100% RAP materials and laboratory mix designs. Gradations, RAP contents, recycled asphalt shingle (RAS) contents, asphalt binder contents, and virgin asphalt binder grades were all obtained from the job mix formulas provided by the contractors supplying the mixes.

TABLE 7 Plant Mix Information

	Plant Mix				
	McCartney Const. Co.	**S.T. Bunn Const. Co.**	**Dunn Const Co.**	**Mobile Asphalt Co.**	**East Alabama Paving Co.**
Sieve Size, mm	**A**	**B**	**C**	**D**	**E**
50	100	100	100	100	100
37.5	100	100	100	100	100
25	100	100	100	100	100
19	84	96	100	99	90
12.5	63	81	90	87	77
9.5	54	72	70	78	67
4.75	45	54	57	56	45
2.36	31	44	44	41	37
1.18	20	37	33	33	29
0.6	14	28	24	26	19
0.3	10	14	13	13	11
0.15	7	9	9	6	7
0.075	4.5	5.2	5.6	3.5	4.4
% RAP	25	15 + 5% RAS	10 + 5% RAS	20	20
Virgin Binder Grade	76-22	64-22	64-22	76-22	64-22
%AC	4.2	5	5.3	4.5	4.5

Organization of the Testing Plan

Binder Tests

The first part of this study included characterizing the virgin and recovered RAP binders used in the study. The virgin PG 64-22 and PG 76-22 binders were tested in accordance with AASHTO M320-05, *Performance Graded Asphalt Binder*, and AASHTO R29-08, *Grading or Verifying the Performance Grade (PG) of an Asphalt Binder* to determine their PG and true binder grades. Specific binder tests in this methodology include:

- viscosity measurements using the Rotational Viscometer (RV) procedure described in AASHTO T316-06,
- short-term aging using the Rolling Thin Film Oven (RTFO) procedure described in AASHTO T240-08,
- long-term aging using the Pressure Aging Vessel (PAV) procedure described in AASHTO R28-06,
- binder complex shear modulus (G^*_{binder}) and phase angle (δ_{binder}) using the Dynamic Shear Rheometer (DSR) at high and intermediate-temperatures, as described in AASHTO T315-08,
- binder frequency sweeps using the DSR to determine G^*_{binder} at different temperatures and frequencies, and

- low-temperature stiffness and relaxation properties from the Bending Beam Rheometer (BBR), as described in AASHTO T313-12.

Critical temperatures are defined as the temperature at which a test criterion is met (for example, the critical temperature for unaged DSR is the temperature at which *G*/sin(δ)* = 1.00 kPa) and are determined by interpolating between two test results that bracket the criteria. The high critical temperature, T_{crit}, High, is based on the lower of the unaged and RTFO-aged DSR results. The low critical temperature, T_{crit}, Low, is based on the warmer of the two BBR results (*S* and *m*-value). The intermediate critical temperature, T_{crit}, Int, is based on the results from the PAV-aged DSR. The true-grade of an asphalt binder is determined from the critical temperatures and is rounded to a standard grade to determine the PG grade (*25*). Table 8 shows a summary of the binder tests and the criteria associated with them.

TABLE 8 Binder Testing Summary

Test	AASHTO Method	Output	Criteria
RV	T316	Viscosity (Pa-S)	Viscosity ≤ 3.0 Pa-S
DSR	T315	*G** (kPa) and *δ* (degrees)	Unaged Binder: *G*/sin(δ)* ≥ 1.00 kPa RTFO Aged Binder: *G*/sin(δ)* ≥ 2.20 kPa PAV aged binder: *G*sin(δ)* ≤ 5,000 kPa
BBR	T313	*S* (Mpa) and *m*-value (no units)	*S* ≤ 300 Mpa *m*-value ≥ 0.300
RTFO	T240	Mass Change, %	Mass change ≤ 1.00%
PAV	R28	aged asphalt binder for further testing	no criteria

Asphalt binder was extracted and recovered from samples of each of the RAP sources and plant produced mixes using the centrifuge extraction method (ASTM D2172-05 Method A) with TCE as the solvent. The rotary evaporator recovery procedure (ASTM D5404-03) was used to remove the solvent from the extracted binder. At least two replicate samples were recovered for each RAP source. Only one sample was recovered for the plant mixes.

The recovered binders were tested to determine their PG and true-grade temperatures. When testing recovered binders, short-term aging in the RTFO is not required. Recovered binder has already been through the mixing and construction phase simulated by the short-term aging procedure and, therefore, does not need further aging. Some agencies use the RTFO aging procedure for their recovered binders as a means of assuring that all the solvent from the extraction/recovery process is removed. Since this is not a standardized procedure and does cause additional aging of the recovered binder, it was not done as part of this testing. The recovered binders were long-term aged because this seemed necessary to provide accurate intermediate and low PG grade temperatures. Binder tests on extracted/recovered binder have long been the preferred method of characterizing RAP binder and are used as the basis for creating blending charts for high RAP mixtures. Consequently, it was felt that recovered binder properties should be used as the benchmark for this project to determine the ability of the chosen model to accurately predict binder stiffness.

Mixture Tests

The mixture test chosen for this project was a torsion bar procedure tested using small bars of mix in the DSR. At the time the testing took place, ASTM D7552 was not an official ASTM standard so modifications were made to the test procedure (mainly sample size and test temperature) and are noted below. The test procedure uses a torsional rectangular geometry (torsion bar) to measure the complex shear modulus (G^*_{mix}) of a small sample of asphalt mixture at multiple temperatures and frequencies.

The torsion bars used for this procedure were cut from samples that had been compacted using the Superpave Gyratory Compactor (SGC). For the 100% virgin samples, four sets of test specimens were compacted:

1. PG 64-22 with limestone 820s screened over a #4 sieve,
2. PG 64-22 with limestone 820s screened over a #8 sieve,
3. PG 76-22 with limestone 820s screened over a #4 sieve, and
4. PG 76-22 with limestone 820s screened over a #8 sieve.

After mixing, the mixes were short-term oven-aged for 2 hours at 150°C and compacted using the SGC. The 100% RAP torsion bars were comprised of RAP with no virgin materials. The RAP materials were heated in the oven, mixed, then allowed to age for an additional hour at 150°C before being compacted. ASTM D7552 does not provide guidance about compactive effort and states that the use of discarded volumetric specimens is acceptable. Because another portion of this project required the compaction of gyratory specimens for mixture performance testing to an air void

level of 7%, the rejected performance specimens were used to cut the torsion bar test specimens. Therefore, the compacted specimens used for this testing were compacted to somewhere between 5-7% air voids. The cut test specimens had air voids that were higher than those of the compacted samples and average values ranged from 7.0 to 11.2% for the virgin and 100% RAP test specimens.

Once compacted, the samples were sliced into small chunks taken from the middle of the compacted specimen. A Master Tiler diamond wheel 7-in. wet saw (Figure 1) was used to further slice the samples into 5.5-mm thick by 11.5-mm wide by 50-mm long bars (Figure 2). This was a change from D7552; the 9 ± 1.5-mm thick by 12 ± 2-mm wide by 49 ± 2-mm long dimension specified in ASTM D7552 was too stiff and maxed out the torque capacity of the DSR at high frequencies and cold temperatures.

Figure 1 Saw Used to Cut Torsion Bar Specimen

Figure 2 Torsion Bar Specimen

After cutting, the torsion bars were measured (length, width, and thickness in mm) and weighed (grams) to calculate bulk specific gravity (G_{mb}) and air voids using dimensional analysis calculations, as shown in Equation 2.

$$Density,(g/cm^3) = \frac{Weight * 1000}{Length * Width * Thickness} \quad (2)$$

The air voids of the sample were calculated using Equation 3.

$$\%AirVoids = \frac{G_{mm} - Density}{G_{mm}} * 100 \quad (3)$$

Several specimens were cut for each group of materials and narrowed down to four replicate test specimens per group. The final test specimens were selected to be within approximately 1% air voids of each other. Care was also taken to select bars that did not vary more than 1 mm from end to end for width or thickness. Finally, the bars were inspected to make sure they did not have any imperfections or roughness at the ends that might interfere with the clamping assembly.

A TA Instruments AR2000 EX DSR with a rectangular solid clamp set-up and environmental temperature chamber with liquid nitrogen hookup for temperature control was used to test the torsion bar samples (Figures 3-4). Before testing, the gap between the clamping fixtures was zeroed at the mid-range of test temperatures. The environmental chamber was opened, and the test specimen was placed in the clamping fixture at ambient temperature. The clamp screws were finger-tightened and the bar visually inspected to ensure it was straight and centered in the fixture. A torque wrench was used to tighten the screws to a torque of approximately 20 dynes, being careful not to introduce a normal load on the specimen as indicated by the DSR software.

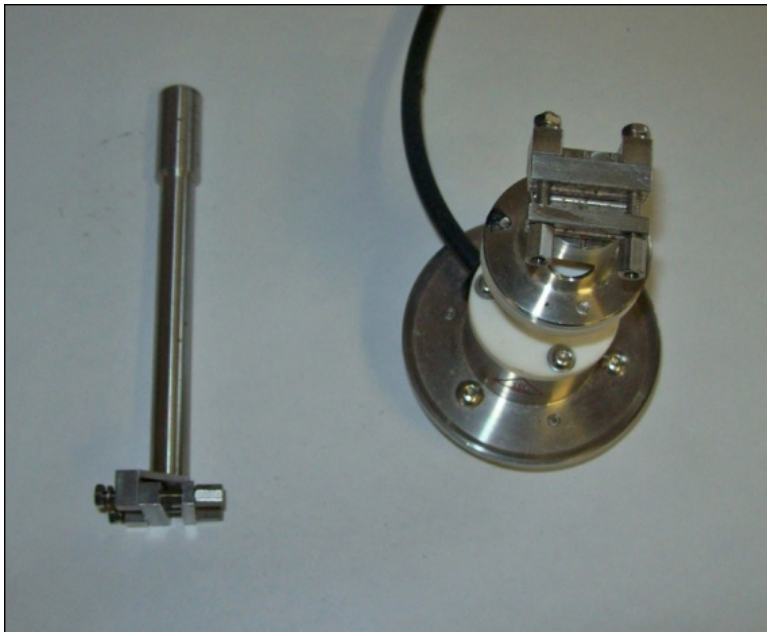

Figure 3 DSR Rectangular Torsion Clamps

Figure 4 AR2000EX Torsion Bar Testing Setup

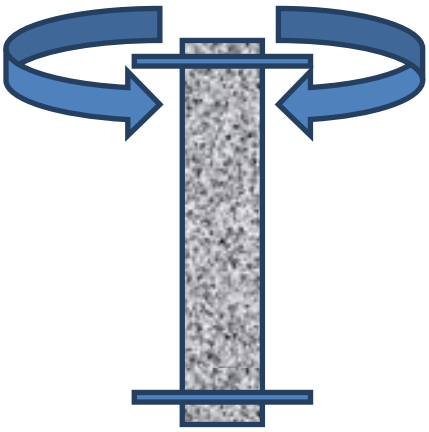

Figure 5 Torsion Bar Loading

After clamping the specimen, the environmental chamber was closed and allowed to equilibrate to the lowest test temperature ± 0.1°C for at least 15 minutes. The testing was conducted in controlled strain mode using a strain of 0.01%. At this strain, ten frequencies ranging from 0.01 to 10 Hz were applied to the bar by oscillating the top clamp in a sinusoidal fashion as shown in Figure 5. Each frequency was tested for a total of 20 cycles. For each cycle, measurements of the shear stress required to

maintain the required frequency and strain level were taken. This stress was used to calculate G^*_{mix} for each cycle as shown in equation 4.

$$G^*_{mix} = \frac{MaxShearStress}{MaxShearStrain} \quad (4)$$

The time lag in seconds between sample loading and movement was also measured and used to calculate δ_{mix} as shown in equation 5.

$$\delta_{mix} = 360 * time * frequency \quad (5)$$

For each frequency, the first 10 cycles of data were discarded, and the results of the second 10 were averaged for the final result. Testing was repeated at five test temperatures (20, 30, 40, 50, and 60°C) to provide multiple isotherms of G^*_{mix} and frequency. These temperatures were chosen instead of the high PG grade temperature required by the climate (64°C for Alabama) recommended in ASTM D7552 because of issues with the mix samples deforming at the warmer temperature.

Description of Models and Master Curves

Models

Many researchers working to improve characterization of high-temperature RAP properties have focused on developing a mixture test (i.e., dynamic modulus) to obtain a mixture stiffness parameter to estimate binder stiffness. Conversely, several models currently exist for calculating mixture stiffness based on tested binder stiffness. In theory these models could be used with known mixture stiffness to backcalculate binder stiffness.

The first predictive models for mixture stiffness were developed in the late 1970s when Witczak began his work developing several versions of a model to predict mixture Dynamic Modulus, E^*_{mix}, using such parameters as binder viscosity, aggregate gradation, testing frequency, volume of air voids, and volume of effective binder. While the models were all able to predict E^*_{mix} reasonably well, earlier versions had several limitations:

- Mixtures with modified asphalt were omitted from model calibration,
- The binder viscosity value used in the models was based on asphalt viscosity or penetration at 25°C only and assumed that the laboratory aging approximated field aging, and
- The models were based on a polynomial form and did not provide accurate predictions at extremely hot or cold conditions.

A version of the Witczak model developed in the 2006 attempted to address these concerns by including the Superpave binder properties G^*_{binder} and phase angle (δ_{binder}), that could be based on test results at any temperature or aging condition desired. The form of the model was changed from a basic polynomial equation to a symmetrical sigmoidal function in order to improve prediction at the extreme values. The final model is shown in Equation 6.

$$\log E^*_{mix} = -0.349 + \left[0.754 G^{*\,-0.0052}_{b}\right] *$$
$$\left[6.65 - 0.032 p_{200} + 0.0027 p_{200}^2 + 0.011 p_4 - 0.0001 p_4^2 + 0.006 p_{38} - 0.00014 p_{38}^2 - 0.08 v_a - 1.06\left(\frac{V_{beff}}{V_a + V_{beff}}\right)\right] +$$
$$\left(\frac{2.56 + 0.03 V_a + 0.71\left(\frac{V_a}{V_a + V_{beff}}\right) + 0.012 p_{38} - 0.0001 p_{38}^2 - 0.01 p_{34}}{1 + e^{\left(-0.7814 - 0.5785 \log(G^*_{binder}) + 0.8834 \log \delta_{inder}\right.}}\right) \quad (6)$$

Where:

E^*_{mix} = asphalt mix dynamic modulus, in 10^5 psi;

G^*_{binder} = dynamic shear modulus of binder, psi;

δ_{binder} = phase angle of binder associated with G^*_b, degree;

F = load frequency, in Hz;

V_a = percent air voids in the mix, by volume;

V_{beff} = percent effective bitumen content, by volume;

P_{34} = percent retained on ¾-in sieve, by total aggregate weight (cumulative);

P_{38} = percent retained on the 3/8-in sieve, by total aggregate weight (cumulative);

P_4 = percent retained on No.4 sieve by total aggregate weight (cumulative); and

P_{200} = percent passing No. 200 sieve, by total aggregate weight.

This version of the Witczak model was found to have excellent statistical correlation based on the database used for its development. The use of the actual binder properties gave it greater flexibility for estimating E^*_{mix} at various temperatures and aging conditions. The nonlinear sigmoidal function also provided better results at high and low-temperatures *(26)*.

Another model frequently used for estimating asphalt mixture modulus (shear or dynamic) from the results of asphalt binder complex shear modulus (G^*_{binder}) testing and mixture volumetric analysis was developed in the early 2000s by Christiansen et al. Several variations of an existing version of the law of mixtures, the Hirsch Model, were evaluated before a final, simple model was chosen. The final version of the model estimates the asphalt mixture modulus directly from the asphalt binder complex shear modulus, the voids in the mineral aggregate (VMA) of the mixture, and the voids filled with asphalt (VFA) of the mixture. The model takes two forms: one for dynamic complex shear modulus, G^*_{mix}, and one for dynamic complex extensional modulus, E^*_{mix}. Equations 7 - 10 show both forms of the finalized model.

$$G^*_{mix} = Pc\left[601{,}000\left(1-\frac{VMA}{100}\right)+G^*_{binder}\frac{VFAxVMA}{10{,}000}\right]+(1-Pc)\left[\frac{1-\frac{VMA}{100}}{601{,}000}+\frac{VMA}{VFAG^*_{binder}}\right]^{-1} \quad (7)$$

$$Pc=\frac{\left[3+\frac{VFAxG^*_{binder}}{VMA}\right]^{0.678}}{396+\left[\frac{VFAxG^*_{binder}}{VMA}\right]^{0.678}} \quad (8)$$

$$E^*_{mix} = Pc\left[4{,}200{,}000\left(1-\frac{VMA}{100}\right)+3G^*_{binder}\frac{VFAxVMA}{10{,}000}\right]+(1-Pc)\left[\frac{1-\frac{VMA}{100}}{4{,}200{,}000}+\frac{VMA}{3VFAG^*_{binder}}\right]^{-1} \quad (9)$$

$$Pc=\frac{\left[20+\frac{VFAx3G^*_{binder}}{VMA}\right]^{0.58}}{650+\left[\frac{VFAx3G^*_{binder}}{VMA}\right]^{0.58}} \quad (10)$$

Where:

G^*_{mix} = complex shear modulus for asphalt mixture, psi;

G^*_{binder} = complex shear modulus for asphalt binder, psi;

VMA = voids in the mineral aggregate;

VFA = voids filled with asphalt;

P_c = contact factor; and

E^*_{mix} = complex extensional modulus for asphalt mixture, psi.

In addition, an equation was developed for calculating mixture phase angle, δ, using the contact factor P_c. This model is shown in equation 11.

$$\delta = -9.5(\log(Pc))^2 - 39\log(Pc) + 9.6 \quad (11)$$

Model verification was completed by estimating mixture shear modulus (G^*_{mix}) for tests performed during the SHRP program. These calculations showed the agreement between predicted and measured values of G^*_{mix}, though good, were slightly under-predicted, while the phase angle prediction was less accurate, especially at higher phase angles. Model calculations were also compared to Witczak's model and had similar accuracy for the data used, although it was theorized that this level of agreement would not always be the case. A comparison using binder creep modulus data from the BBR in the Hirsch model showed that when compared to the mixture creep compliance results from SHRP, the Hirsch model tended to under estimate mixture values (*27*).

The Hirsch model for G^*_{mix} shown in equations 7 and 8 was chosen as the starting point for the high and intermediate-temperature backcalculation testing for this project. This model was chosen over the Witczak model due to its simple form and use of a single, easily tested binder parameter (G^*_{binder}). For the first step in the analysis of the test results, the G^*_{binder} values from the tested virgin and recovered RAP binder frequency sweeps were used with the Hirsch model to calculate G^*_{mix} for the individual torsion bar samples (forward-calculation). In order to obtain replicate results so that statistical analysis could be performed, values of VMA and VFA were calculated from the dimensional analysis of the torsion bar samples and each set of values used to calculate a value of $G^*_{mix.}$ The calculated G^*_{mix} values were compared to those obtained from the torsion bar mixture testing and analyzed to determine the model's ability to accurately estimate the torsion bar mixture stiffness.

Once it was determined that the Hirsch model could accurately forward-calculate mixture stiffness, a Microsoft Excel® spreadsheet was used to iteratively solve for the binder stiffness using mixture stiffness values measured using the torsion bar test procedure. Backcalculations were done for G^*_{binder} at each of the temperature-frequency combinations tested during the torsion bar test so that master curves of the backcalculated binder data could be created. The same VMA and VFA values as before were used for this process so that replicate test results could be obtained. A complete example of the backcalculation procedure is included in Appendix B.

Master Curves

To obtain G^*_{binder} values at the temperatures and frequencies necessary for accurately estimating the true and PG binder grades from the backcalculated binder stiffness results it was necessary to construct master curves. Master curves help define both time dependency (the location and shape of the master curve) and temperature dependency (shift factors) of a material and allow for determination of stiffness properties at temperature and frequencies that are not easily tested in a laboratory setting. Figure 6 shows an example of a master curve for complex shear modulus, G^*_{binder}.

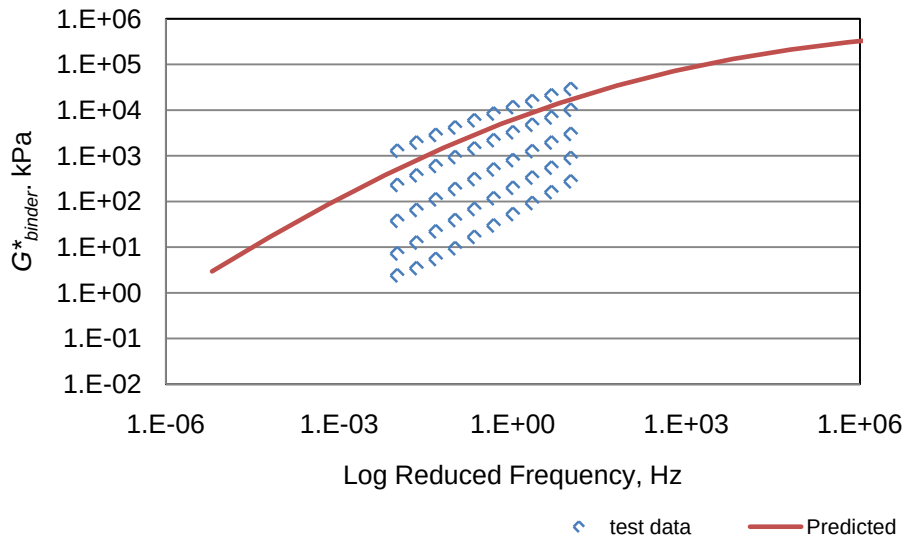

Figure 6 Example Isotherm and Master Curve Plot for G*,kPa

Many methods have been suggested for the creation of master curves using modulus verses frequency data. These range from simple manual shifting of the isotherms (plots of some parameter at different temperatures) to more complex models. For this project, the model developed by Christensen and Anderson (CA) during SHRP A-002A was chosen for constructing master curves of the tested and backcalculated G^*_{binder} data. It is shown below in Equation 12.

$$G^*_{binder}(\omega) = G_g\left[1+\left(\frac{\omega_0}{\omega}\right)^{\frac{\log 2}{R}}\right]^{\frac{-R}{\log 2}} \quad (12)$$

Where:

G_g = glassy modulus, typically 1GPa;

ω_o = crossover frequency, rad/s; and

R = rheological index.

The shift factors used to manipulate the *G** isotherms to a reference temperature (25°C for this project) were defined using the Williams-Landel-Ferry (WLF) equation for temperatures above the reference temperature and the Arrhenius equation for temperatures below the reference temperature. The shift factor equations are shown in Equations 13 and 14.

$$\log\left(\frac{a(T)}{a(T_r)}\right) = \frac{-C_1(T - T_r)}{(C_2 + T - T_r)} \tag{13}$$

Where:

$a(T)/a(T_r)$ = WLF shift factor relative to the reference temperature;

C_1, C_2 = empirically determined constants;

T = Selected temperature, in °C or °K; and

T_r = Refining temperature, in °C or °K.

$$\log\left(\frac{a(T)}{a(T_r)}\right) = \frac{2.303E_a}{R\left(\frac{1}{T} - \frac{1}{T_r}\right)} \tag{14}$$

Where:

$a(T)/a(T_r)$ = Arrhennius shift factor relative to the reference temperature;

E_a = Activation energy for flow below Tr; and

R = Ideal gas constant = 8.34 J/mol -°K.

The phase angle, δ, was determined from the master curves relative to frequency using Equation 15 (*28*).

$$\delta(\omega) = \frac{90}{\left[1 + \left(\frac{\omega}{\omega_0}\right)^{\frac{\log 2}{R}}\right]} \quad (15)$$

A master curve model developed by Rowe and Sharrock and shown in equation 16 was chosen for creating master curves for mixture stiffness results.

$$\log E^*_{mix} = \delta + \frac{\alpha}{\left[1 + \lambda e^{(\beta + \gamma(\log \omega))}\right]^{\frac{1}{\lambda}}} \quad (16)$$

Where:

δ = Lower asymptote;

$\delta+\alpha$ = Upper asymptote;

$-(\beta/\gamma)$ = Inflection point/frequency;

ω = Reduced Frequency; and

λ = Constant.

During the development of this model, the researchers evaluated conventional forms of the shift factor equations including WLF, Arrhenius, and polynomial versions. They assessed the effectiveness of each model in determining the shift factors needed for master curve creation. Using a heavily modified SBS asphalt binder, it was shown that while the above-mentioned shift factors provide a reasonable fit for the data, some deviations do occur. The WLF shift factors began to deviate at colder temperatures while the Arrhenius factors had issues at the extremes and the intermediate points of the master curves. It was theorized based on previous research that a modified version of the WLF relationship was a better fit. The modified function introduced the parameter

T_d as a way of separating the data above and below the glass transition temperature. At temperatures above the glass transition temperature, the relationship behaved identically to the WLF equation. Below the glass-transition temperature, the log a_T did not increase as rapidly as the WLF values, thus introducing an inflection point in the master curve, changing its shape from hyperbolic to sigmoidal. The modified WLF equation, or Kaeble shift factor, is shown in Equation 17.

$$\log a_T = -C_1\left(\frac{T - T_d}{C_2 + |T - T_d|} - \frac{T_r - T_d}{C_2 + |T_r - T_d|}\right) \quad (17)$$

Where:

C_1, C_2 = empirically determined constants

T = Selected temperature, in °C or °K;

T_r = Reference temperature, in °C or °K;

T_d = Defining temperature, in °C or °K.

Use of the generalized logistic model in Equation 16 combined with the modified Kaeble shift factors should provide a better fit for asphalt mixture data than the CA model. A benefit of this relationship is the use of a single shift factor relationship for temperatures above and below the glass transition temperature *(29)*.

BINDER TEST RESULTS

This chapter presents the results from the testing of the virgin and recovered RAP binders. The results shown include Superpave performance grades (PG), frequency sweep tests, and master curves created using the CA model.

Virgin Binder Results

The virgin binders were tested according to AASHTO M320-05 to determine their PG and true-grade critical high, intermediate, and low-temperatures. Table 9 shows the results of the PG classification testing from a singular test. As can be seen, both virgin binders meet the requirements for the designated PG grade.

TABLE 9 Virgin Binder Critical Temperatures, °C

	T_{crit}, °C					
Binder	**High**	**Int.**	**Low - S**	**Low - m**	**True-Grade**	**PG Grade**
PG 64-22	70.2	23.9	-24.3	-23.2	70.2 - 23.2	70 - 22
PG 76-22	78.6	21.6	-24.9	-24.1	78.6 - 24.1	76 - 22

Binder master curves at a standard reference temperature of 25°C were created from the frequency sweep isotherms using the CA model (shown in Equation 12) for both virgin binders. Figure 7 shows the G^*_{binder} master curves for the virgin binders.

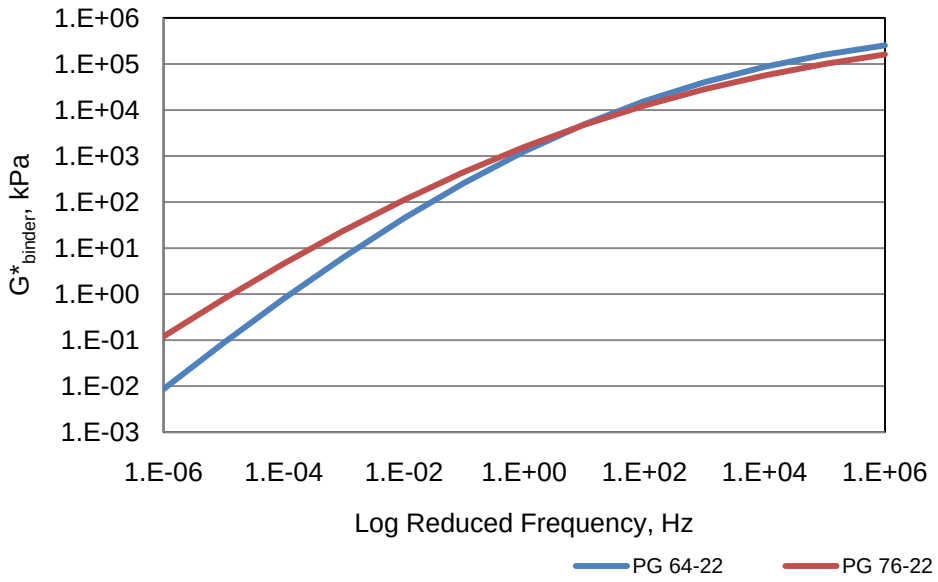

Figure 7 Virgin Binder Master Curves @ 25°C

RAP Binder Results

Table 10 shows the PG and critical temperatures for the asphalt binders recovered from the five RAP materials. This testing was performed in the same manner as the virgin binders with the exception of the original DSR, which was omitted due to the aged condition of the recovered binders. Duplicate tests were done for the recovered RAP binders, as they tend to be more variable than virgin binders.

TABLE 10 Recovered RAP Binder Critical Temperatures, °C

		T_{crit}, °C					
RAP	**Replicate**	**High**	**Int.**	**Low - S**	**Low - m**	**True-Grade**	**PG Grade**
1	1	99.0	39.7	-15.4	-9.5	99.0 -9.5	94 - 4
	2	97.8	38.1	-15.4	-9.2	97.8 -9.2	94 - 4
2	1	92.1	31.5	-23.3	-14.3	92.1 -14.3	88 - 10
	2	91.2	30.8	-22.3	-13.3	91.2 -13.3	88 - 10
3	1	95.7	32.1	-18.5	-13.0	95.7 -13.0	94 - 10
	2	94.2	32.2	-33.1	-11.3	94.2 -11.3	94 - 10
4	1	88.4	29.1	-19.1	-16.2	88.4 -16.2	88 - 16
	2	88.2	29.8	-19.0	-16.0	88.2 -16.0	88 - 16
5	1	85.7	26.7	-25.3	-15.8	85.7 -15.8	82 - 10
	2	85.6	25.2	-24.1	-15.3	85.6 -15.3	82 - 10

The high true grade temperatures of the recovered RAP binders ranged from 85.6 to 99.0°C. The low true-grade temperatures ranged from -9.2 to -16.1°C. The high-temperature grades of the recovered RAP binders match expectations for RAP sources in Alabama as do the low-temperature grades. The intermediate grades ranged from 25.2 to 39.7°C and were considered reasonable based on the high and low-temperature values for the individual binders. Figure 8 shows the CA master curves for the RAP

binders. Figure 9 shows a summary of the master curves for all seven binders that were tested as part of this study.

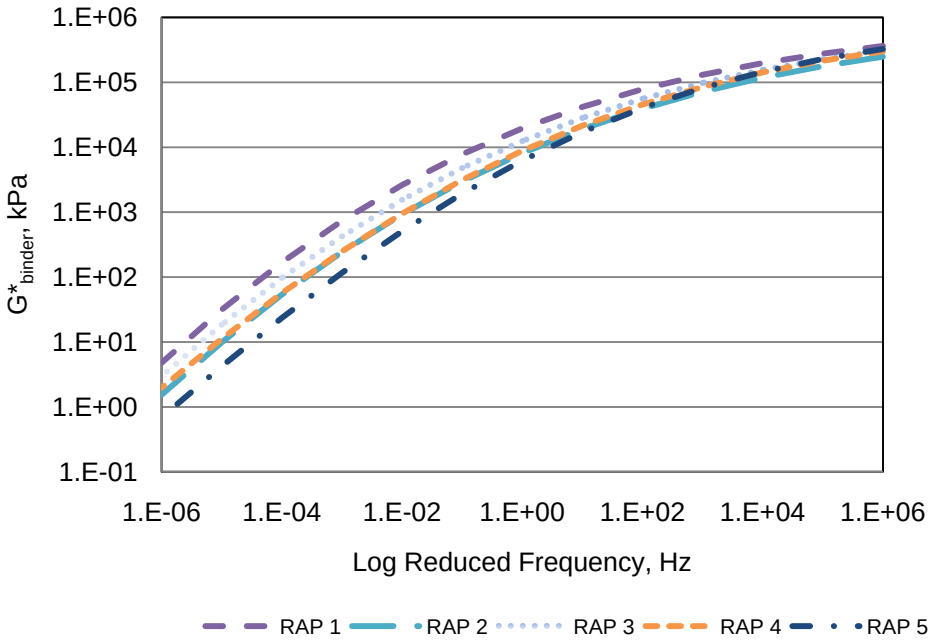

Figure 8 Recovered Binder Master Curves @ 25°C

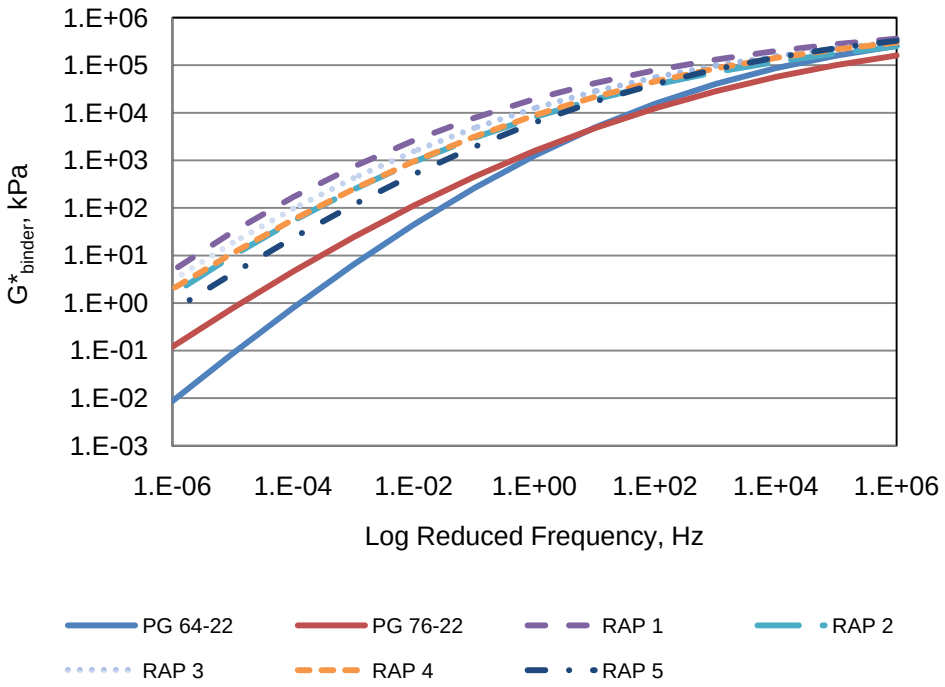

Figure 9 Master Curves for all Binders @ 25°C

As expected based on the PG grades, the RAP binder master curves are stiffer than the virgin binder master curves. RAP 1 is the stiffest binder at high-temperatures while RAP 5 is the least stiff. As the temperature decreases, the differences between the stiffnesses of the seven binders are reduced. This can be seen in the master curves, with RAP 1 and RAP 5 converging as frequency increases. RAP 2, RAP 3, and RAP 4 are very similar in their stiffness properties, which again is reflected in the master curves.

TORSION BAR STIFFNESS TEST RESULTS

In this chapter, the results obtained from torsion bar testing of the virgin and 100% RAP materials are presented and analyzed. The goal of this portion of the study was to determine if the torsion bar procedure produced mixture stiffness data of suitable

quality. The factors considered included repeatability, data trends, and suitability for creating the master curves needed for backcalculation.

Virgin Torsion Bars

For ease of reference in this and later sections, the torsion bar specimens made with aggregate that was split over the #4 sieve will be referred to as -4 while the specimens made with aggregate that was split over the #8 sieve will be referred to as -8. Figures 10 and 11 show the G^*_{mix} and δ_{mix} results at 20°C for the virgin binders. The results shown are the average of four replicate test specimens. Error bars showing the standard deviation of the test results are included to show the variability within each set of replicate tests.

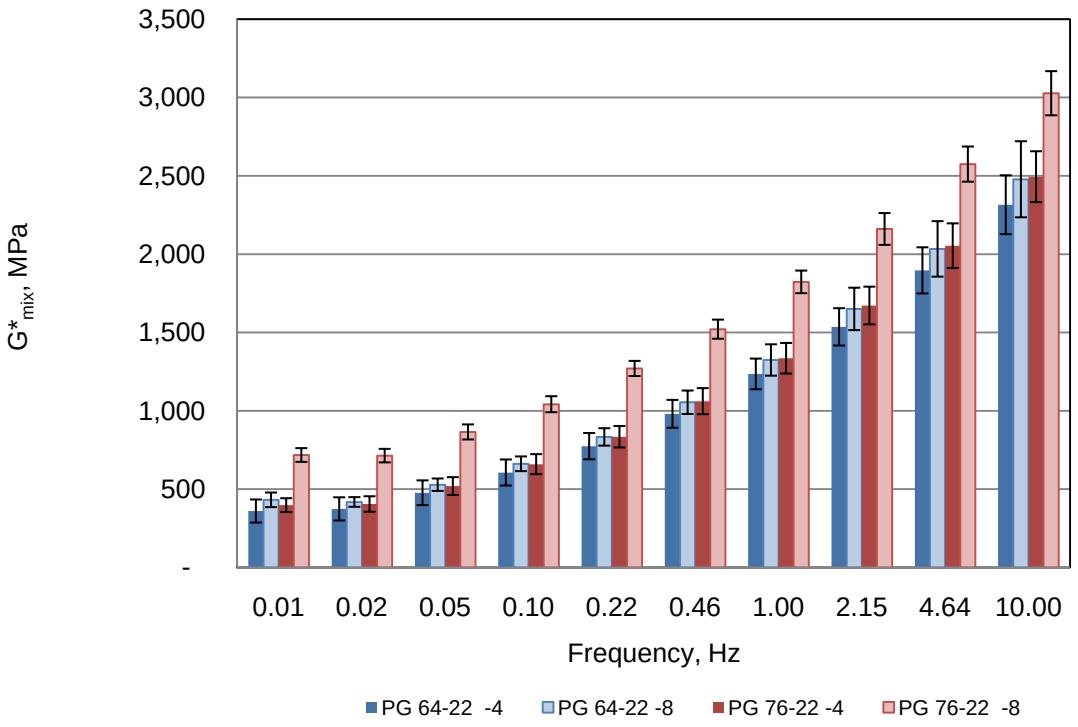

Figure 10 Virgin Torsion G^*_{mix} Results @ 20°C

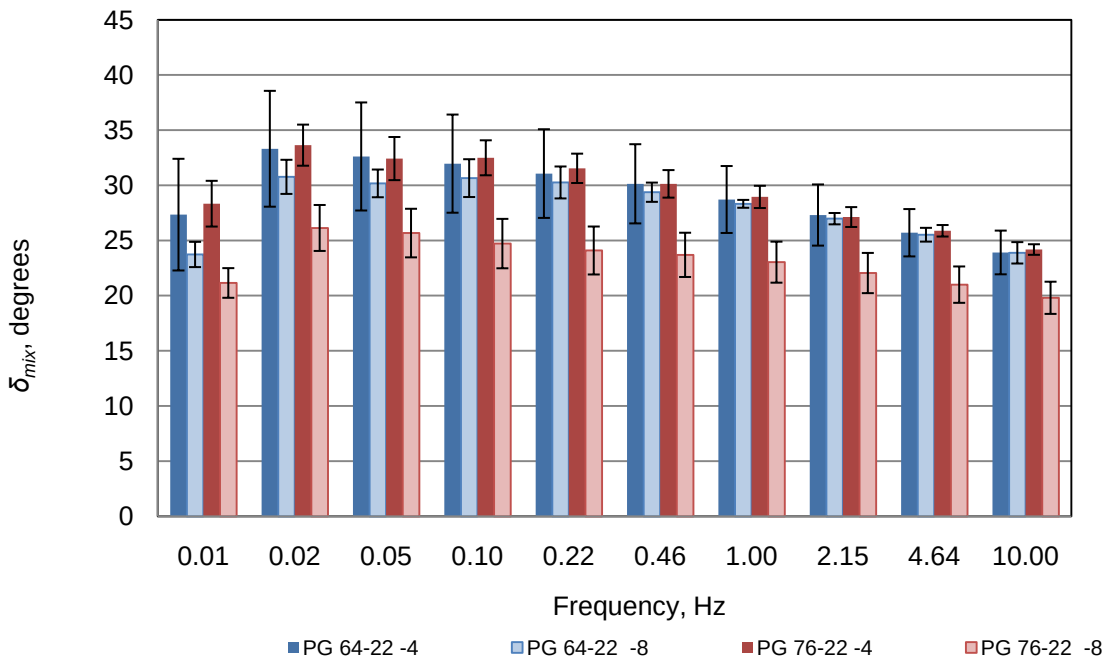

Figure 11 Virgin Torsion δ_{mix} Results @ 20°C

Trends for G^*_{mix} and δ_{mix} at the other test temperatures were similar to the results shown. Complete torsion bar results for these mixes can be found in Appendix C.

The torsion bar results for the virgin materials followed the expected trends for mixture stiffness testing using other test methods. The G^*_{mix} values increase with increasing frequency and decrease with increasing temperature. The change in stiffness with increasing frequency as more pronounced at lower temperatures, with an almost 500% increase in G^*_{mix} between the 0.01 and 10 Hz frequencies at 20°C. At 60°C, the G^*_{mix} values are significantly lower at all frequencies and do not increase as much from 0.01 to 10 Hz. At warmer temperatures and frequencies where the binder is

softer, the aggregate structure begins to play more of a role in the stiffness properties of the mixture, and differences in binder stiffness may become less pronounced.

For both virgin binders, the -8 G^*_{mix} values were higher than the -4 G^*_{mix} values. Of the four datasets, the PG 76-22 test specimens made with -8 aggregate had the highest G^*_{mix} values. The PG 76-22 test specimens made with -4 aggregate had much lower G^*_{mix} values than the -8 specimens, and in some cases were less stiff than the PG 64-22 test specimens made with -4 aggregate. The PG 64-22 virgin binder test specimens made with both the -4 and -8 aggregate generally had lower G^*_{mix} than the PG 76-22 test specimens, although in a few instances they were slightly higher than the PG 76-22 -4 values.

The δ_{mix} results for the virgin torsion bars also matched expected behavior for asphalt mixture testing. The δ_{mix} values decrease with increasing frequency for the 20°C tests. This is typical behavior seen in asphalt binder testing (phase angle decreases as the binder stiffness increases, indicating that the binder is approaching an elastic state) and is expected given the increased role of the asphalt binder in the mix at the colder temperatures. The δ_{mix} appear to plateau and change very little with increasing frequency at 30°C. At 40°C and above, the δ_{mix} plateau at the lower frequencies, then increase with increasing frequency, indicating the increased role of the aggregate as the asphalt binder softens at high-temperatures.

Differences in δ_{mix} between the datasets are less pronounced than the differences in G^*_{mix}. Mix tests tend to be less sensitive to phase angle than binder tests. The PG 76-22 test specimens made with -8 aggregate had the lowest δ_{mix}, which

was expected given that this dataset had the highest G^*_{mix} and also because the PG 76-22 is a polymer modified binder. Both of these conditions lead to reduced phase angles. The PG 76-22 made with the -4 aggregate did not follow the expected trends at lower temperatures and had δ_{mix} that were higher than the PG 64-22 datasets. At 50 and 60°C, the PG 76-22 made with -4 aggregates had δ_{mix} values that were lower than the PG 64-22 datasets, better matching expected behavior. The PG 64-22 -4 and -8 datasets had δ_{mix} values that were typically higher than the PG 76-22 test results. For the PG 64-22 test specimens, the different aggregate sizes didn't show large differences in δ_{mix}. Overall, the δ_{mix} values for the virgin binder tests had a very limited range. Most δ_{mix} values, regardless of testing conditions, fell between 20 and 35°.

Figures 12 and 13 show the coefficient of variation (COV) values at 10Hz for both G^*_{mix} and δ_{mix}.

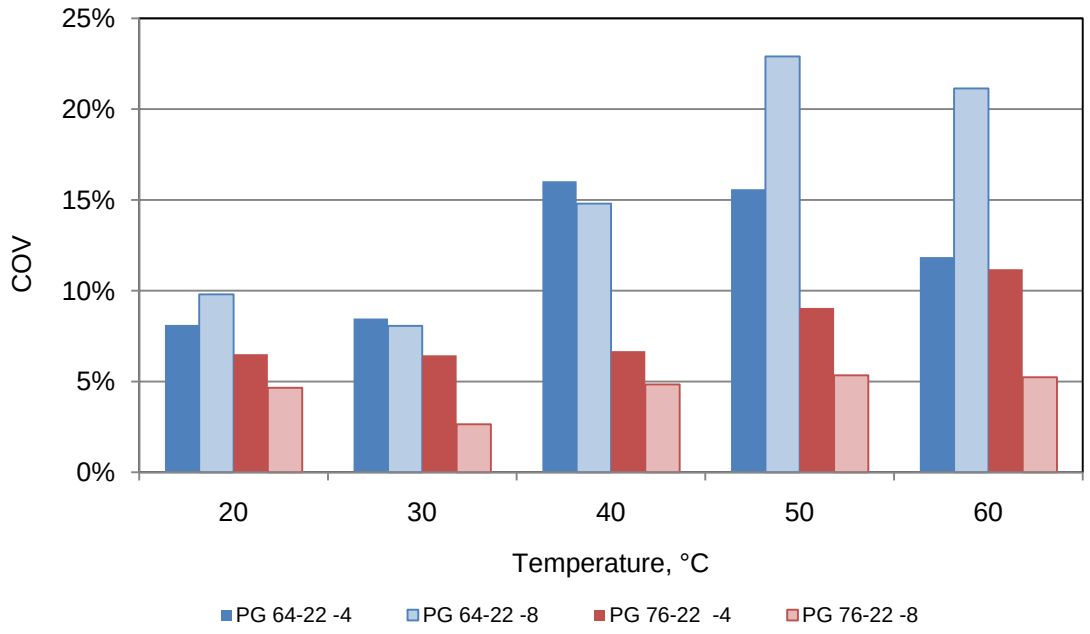

Figure 12 COV at 10Hz for all Test Temperatures – Virgin Binder Torsion Bars G^*_{mix}

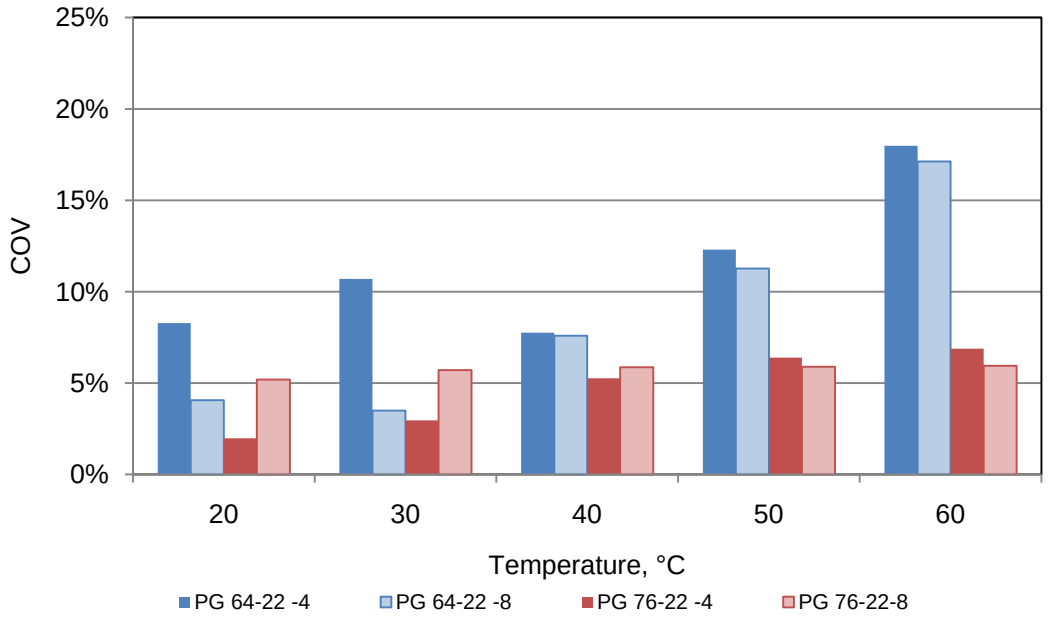

Figure 13 COV at 10Hz for all Test Temperatures – Virgin Binder Torsion Bars δ_{mix}

At the time the testing was conducted, there was no official recommendation for acceptable variability between replicate samples. However, the ASTM D7552-09 test method, published after testing was completed, requires that COV values for replicate data at the 10Hz frequency level for all temperatures be less than 15%. As can be seen from Figure 12, a few of the test results at high-temperature/low frequency conditions had COV values above 20% but were in all cases less than 25% and in most cases met the 15% requirement. There also appears to be a trend of increasing COV with increasing temperature (for all but the PG 76-22 -8 specimens). The softer PG 64-22 torsion bar specimens have higher COV than the stiffer PG 76-22 specimens. Although ASTM D7552 does not recommend a COV level for δ_{mix}, it can be seen from Figure 13 that the δ_{mix} results at 10Hz are all below 15% COV, with the exception of the PG 64-22 results at 60°C. Again, there appears to be less variability in the data at the colder temperatures.

The quality of the data for creating master curves was evaluated using Black Space diagrams. Plots of δ_{mix} verses the log (G^*_{mix}) were plotted for the average results at all temperatures and a polynomial trend-line fitted to the data. The smoothness of the data points indicates whether the data is of acceptable quality. Typically values of R^2 less than 0.90 are rejected *(30)*. Figures 14 and 15 show the Black Space diagrams for the virgin binder torsion bar results. The data shown is an average of the 4 replicates for each material.

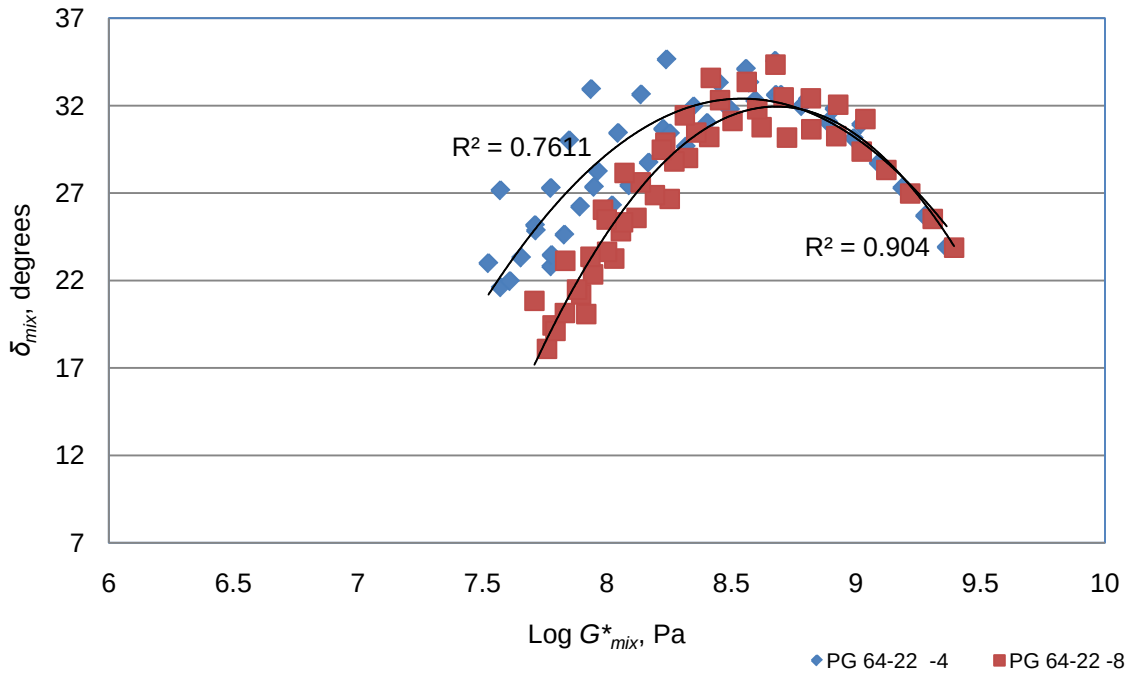

Figure 14 Black Space Diagram for PG 64-22 Virgin Torsion Results

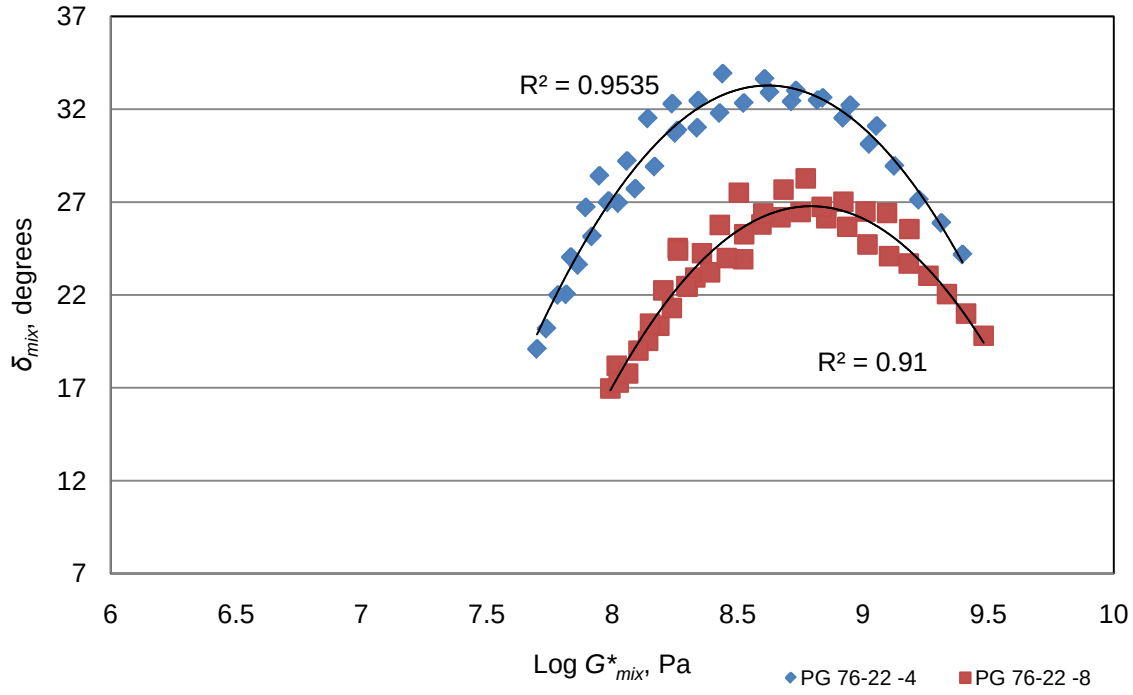

Figure 15: Black Space Diagram for PG 76-22 Virgin Torsion Results

For the PG 64-22 materials, the R^2 value for the -4 mix did not meet the smoothness requirement. The PG 64-22 -8 mix did have an acceptable R^2 (0.92). The low R^2 for the PG 64-22 -4 mixes may be due to increased variability in the lower frequencies of the 50 and 60°C data (and removal of these data sets would have improved the R^2 value for this mix to 0.90, although no data was actually removed from the analysis at this time). Both sets of PG 76-22 virgin mixes had adequate R^2 values. Overall, excepting a few issues with the high-temperature tests, the DSR torsion bar tests on the virgin mixes provided reasonable results that could be used to create master curves.

For the mixture tests, master curves were created using the generalized logistic equation shown in Equation 16. Figure 16 shows a comparison of the four sets of virgin torsion bar master curves while Figure 17 shows a comparison of the torsion bar and binder master curves. Again, the results shown are the average values for four replicates.

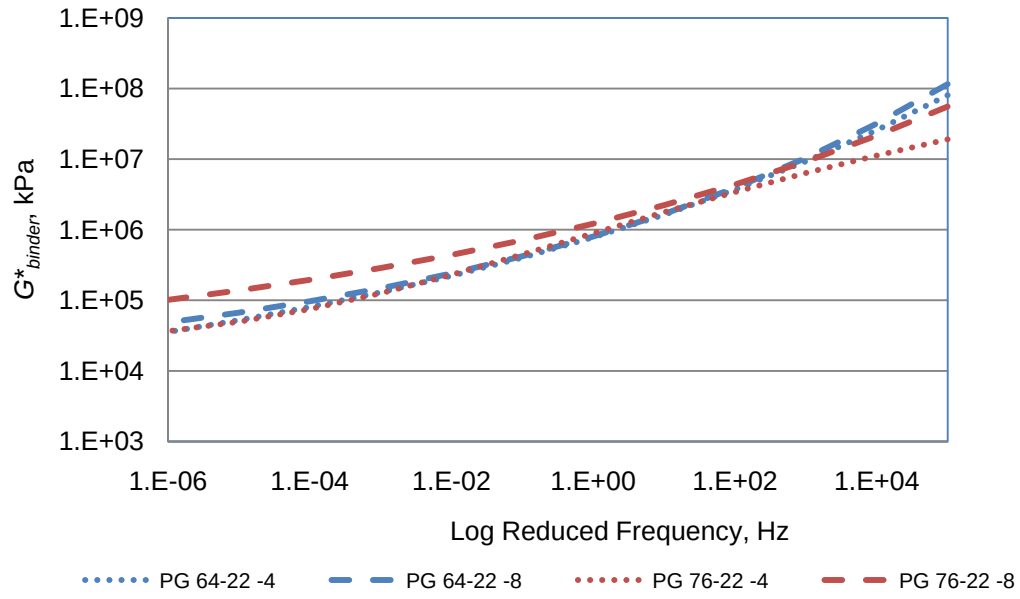

Figure 16 Virgin Torsion Bar Master Curve – PG 64-22 -4

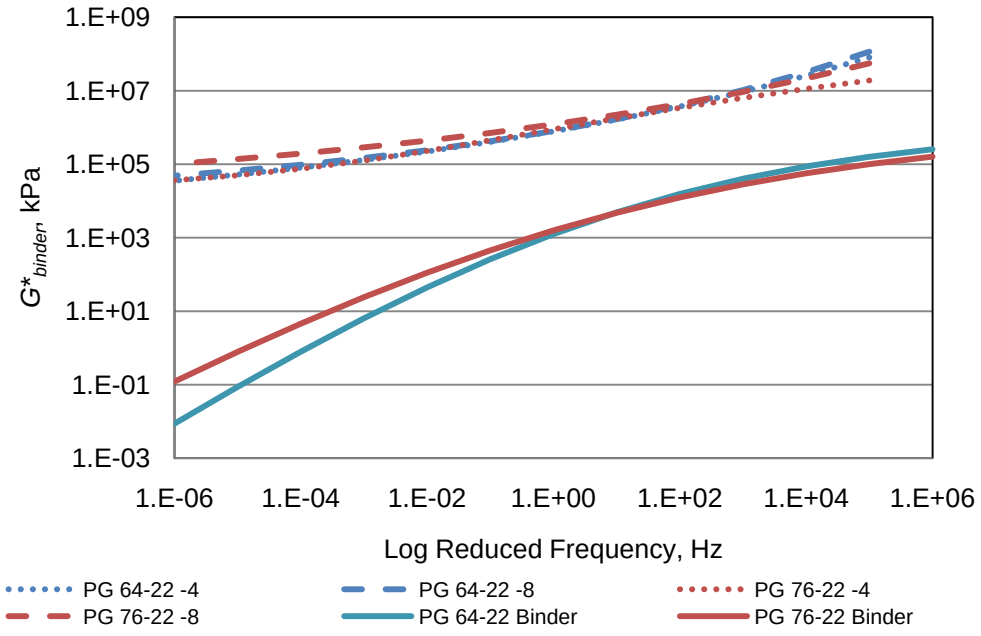

Figure 17 Virgin G^*_{mix} and G^*_{binder} Master Curves @ 25°C

The master curves show that, as expected, the torsion bar stiffness results were stiffer than the binder stiffness values. For the torsion bars, the PG 76-22 -8 specimens appear to be the stiffest at lower frequencies while the other three mixtures have similar stiffnesses. At the higher frequencies, the PG 76-22 -4 specimens are the least stiff while the other combinations have similar stiffness values. Based on these results, it does not appear that there is a great difference in stiffness values between the binders or aggregates except at the extremes of high or low stiffness.

Statistical analyses were performed on the virgin torsion bar results to compare the effects of aggregate size and binder type on the G^*_{mix} values. The aggregate size comparison was made to determine if the different aggregate sizes affected the mixture stiffness results. The binder type comparison was to determine if the torsion bar test is sensitive enough to identify differences in mixture stiffness due to different binder types. Table 11 shows the summary of a two-sample statistical *t*-test analysis ($\alpha = 0.05$) on aggregate size for both virgin binders (H_0: $\bar{x}_{-4} = \bar{x}_{-8}$). A separate analysis was performed at each test temperature and frequency (0.1, 1.0, and 10.0 Hz) to see if aggregate size caused a significant difference in the G^*_{mix} values measured by the test results.

TABLE 11 *t*-test Analysis for Aggregate Size – p-values

		Average G^*_{mix}, kPa					
		PG 64-22			PG 76-22		
Freq.	Temp, °C	-4	-8	*p*-value	-4	-8	*p*-value
0.1Hz	20	606,000	661,725	0.288	659,200	1,042,000	0.000
	30	252,700	257,525	0.895	268,150	468,300	0.000
	40	110,498	131,410	0.253	123,550	245,600	0.000
	50	67,543	87,930	0.137	73,128	154,025	0.000
	60	40,833	62,115	0.051	50,105	106,075	0.000
1 Hz	20	1,235,250	1,324,250	0.251	1,335,500	1,822,750	0.000
	30	500,150	512,125	0.796	540,275	834,900	0.000
	40	218,475	228,400	0.634	220,150	400,025	0.000
	50	110,950	136,700	0.113	114,488	227,925	0.000
	60	59,590	85,828	0.006	68,358	141,450	0.000
10Hz	20	2,315,250	2,477,750	0.330	2,494,250	3,027,000	0.003
	30	1,050,150	1,090,500	0.543	1,134,250	1,531,250	0.000
	40	491,950	474,975	0.985	459,625	729,400	0.000
	50	225,850	261,375	0.346	219,175	389,725	0.000
	60	109,145	143,475	0.082	112,085	215,775	0.000

The p-values shown in Table 11 represent the probability of getting similar results if the null hypothesis, H_0, is true. The farther away the test statistic from the *t*-test is located on the tails of the standard normal distribution, the smaller the p-value will be. For the chosen significance level of 0.05, a p-value of greater than 0.05 will result in a failure to reject the null hypothesis. P-values less than 0.05 indicate that the results are too far apart and therefore the null hypothesis must be rejected. Based on the statistical analysis the PG 64-22 -4 G^*_{mix} results were statistically the same as the -8 G^*_{mix} results for 14 out of the 15 cases (failed to reject H_0: $\bar{x}_{-4} = \bar{x}_{-8}$). The PG 76-22 G^*_{mix} results for the two aggregate sizes were statistically different in all cases. These

results indicate that aggregate structure may have an influence on the results of the torsion bar tests.

A similar statistical analysis was done comparing the G^*_{mix} results across binder type to determine if the torsion bar test was sensitive enough to distinguish between the two virgin binders (H_0: $\bar{x}_{64} = \bar{x}_{76}$) . Table 12 shows the *p*-values for comparisons of the PG 64-22 and PG 76-22 mixes including comparisons of both aggregate sizes and when separated into -4 and -8 aggregate. Again, cells with p-values less than 0.05 indicate a statistically significant difference (rejection of H_0) between the PG 64-22 and PG 76-22 tests.

TABLE 12 *t*-test Analysis for Binder Type – p-value

		Average G^*_{mix}, kPa								
		All			-4			-8		
Freq, Hz	Temp, °C	PG 64-22	PG 76-22	*p*-value	PG 64-22	PG 76-22	*p*-value	PG 64-22	PG 76-22	*p*-value
0.1	20	633,863	850,600	0.025	606,000	659,200	0.357	661,725	1,042,000	0.000
	30	255,113	368,225	0.051	252,700	268,150	0.655	257,525	468,300	0.001
	40	120,954	184,575	0.031	110,498	123,550	0.966	131,410	245,600	0.003
	50	77,736	113,576	0.008	67,543	73,128	0.566	87,930	154,025	0.003
	60	51,474	78,090	0.004	40,833	50,105	0.241	62,115	106,075	0.003
1	20	1,279,750	1,579,125	0.020	1,235,250	1,335,500	0.207	1,324,250	1,822,750	0.000
	30	506,138	687,588	0.018	500,150	540,275	0.388	512,125	834,900	0.000
	40	223,438	310,088	0.049	218,475	220,150	0.826	228,400	400,025	0.001
	50	123,825	171,206	0.079	110,950	114,488	0.715	136,700	227,925	0.002
	60	72,709	104,904	0.069	59,590	68,358	0.249	85,828	141,450	0.002
10	20	2,396,500	2,760,625	0.020	2,315,250	2,494,250	0.209	2,477,750	3,027,000	0.017
	30	1,070,325	1,332,750	0.012	1,050,150	1,134,250	0.204	1,090,500	1,531,250	0.001
	40	483,463	594,513	0.064	491,950	459,625	0.722	474,975	729,400	0.003
	50	243,613	304,450	0.133	225,850	219,175	0.758	261,375	389,725	0.027
	60	126,310	163,930	0.123	109,145	112,085	0.757	143,475	215,775	0.021

The statistical analysis showed that the G^*_{mix} results could distinguish between the different binder types at 9 out of the 15 temperatures and frequencies shown when the two aggregate sizes were combined and analyzed together. When analyzing the two aggregate sizes separately, the -8 aggregate test specimens could distinguish between binder type in all cases while the -4 aggregate size could not.

Based on the quality of the data shown, the torsion bar test was considered to be an adequate candidate for further testing. The G^*_{mix} and δ_{mix} results measured by the test were reasonable in behavior and repeatability and seemed to be of adequate quality for the creation of master curves. The lack of ability to distinguish between the two virgin binders for one aggregate size was a concern, but since two out of the three comparisons (all aggregate and -8 aggregates) did show statistically significant differences in $G^*_{mix,}$ it was decided to continue testing for the 100% RAP mixes.

RAP Torsion Bars

Figures 18 and 19 show the G^*_{mix} and δ_{mix} results for the torsion bar samples made using the five RAP materials at 20°C. Due to time and material restrictions, it was decided to use only the -4 aggregate size for the RAP specimens. This size was chosen due to some testing issues that occurred with the -8 virgin specimens (high rate of sample breakage and difficulty getting consistent air voids) and also because this seems to be the most commonly used size for separating coarse and fine RAP materials and allowed for direct sampling at the mix plant if necessary. The results shown are the average of four replicate test specimens. Complete torsion bar results for the RAP samples can be found in Appendix C.

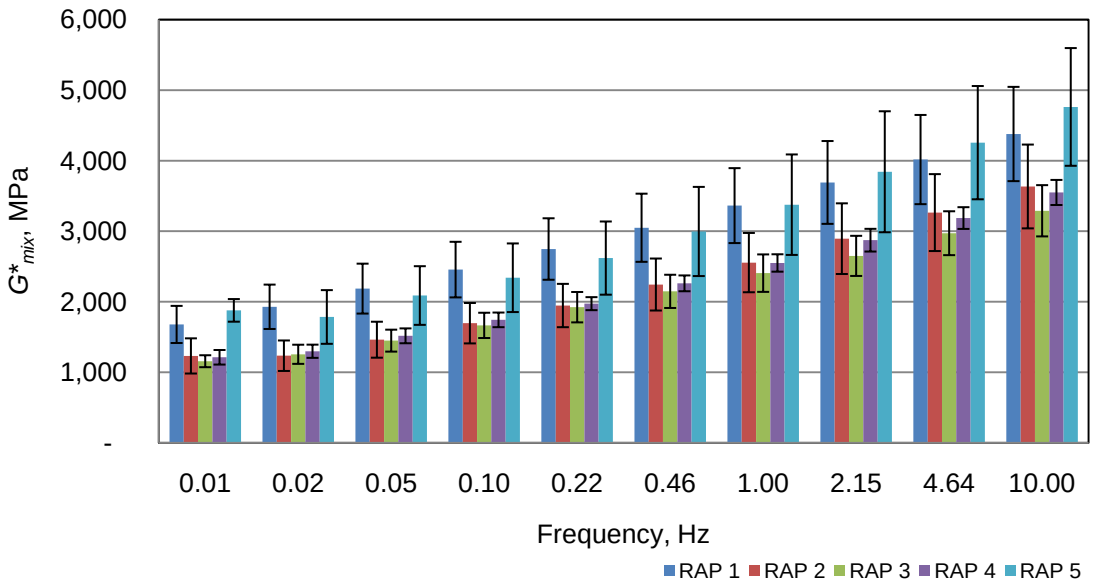

Figure 18 RAP Torsion G*$_{mix}$ Results @ 20°C

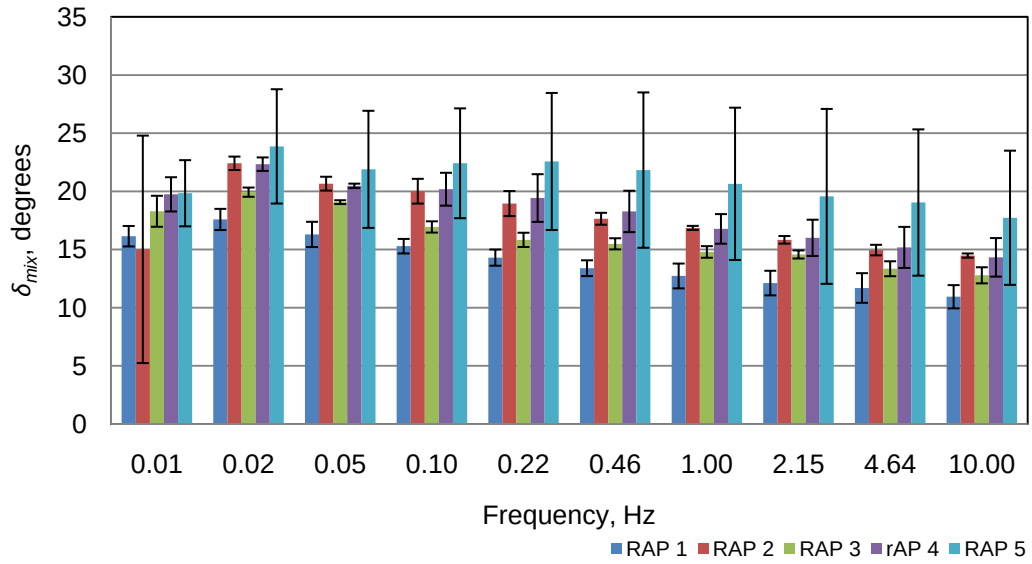

Figure 19 RAP Torsion δ$_{mix}$ Results @ 20°C

The torsion bar test results for the RAP materials followed the same trends as the virgin torsion bar tests. The G^*_{mix} values increased with increasing frequency and decreased with increasing temperature. Differences in stiffness between RAPs are

more apparent at colder temperatures where the asphalt binder influence on stiffness is strongest. As the test temperature increased and test frequency decreased, the differences in G^*_{mix} values decreased. RAPs 1 and 5 had higher G^*_{mix} values at all temperatures and frequencies than the other RAP sources. RAPs 2, 3, and 4 all had much lower G^*_{mix} values. RAP 3 appears to have less sensitivity to changes in temperature or frequency than the other RAPs, and therefore had higher G^*_{mix} than RAPs 2 and 4 as the test temperature increases.

The δ_{mix} decreased with increasing frequency at the lower temperature, appeared to plateau around 50°C, and then decreased with increasing frequency. Figures 20 and 21 show the COV values for the RAP specimens at 10Hz. RAPs 1 and 5 had the lowest overall δ_{mix} compared to the other RAP sources, followed by RAP 3. RAPs 2 and 4 had the highest δ_{mix}.

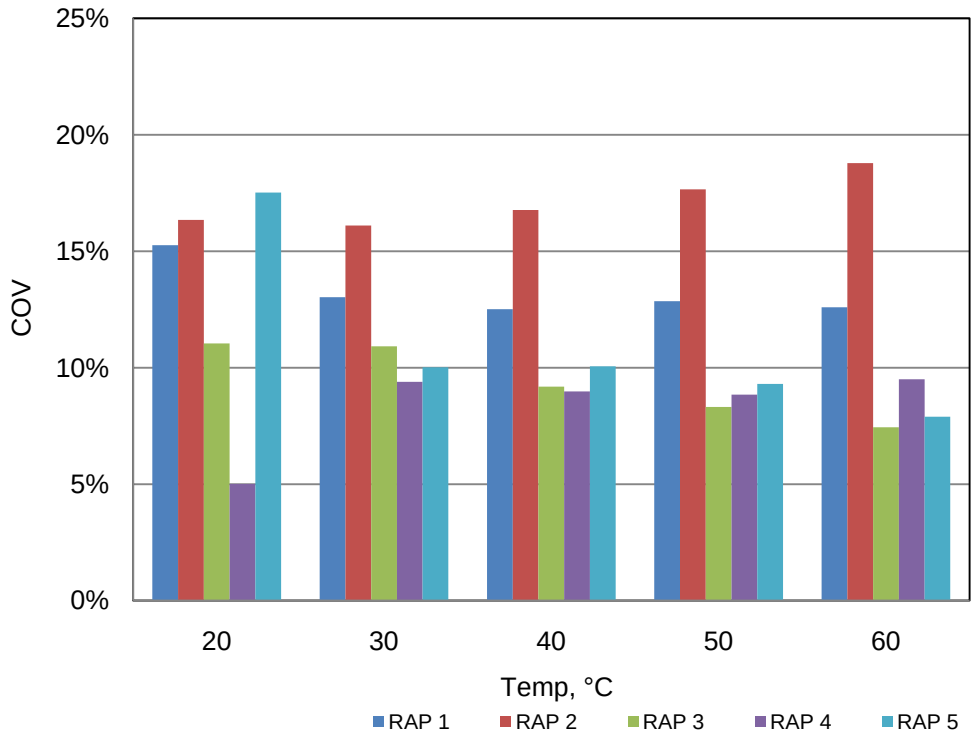

Figure 20 COV at 10Hz for all Test Temperatures – RAP Torsion Bars G^*_{mix}

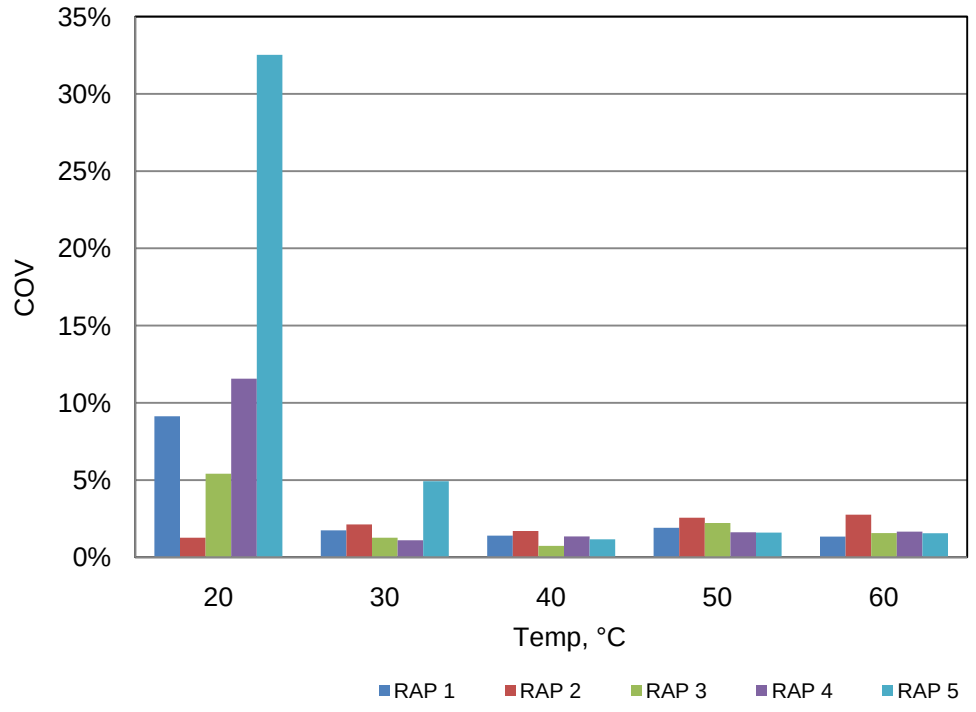

Figure 21 COV at 10Hz for all Test Temperatures – RAP Torsion Bars δ_{mix}

Like the virgin binder torsion bars, the RAP torsion bar specimens for the most part had acceptable COV values. RAP 2 had COV values for G^*_{mix} that were slightly higher than the 15% limit. RAP 5 had G^*_{mix} and δ_{mix} COV that were high at 20°C. The trend of increasing COV with decreasing binder stiffness as seen in the specimens with virgin binders was not apparent with the RAP specimens. This may be due to the higher stiffness of the RAP binders at the test temperatures that reduced the influence of the aggregate structure.

When used to make Black Space diagrams, all the RAP torsion results had R^2 values greater than 0.90. This indicates that the G^*_{mix} results from the torsion bar tests on RAP specimens provided data that was of acceptable quality for the creation of master curves. Figure 22 shows the master curves created from the RAP torsion bar G^*_{mix} results. Figure 23 shows the RAP G^*_{mix} master curves compared to the master curves created from the G^*_{binder} frequency sweeps on the recovered RAP binders. The values shown are averages of 4 replicate test specimens for each RAP source.

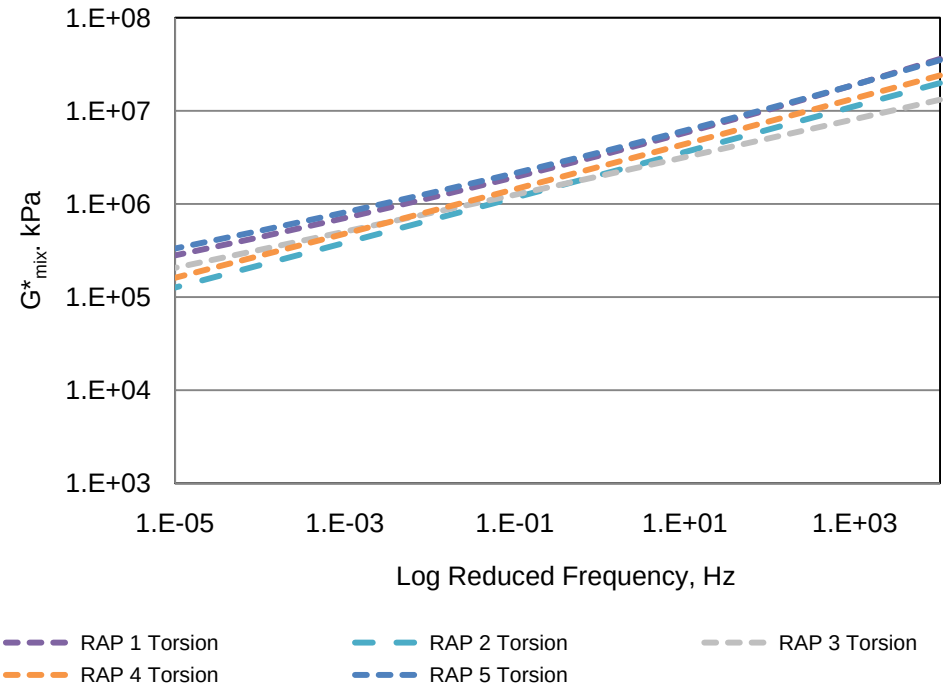

Figure 22 RAP Torsion Bar Master Curves @ 25°C

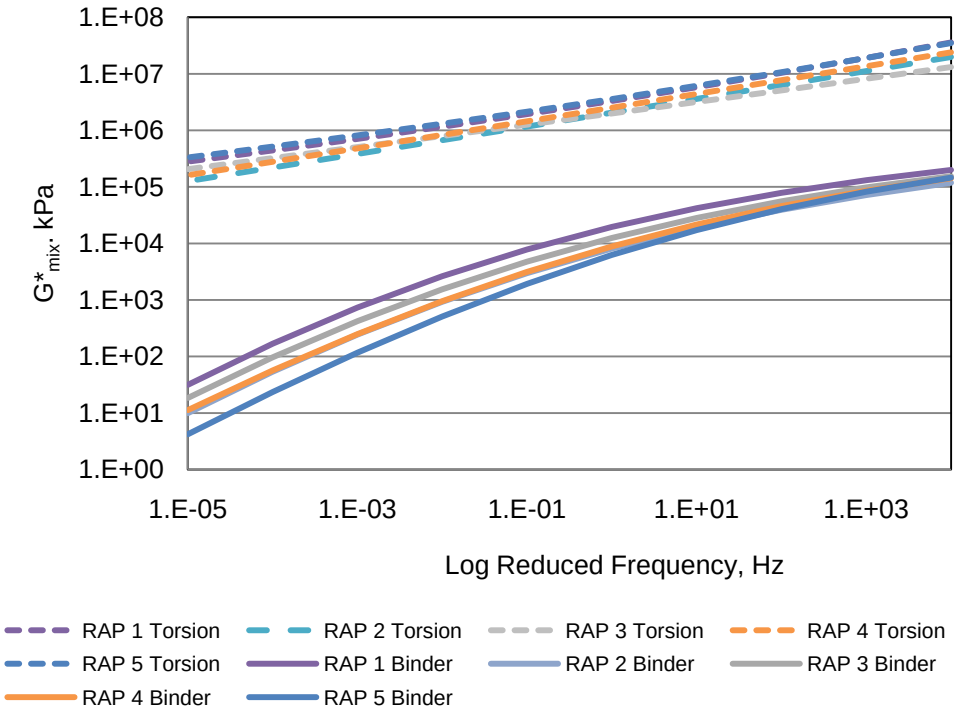

Figure 23 Comparison of RAP Binder and Torsion Bar Master Curves @ 25°C

The G^*_{mix} master curves ranked the RAP sources slightly differently than the G^*_{binder} master curves. For the binders, RAP 1 was the stiffest material while RAP 5 was the softest. RAP 2 and RAP 4 were very similar according to the binder master curves. RAP 3 was the second stiffest after RAP 1. For the mixes, RAPs 1 and 5 appeared to have very similar stiffness values while RAP 2 was the least stiff at high-temperature, low frequencies. RAPs 3 and 4 were similar at the high-temperature, low stiffness region, but diverged as stiffness increased. There are several possible reasons for these differences, mainly the effect of aggregates and air voids on the stiffness properties of the mixture test specimens. There may also be some differences in binder properties between the recovered RAP binders that have been through the extraction/recovery process and the actual RAP binder in the RAP mixtures.

A statistical general linear model Analysis of Variance (ANOVA) test was performed on the 100% RAP G^*_{mix} results to determine if there was any statistical difference between the RAP stiffness values for the different RAP sources (H_0: $\bar{x}_1 = \bar{x}_2 = \bar{x}_3 = \bar{x}_4 = \bar{x}_5$). In the cases where there were statistical differences found, Tukey-Kramer comparisons ($\alpha = 0.05$) were performed on the replicate data for the RAP torsion bars to determine which of the datasets differed from the others. The analysis was done for each temperature and at three frequencies (0.1, 1.0, and 10.0 Hz). The results of the ANOVA analysis are summarized in Table 13. For each row in the table, RAP sources with the same letter indicate that the average G^*_{mix} values were found to be statistically the same. RAP sources with different letters were found to be statistically different. RAP sources with two letters had average G^*_{mix} values that were

statistically the same as two other RAP sources that were not statistically the same. For example, at 50°C and 0.1Hz, the statistical analysis found the average G^*_{mix} values for RAPs 1 and 5 to be statistically the same. The average G^*_{mix} values for RAP 5 were also statistically the same as for RAP 3, although RAP 3 was not a statistical match for RAP 1. The average G^*_{mix} values for RAPs 2 and 4 were statistically the same as each other and different from RAPs 1, 3, and 5.

TABLE 13 ANOVA Analysis of RAP Source

		RAP				
Freq	**Temp, °C**	**1**	**2**	**3**	**4**	**5**
0.1Hz	20	A	B	B	B	AB
	30	A	B	B	B	A
	40	A	C	B	BC	A
	50	A	C	B	C	AB
	60	B	C	B	C	A
1 Hz	20	A	A	A	A	A
	30	A	B	B	B	A
	40	A	B	B	B	A
	50	A	C	B	C	A
	60	A	B	A	B	A
10Hz	20	AB	AB	B	AB	A
	30	AB	C	C	BC	A
	40	A	B	B	B	A
	50	A	B	B	B	A
	60	A	C	B	C	A

Per the statistical analysis, the average G^*_{mix} values for RAPs 1 and 5 were statistically the same in most cases. The average G^*_{mix} values for RAPs 2, 3, and 4 were also statistically the same at lower temperatures, while differing at higher temperatures. When the virgin binder torsion bar results were compared to the torsion bar results using a similar analysis, the Tukey groupings placed them in a separate

group from the RAP torsion bar results in all cases. This indicated that the torsion bar results could distinguish between the virgin mix specimens and the much stiffer RAP specimens.

Summary

The following observations were made at the conclusion of the torsion bar mixture stiffness testing:

1. The mixture stiffness data obtained from the torsion bar tests resembled that of other mixture stiffness tests in both behavior and quality.
2. The mixture stiffness data obtained for both the virgin binders and 100% RAP test specimens met the data quality requirements for the construction of master curves according to the use of Black Space diagrams. The only exception was the PG 64-22 binder which had issues with testing variability at the high-temperature and low-frequency test parameters. It appears from this dataset that the torsion bar procedure may not be suited for mixtures with very low stiffness values. The stiffer PG 76-22 and 100% RAP mixes did not have the same problem, nor did the PG 64-22 mixes at lower temperatures or higher frequencies.
3. While the backcalculated torsion bar G^*_{mix} values could not distinguish between the two virgin binders at one of the aggregate sizes, they could distinguish between the 100% RAP sources in several instances. The torsion bar G^*_{mix} values were also able to group the results of the virgin binder specimens as being statistically different than the 100% RAP specimens. It was unclear how

much influence the effects of aggregate structure and air voids have on the mixture stiffness values, but analysis of the -4 and -8 aggregate sizes for the virgin binders indicates that aggregate structure may be an important factor. This was also indicated by the different rankings of the RAP torsion bar results and the recovered RAP binder results.

4. Even though it was unclear how well the mixture stiffness results could distinguish between the materials in the torsion specimens, the ultimate goal of this research was the estimation of the properties of the asphalt binder in the mixes. The Hirsch model chosen for this calculation takes the volumetric factors into account; therefore the estimated binder properties may not be as affected by the aggregate structure as the mixture stiffness values.

BACKCALCULATION RESULTS

Once a complete set of mixture stiffness data had been obtained for the virgin and 100% RAP test specimens, the next step in the study evaluated the ability of the Hirsch model to accurately predict G^*_{binder}. The first evaluation performed was to determine the effectiveness of the Hirsch model as written for calculating G^*_{mix} based on tested G^*_{binder}. Theoretically, if the model can accurately forward-calculate $G^*_{mix,}$ it should also be able to backcalculate G^*_{binder}. It was expected that the model would need to be adjusted to improve its accuracy as the original version of the model was calibrated for a different test procedure. Once a revised version of the model was developed to forward-calculate $G^*_{mix,}$ both versions of the formula were used to backcalculate a set of binder test results.

Evaluation of Hirsch Model for High and Intermediate-temperatures

In theory, if the Hirsch model can accurately estimate the G^*_{mix} based on tested G^*_{binder}, then the model might also be capable of estimating G^*_{binder} based on tested G^*_{mix} values. The Hirsch model for G* is shown in Equations 7 and 8 and is repeated below.

$$G^*_{mix} = \left[P_c \left[601{,}000\left(1 - \frac{VMA}{100}\right) + G^*_{binder}\left(\frac{VMA * VFA}{10{,}000}\right)\right] + \frac{(1 - P_c)}{\left(\frac{1 - \frac{VMA}{100}}{601{,}000} + \frac{VMA * VFA}{G^*_{binder}}\right)}\right] \quad (7)$$

Where: *VMA* = voids in mineral Aggregate, %;

VFA = voids Filled with asphalt, %;

G^*_{binder} = binder complex shear modulus, psi;

P_c = contact factor, obtained from Equation 8; and

G^*_{mix} = mix complex shear modulus, psi – obtained from torsion bar test.

$$P_c = \frac{\left(3 + \frac{VFA * G^*_{binder}}{VMA}\right)^{0.678}}{396 + \left(\frac{VFA * G^*_{binder}}{VMA}\right)^{0.678}} \quad (8)$$

The *G** version of the Hirsch model was chosen for this project because the torsion bar test method results in a measurement of complex shear modulus. The torsional sinusoidal loading used in the torsion bar procedure also more closely matched the

loading used in the SST Frequency Sweep at Constant Height test used to measure G^*_{mix} than it does the compressive loading used to measure E^*_{mix}. The original version of the model was not expected to be an exact fit for the torsion bar data G^*_{mix} results since it was calibrated for a much larger sample and a straight shear load instead of the small torsion bars subjected to a torsional twisting load. As such, the first step in evaluating the effectiveness of the model was to use the DSR data obtained from the RTFO-aged virgin binder frequency sweeps to calculate values of G^*_{mix}. The VMA and VFA values measured by the dimensional analysis of the individual torsion specimens were used to calculate replicate test results. The calculated G^*_{mix} values were then compared to the individual G^*_{mix} values measured in the previous section. The results of the comparison were used to verify the accuracy of the model shown in Equations 7 and 8 for estimating G^*_{mix} for the torsion bars. Figures 24 and 25 show the comparison of calculated and tested G^*_{mix} values using the original Hirsch G^*_{mix} model for the virgin materials. The data in these figures includes the entire set of test results for both the -4 and -8 aggregate sizes. Linear regression was performed to determine the line of best fit for the data, along with 95% confidence intervals for the results.

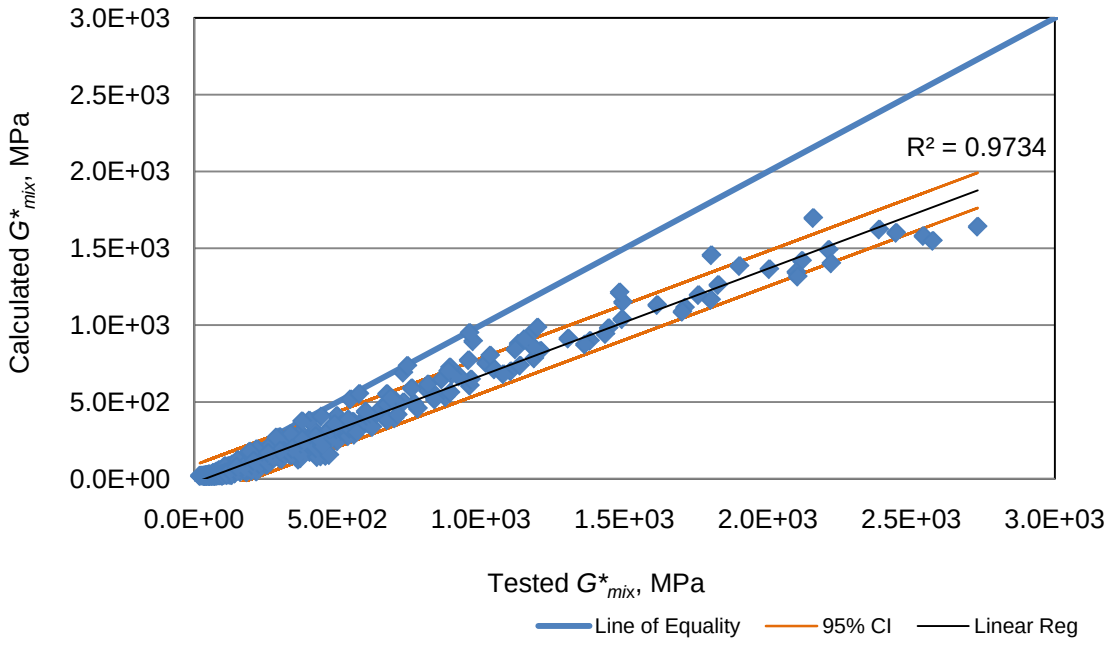

Figure 24 Comparison of Calculated vs. Tested G^*_{mix} for Virgin PG 64-22 – Original Model

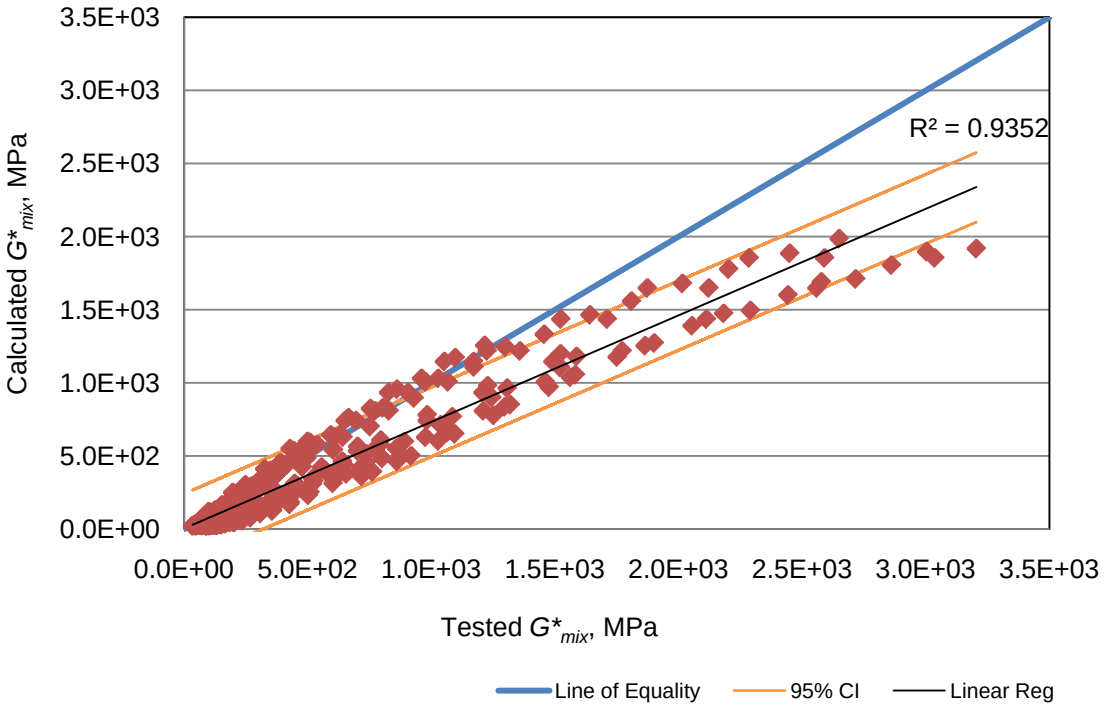

Figure 25 Comparison of Calculated vs. Tested G^*_{mix} for Virgin PG 76-22 – Original Model

The 95% confidence interval for the data was calculated using equation 18 as follows:

$$CI = \bar{x} \pm t_{n-1}\left(\frac{s}{\sqrt{n}}\right) \quad (18)$$

Where:

$\bar{x}$ = sample mean;

t_{n-1} = t-value representing n-1 degrees of freedom, 0.05 confidence level;

n= sample size;

s = sample standard deviation.

A confidence interval expresses the degree of uncertainty about the linear regression. If the formula generated by the linear regression line is used to calculate G^*_{mix} based on a tested G^*_{mix} value, the result will lie within this interval 95% of the time. The width of a confidence interval gives an indication of how uncertain the data is. The wider the interval, the more uncertain the data.

As seen in the figures, the original version of the Hirsch model almost always under-estimated G^*_{mix} when compared to actual tested data from the torsion bars. A paired -sample *t*-test (α = 0.05) analysis comparing the difference between the individual pairs of tested and calculated data showed the tested results were statistically larger than the calculated G^*_{mix} values and confirmed that the calculated results were statistically different from the line of equality.

To improve the accuracy of the calculated G^*_{mix} results, a calibration of the model was performed. In order to complete this task, the calculated G^*_{mix} values for the virgin materials were compared to the tested G^*_{mix} values and a non-linear least

squares analysis was performed to find constants for the Hirsch model that would minimize the differences between the two data sets. Only the virgin binder results were used in the calibration, as it was felt that the recovered RAP binders may not accurately represent the binder in the RAP torsion bars and could possibly skew the results. For ease of reference, the original Hirsch model will be referred to as OH while the revised Hirsch model will be referred to as RH. Table 14 shows the constants for the original Hirsch (OH) and revised Hirsch (RH) models.

TABLE 14 Revised Hirsch Model Constants

Parameter	OH	RH
P_o	3.0	18.5
P_1	0.678	0.762
P_2	396	395
E_a	601000	601000

Using the new constants, the revised Hirsch model was used to calculate G^*_{mix}. Figures 26 and 27 show the results.

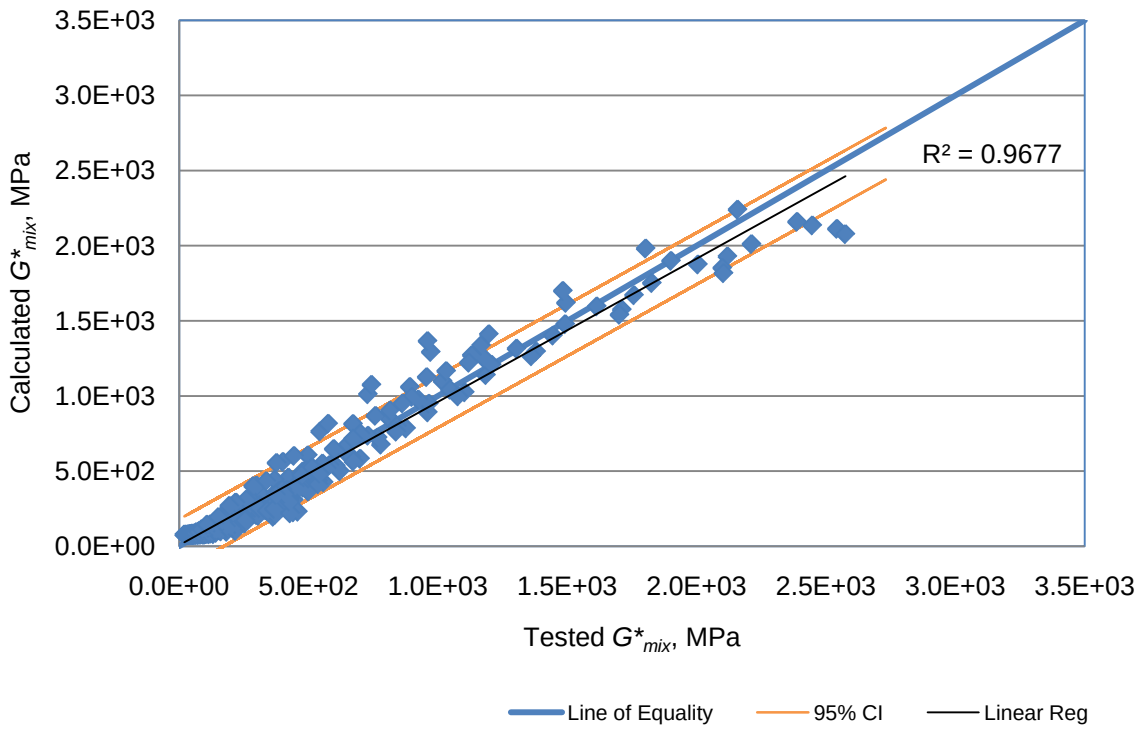

Figure 26 Comparison of Calculated vs. Tested G^*_{mix} for Virgin PG 64-22 – Revised Model

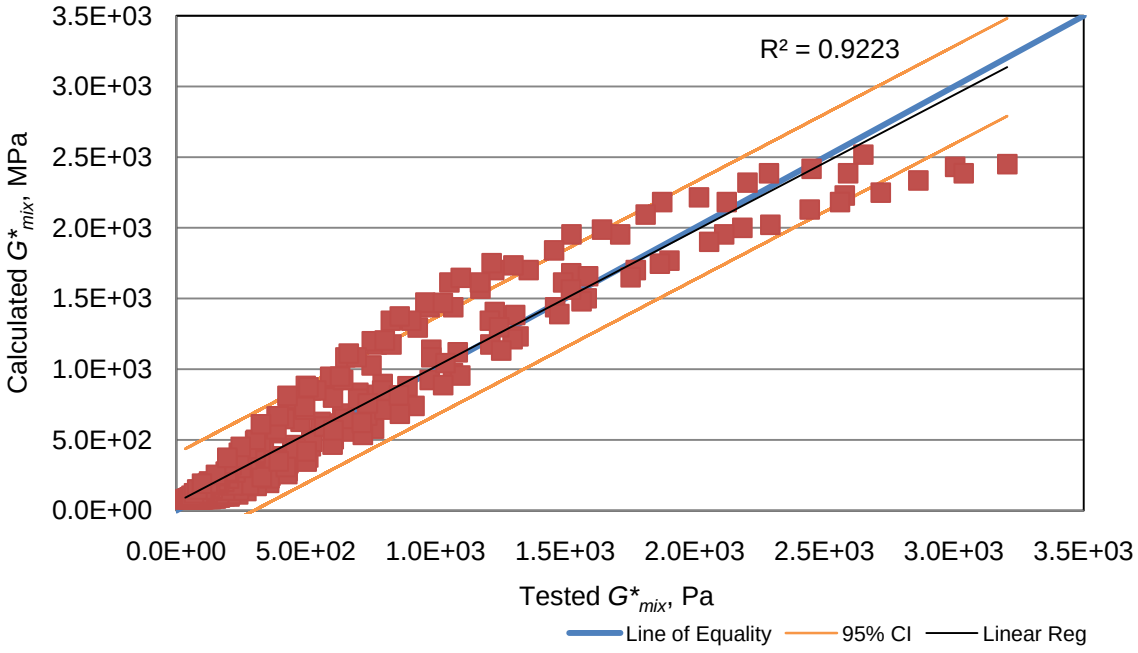

Figure 27 Comparison of Calculated vs. Tested G^*_{mix} for Virgin PG 76 - 22 – Revised Model

For the revised version of the Hirsch model, a paired-sample *t*-test analysis ($\alpha = 0.05$) indicated that the calculated and tested G^*_{mix} values were still not statistically equal. Visually, however, the revised version of the Hirsch model resulted in an improved estimation of G^*_{mix} obtained from the virgin torsion bar samples.

Once it was determined that the revised Hirsch model gave an improved estimate of the virgin binder torsion bar properties, it was used to calculate the G^*_{mix} values for the 100% RAP torsion bar specimens using the DSR data from the recovered RAP binders. Figure 28 shows a comparison of the actual and calculated G^*_{mix} using both the original and revised Hirsch model coefficients for the five RAP samples used in the study.

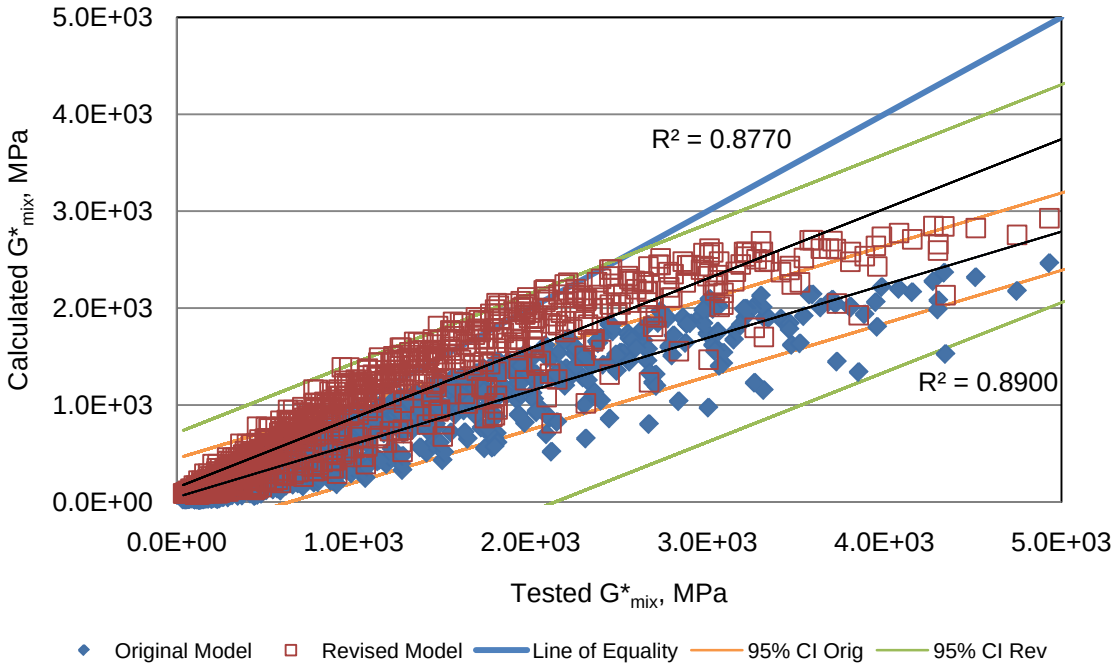

Figure 28 Comparison of Calculated vs. Tested G^*_{mix} for RAP Torsion Samples

Figure 28 shows a similar trend for the RAP materials as for the virgin materials. The original Hirsch model formula underestimated the calculated G^*_{mix} values. The revised Hirsch model, while not improving the RAP results as much as the virgin results, does bring the results closer to the line of equality. A paired-sample *t*-test ($\alpha = 0.05$) analysis comparing the calculated and tested G^*_{mix} values that the two sets of data (original and revised Hirsch) are statistically different, both from each other and from the line of equality. Figure 29 shows the comparison results for RAP 1. Plots of the comparison for the other RAP sources can be found in Appendix D.

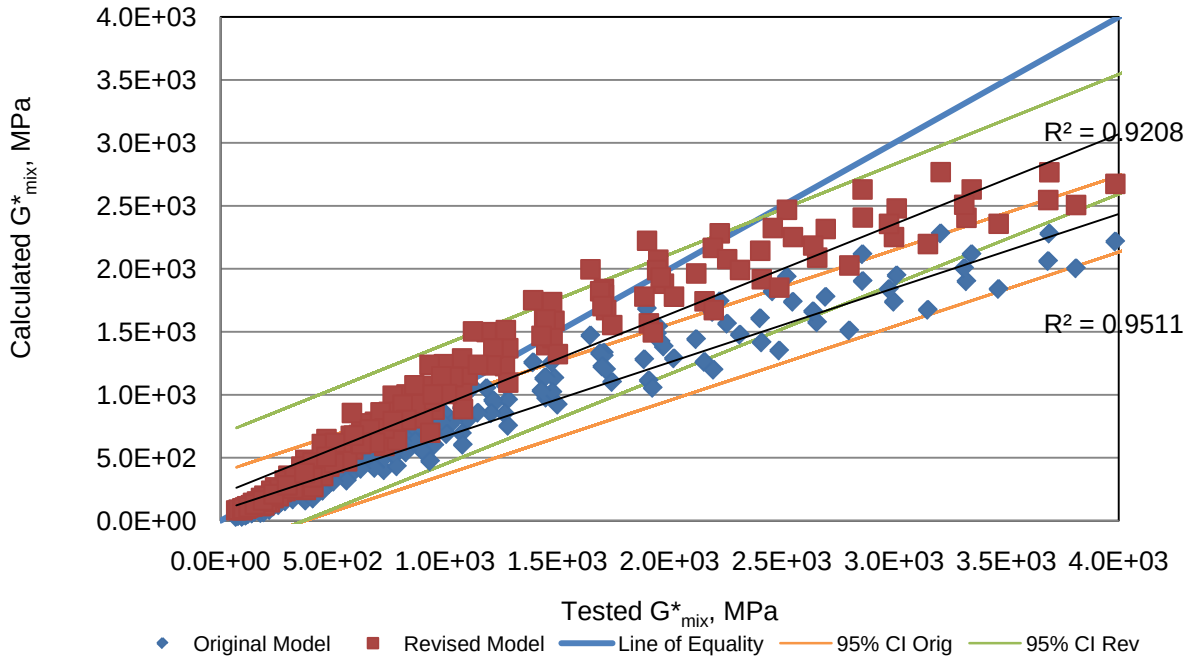

Figure 29 RAP 1 Calculation Comparison for Original and Revised Hirsch

The figure shows that, even though the revised Hirsch model provides improved correlation between the tested and calculated G^*_{mix} values for the RAP materials, the improvement is not quite as good as for the virgin materials. For RAPs 2 and 5, the improvement was only slight, while RAPs 1, 3, and 4 showed better agreement between calculated and tested G^*_{mix}. This is not necessarily the fault of the calculation and may be due to the inability to adequately characterize RAP binders using extracted and recovered binder. Figure 29 also shows what appears to be a plateau in the G^*_{mix} results at higher stiffness values (high frequency, cold temperature region). This plateau behavior was seen in all the RAP G^*_{mix} plots and to a lesser extent in Figures 24 – 27. Christensen et al. noted the tendency of the G^*_{mix} values calculated using the Hirsch model to plateau in this region and attributed it to the use of the estimated constant aggregate modulus value (601,000 psi for the original Hirsch model) in the

calculation. This value acts as a limiting value for the asphalt mixture stiffness calculated using the model. This behavior was not believed to be of any concern, as the range of stiffness values at which it occurs is much higher than any the asphalt mixture would experience in a pavement (*27*).

Based on the forward calculation results, it was felt that the revised Hirsch model might be able to provide an improved estimate of backcalculated G^*_{binder} results. In the following section, both the original and revised forms of the model were used for backcalculation so that the final results could be compared to further study the accuracy of the revised model.

Virgin Torsion Bars Backcalculation Results

To determine the PG grades of the virgin binders based on the torsion bar results, it was necessary to find the backcalculated G^*_{binder} and δ_{binder} values at the same temperatures that were used for the binder testing. Since the torsion bar tests were not run at the necessary temperatures (and in some cases the temperatures were outside the testable range), the results were estimated from CA master curves created using the backcalculated G^*_{binder} results. The backcalculated G^*_{binder} results at the required temperatures could also have been extrapolated from the individual temperature and frequency sweep results, but developing master curves was necessary for determining δ_{binder}. Once the backcalculated G^*_{binder} and δ_{binder} were determined, the Superpave PG criteria of $G^*/\sin\delta$ and $G^*\sin\delta$ were calculated at each temperature and the high and intermediate critical temperatures for the virgin binders determined using the criteria listed in AASHTO M320. Since the virgin binders were able to be tested in

the laboratory without the effect of extraction and recovery procedures it was expected that the backcalculated results would match the tested results fairly well.

A total of eight sets of backcalculated results were obtained for the virgin binders (2 binders X 2 aggregate sizes X 2 Hirsch model versions). Each set consisted of backcalculated results for four replicate test specimens. For ease of reference, the results using the original Hirsch model were identified as OH while the results using the revised Hirsch model were identified as RH. A -4 or -8 was added to indicate aggregate size; for example, PG 64-22 OH-4 refers to the set of test results backcalculated using the original Hirsch model and torsion results from the PG 64-22 test specimens made with material passing the #4 sieve. In the following sections, G^*_{binder} and δ_{binder} are discussed separately, followed by a discussion of the critical temperature results.

Virgin Backcalculated G^*_{binder}

Figures 30 – 33 show the backcalculated G^*_{binder} results compared to the tested G^*_{binder} data for the virgin binders. Both the -4 and -8 data are included in each figure for the entire range of temperatures and frequencies tested. Separate comparisons were made for the OH and RH results.

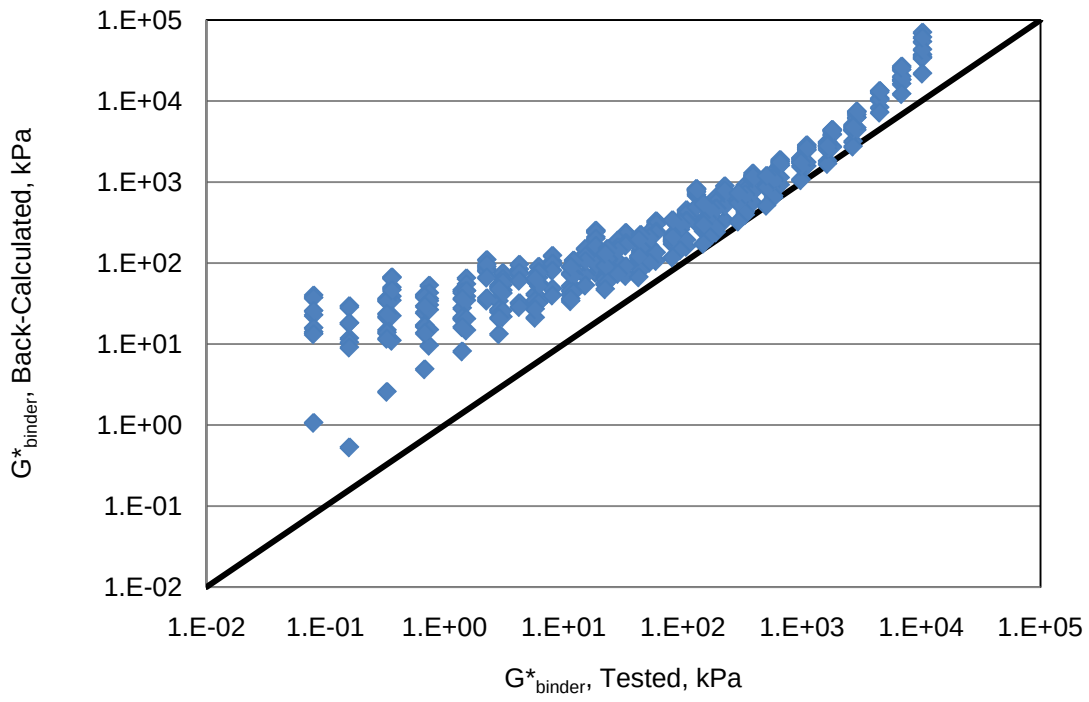

Figure 30 PG 64-22 Backcalculation Results – OH

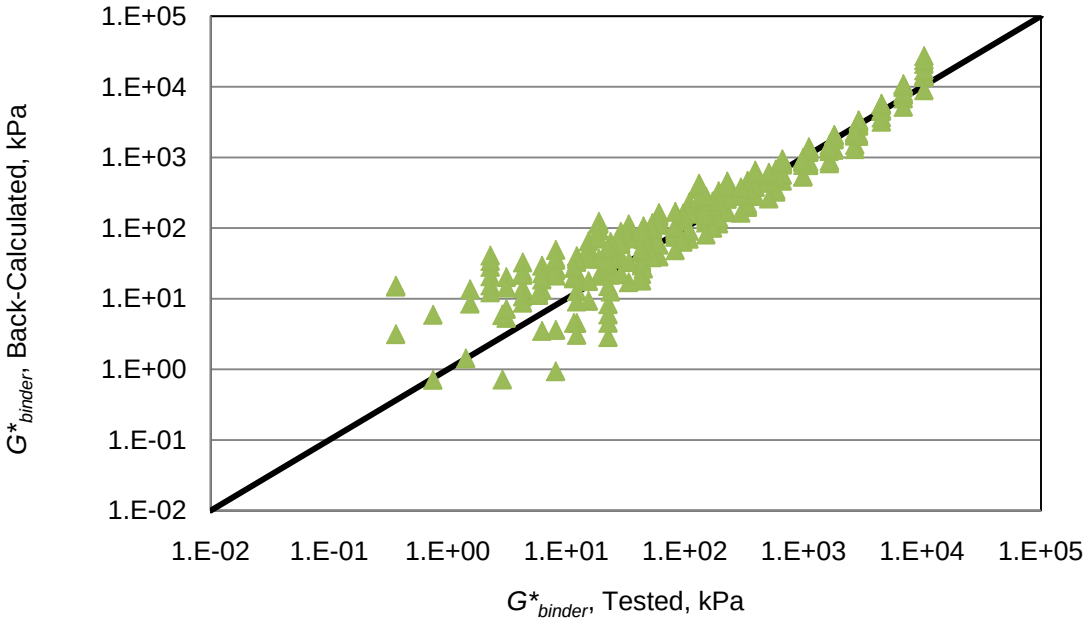

Figure 31 PG 64-22 Backcalculation Results – RH

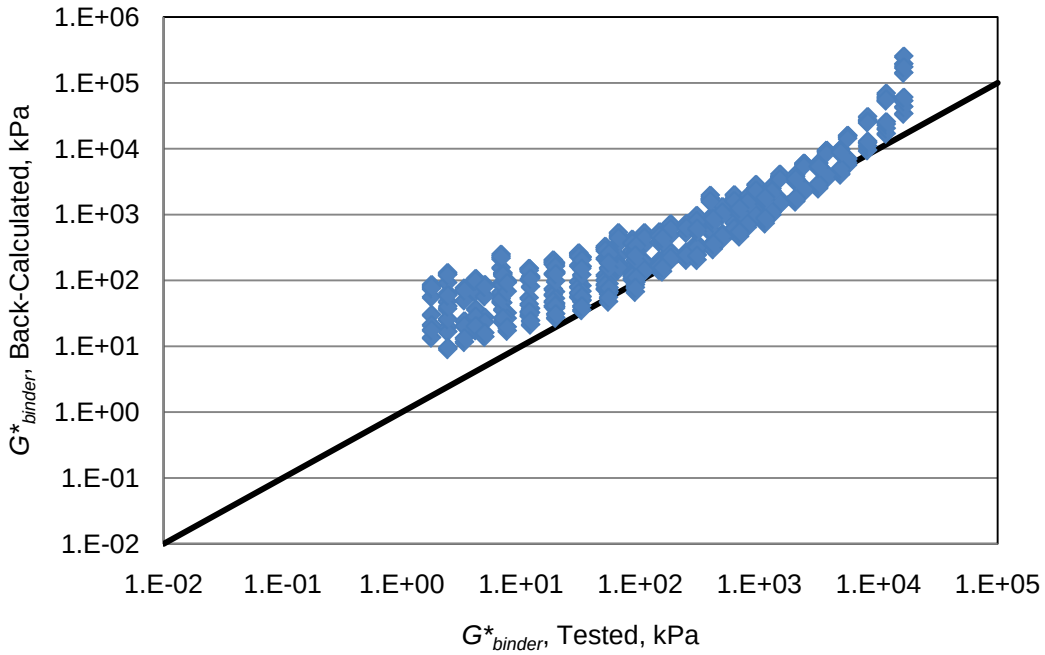

Figure 32 PG 76-22 Backcalculation Results – OH

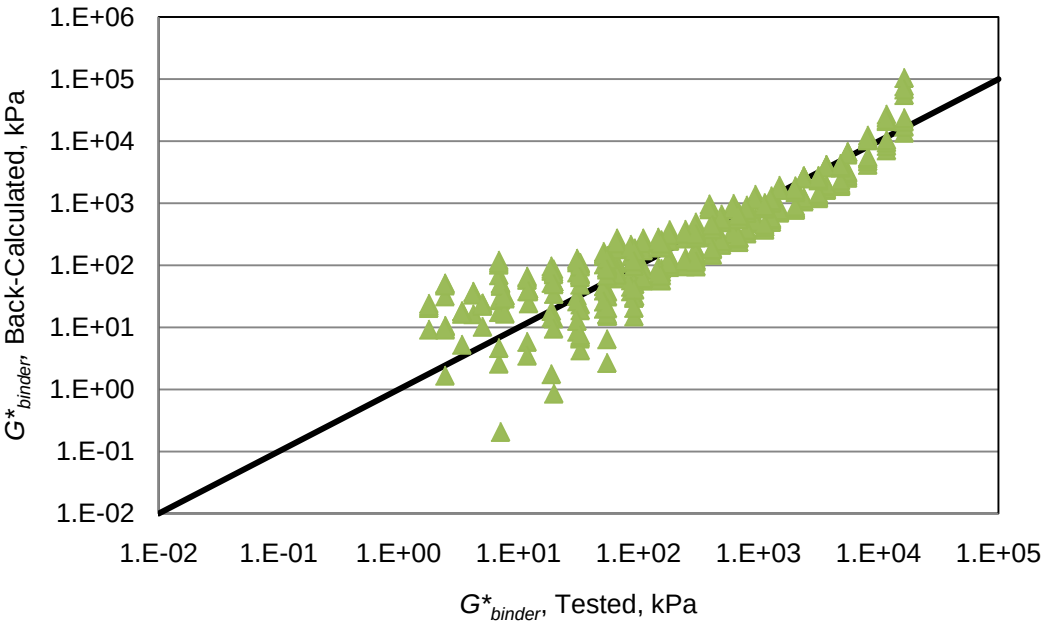

Figure 33 PG 76-22 Backcalculation Results – RH

The OH model mostly over-estimated the G^*_{binder} compared to the tested values for both virgin binders. There is also a great deal of scatter in the data. Although the scatter appears to be higher at the lower stiffness values, this is probably just an artifact of the log-log scale. A sharp increase in backcalculated G^*_{binder} at the higher stiffness range was noted as well, most likely a function of the limiting modulus value discussed in the previous section. Changing to the RH model improved the correlation between tested and backcalculated values for a portion of the data, but still showed increased scatter at lower stiffness values and did not match the tested G^*_{binder} at the higher stiffness values. It was noted during the backcalculation process, that the Hirsch model does not handle extremes in mixture stiffness data well. G^*_{mix} values of less than approximately 18,000 kPa for the OH Model and 72,000 kPa for the RH model could not be used to backcalculate G^*_{binder} as they gave results that were either unrealistically low (10^{-08} kPa) or negative. This matches findings from previous research using the Hirsch model for backcalculation (*31*). Both versions of the Hirsch model were also very sensitive to possible issues at cold temperatures and high frequency levels. A slight flattening of the 20°C G^*_{mix} isotherm at high frequencies translated into a sharp increase in G^*_{binder} after backcalculation, although this could also be attributed to limitations of the model discussed earlier. Since there were more than enough data points available to form the master curves for these test results, data points that appeared unreasonably high or low (due to the limitations of the model at extreme conditions) were removed from the backcalculated isotherms. For the virgin binder, in most cases this was the entire 60°C data set and the two highest frequencies for the 20°C data set.

Figures 34 and 35 show the master curves of the backcalculated G^*_{binder} results (both versions of the model) compared to the G^*_{binder} values obtained from testing the virgin binder.

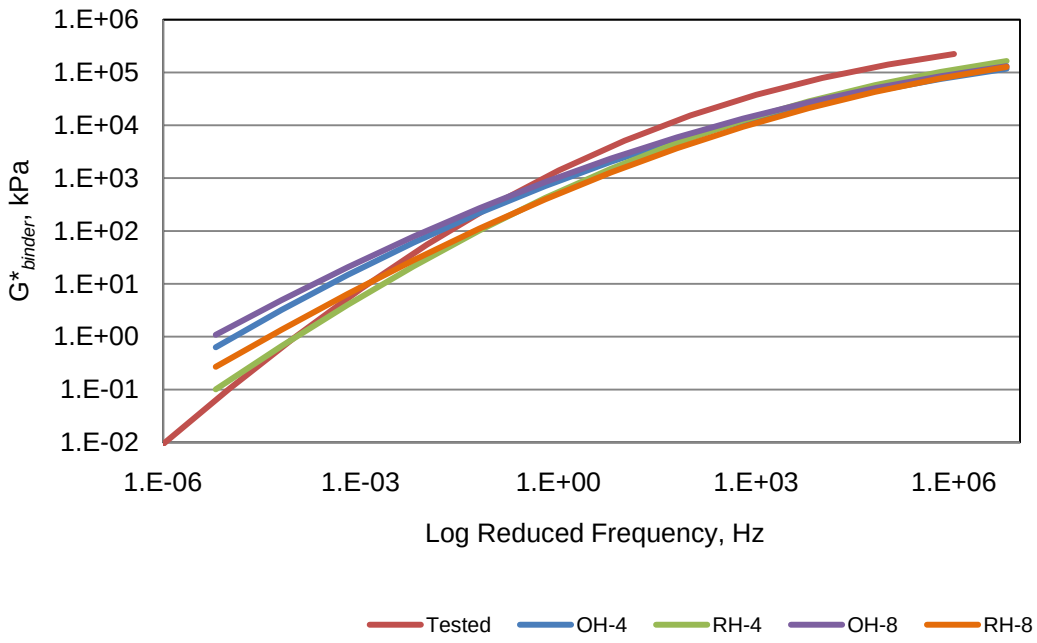

Figure 34 Backcalculated and Tested Binder Master Curves – PG 64-22

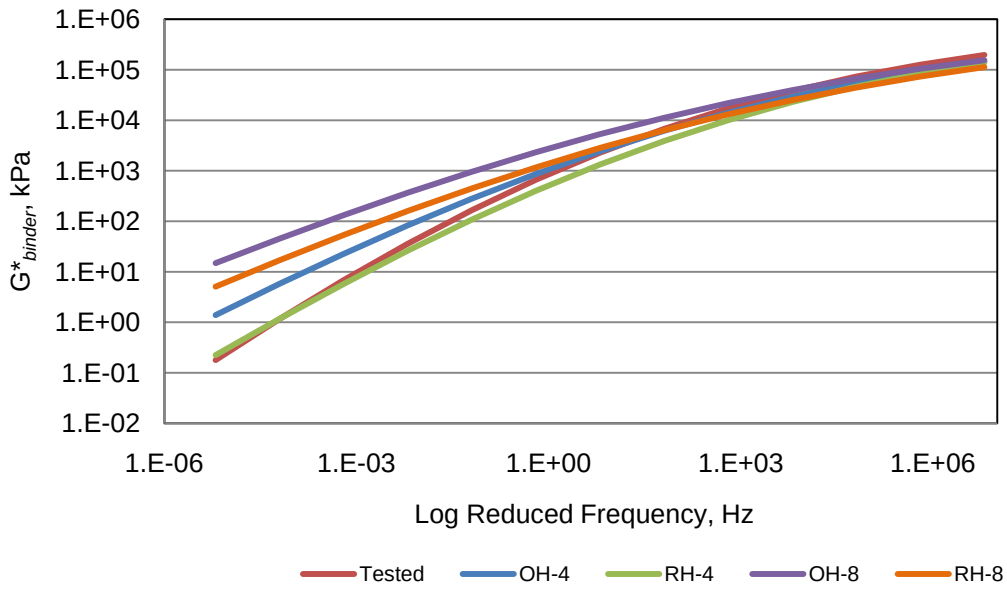

Figure 35 Backcalculated and Tested Binder Master Curves – PG 76-22

The master curves show that none of the backcalculated master curves appear to follow the tested binder master curves. The backcalculation procedure under-estimated G^*_{binder} for the higher stiffness values of the curve and over-estimated it at the lower stiffness values.

Figures 36 and 37 show the percent difference between the tested G^*_{binder} values and the backcalculated G^*_{binder} values at high and intermediate-temperatures. Since the backcalculation was done at four temperatures (two high and two intermediate) for each dataset, there are two values of percent difference for each test replicate in each figure. For example, for Replicate 1, G^*_{binder} was backcalculated at 64 and 70°C as these were the temperatures corresponding to the passing and failing binder test results. At 64°C, the calculated percent difference for the OH model was approximately 200% while at 70°C, the calculated percent difference was approximately 190%. For

the RH model, the calculated percent at 64°C difference was 7% for the first temperature and 15% at 70°C.

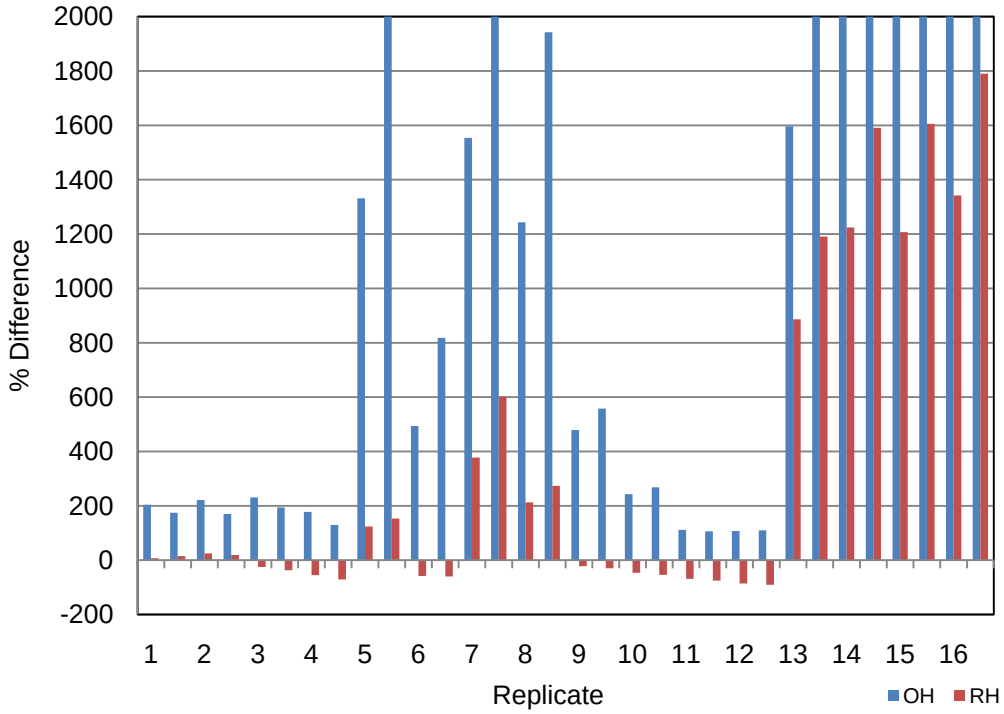

Figure 36 Percent Difference in G^*_{binder} for High-temperature Results- Virgin Binder

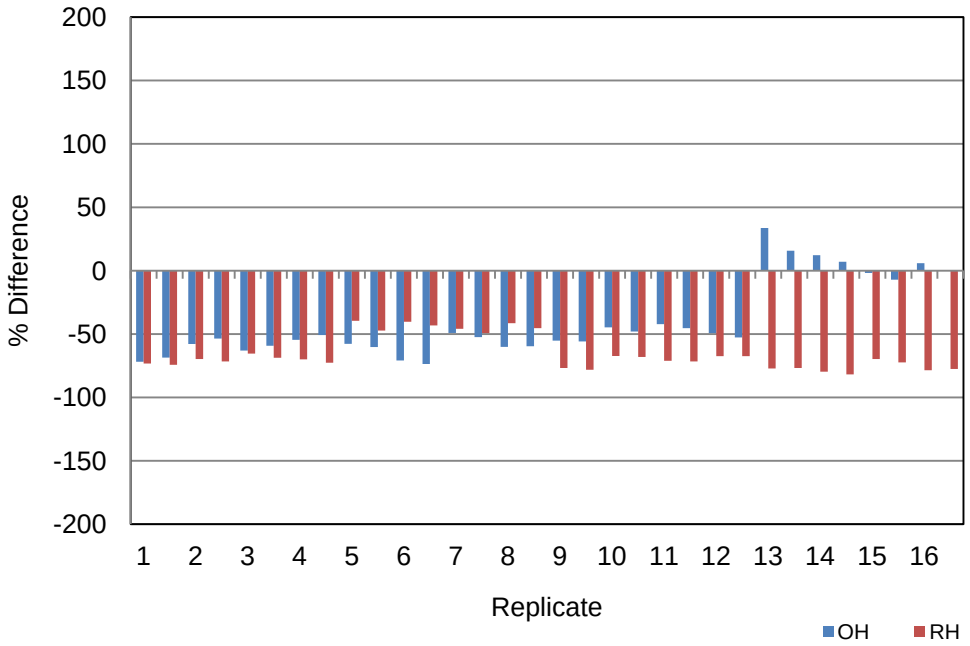

Figure 37 Percent Difference in G^*_{binder} for Intermediate-temperature Results- Virgin Binder

The figures show that at high-temperatures, both versions of the model tended to over-estimate the backcalculated G^*_{binder} values. The RH model in most cases had lower differences between tested and backcalculated G^*_{binder} values than the OH model; however, the average model error was still 370%. The average model error for the OH model was 1,285%.

At intermediate-temperatures, the differences between the two versions of the model were not as pronounced as at the high-temperatures. Both versions of the model tended to under-estimate G^*_{binder} at intermediate-temperatures, and in some cases the RH model (average error = 65%) was worse than the OH model (average error = 40%).

Figures 38 - 41 compare the differences between the average backcalculated and tested G^*_{binder} values. Results are separated by binder type, high or intermediate-temperature range, aggregate size, and version of the model. Error bars showing the standard deviation are included to show the high variability seen in the calculation.

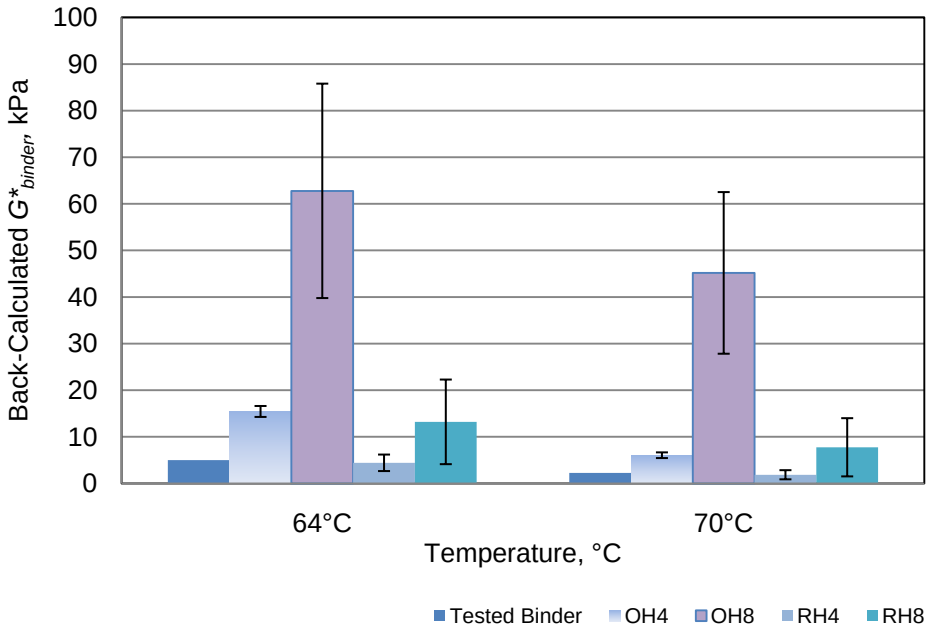

Figure 38 High-temperature Backcalculated G^*_{binder} Results for PG 64-22

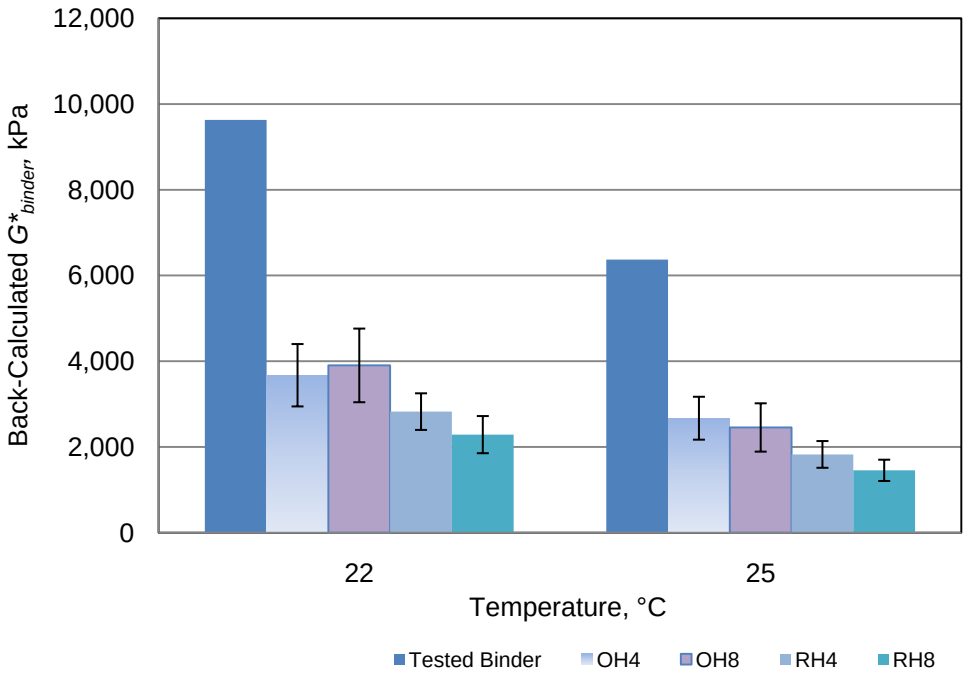

Figure 39 Intermediate-temperature Backcalculated G^*_{binder} Results for PG 64-22

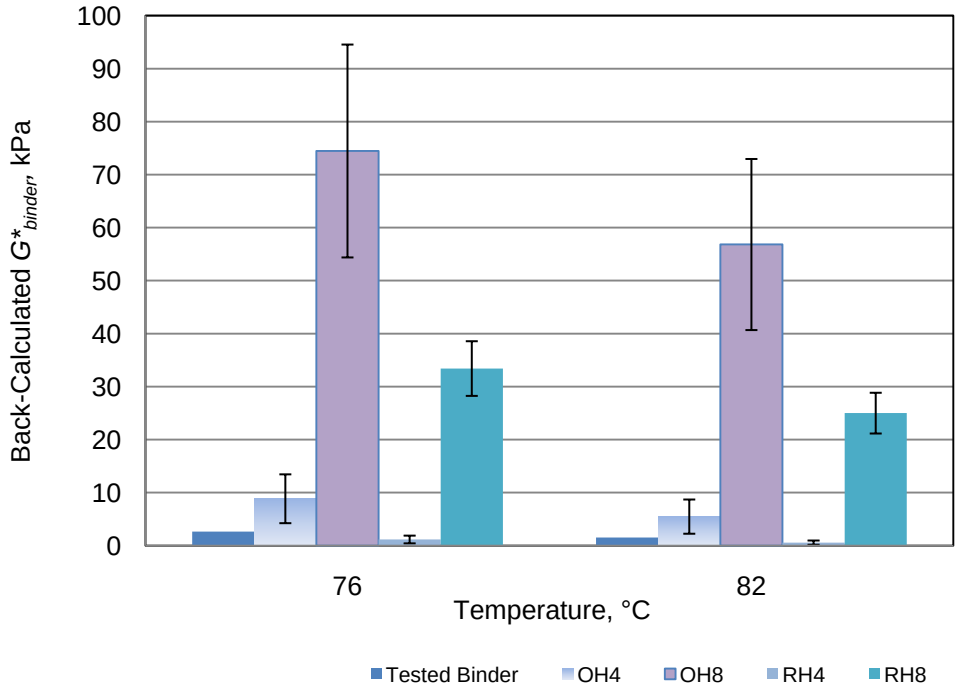

Figure 40 High-temperature Backcalculated G^*_{binder} Results for PG 76-22

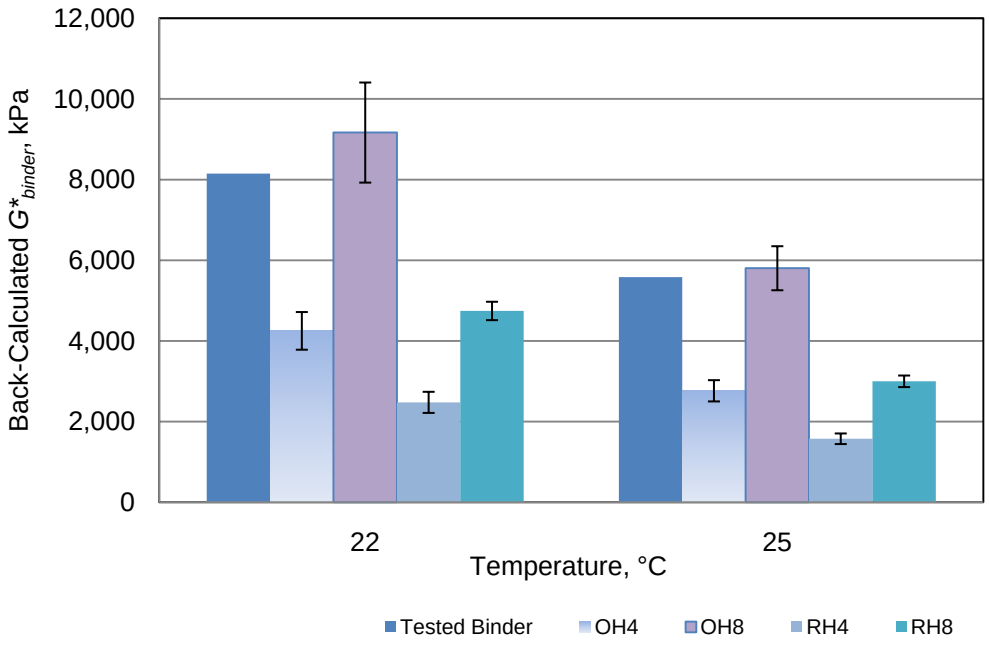

Figure 41 Intermediate-temperature Backcalculated G^*_{binder} Results for PG 76-22

Variability for the back-calculation procedure was very high in some cases, particularly for the high-temperatures which had COV values of up to 81%. The intermediate-temperature backcalculation results had lower COV values (between 11 and 22%). The variability in the high-temperature results was most likely due to issues with the Hirsch model at low mixture stiffness values.

Table 15 shows the average backcalculated G^*_{binder} values compared to the tested G^*_{binder} values for the virgin materials. A one-sample statistical *t*-test (α=0.05) was used to compare the average backcalculated results to the tested values (H_0: backcalculated G^*_{binder} = tested G^*_{binder}). The p-values obtained from the comparisons are included in the table.

Table 15 Comparison of Backcalculated to Tested G^*_{binder}, kPa

			-4 Aggregate				-8 Aggregate			
		Tested	RH		OH		RH		OH	
Binder	Temp °C	G^*_{binder}	G^*_{binder}	*p*-value	G^*_{binder}	*p*-value	G^*_{binder}	*p*-value	G^*_{binder}	*p*-value
64-22	64	5.00	4.40	0.548	15.42	0.000	13.19	0.169	67.74	0.015
	70	2.26	1.84	0.546	6.03	0.001	7.74	0.178	49.85	0.016
	22	9631	2825	0.000	3674	0.001	2288	0.000	3857	0.001
	25	6373	1827	0.001	2671	0.001	1456	0.000	2412	0.001
76-22	76	2.64	1.17	0.027	8.85	0.074	33.42	0.001	74.47	0.006
	82	1.52	0.57	0.018	5.48	0.091	25.01	0.001	56.83	0.006
	22	8149	2477	0.000	4250	0.000	4744	0.000	9167	0.199
	25	5581	1575	0.000	2764	0.000	2999	0.000	5803	0.476

For the PG 64-22 virgin materials tested at high-temperatures, the RH-4 results were a statistical match for the tested G^*_{binder} results. The RH-8, and OH-8 results were not a statistical match and were higher than the tested values. The RH -4 G^*_{binder} results were a stastical match for the tested G^*_{binder}, but based on the average value of 13.19 kPa, it appears that the high variability of the dataset is affecting the statistical results. At intermediate-temperatures, none of the PG 64-22 backcalculated results matched the tested values. For the PG 76-22 virgin materials, the OH-4 results were the only statistical match at high-temperatures and the OH-8 results were the only statistical match at intermediate-temperatures.

Virgin Backcalculated δ_{binder}

Figures 42 and 43 show the percent difference between the tested δ_{binder} and the backcalculated δ_{binder} for both versions of the Hirsch model.

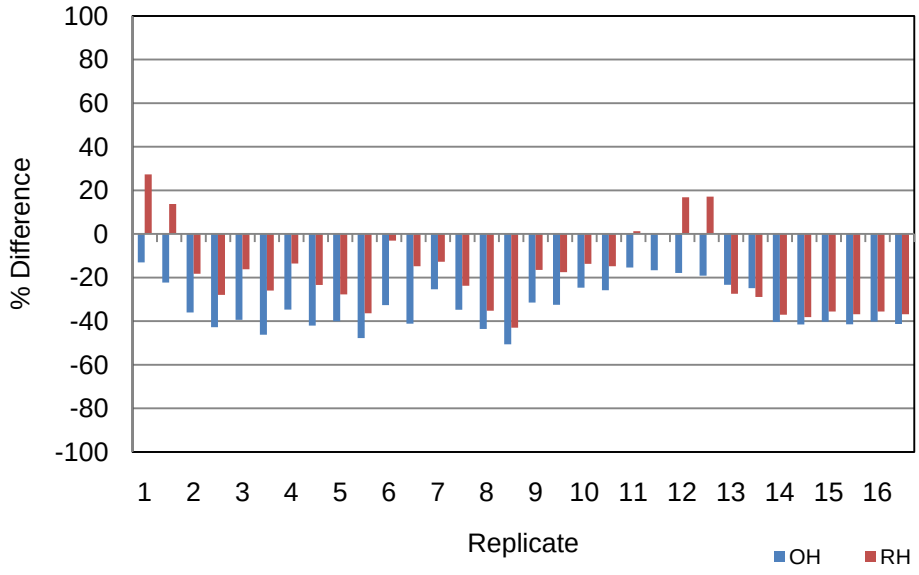

Figure 42 Percent Difference in δ_{binder} for High-temperature Results

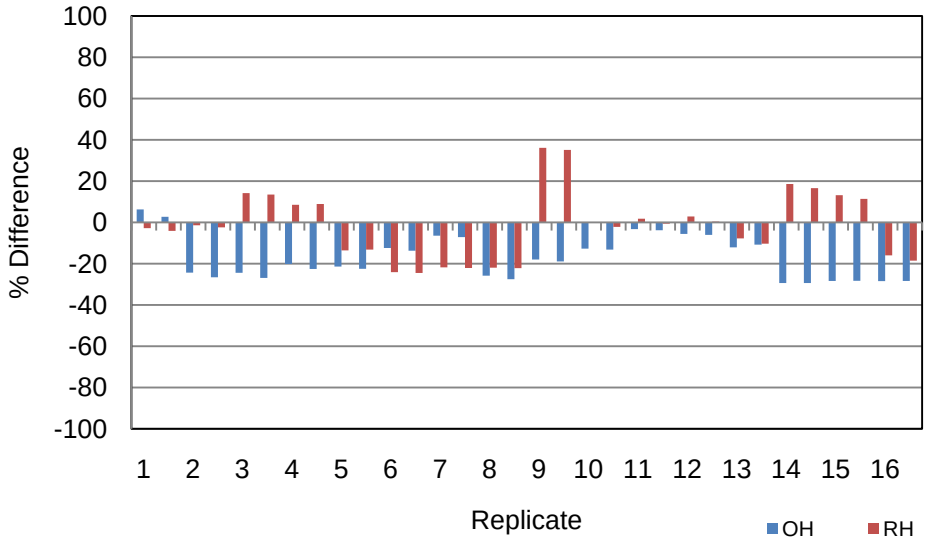

Figure 43 Percent Difference in δ_{binder} for Intermediate-temperature Results

The figures show that the backcalculation method under-estimates δ_{binder} in many cases at both high and intermediate-temperatures. The RH model typically has a better correlation (average of -18% difference at high-temperatures and -1.5% difference at intermediate-temperatures) between the tested and backcalculated results than the OH model (average percent difference of -33% at high-temperatures and -17% at intermediate-temperatures), but not always, and in many cases the improvement is minor.

Figures 44 - 47 compare the average backcalculated δ_{binder} results for the virgin materials to the tested results at high and intermediate-temperatures.

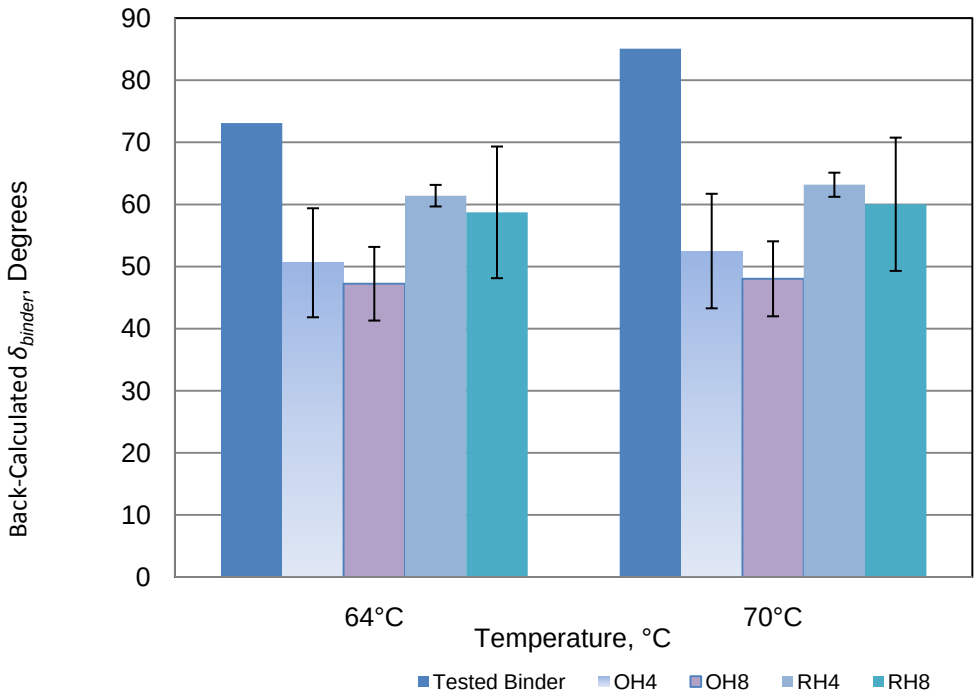

Figure 44 High-temperature Backcalculated δ_{binder} Results for PG 64-22

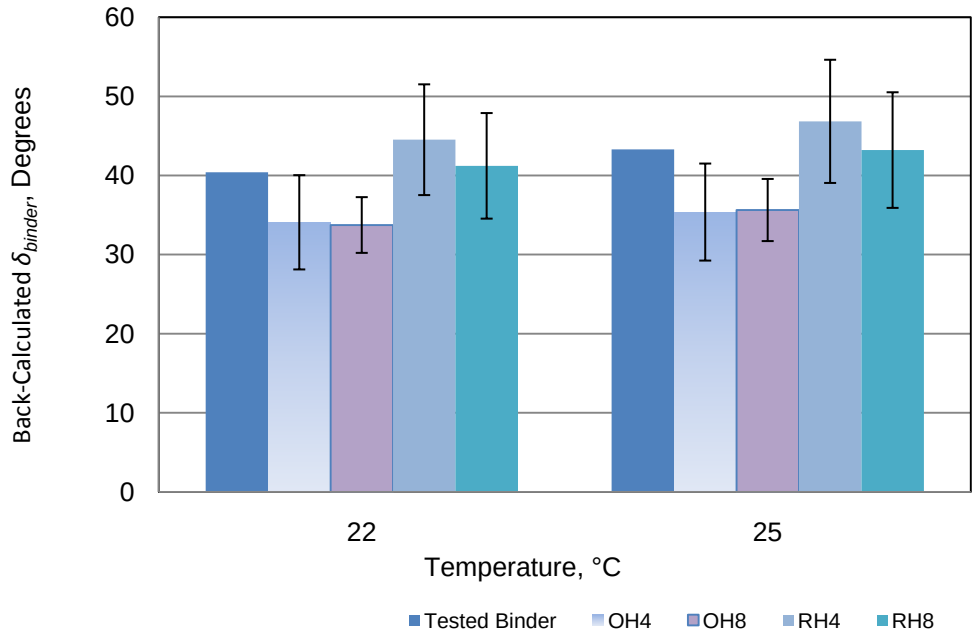

Figure 45 Intermediate-temperature Backcalculated δ_{binder} Results for PG 64-22

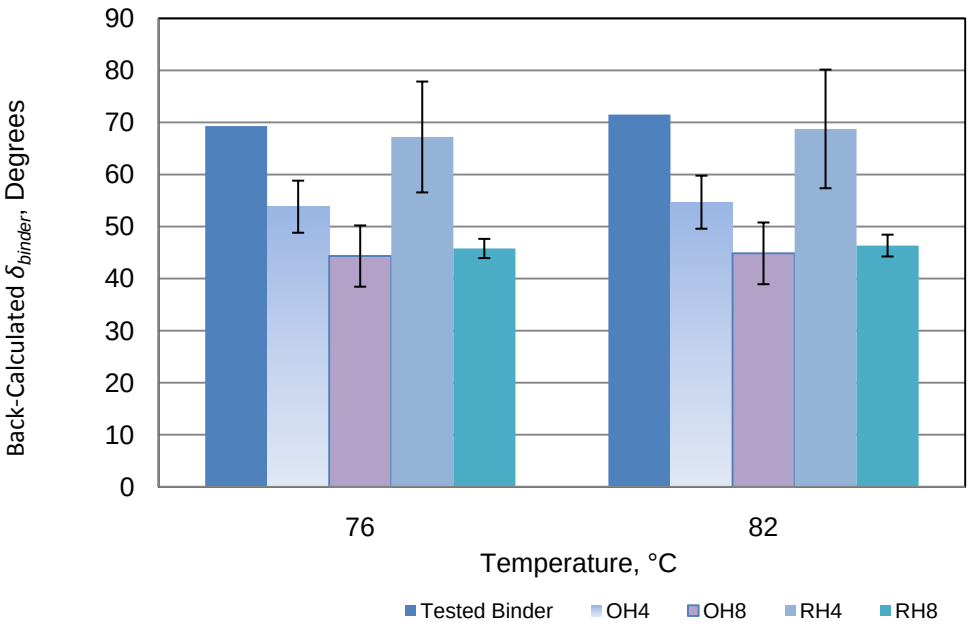

Figure 46 High-temperature Backcalculated δ_{binder} Results for PG 76-22

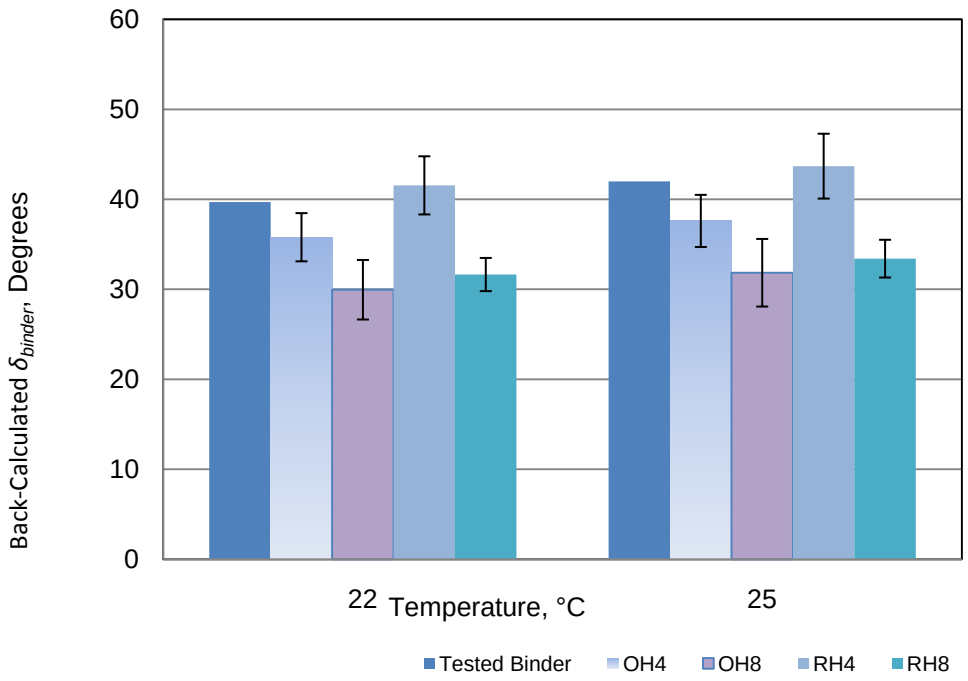

Figure 47 Intermediate-temperature Backcalculated δ_{binder} Results for PG 76-22

A one-sample *t*-test (α=0.05) was used to compare the backcalculated δ_{binder} values to the tested δ_{binder} values. Results of the statistical analysis are shown in Table 16 along with a summary of the average δ_{binder} results for each dataset.

Table 16 Comparison of Backcalculated to Tested δ_{binder}, °

			-4 Aggregate				-8 Aggregate			
		Tested	RH		OH		RH		OH	
Binder	Temp, °C	$\delta_{binder,}$	δ_{binder}	*p*-value	δ_{binder}	*p*-value	δ_{binder}	*p*-value	δ_{binder}	*p*-value
64-22	64	73.1	61.4	0.007	50.6	0.014	58.7	0.073	46.2	0.003
	70	85.1	63.2	0.003	52.5	0.006	60.0	0.019	46.9	0.001
	22	40.4	44.5	0.324	34.1	0.124	41.2	0.822	33.6	0.032
	25	43.3	46.8	0.430	35.4	0.081	43.2	0.982	35.4	0.030
76-22	76	69.3	67.2	0.722	53.8	0.009	45.8	0.001	44.3	0.003
	82	71.5	68.8	0.664	54.7	0.007	46.4	0.000	44.9	0.063
	22	39.7	41.6	0.335	35.8	0.061	31.6	0.003	30.0	0.010
	25	42.0	43.7	0.419	37.6	0.056	33.4	0.004	31.8	0.012

When compared to the tested δ_{binder} results, none of the backcalculated datasets showed a consistent statistical match. The RH-4 dataset had the best results with statistical matches for all but the PG 64-22 high-temperature dataset. The OH-4 dataset only showed a statistical match between tested and backcalculated δ_{binder} for the intermediate-temperatures. The RH-8 dataset correctly estimated δ_{binder} for three out of four temperatures for the PG 64-22 binder, but was not a statistical match for the PG 76-22 δ_{binder} at any temperature. The OH-8 dataset only had one statistical match.

Virgin Binder Critical Temperatures

Figures 48 and 49 show how the estimated binder critical temperatures compared to the tested values for the virgin materials.

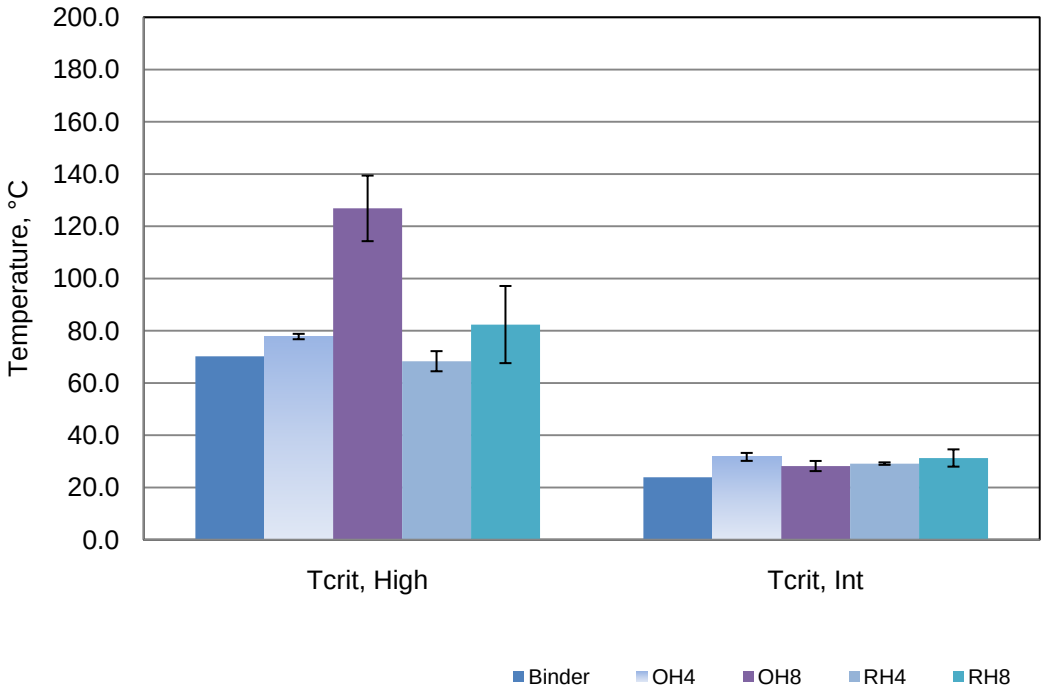

Figure 48 PG 64-22 Backcalculated T_{crit}

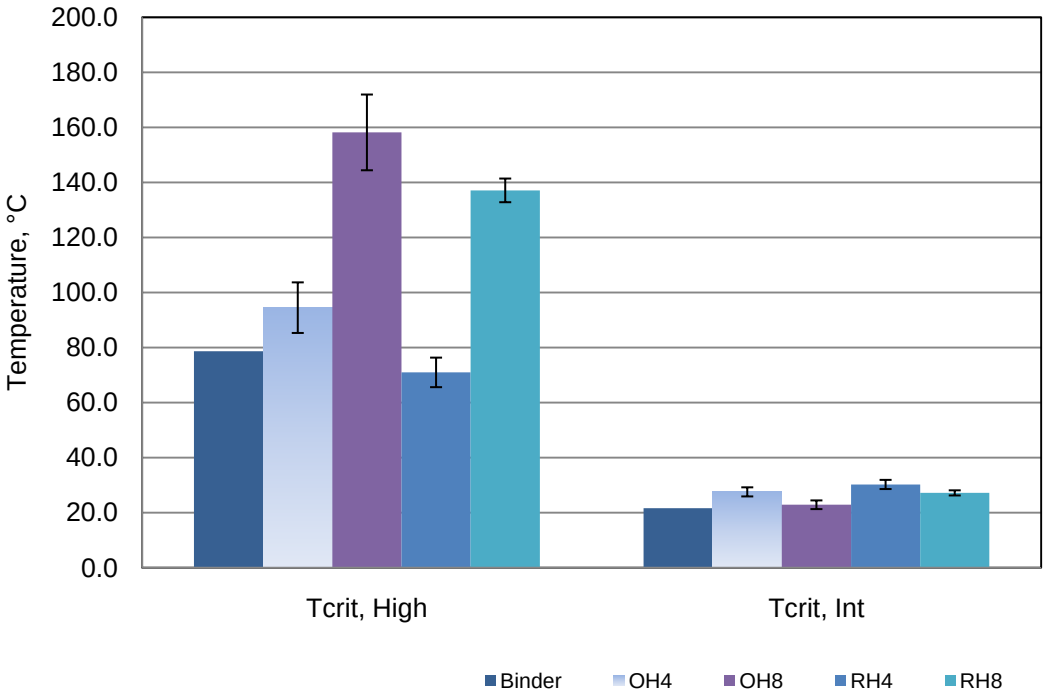

Figure 49 PG 76-22 Backcalculated T_{crit}

Table 17 shows the results of a one-sample *t*-test (α=0.05) analysis comparing the high and intermediate backcalculated critical temperatures to the tested values.

Table 17 p-Values for Comparison of Backcalculated Critical Temperature, °C

			-4 Aggregate				-8 Aggregate			
			OH		RH		OH		RH	
Binder	**Temp.**	**Tested**	**T_{crit}**	**p-value**	**T_{crit}**	**p-value**	**T_{crit}**	**p-value**	**T_{crit}**	**p-value**
64-22	High	70.2	77.8	0.001	68.3	0.490	126.9	0.003	82.4	0.198
	Int	23.9	31.7	0.002	31.3	0.000	28.2	0.021	31.3	0.021
76-22	High	78.6	94.5	0.041	71.0	0.066	158.2	0.001	137.1	0.000
	Int	21.6	27.5	0.006	30.2	0.002	22.9	0.207	27.2	0.001

For both binders, the statistical analysis shows that there are only four statistical matches between the tested and backcalculated T_{crit} values for either model: RH-4 at high-temperatures for both binders, OH-8 at intermediate-temperatures for the PG 76-22, and RH-8 for the PG 64-22 at high-temperatures.

It is important to remember that the desired result of this project was a method to estimate the properties of the binder in the torsion bar specimens. Although an exact statistical match for the tested values would be ideal, it is not necessarily required as long as the backcalculated results are reasonably close to the tested results. Table 18 shows the high and intermediate PG grades of the virgin binders based on the average backcalculated results. Note that the intermediate critical temperature is not normally stated as part of the PG grade of the binder and therefore does not have standard values. For the sake of comparison, a value equal to the higher standard DSR test temperature (25, 28, 31, etc) bracketing the critical temperature was assigned as the intermediate PG grade. For example, a critical temperature of 29.1°C would be assigned a standard value of 31.

Table 18 Standard PG Grades for Virgin Materials

	PG 64-22		PG 76-22	
	High	**Intermediate**	**High**	**Intermediate**
Binder	**70**	**25**	**76**	**22**
OH-4	76	34	94	28
OH-8	124	31	154	25
RH-4	64	31	70	31
RH-8	82	34	136	28

At high-temperatures, the RH-4 dataset was the closest match for the high standard PG grade of both binders, although it under-estimated the critical temperature by one standard grade for both binders. All the other datasets significantly over-estimated the high PG grades, sometimes by as many as thirteen grades. At intermediate-temperatures, both versions of the model estimated PG grades that were higher than the binder PG grade; although all were within three standard grades.

RAP Torsion Bars Back-Calculation Results

This section discusses the backcalculated results obtained for the 100% RAP torsion bar specimens. The analysis was similar to the virgin binder back-calculation results except that only one aggregate size was used. Also, instead of RTFO-aged binder, the backcalculated results were compared to the values obtained from testing the asphalt binder that was extracted and recovered from the RAP materials.

RAP Backcalculated G^*_{binder}

Figures 50 and 51 compare the backcalculated G^*_{binder} results to the tested G^*_{binder} obtained from the extracted binders.

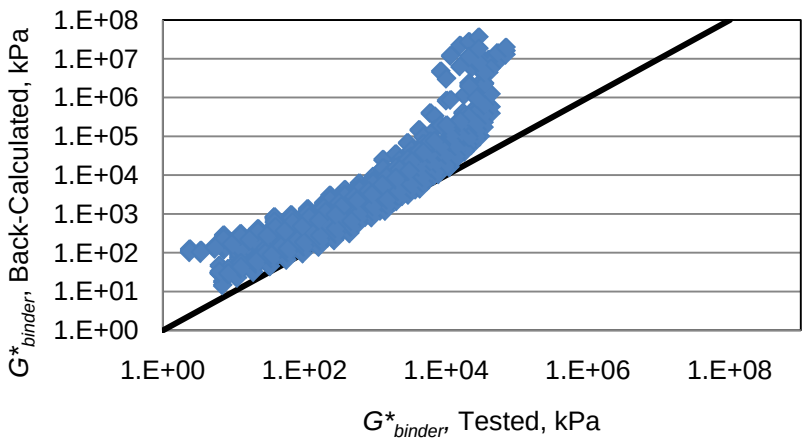

Figure 50 Comparison of Tested G^*_{binder} and Backcalculated G^*_{binder} – OH

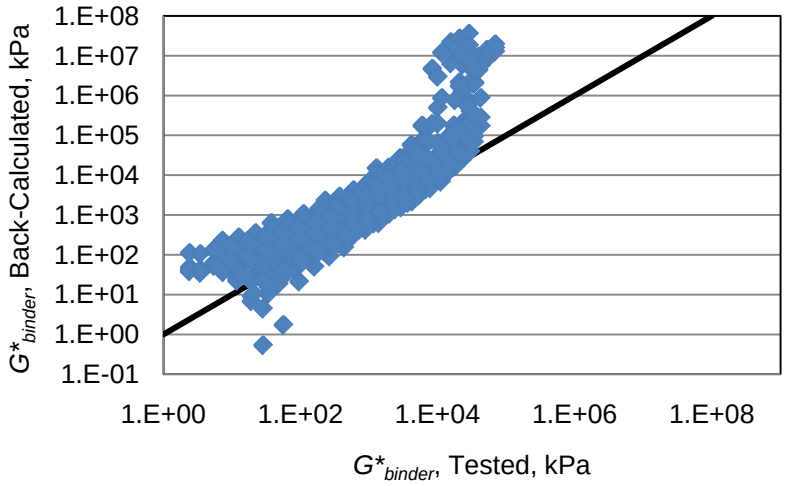

Figure 51 Comparison of Tested and Backcalculated G^*_{binder} – RH

The comparison of RAP backcalculated and tested G^*_{binder} values looks similar to that of the virgin binder results. The data follow a linear trend for a portion of the curve, but not at the ends. The RAP torsion bars were stiffer than the virgin torsion bars and therefore did not have as many issues with back-calculation at the lower frequencies, although

there is still some scatter in the low stiffness data. The backcalculated values had the same sharp increase in the higher stiffness range. Since there were more than enough data points available to form the master curves for these test results, backcalculated data points that appeared to be beyond the capability of the model were removed. In most cases this was the entire 20°C data set for the RAP binders.

Figures 52 and 53 show the percent difference between the individual tested G^*_{binder} values and the G^*_{binder} values backcalculated using both versions of the Hirsch model. The results shown were backcalculated at the same temperatures as the recovered RAP binder testing.

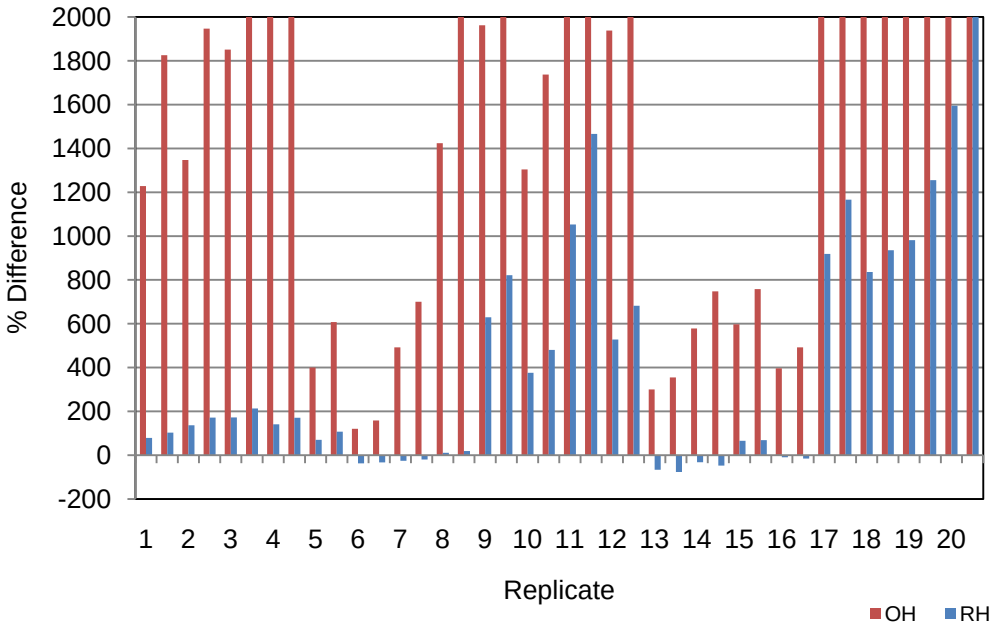

Figure 52 Percent Difference in G^*_{binder} for High-temperature Results-100% RAP

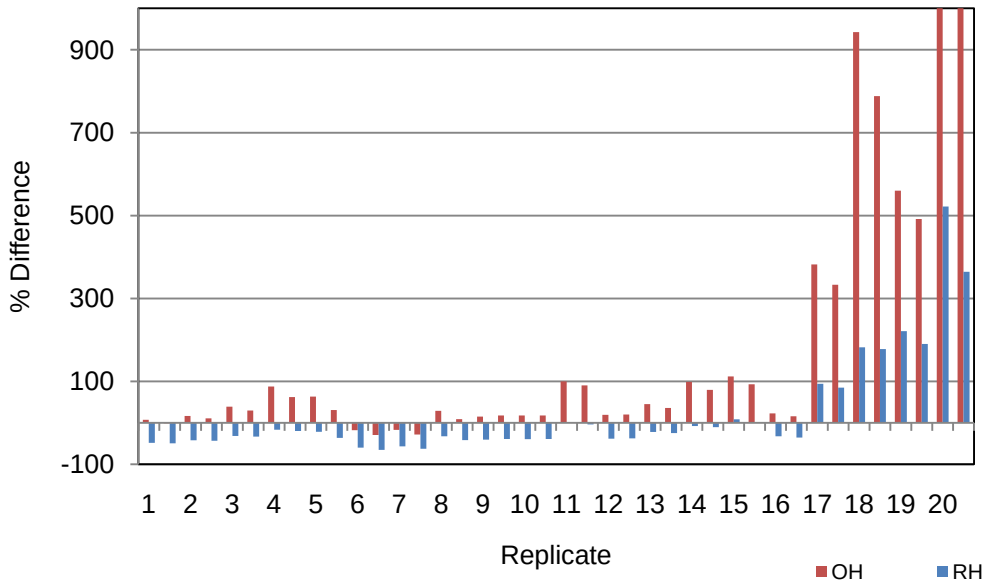

Figure 53 Percent Difference in G^*_{binder} for Intermediate-temperature Results-100% RAP

As with the virgin torsion bar results, the OH model over-estimated G^*_{binder} at high-temperatures for the 100% RAP samples, in some cases by over 2,000% with an average percent difference for the OH model results of 1,980%. Using the RH model reduced the average percent difference at high-temperatures to 430%. At intermediate-temperatures, the OH model over-estimated almost all of the G^*_{binder} values by an average of 230% while the RH model under-estimated them by an average of 20%.

Figures 54 and 55 compare the average backcalculated G^*_{binder} values to those obtained by testing the extracted and recovered binder for RAP 1. Error bars showing the standard deviations of the test results are included to show the high variability seen in the backcalculated results. The results for the other four RAP sources were similar and are included in Appendix E.

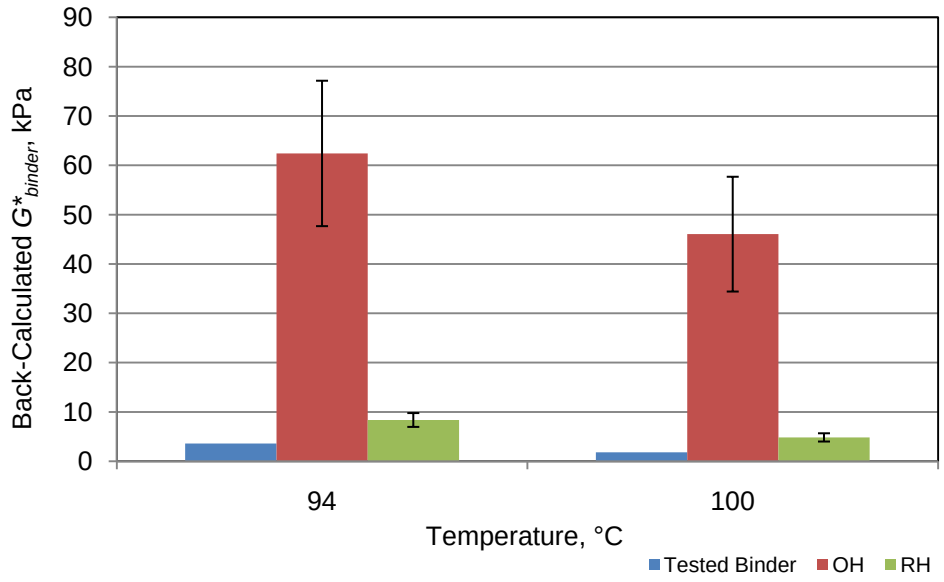

Figure 54 High-temperature Backcalculated G^*_{binder} Results for RAP 1

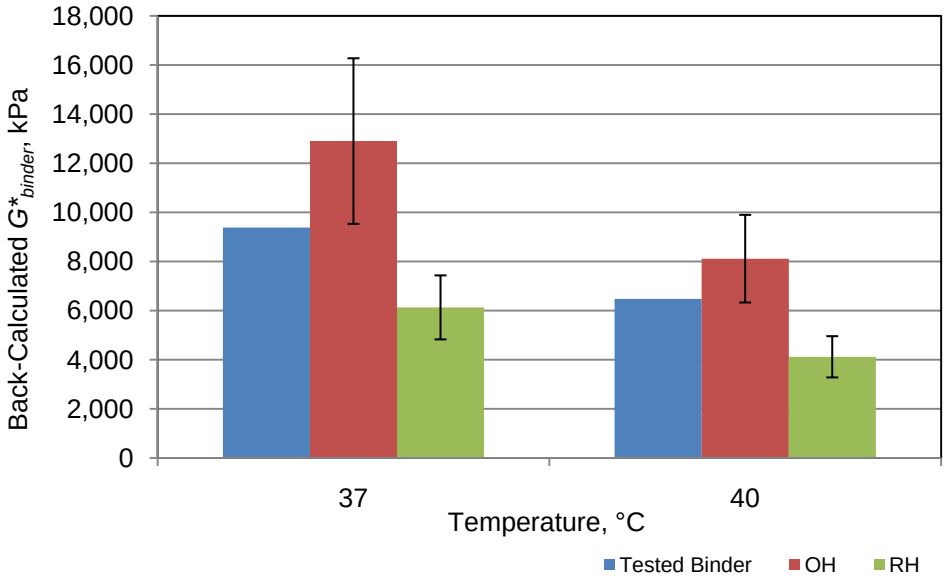

Figure 55 Intermediate-temperature Backcalculated G^*_{binder} Results for RAP 1

At high-temperatures, both versions of the model over-estimated the G^*_{binder} results when compared to the tested values. The RH model had lower values than the OH model in most cases and appears to be a closer match to the tested results, although

they may not be a statistical match. Both versions of the model have high variability between the replicate data, with COV values approaching 80% in some cases.

At intermediate-temperatures, the OH model over-estimated G^*_{binder} for all five RAPs. The RH model under-estimated G^*_{binder} for all the RAP materials except RAP 5. Variability was high for these results as well. Neither version of the model stands out as a consistent best match for the intermediate-temperature G^*_{binder} tested values. Table 19 shows the one-sample *t*-test results (α=0.05) for comparing the tested values to the backcalculated values for each model.

Table 19 p-values for RAP G^*_{binder}

		G^*_{binder}, kPa				
RAP	**Temp, °C**	**Binder**	**OH**	***p*-value**	**RH**	***p*-value**
1	94	3.61	62.41	0.004	8.37	0.007
	100	1.83	46.05	0.005	4.84	0.006
	37	9380	12903	0.128	6129	0.016
	40	6475	8113	0.164	4117	0.011
2	88	3.32	23.54	0.120	3.47	0.867
	94	1.65	16.57	0.127	1.95	0.610
	31	8735	9994	0.516	5016	0.020
	34	6591	6295	0.780	3203	0.006
3	94	2.43	18.14	0.012	53.02	0.021
	100	1.24	11.94	0.016	37.31	0.027
	31	9410	6621	0.164	12986	0.055
	34	6730	4717	0.136	9181	0.041
4	82	4.19	3.74	0.007	23.79	0.727
	88	2.00	1.64	0.010	13.76	0.611
	28	9732	8424	0.047	16510	0.229
	31	6942	5733	0.053	10834	0.118
5	82	3.30	39.03	0.006	108.84	0.008
	88	1.67	25.43	0.012	77.35	0.020
	25	9018	31996	0.142	121559	0.071
	28	6305	19195	0.058	55578	0.039

The statistical analysis comparing the backcalculated G^*_{binder} values and the tested G^*_{binder} values for the RAP materials showed that at high-temperatures, neither model was a statistical match for G^*_{binder} except for the OH model for RAP 2 and the RH model for RAPs 2 and 4. The average results for the RAP 2 G^*_{binder} backcalculated using the OH model and the RAP 4 G^*_{binder} backcalculated using the RH model appear to be much larger than the average recovered binder values for these RAP sources. Both of these datasets had extremely high COV values at high temperatures (83% for RAP 2 and 70% for RAP 4). The variability in these results is most likely affecting the results of

the statistical analysis in this case and it is likely that these backcalculated values are not actually equal to the tested values.

At intermediate-temperatures, the OH G^*_{binder} dataset is the best match for all the RAPs. The RH model is also a statistical match for RAP 4 (both temperatures) and RAPs 3 and 5 (one temperature only) at intermediate-temperatures.

RAP Backcalculated δ_{binder}

Figures 56 and 57 show the percent difference between the tested δ_{binder} and the backcalculated δ_{binder} for the 100% RAP results using both versions of the Hirsch model.

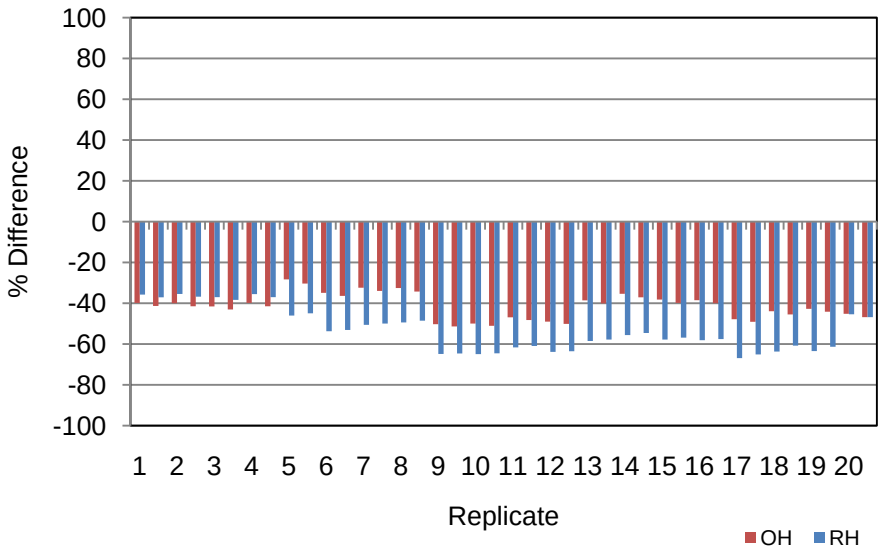

Figure 56 Percent Difference in δ_{binder} for HighTemperature Results

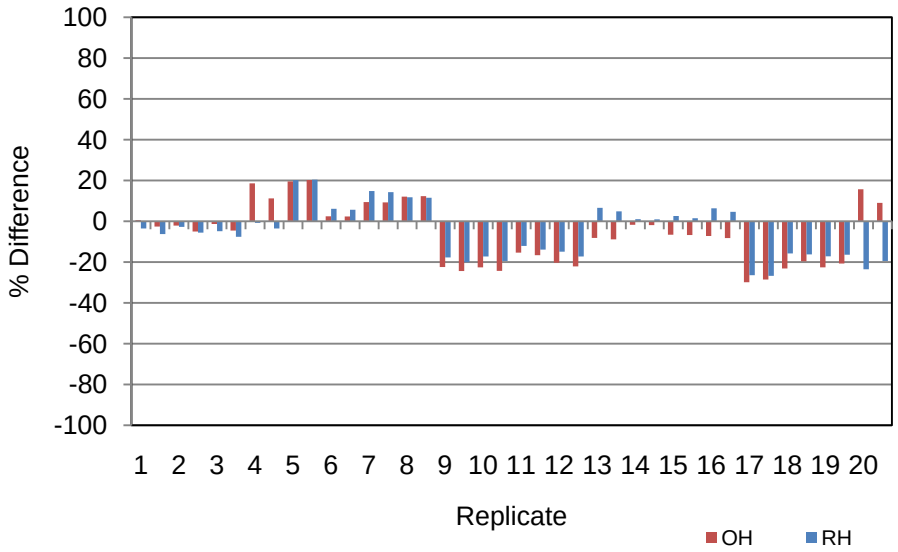

Figure 57 Percent Difference in δ_{binder} for Intermediate-temperature Results

Similar to the virgin material results, both versions of the Hirsch model under-estimated δ_{binder} for the 100% RAP materials at high-temperatures with the RH model (average percent difference = -53%) as being worse than the OH model (average % difference = -42%). At intermediate-temperatures, some of the test results are under-estimated and some are over-estimated. In most cases, the RH model was slightly closer to the tested values than the OH model. Both versions of the model had average percent differences of approximately 5%.

Figures 58 and 59 compare the backcalculated δ_{binder} values to those obtained from testing the recovered RAP binders. RAP 1 is shown while the other RAP source results are included in Appendix D. Trends were similar for all the RAP sources.

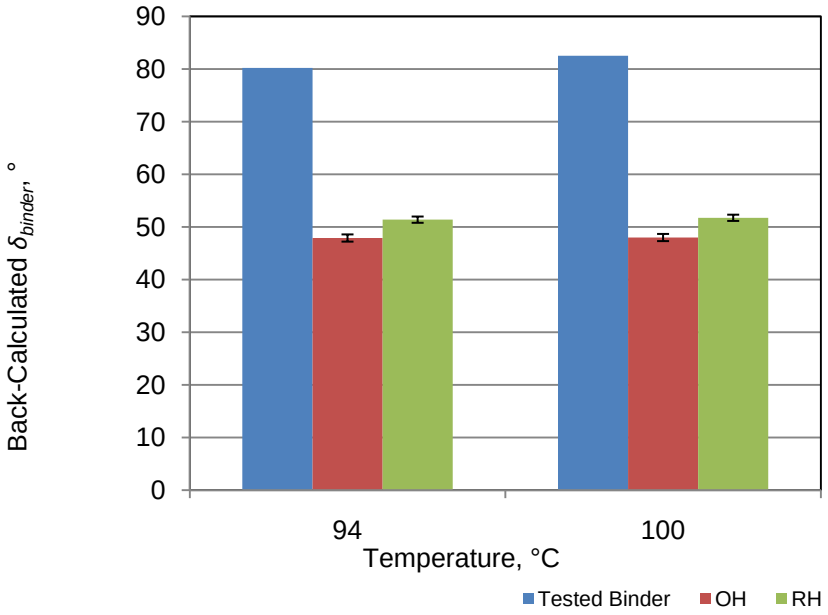

Figure 58 High-temperature Backcalculated δ_{binder} Results for RAP 1

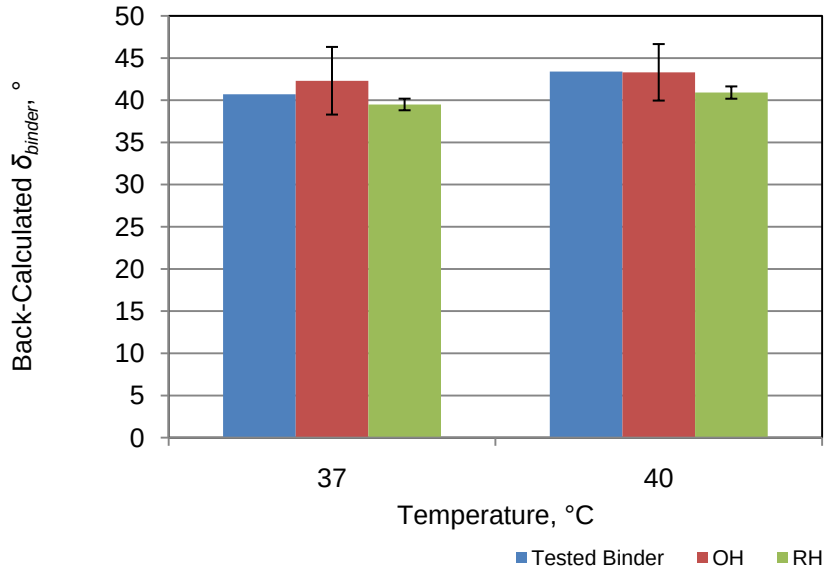

Figure 59 Intermediate-temperature Backcalculated δ_{binder} Results for RAP 1

At high-temperatures neither model was a close match for the tested binder data, with RAP 2 being the only exception. The models do a better job of estimating δ_{binder} at intermediate-temperatures. Table 20 shows the one-sample *t*-test results (α=0.05) comparing the tested and calculated δ_{binder} results.

Table 20 p-values for Backcalculated δ_{binder}

		δ_{binder}, °				
RAP	**Temp, °C**	**Binder**	**OH**	***p*-value**	**RH**	***p*-value**
1	94	80.2	47.9	0.000	51.4	0.000
	100	82.5	48.0	0.000	51.7	0.000
	37	40.7	42.3	0.481	39.5	0.040
	40	43.4	43.3	0.959	40.9	0.006
2	88	79.9	54.3	0.000	57.4	0.000
	94	82.5	54.7	0.000	58.0	0.000
	31	36.1	40.0	0.055	40.9	0.020
	34	37.8	42.0	0.058	42.7	0.024
3	94	80.3	40.9	0.015	43.6	0.501
	100	82.9	41.3	0.012	44.1	0.466
	31	36.4	29.1	0.051	30.8	0.658
	34	38.8	30.3	0.087	31.9	0.794
4	82	78.7	49.1	0.000	59.4	0.013
	88	81.6	49.6	0.000	60.7	0.015
	28	35.5	33.4	0.027	37.0	0.055
	31	37.7	35.3	0.028	38.9	0.058
5	82	80.3	44.2	0.000	46.9	0.000
	88	82.8	44.4	0.000	47.3	0.000
	25	37.9	32.2	0.245	30.1	0.004
	28	40.4	34.4	0.167	32.4	0.004

Based on the statistical analysis of the δ_{binder} results, only the RAP 3 δ_{binder} dataset calculated using the RH model was a statistical match for the tested δ_{binder} values at high-temperatures. Based on the average values for RAP 3, the statistical match is

most likely due to sample variability. All the other δ_{binder} datasets were lower than the tested values. At intermediate-temperatures, the δ_{binder} values calculated for all the RAPs except RAP 4 using the OH dataset were statistical matches for the tested δ_{binder} values. The RH dataset was a statistical match for RAPs 3 and 4 at intermediate-temperatures.

RAP Critical Temperatures

Figure 60 shows how the backcalculated binder critical temperatures values compared to the tested values for RAP 1.

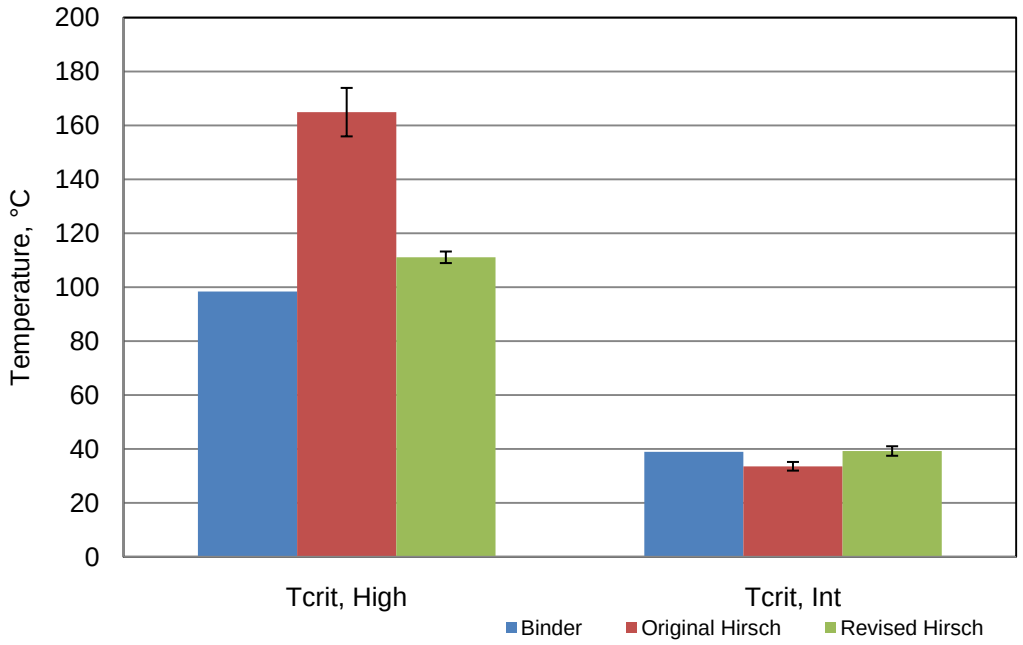

Figure 60 RAP 1 Backcalculated T_{crit}

Table 21 shows the one-sample *t*-test results (α=0.05) comparing the high and intermediate backcalculated critical temperatures to the tested values.

Table 21 p-Values for Comparison of Backcalculated Critical Temperature, °C

			OH		RH	
		Tested	**T_{crit}**	***p*-value**	**T_{crit}**	***p*-value**
RAP 1	High	98.4	164.9	0.001	111.1	0.001
	Int	38.9	33.5	0.007	39.2	0.762
RAP 2	High	91.8	126.2	0.040	93.8	0.487
	Int	31.3	29.7	0.301	34.5	0.102
RAP 3	High	95.0	152.8	0.003	127.7	0.006
	Int	32.2	29.2	0.104	35.3	0.118
RAP 4	High	87.3	110.4	0.002	82.1	0.045
	Int	29.4	23.4	0.010	30.1	0.633
RAP 5	High	85.7	150.8	0.009	125.9	0.015
	Int	26.0	12.4	0.002	17.2	0.005

At high-temperatures, the RH dataset provided backcalculated critical temperatures that were not a statistical match for the tested critical temperatures for any of the RAP sources except for RAP 2. At intermediate-temperatures, the RH results were a statistical match for all of the RAPs except for RAP 5. The critical temperatures calculated based on the OH results were statistical matches only for RAPs 2 and 4 at intermediate-temperatures.

As for the virgin materials, it is important to remember that the desired result of this project was a method for estimating the binder properties of the RAP sources, not necessarily to obtain an exact statistical match. Table 22 shows the high and intermediate PG grades of the RAP binders based on the average of the backcalculated results.

Table 22 Standard PG Grades for RAP Materials

	RAP 1		RAP 2		RAP 3		RAP 4		RAP 5	
	High	**Int**	**High**	**Int**	**High**	**Int**	**High**	**Int**	**High**	**Int**
Binder	94	40	88	34	94	34	82	31	82	28
OH	160	34	124	31	148	31	106	25	148	13
RH	106	40	88	37	124	37	82	31	124	19

At high-temperatures, the RH dataset did the best job of estimating the high standard PG grade of the RAP binders, although it was off by as many as seven standard grades in some cases. At intermediate-temperatures, the RH datasets were within one standard temperature of the intermediate-temperature grade for all the RAP sources except for RAP 5. The OH dataset over-estimated the high PG grade by a minimum of four and up to eleven standard grades. The intermediate-temperature PG grades were within two standard grades for all but RAP 5.

Summary

Based on the results presented in this chapter, the following conclusions can be made:

1. The original version of the Hirsch model was not calibrated for the DSR torsion bars and could not accurately predict G^*_{mix} using G^*_{binder} for either the virgin materials or the 100% RAP materials. A calibration of the model based on the virgin materials showed that the accuracy of the model compared to the tested G^*_{mix} results could be improved.

2. The original version of the Hirsch model over-estimated G^*_{binder} at high-temperatures by as much as 2,000% for some samples. The revised version of the model also tended to over-estimate G^*_{binder} at high-temperatures but in most cases was not as severe (40 – 65%). δ_{binder} was almost always under-estimated by both versions of the model and was usually better estimated using the original model results.
3. At intermediate-temperatures, the virgin G^*_{binder} values were all over-estimated by as much as 65% with no clear trend as to which version of the model is better. The original Hirsch model severely over-estimated the RAP G^*_{binder} as well, while the revised model under-estimated it for all but one RAP source. δ_{binder} also showed no clear trend at intermediate-temperatures as to which version of the Hirsch model was better.
4. When analyzing the estimated PG grades for the virgin binders, the results backcalculated using the revised version of the Hirsch model with the -4 aggregate gave to the closest estimate for the high and intermediate PG grade for both virgin binders. The PG 64-22 binder (which actually graded to be PG 70+25 based on its high and intermediate temperature properties) was estimated to be a PG 64+31(high and intermediate PG grades) based on the backcalculated results. The PG 76-22 binder (PG 76+22 based on its high and intermediate temperature properties) was estimated to be a PG 70+31.
5. The revised Hirsch model gave a closer estimate of the extracted binder RAP PG grades compared to the original Hirsch model results.

LABORATORY RAP BLENDS AND PLANT MIXES

A potential application for the torsion bar back-calculation procedure is the characterization of asphalt binder properties of HMA mixtures containing RAP. Currently there is no method for directly testing the asphalt binder properties of RAP blends other than using solvent extraction and recovery procedures to obtain the binder to test or by estimating the asphalt binder properties from blending charts (which also require recovered asphalt binder). If the backcalculation procedure can successfully identify the asphalt binder properties of mixes with RAP, then it may eliminate the need for asphalt binder testing to quantify changes in mixture stiffness due to increasing RAP content or to identify the maximum amount of RAP that can be added to a mix while still maintaining a target PG binder grade.

In this section of the project, the virgin and recovered binder high and intermediate critical temperatures obtained during previous testing were used to create blending charts for three of the RAP materials (RAP 2, RAP 3, and RAP 5). The recovered values were used instead of the backcalculated since this is the current method of creating blending charts according to AASHTO M323. Torsion bars made from laboratory HMA mixes containing three different percentages of RAP (20, 35, and 50%) were tested and their binder properties backcalculated using both versions of the model. The backcalculated values were compared to the critical temperatures estimated by the blending charts. Five plant-produced mixes were also tested to see how their backcalculated binder properties compared to the blending chart estimations.

Laboratory RAP Blends

The laboratory RAP blend evaluation was conducted using laboratory-produced mixes containing three of the RAP sources from the previous section. Mix designs were created using three percentages of RAP and test specimens were fabricated using both virgin binders. Aggregate gradations for the mixes were designed to be as similar as possible, accounting for the additional RAP aggregates. Figures 61-64 show an example of the master curves created from the average backcalculated G^*_{binder} values for RAP 2 with the virgin PG 64-22 binders. Also included in the figures are the G^*_{binder} master curves obtained from testing the recovered RAP 2 binder and the RTFO-aged virgin binder master curves. No recovery testing was done for these mixes; therefore, there are no master curves shown for the recovered asphalt binders from the individual blends.

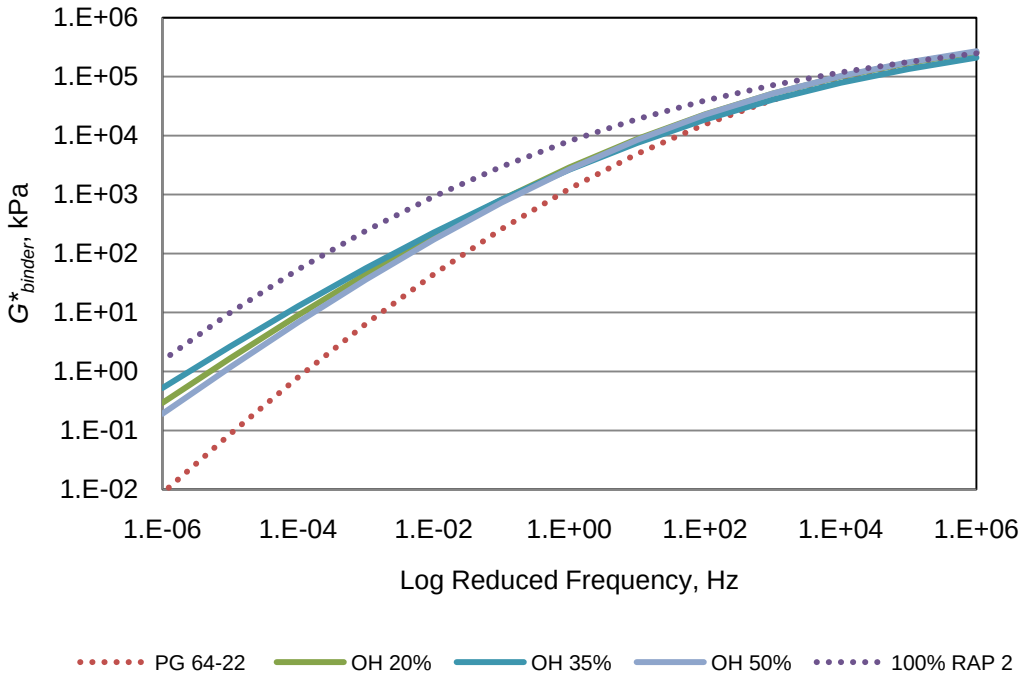

Figure 61 PG 64-22 RAP 2 Master Curve – OH Model

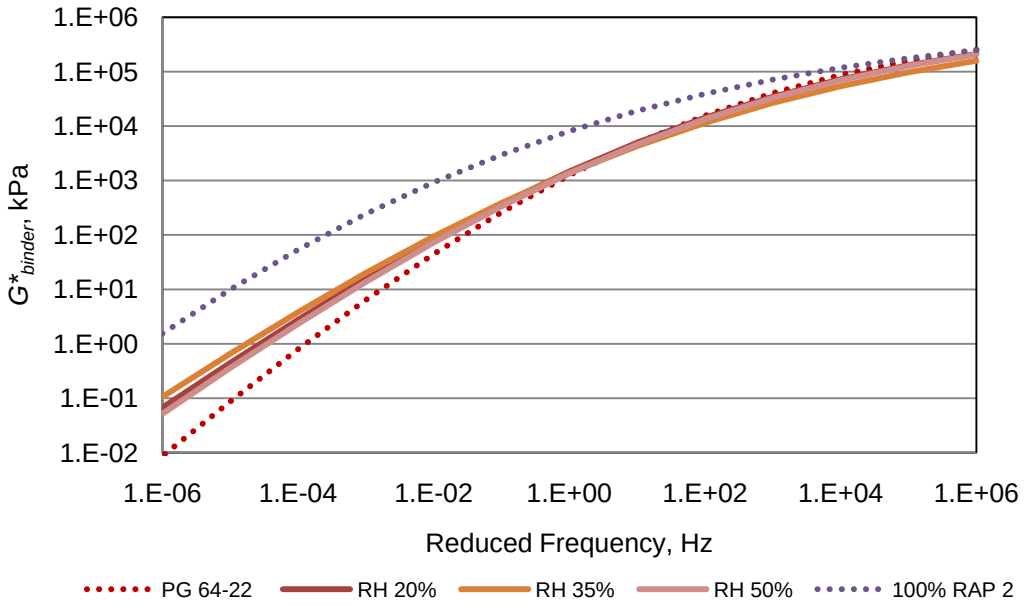

Figure 62 PG 64-22 RAP 2 Master Curve – RH Model

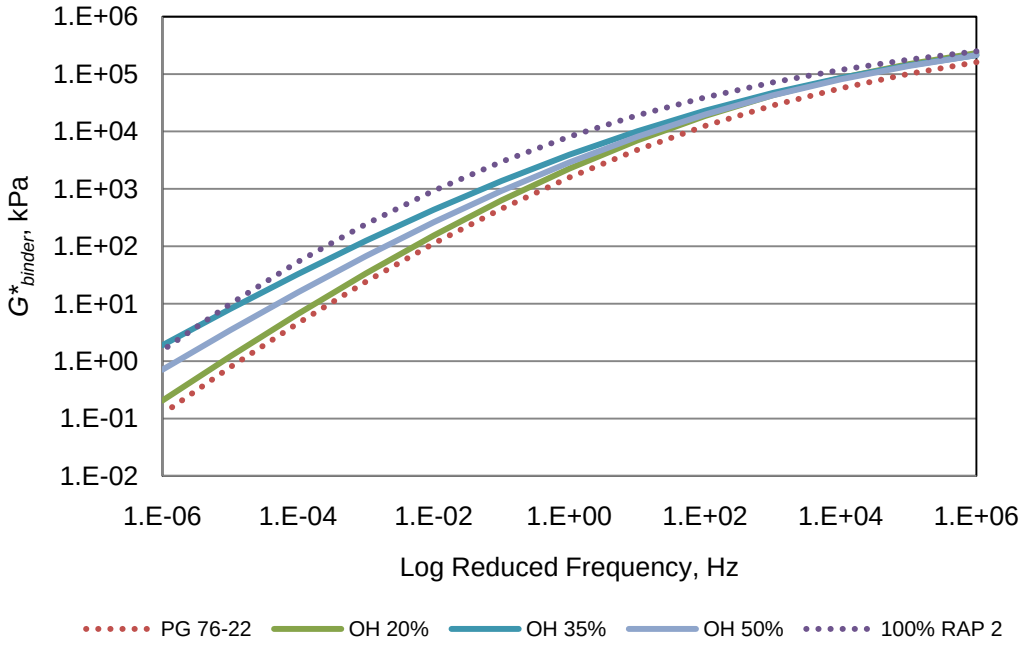

Figure 63 PG 76-22 RAP 2 Master Curve – OH Model

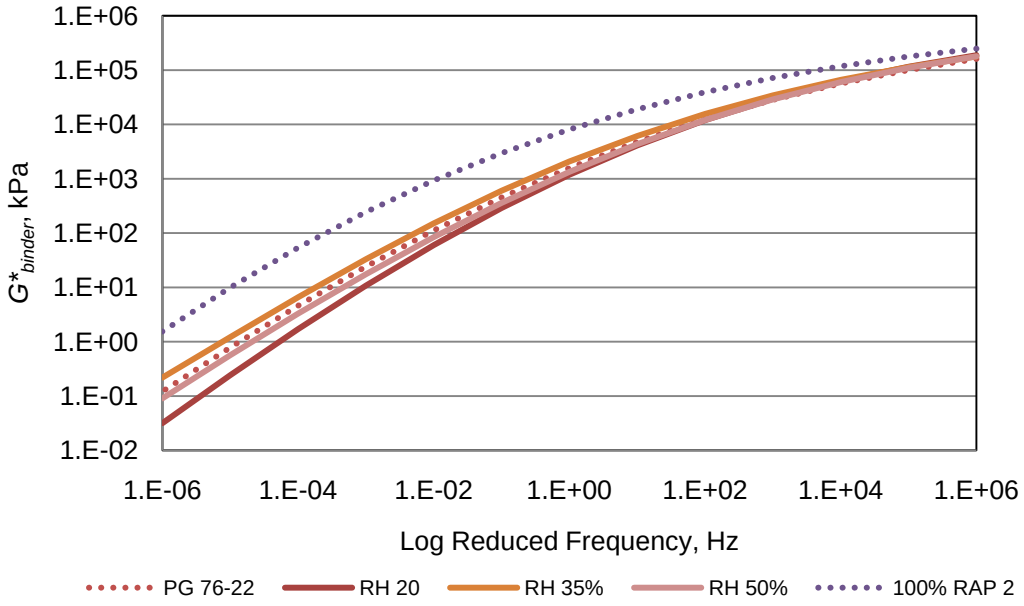

Figure 64 PG 76-22 RAP 2 Master Curve – RH Model

Trends for the other RAP blends were similar and the master curves for RAPs 3 and 5 are included in Appendix E, along with a summary of the backcalculated G^*_{binder} and δ_{binder} results. The expected behavior for RAP mixes is increased stiffness with increasing RAP content with the stiffness values for the blends being somewhere between the virgin and 100% RAP binder values. Neither version of the model appears to consistently rank the results from the different RAP contents in the expected manner for the RAP blends. In a few cases, the G^*_{binder} values backcalculated using the RH model for the RAP blends are softer than the virgin binder values. In other cases, the backcalculated G^*_{binder} values are stiffer than the recovered RAP binder master curve. In several cases, the 35% RAP blends appear to be stiffer than the 50% RAP blends.

Figure 65 shows the blending chart created for the laboratory blends containing RAP 2 and the PG 64-22 virgin binder. The high and intermediate critical temperatures for the virgin binder (0%) RAP and the recovered RAP 2 binder (100% RAP) were plotted on the chart and lines drawn from the 0 to 100% RAP conditions. From these lines, estimates were made for the high and intermediate critical temperatures at 20, 35, and 50% RAP. For the RAP 2 blends shown in Figure 65, the estimated high critical temperatures were found to be higher than the backcalculated critical temperatures. Blending charts for the other RAP sources are included in Appendix F.

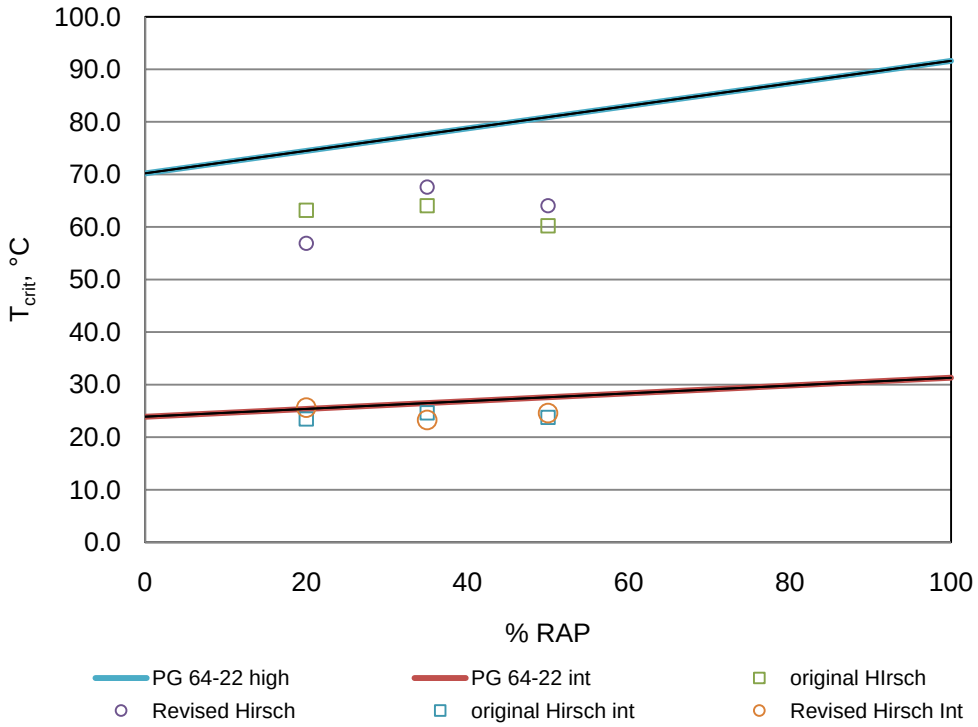

Figure 65 PG 64-22 RAP 2 Blending Chart

As can be seen from the figure, the back-calculation procedure was not successful at estimating the high-temperature binder properties of the RAP blends compared to the blending charts. For both versions of the Hirsch model, the high critical temperatures based on the backcalculated results were significantly lower than those estimated from the blending charts. For RAP 2, the backcalculated high critical temperatures are also not following the expected trends of increasing values with increasing RAP contents and are lower at 50% RAP than at the 35% and the 20% values.

At intermediate-temperatures, the backcalculated critical temperature results are a better match for the values estimated from the blending charts. A one-sample *t*-test

analysis (α=0.05) was used to compare the critical temperatures estimated from the blending charts to the backcalculated values for all the RAP and virgin binder combinations. Tables 23 and 24 show the average estimated and backcalculated critical temperatures and the p-values obtained from the statistical analysis.

Table 23 p-values for Laboratory RAP Blends with PG 64-22

			PG 64-22				
			Blending	OH		RH	
	% RAP	Range	Chart T_{crit}	T_{crit}	*p*-value	T_{crit}	*p*-value
RAP2	20%	High	74.5	63.2	0.009	56.9	0.003
		Int	25.4	23.5	0.188	26.6	0.327
	35%	High	77.7	64.0	0.002	56.6	0.001
		Int	26.5	24.6	0.024	27.8	0.102
	50%	High	80.9	60.2	0.000	55.8	0.001
		Int	27.6	23.8	0.029	26.8	0.202
RAP 3	20%	High	75.2	60.3	0.004	55.5	0.000
		Int	25.6	23.1	0.148	26.3	0.487
	35%	High	78.9	73.5	0.034	63.9	0.000
		Int	26.8	15.9	0.004	20.7	0.008
	50%	High	82.6	76.2	0.030	66.1	0.007
		Int	28.1	12.5	0.002	17.4	0.004
RAP 5	20%	High	73.3	63.0	0.066	62.5	0.070
		Int	24.3	24.4	0.968	28.2	0.457
	35%	High	75.6	66.1	0.026	60.9	0.038
		Int	24.6	17.7	0.003	20.6	0.006
	50%	High	78.0	68.3	0.014	64.7	0.001
		Int	25.0	20.1	0.060	25.0	0.993

Table 24 p-values for Laboratory RAP Blends with PG 76-22

			PG 76-22				
			Blending	OH		RH	
	% RAP	Temp.	Chart T_{crit}	T_{crit}	*p*-value	T_{crit}	*p*-value
RAP2	20%	High	81.2	63.6	0.001	56.3	0.004
		Int	23.5	25.6	0.001	28.1	0.001
	35%	High	83.2	67.6	0.003	61.0	0.005
		Int	25.0	23.3	0.163	26.8	0.123
	50%	High	85.1	64.0	0.002	57.5	0.011
		Int	26.5	24.6	0.074	28.3	0.216
RAP 3	20%	High	81.9	65.5	0.001	57.4	0.001
		Int	23.7	27.8	0.037	30.7	0.009
	35%	High	84.3	67.8	0.005	61.9	0.001
		Int	25.3	19.7	0.024	24.2	0.322
	50%	High	86.8	72.8	0.009	65.8	0.001
		Int	26.9	16.5	0.000	21.5	0.002
RAP 5	20%	High	80.0	67.6	0.004	61.1	0.000
		Int	22.5	21.7	0.539	24.3	0.273
	35%	High	81.1	68.4	0.000	62.7	0.000
		Int	23.1	19.6	0.013	23.3	0.738
	50%	High	82.2	70.2	0.004	65.1	0.002
		Int	23.8	18.3	0.001	21.9	0.011

The statistical analysis confirmed that neither model could provide backcalculated high critical temperatures that were a statistical match for the critical temperatures estimated from the blending charts. In all cases, the back-calculation under-estimated the binder properties.

At intermediate-temperatures, the RH model was a statistical match for the critical temperatures estimated from the blending chart for seven out of nine cases for the PG 64-22 binder. The OH model was only a statistical match in four cases. For the PG 76-22 test specimens at intermediate-temperatures, the RH model was a statistical

match in five out of nine cases while the OH model was only a statistical match in three cases.

Table 25 shows the results of a general linear model analysis of variance (ANOVA) test (α=0.05) with Tukey comparisons to determine if the effects of RAP content or model type were significant. No comparison was done between the two virgin binders or between the critical temperatures for the different RAP sources. Within the PG 64-22 or PG 76-22 columns for each RAP source, cells with the same letter designation are statistically the same.

The results shown in Table 25 indicate that while the backcalculated critical temperature can distinguish between changes in RAP percentage in some cases, especially for the 50% RAP case, it cannot always do so. The difference in critical temperatures between the two versions of the model was found to be statistically significant in all cases. Table 26 shows the final high and intermediate PG grades for the blends compared to the PG grades estimated from the blending charts.

Table 25 ANOVA Results for Laboratory Blends

			PG 64-22		PG 76-22	
		RAP, %	OH	RH	OH	RH
RAP 2	High Temps	20	A	C	A	C
		35	A	C	B	D
		50	B	D	B	D
	Int Temps	20	A	B	A	C
		35	A	B	AB	CD
		50	A	B	B	C
RAP 3	High Temps	20	A	D	A	D
		35	B	E	B	E
		50	C	F	C	F
	Int Temps	20	A	D	A	D
		35	B	E	B	E
		50	C	F	C	F
RAP 5	High Temps	20	A	B	A	D
		35	A	B	B	E
		50	A	B	C	F
	Int Temps	20	A	C	A	D
		35	AB	CD	B	E
		50	AB	C	C	F

Table 26 PG Grades for Laboratory Blends

		PG 64-22			PG 76-22		
	RAP, %	Blending Chart	OH	RH	Blending Chart	OH	RH
RAP 2	20	70	58	52	76	58	52
	35	76	64	64	82	52	58
	50	76	58	64	82	52	52
	20	28	25	28	25	28	31
	35	28	25	25	28	28	28
	50	28	25	25	28	28	31
RAP 3	20	70	58	64	76	52	52
	35	76	70	64	82	58	58
	50	82	76	70	82	64	64
	20	28	25	28	25	28	31
	35	28	16	22	28	22	25
	50	31	13	19	28	19	22
RAP 5	20	70	58	64	76	58	58
	35	70	64	64	76	58	58
	50	76	64	70	82	64	64
	20	25	22	22	25	28	25
	35	25	19	22	25	22	25
	50	25	22	19	25	25	22

At high-temperatures, the backcalculated PG grades were at least one grade and as many as three grades lower than those estimated from the blending charts for all of the blends. At intermediate-temperatures, there was no trend in the results, with some RAP/binder combinations having lower intermediate grades than those estimated from the blending charts and some having higher intermediate PG grades.

Plant Mix Analysis

The final portion of the project involved testing plant-produced HMA to determine if the back-calculation method could identify the properties of the asphalt binder in the mix. Torsion bar test specimens were constructed from five plant-produced mixes

containing various percentages of RAP and either a PG 64-22 or PG 76-22 virgin binder. Asphalt binder properties were backcalculated from the torsion results and compared to those obtained by testing asphalt binder recovered using solvent extraction and recovery procedures. The backcalculated binder results were also compared to the critical temperatures estimated from blending charts created using the recovered RAP binder properties for the RAP sources used in the mixes.

Figures 66 – 69 show the backcalculated G^*_{binder} master curves compared to the G^*_{binder} obtained from the recovered binder for four of the mixes. Plant mix C did not have enough material to do extractions and therefore is not shown.

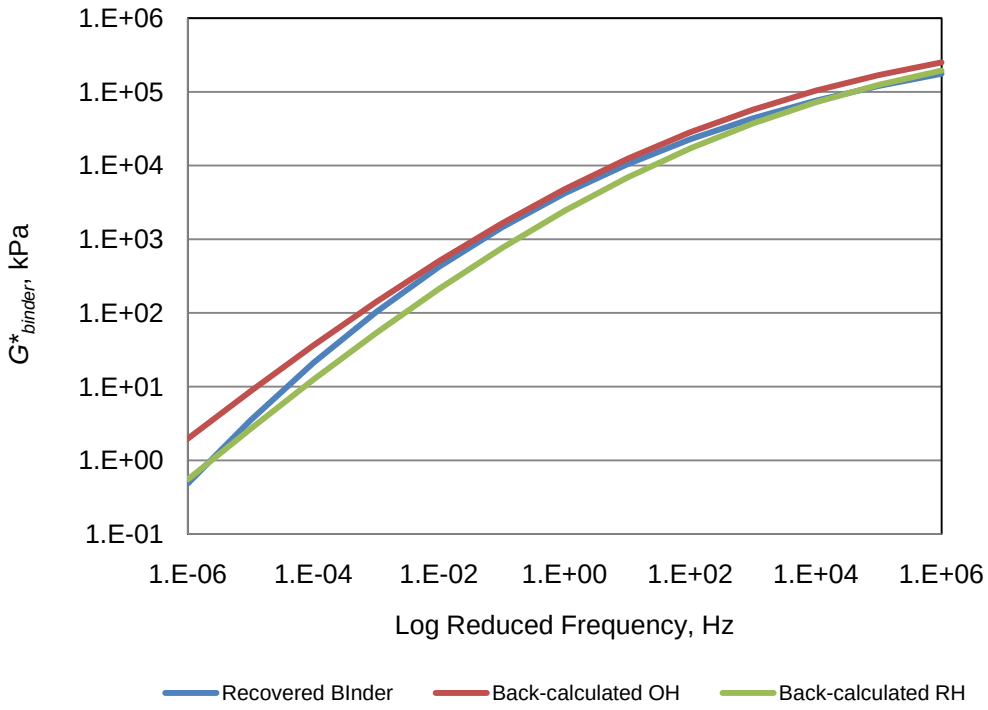

Figure 66 G^*_{binder} Master Curves – Plant Mix A

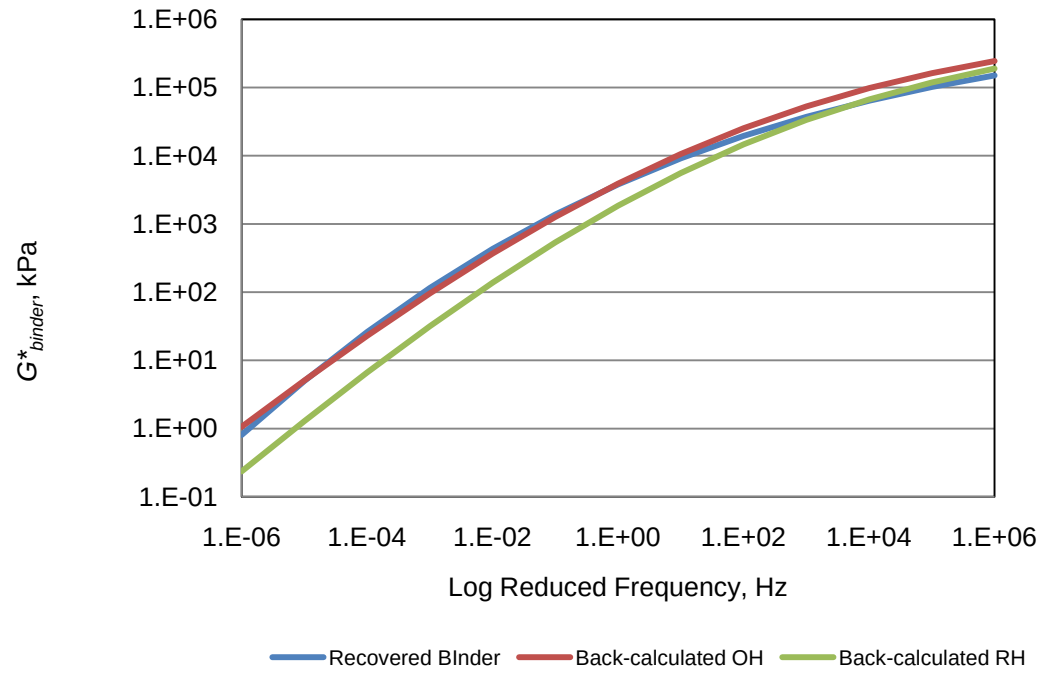

Figure 67 G^*_{binder} Master Curves – Plant Mix B

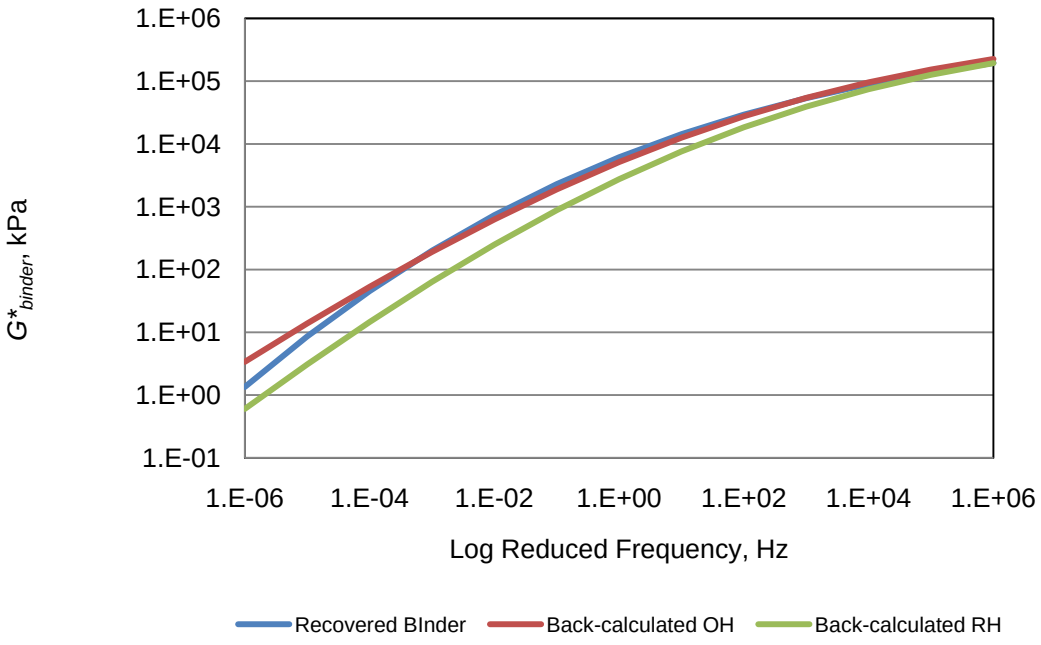

Figure 68 G^*_{binder} Master Curves – Plant Mix D

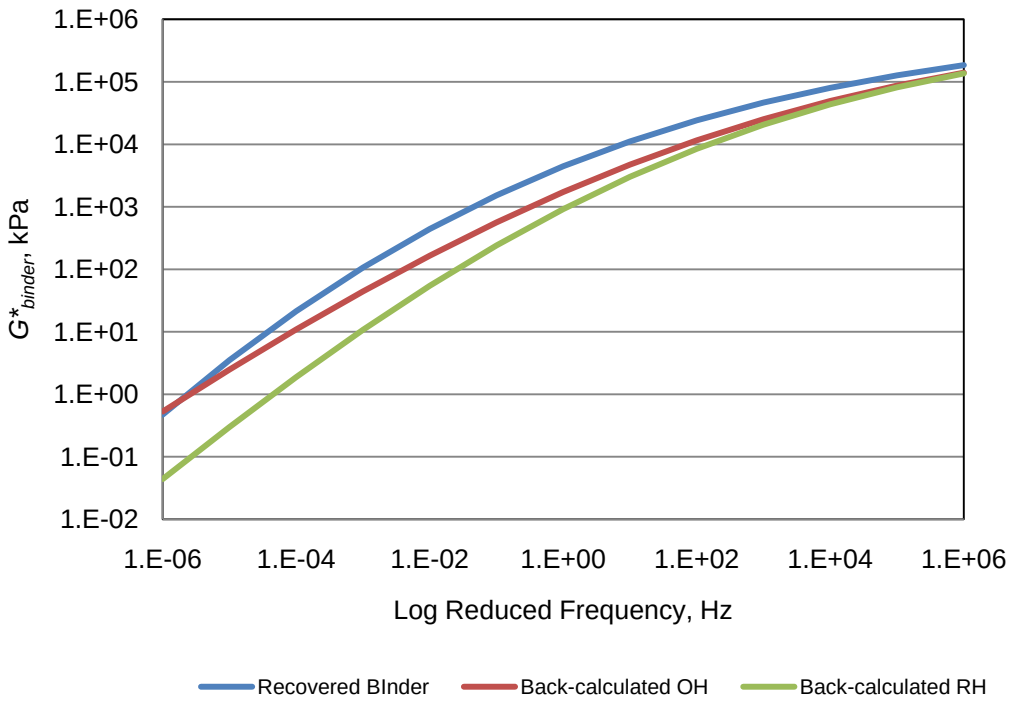

Figure 69 G^*_{binder} Master Curves – Plant Mix E

The figures show varying degrees of agreement between the recovered asphalt binder and the results backcalculated using the OH model. The master curves for mixes A, B and D are very similar for a portion of the curve, then diverge at the lower frequencies. The master curve backcalculated for mix E using the OH model is stiffer than the recovered binder master curve. The RH model master curves are less stiff than the recovered binder master curve for all of the mixes.

Plant mixes B and C contain 5% RAS in addition to RAP. The blending charts for these materials were created using a two-step process to account for the additional binder stiffness from the RAS binder. First, blending charts were made using the virgin binder and recovered RAS binder critical temperatures. The critical temperatures for a mix containing 5% RAS were estimated from the blending chart. A second blending

chart was then created using the 5% RAS binder critical temperatures as the 0% RAP condition along with the recovered RAP properties. The second blending chart was used to compare the backcalculated results for these two mixes. Figures 70-74 show the blending charts created for the plant mixes using the recovered RAP binder properties.

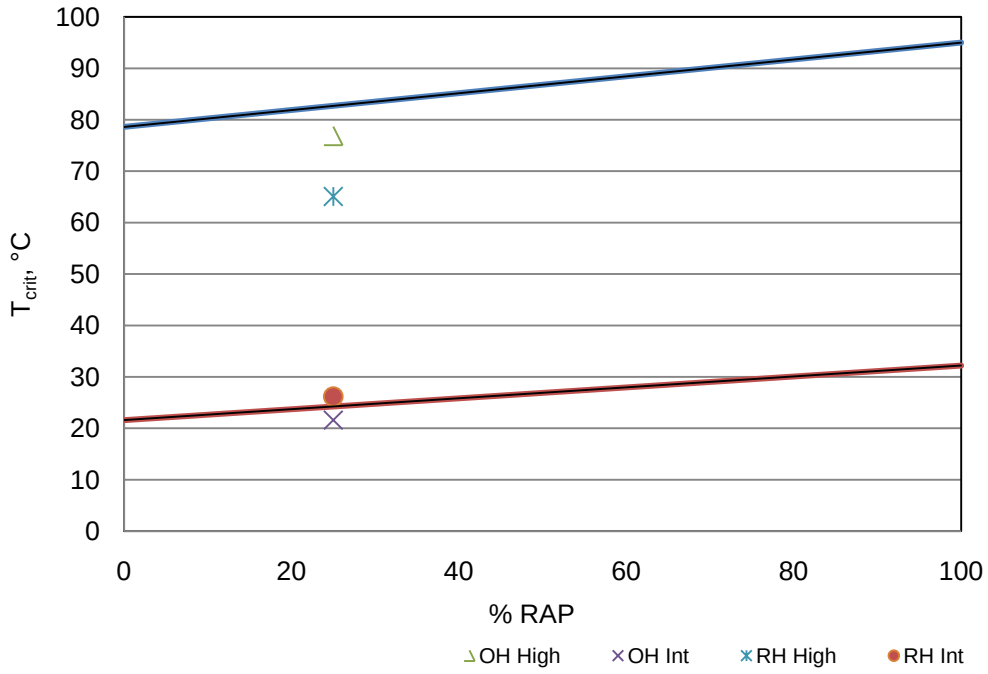

Figure 70 Plant Mix A Blending Chart

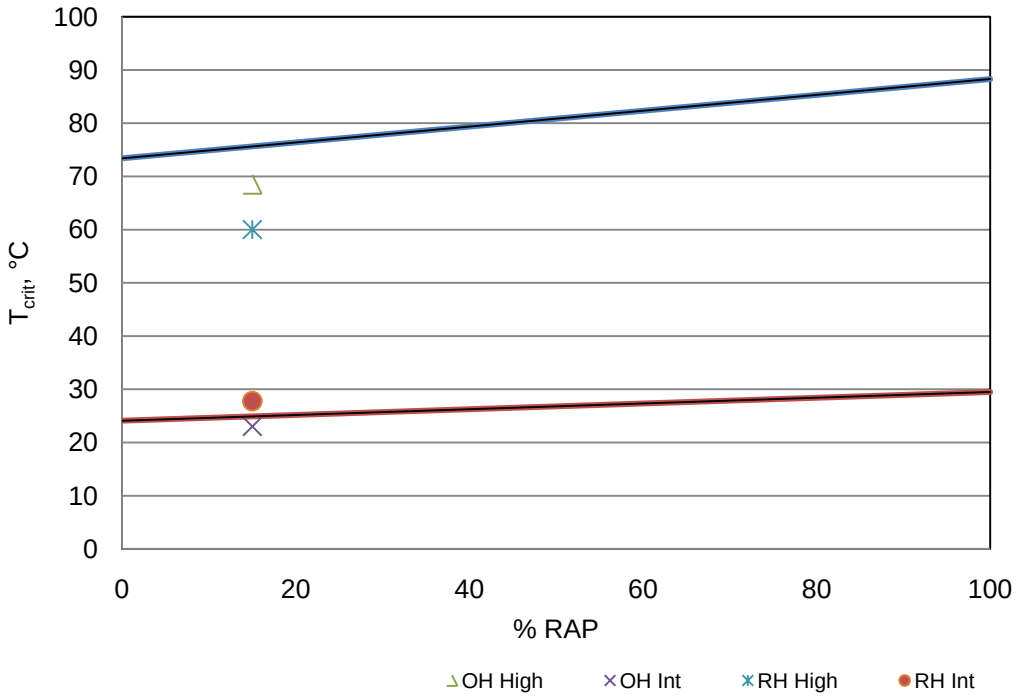

Figure 71 Plant Mix B Blending Chart

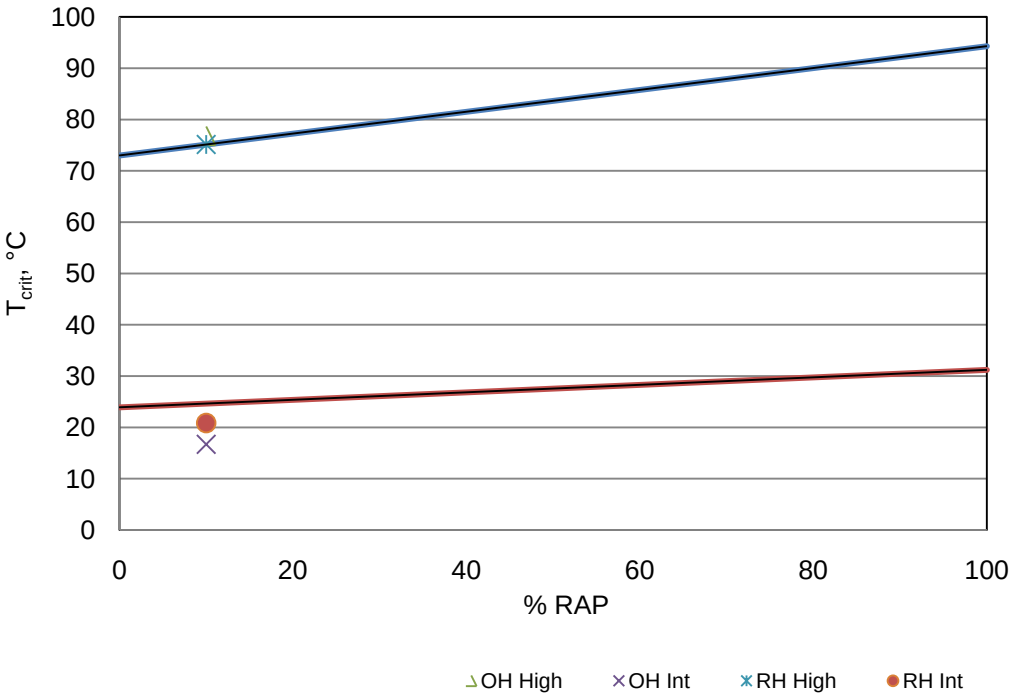

Figure 72 Plant Mix C Blending Chart

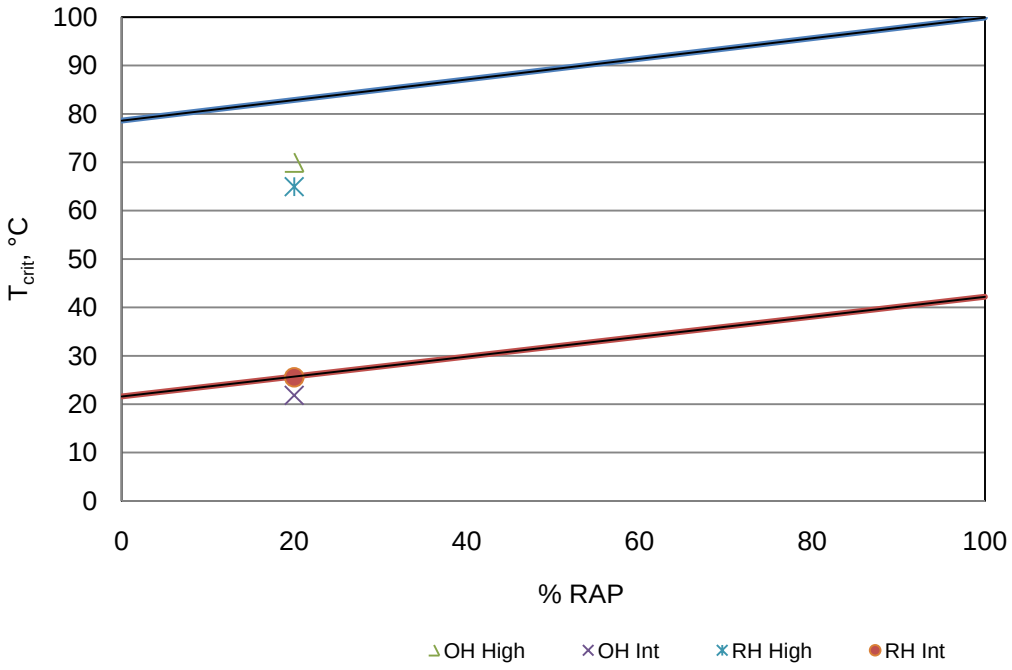

Figure 73 Plant Mix D Blending Chart

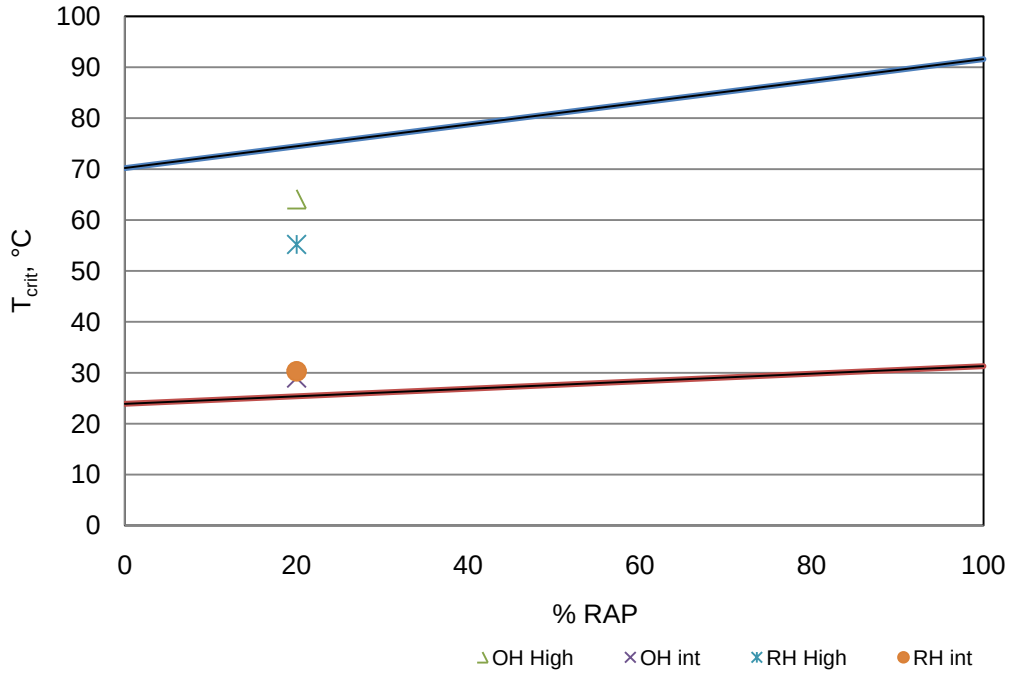

Figure 74 Plant Mix E Blending Chart

The blending charts show that the backcalculated high critical temperatures for the plant-produced mixes were usually lower than the estimated critical temperatures. The intermediate backcalculated critical temperatures match those estimated from the blending charts fairly well in most cases. Table 27 shows results of a one sample *t*-test (α=0.05) comparison of backcalculated and estimated critical temperatures.

Table 27 p-values Comparing Backcalculated Critical Temperature to Blending Chart Values

	T_{crit}, High, °C					T_{crit}, Intermediate, °C				
Mix	**Blending Chart**	**OH**	**p-value**	**RH**	**p-value**	**Blending Chart**	**OH**	**p-value**	**RH**	**p-value**
A	82.7	76.9	0.079	65.1	0.005	24.3	21.6	0.072	26.2	0.234
B	75.6	68.5	0.002	60.0	0.005	24.9	23.0	0.248	27.8	0.308
C	75.1	76.8	0.030	75.1	0.972	24.6	16.7	0.002	20.8	0.012
D	82.9	70.0	0.004	65.0	0.003	25.7	21.8	0.087	25.5	0.916
E	74.5	64.1	0.001	55.2	0.001	25.4	29.0	0.008	30.3	0.002

The statistical analysis shows that only the high critical temperatures backcalculated for plant mix A using the original Hirsch model and plant mix C using the revised Hirsch model match the values estimated from the blending chart. All the other plant mix backcalculated high critical temperatures were significantly lower than the blending chart values. At intermediate-temperatures, only plant mixes C and E did not match the blending chart values for either version of the model. Plant mixes A, B, and D backcalculated intermediate critical temperatures were a statistical match for the blending chart values regardless of the model used.

Table 28 shows the statistical analysis results using a 1-sample *t*-test (α=0. 05) comparing the critical temperatures from the recovered binder testing and those backcalculated from the torsion bar results.

Table 28 p-value Results Comparing Backcalculated to Tested Recovered Binder Properties

	High Critical Temperture, °C					Intermediate Critical Temperature, °C				
Mix	Rec. Binder	OH	p-value	RH	p-value	Rec. Binder	OH	p-value	RH	p-value
A	90.1	76.9	0.017	65.1	0.003	23.3	21.6	0.156	26.2	0.123
B	86.4	68.5	0.000	60.0	0.002	24.2	23.0	0.417	27.8	0.235
D	93.5	70.0	0.001	65.0	0.001	26.7	21.8	0.057	25.5	0.463
E	87.2	64.1	0.000	55.2	0.000	24.1	29.0	0.004	30.3	0.001

At high-temperatures, none of the backcalculated critical temperatures for either version of the model were a statistical match for the tested recovered binder critical temperatures. At intermediate-temperatures, only the results for plant mix E were not statistical matches.

Table 29 shows the final PG grades of the backcalculated plant mix binders compared to those from the recovered binder testing and from the blending chart.

Table 29 Comparison of Backcalculated PG Grades

	A		B		C		D		E	
	High	Int	High	Int	High	Int	High	Int	High	Int
Binder	88	25	82	25			94	28	82	25
Blending Chart	82	25	70	25	70	25	82	28	70	28
OH	76	22	76	22	76	19	70	22	64	31
RH	64	28	64	28	70	22	64	28	52	31

The high PG grades for the OH back-calculations matched those from the blending chart within one PG grade except plant mix D. Intermediate PG grades for the OH model matched well for mixes A, B, and E but were two PG grades off for mixes C and D. The RH back-calculations did not match the high PG grades from the blending charts except for mix C. Intermediate PG grades for the RH back-calculations were

within one PG grade. All the backcalculated PG grades were under-estimated compared to those from the recovered binder tests.

Summary

The following observations were made from the results of the laboratory and plant-produced mixes:

1. Neither version of the Hirsch model could accurately estimate the high critical temperatures of the laboratory mixes. Both versions under-estimated the high-temperature grade by at least one standard PG grade. In many cases, the backcalculated critical temperature was lower than the high critical temperature for the virgin binder. The revised Hirsch model was a better match than the original Hirsch model for the intermediate critical temperatures.
2. Neither version of the model could consistently identify changes in asphalt binder stiffness due to increasing RAP content and showed the 50% RAP case to be less stiff than the 35% case in several instances. The stiffer PG 76-22 mixes better identified changes in mix stiffness than the PG 64-22 mixes.
3. As with the laboratory mixes, both versions of the model under-estimated the high critical temperatures of the plant mix. The revised Hirsch model backcalculated values were lower than the original Hirsch model. At intermediate-temperatures, the backcalculated values for both versions of the model were more likely to be a statistical match for the blending chart critical

temperatures. The same was true for the backcalculated critical temperatures (high and Intermediate) compared to the recovered asphalt binder values.

CONCLUSIONS

The results of this study led to the following conclusions:

1. The current extraction/recovery methods used to characterize RAP binders provide an estimate of binder properties that may or may not match what is actually in an asphalt mix.
2. The torsion bar procedure used in this project provided reasonable values of G^*_{mix} at differing frequencies and temperatures. The repeatability of the test was adequate (COV less than 15% in most cases) and the data trends match those seen in other mixture tests.
3. Black Space diagrams for the torsion bar data show that the data appears to be of adequate quality for creating master curves. The softer virgin binder specimens had issues with data quality at high-temperatures and low frequency values, most likely due to variability in the dataset at these levels.
4. The torsion bar results appear to distinguish between samples with differing binder stiffness in most cases, although they had difficulty doing so with the virgin binders.
5. The size of the aggregate in the virgin torsion bar specimens appeared to have an effect on the stiffness values. It is unclear whether this effect is significant due to differences in the air voids between the sets of samples.

6. The original Hirsch model formula could not accurately forward calculate G^*_{mix} using either the virgin G^*_{binder} or the recovered RAP G^*_{binder}. Calculated G^*_{mix} values were usually under-estimated for both sets of materials.
7. A calibration of the Hirsch model using the virgin binder data resulted in a revised model that provided an improved correlation between tested and calculated G^*_{mix} for the virgin binder specimens. Calculation of G^*_{mix} using the revised Hirsch model also showed an improved correlation to the tested G^*_{mix} for the 100% RAP specimens, although the calculated values were still under-estimated compared to the tested values.
8. Both versions of the model had problems with scatter in the backcalculated results at the high-temperature/low frequency condition. Both versions also had problems with the limitations of the model at low-temperature/high frequency values and large variability between the backcalculated results compared to that of the G^*_{mix} data (up to 83% in some cases).
9. For the virgin materials, neither verson of the model could accurately predict the PG grade of the binders. The original Hirsch with -4 aggregate dataset (PG 76+34) or the revised Hirsch with passing -4 dataset (PG 64+31) gave the closest estimate of PG temperature for the PG 64-22 results. The revised Hirsch with passing -4 aggregate dataset gave the closest estimate for the PG 76-22 at high temperatures (PG 70) while the original Hirsch with passing -8 aggregate dataset gave the closest estimate at intermediate temperatures (PG +25).

10. Neither of the versions of the model could accurately estimate the PG grade of the RAP binders compared to the recovered RAP binder tests in all cases. When estimating the PG grades for the 100% RAP materials, the revised HIrsch model gave the closest estimate of high PG grade, with exact matches for two of the five RAP sources. Estimated PG grades for the other three RAP sources were within two and seven PG grades. At intermediate temperatures, both versions of the model estimated PG grades that were within one or two grades for all but one RAP.
11. Neither model could accurately predict the high-temperature PG grades of laboratory or plant-produced mixes. Comparisons were made using both blending charts and recovered binder from the actual mixes (plant mixes only). In all cases, the backcalculated results were significantly lower than the actual tested values.
12. Both models adequately estimated the intermediate-temperature PG grades of the laboratory blends and plant-produced mixes. Backcalculated PG grades were within 1 standard grade in most cases.
13. The results backcalculated from the torsion bars G^*_{mix} for the laboratory mixes were not able to distinguish between changes in binder stiffness due to increasing RAP content.

Overall, the torsion bar test procedure for measuring G^*_{mix} appear to be promising, but much more work is needed to improve repeatability. The values of G^*_{mix} it provides are of reasonable quality and provide the expected trends with changes in materials and testing conditions. Repeatability may be improved in the future by using tighter controls

on air voids so that the percent of air voids does not vary by more than 0.5% between test specimens. Air voids should also be kept to the normal ranges used in asphalt mixture testing. The air voids seen in the torsion bars were several percent higher than normal target values. Repeatability may also be improved by using a larger specimen size than the 5.5-mm thick by 11.5-mm wide by 50-mm long bars used in this research. Finally, repeatability may be improved with a better quality saw blade than the one used to cut the tested specimens. Using the tile saw, it was difficult to cut test specimens that had similar dimensions and flawless surfaces.

The Hirsch model back-calculation procedure may have some promise as a means of estimating the PG grades of RAP materials, but needs much more work to improve accuracy and reduce variability in the backcalculate data. The calibration process described in this report improved the estimated high temperature PG grades, but still gives values that are over- or under-estimated by at least one grade. A more thorough calibration using multiple binder and aggregate combinations may provide a better calibration of the model. The results obtained from the model may also be improved by using larger test specimens with lower percentages of air voids. This will lead to higher G^*_{mix} values which may be handled better by the model.

The back-calculation procedure does not appear to be a good candidate for quality control of laboratory- and plant-produced mixes. The backcalculated PG grades for the high-temperature tests did a poor job of estimating the binder properties for these mixes and neither version of the model could consistently distinguish between different RAP contents.

REFERENCES

1. "Average Cost of Asphalt Cement Based on the NCDOT Liquid Index" http://www.stwcorp.com/en/34/Default.aspx?&Year=2012.

2. "Oklahoma Department of Transportation Monthly Asphalt Binder Price Index" http://www.okladot.state.ok.us/contractadmin/pdfs/binder-index.pdf.

3. Fournier, Paul. "What's Driving Asphalt Prices Up?" *www.acppubs.com,* http://www.superpave.psu.edu/downloads/pdf/What%27s%20driving%20asphalt.pdf, October, 2008.

4. "Recycled HMA" www.asphaltwa.com, http://www.asphaltwa.com/2010/09/18/pavement-types-recycled-hma, 2010.

5. "Reclaimed Asphalt Pavement" www.graniterock.com, http://www.graniterock.com/technical_notes/reclaimed_asphalt_pavement.html

6. McDaniel, R., H. Soleymani, R. Anderson, P. Turner, and R. Peterson. *NCHRP Web Document 30: Recommended Use of Reclaimed Asphalt Pavement in the Superpave Mix Design Method*, Transportation Research Board, National Research Council, Washington, D.C., 2000.

7. Peterson, R.L., H.R. Soleymani, R.M. Anderson, and R.S. McDaniel. "Recovery and Testing of RAP Binders from Recycled Asphalt Pavements," *Journal of the Association of Asphalt Paving Technologists*, Vol. 69, 2000.

8. VWR Scientific Price Sheet (2011).

9. Abson, G. "Method and Apparatus for the Recovery of Asphalt*,"* Proceedings ASTM Vol II, 1933.

10. Burr, B.L., R.R. Davison, C.J. Glover, and J.A. Bullin. "Solvent Removal from Asphalt," *Transportation Research Record 1269*, Transportation Research Board, National Research Council, Washington, D.C., 1990.

11. Soleymani, H., H. Bahia, and A. Bergan. "Time-Temperature Dependency of Blended and Rejuvenated RAP Binders," *Journal of the Association of Asphalt Paving Technologists*, Vol. 68, 1999

12. McDaniel, S.R., and A. Shah. “Use of Reclaimed Asphalt Pavement (RAP) Under Superpave Specifications,” *Journal of the Association of Asphalt Paving Technologists*, Vol. 72, 2003.

13. Daniel, J.S., J.L. Pochily, and D.M. Boisvert. “Can More Reclaimed Asphalt Pavement be Added?” *Transportation Research Record No. 2180*, Transportation Research Board of the National Academies, Washington, D.C., 2010.

14. Hajj, E.Y., P.E. Sebaaly, L. Loria, K. Said. Kass, T. Liske. “Impact of High RAP Content on the Performance Characteristics of Asphalt Mixtures in Manitoba,” Paper presented at The Innovative Developments in Sustainable Pavements Session of the 2011 Annual Conference of the Transportation Association of Canada, 2011.

15. Mogawer, W.S., T. Bennert, J.S. Daniel, R. Bonaquist, A. Austerman, A. Booshehrian. “Performance Characteristics of Plant Produced High RAP Mixtures,” presented at the 87th Annual Meeting of the Association of Asphalt Paving Technologists, Austin, TX., 2012.

16. McDaniel, R.S., A. Shah, and G. Huber. “Investigation of Low- and High-Temperature Properties of Plant-Produced RAP Mixtures,” FHWA-HRT-11-058, Federal Highway Administration, 2012.

17. Zhao, S., B.Huang, X.Shu, X. Jia, and M. Woods. “Laboratory Performance Evaluation of Warm Mix Asphalt Containing High Percentages of RAP,” Paper presented at the Transportation Research Board Annual Meeting, Washington, D.C., 2012.

18. Roque, R., B. Birgisson, C. Drakos, and B. Dietrich. “Development and Field Evaluation of Energy-Based Criteria for Top-down Cracking Performance of Hot Mix Asphalt,” *Journal of the Association of Asphalt Paving Technologists, Vol. 73*, 2004.

19. Zofka, A., M.O. Marasteanu, T.R. Clyne, X. Li, and O. Hoffmann. “Development of Simple Asphalt Test for Determination of RAP Blending Charts,” *Report 2004-44*, Minnesota Department of Transportation, St. Paul, MN, 2004.

20. Zofka, A., Mihai Marasteanu, X. Li, T. Clyne, and J. McGraw. “Simple Method to Obtain Asphalt Binders Low-temperature Properties from Asphalt Mixtures Properties,” *Journal of the Association of Asphalt Paving Technologists, Vol.74*, 2005.

21. Velasquez, R., M. Marasteanu, J. Labuz, and M. Turos. “Evaluation of Bending Beam Rheometer for Characterization of Asphalt Mixtures, “*Journal of the Association of Asphalt Paving Technologists, Vol 79,* 2010.

22. Bennert, T., and R. Dongre. “A Backcalculation Method to Determine Effective Asphalt Binder Properties of RAP Mixtures,” *Transportation Research Record 2179*, Transportation Research Board, National Research Council, Washington, D.C., 2010.

23. Tran, N., A. Taylor, R. West, and A. Kvasnak. “Evaluation of Predictive Models for Determination of Binder Critical High-temperature from Mixture Properties,” *Transportation Research Record 2179*, Transportation Research Board, National Research Council, Washington, D.C., 2010.

24. Swiertz, D., E. Mahmoud, and H.U. Bahia. “Estimating the Effect of Recycled Asphalt Pavements and Asphalt Shingles on Fresh Binder, Low-Temperature Properties without Extraction and Recovery,” *Transportation Research Record No. 2208,* Transportation Research Board of the National Academies, Washington, D.C., 2011.

25. Performance Graded Asphalt Binder Specification and Testing, *Asphalt Institute Superpave Series No. 1 (SP-1),* Lexington, KY., 1997.

26. Javed, B., and M.W. Witczak. “Development of a New Revised Version of the Witczak E* Predictive Model for Hot Mix Asphalt Mixtures,” *Journal of the Association of Asphalt Paving Technologists, Vol. 75*, 2006.

27. Christensen, D.W., T. Pellinen, and R. Bonaquist. “Hirsch Model for Estimating the Modulus of Asphalt Concrete,” *Journal of the Association of Asphalt Paving Technologists, Vol. 72*, 2003.

28. Christensen, D.W., and D.A. Anderson. “Interpretation of Dynamic Mechanical Test Data for Paving Grade Asphalt Cements, *Journal of the Association of Asphalt Paving Technologists, Vol. 62*, 1992.

29. Rowe, G.M., and M.J. Sharrock. “Alternate Shift Factor Relationship for Describing the Temperature Dependency of the Visco-Elastic Behaviour of Asphalt Materials,” *Transportation Research Record No. 2208,* Transportation Research Board of the National Academies, Washington, D.C., 2011.

30. Rowe, G. “Phase Angle Determination and Interrelationships within Bituminous Materials,” Presented at 45th Petersen Asphalt Research Conference, Laramie, WY., 2008.

31. Dongre, R., L. Myers, J. D'Angelo, C. Paugh, and J. Gudimettla. "Field Evaluation of Witczak and Hirsch Models for Predicting Dynamic Modulus of Hot-Mix Asphalt," *Journal of the Association of Asphalt Paving Technologists, Vol. 74*, 2005.

Appendix A

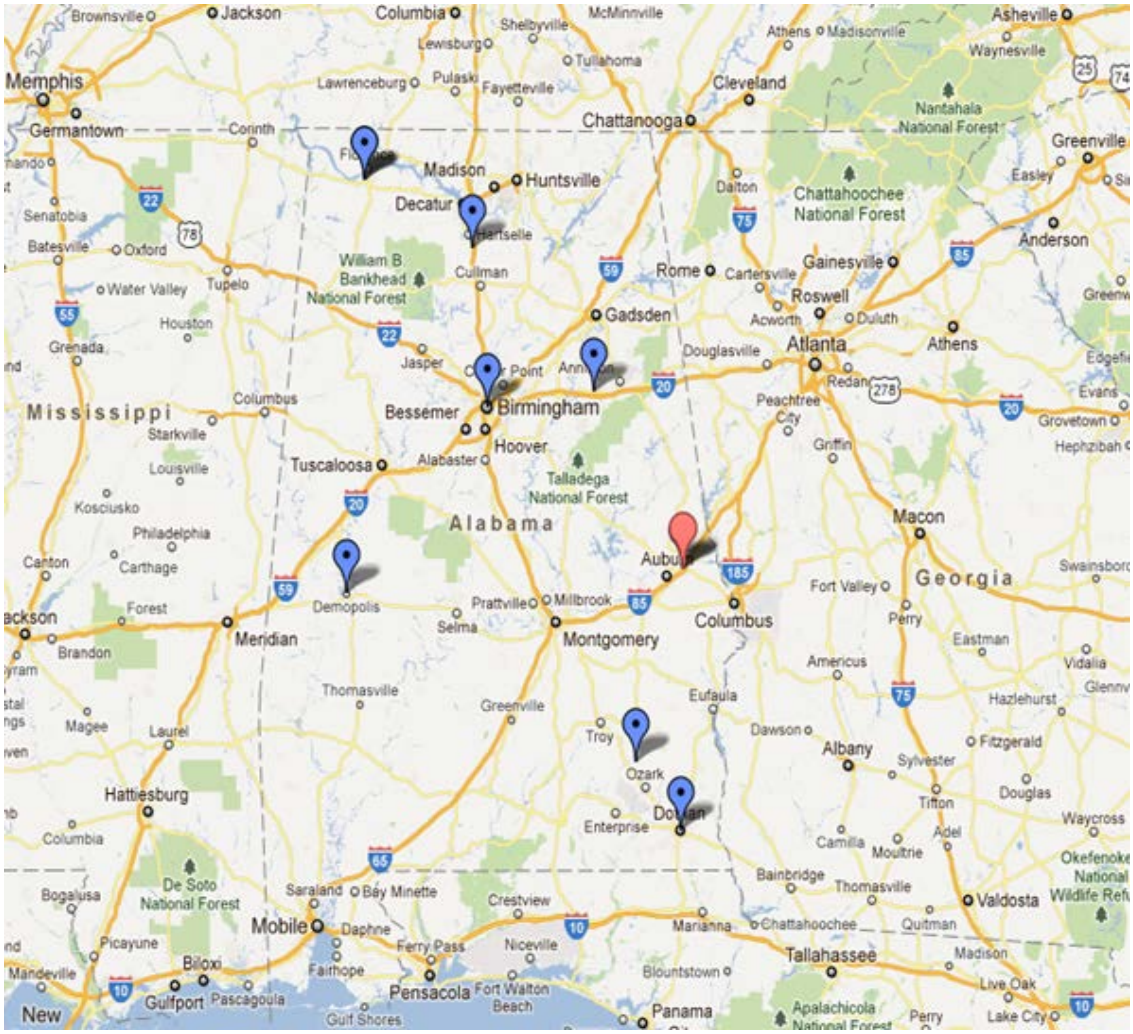

Figure A-1 Alabama Contractor Locations

Appendix B

The following section describes the process used to determine backcalculated values of G^*_{binder} and δ_{binder} based on DSR torsion bar results. The example calculation shown uses the original version of the Hirsch model. The procedure used for the revised version was identical with the exception of the formula used.

1. Obtain a set of torsion bar G^*_{mix} data as shown in Table B-1:

Table B-1 Sample Torsion Bar Results

Temp	frequency	|G*|	delta
°C	Hz	Pa	degrees
20	0.1	1.458E+09	20.82
20	1	2.250E+09	16.92
20	10	3.251E+09	14.26
30	0.1	6.409E+08	27.65
30	1	1.139E+09	23.01
30	10	1.873E+09	19.24
40	0.1	2.695E+08	31.49
40	1	5.231E+08	28.63
40	10	9.744E+08	24.99
50	0.1	1.226E+08	32.83
50	1	2.444E+08	32.09
50	10	5.028E+08	30.44
60	0.1	5.691E+07	31.80
60	1	1.078E+08	33.87
60	10	2.297E+08	34.89

2. Create a spreadsheet as shown in Table B-2 to determine the value of backcalculated G^*_{binder} that will provide predicted G^*_{mix} equal to measured G^*_{mix} using equations 2 and 3. This can be done by either manually changing the values of G^*_{binder} or by setting up a Microsoft Excel solver or goal-seek function.

Table B-2 Iterative Spreadsheet to solve for Backcalculated G^*_{binder}

Temp	Freq	Measured G^*_{mix}		Volumetrics (%)		Backcalculated G^*_{binder}		Pc	Predicted G^*_{mix}	Difference
(oC)	(Hz)	Pa	(psi)	VMA	VFA	(psi)	kPa		(psi)	
20	0.10	1.46E+09	211465.02	15.7	53.6	1,174.7	8099.2	0.41	211465	0
20	1.00	2.25E+09	3.26E+05	15.7	53.6	4,418.8	30466.7	0.63	326335	0
20	10.00	3.25E+09	4.72E+05	15.7	53.6	47,747.8	329209.2	0.90	471518	0
30	0.10	6.41E+08	9.30E+04	15.7	53.6	215.2	1484.0	0.18	92955	0
30	1.00	1.14E+09	1.65E+05	15.7	53.6	663.3	4573.1	0.32	165198	0
30	10.00	1.87E+09	2.72E+05	15.7	53.6	2,342.1	16148.1	0.53	271656	0
40	0.10	2.70E+08	3.91E+04	15.7	53.6	49.6	342.2	0.08	39088	0
40	1.00	5.23E+08	7.59E+04	15.7	53.6	150.3	1036.0	0.15	75869	0
40	10.00	9.74E+08	1.41E+05	15.7	53.6	478.2	3296.9	0.28	141325	0
50	0.10	1.23E+08	1.78E+04	15.7	53.6	14.0	96.2	0.04	17782	0
50	1.00	2.44E+08	3.54E+04	15.7	53.6	42.4	292.1	0.07	35447	0
50	10.00	5.03E+08	7.29E+04	15.7	53.6	140.3	967.3	0.14	72925	0
60	0.10	5.69E+07	8.25E+03	15.7	53.6	3.8	26.0	0.02	8254	0
60	1.00	1.08E+08	1.56E+04	15.7	53.6	11.3	78.0	0.03	15635	0
60	10.00	2.30E+08	3.33E+04	15.7	53.6	38.3	264.3	0.07	33315	0

For the first Row of Table B-2:

The measured value of G^*_{mix} at 0.1Hz is 211,465 psi. The Excel solver function had found that a value of backcalculated G^*_{binder} (psi)= 1174.7 psi will return a value of predicted G^*_{mix} = 211,465 psi. This is repeated until all of the predicted G^*_{mix} values match the measured G^*_{mix}.

3. Create a CA master curve (equations 7 and 13) using the backcalculated G^*_{binder} values (in kPa) shown in Table B-2. A typical chosen reference temperature is 25°C (298.15K). Table B-3 and Figure B-1 show the CA constants and shift factors for the master curve.

Table B-3 CA Master Curve Constants

Constant	Value
G_g, kPa	1,000,000
$\omega_{0,}$ Hz	0.003
T_D, K	268.3
R	3.1
c_1 =	22.6
c_2 =	42.6

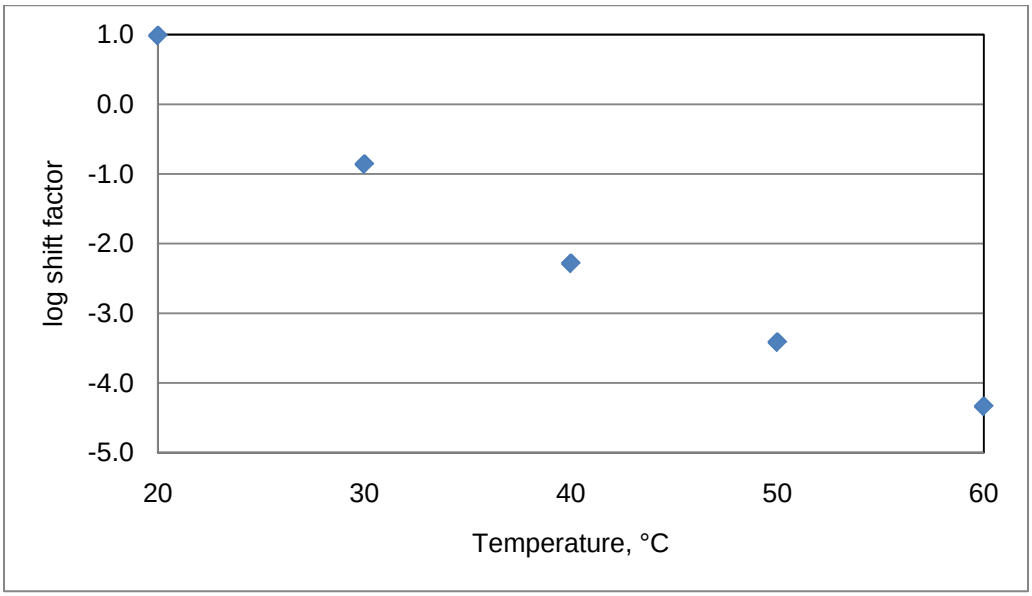

Figure B-1 Kaeble Shift Factors

4. Additional temperatures of G^*_{binder} and δ_{binder} can be calculated using the constants shown in Table B-3. For example, to determine the backcalculated binder properties at 64°C (337.15K) and 1.59 Hz (typical DSR frequency) use the following steps:

   a. Calculate the shift factor for 64°C:

$$\log(shiftfactorto64) = -22.6\left(\frac{337.2-268.3}{42.6+|337.2-268.3|} - \frac{298.15-268.3}{42.6+|298.15-268.3|}\right) = -4.659$$

b. Calculate the reduced frequency:

$$Freq_r = 10^{(\log(1.59)+(-4.659))} = 0.000348$$

c. Use equations 7 and 11 to calculate G^*_{binder} and δ_{binder}:

$$G^*(\omega) = G_g\left[1+\left(\frac{\omega_0}{\omega}\right)^{\frac{\log 2}{R}}\right]^{\frac{-R}{\log 2}} = 1e06\left[1+\left(\frac{.003}{.0000348}\right)^{\frac{\log 2}{3.1}}\right]^{\frac{-3.1}{\log 2}} = 69.7kPa$$

$$\delta(\omega) = \frac{90}{\left[1+\left(\frac{\omega}{\omega_0}\right)^{\frac{\log 2}{R}}\right]} = \frac{90}{\left[1+\left(\frac{.0000348}{.003}\right)^{\frac{\log 2}{3.41}}\right]} = 53.7°$$

Appendix C

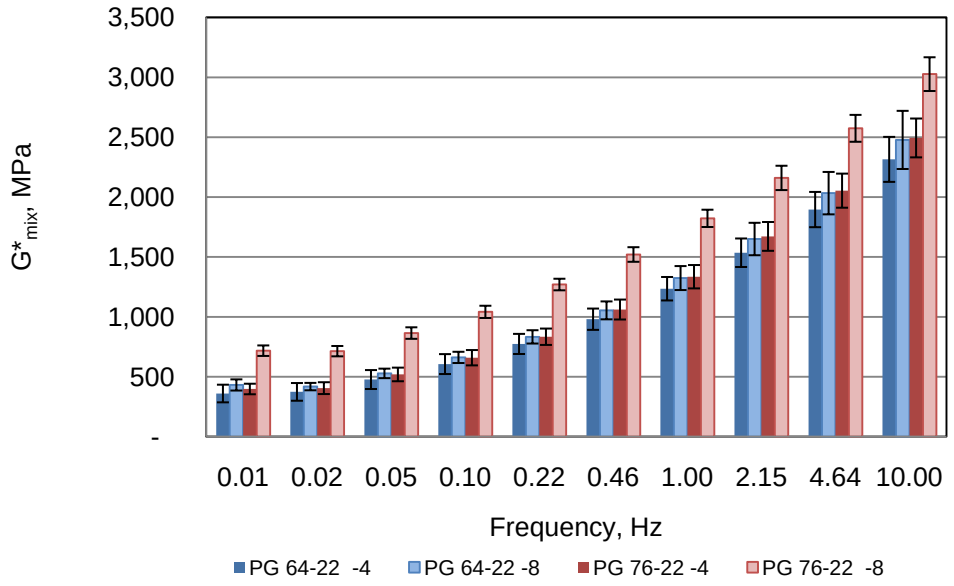

Figure C-1 Virgin Torsion G^*_{mix} Results @ 20°C

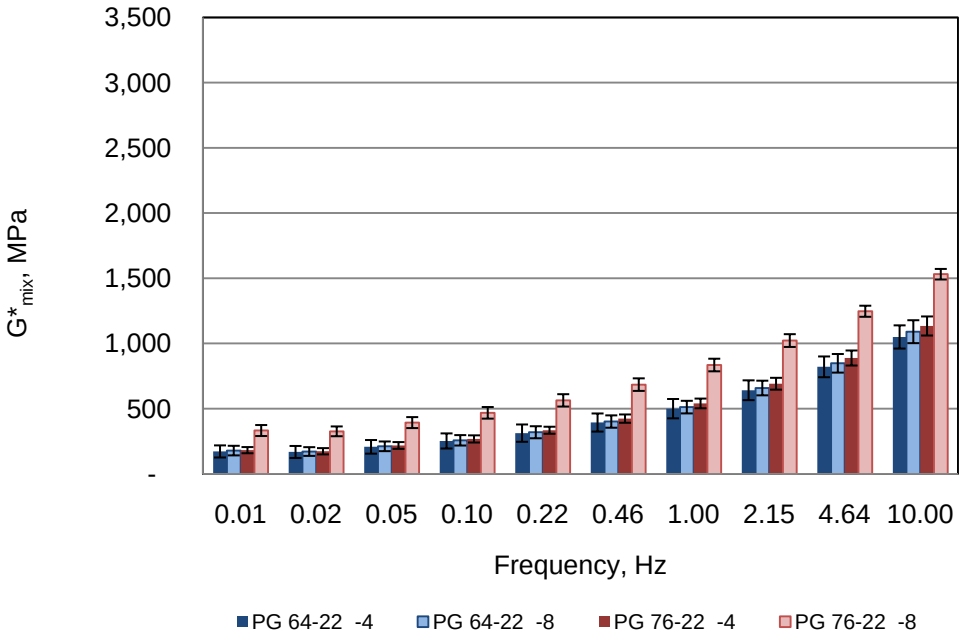

Figure C-2 Virgin Torsion G^*_{mix} Results @ 30°C

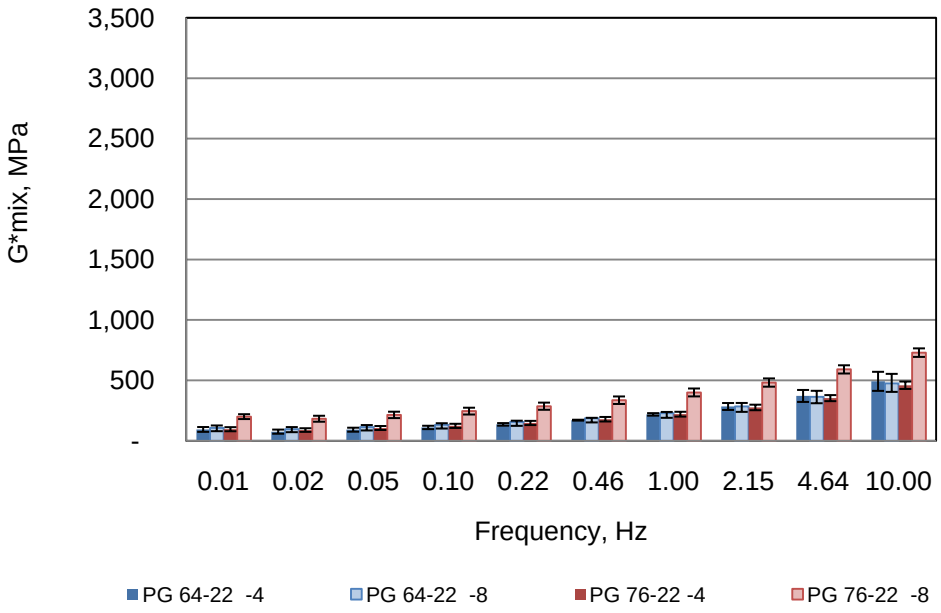

Figure C-3 Virgin Torsion G*$_{mix}$ Results @ 40°C

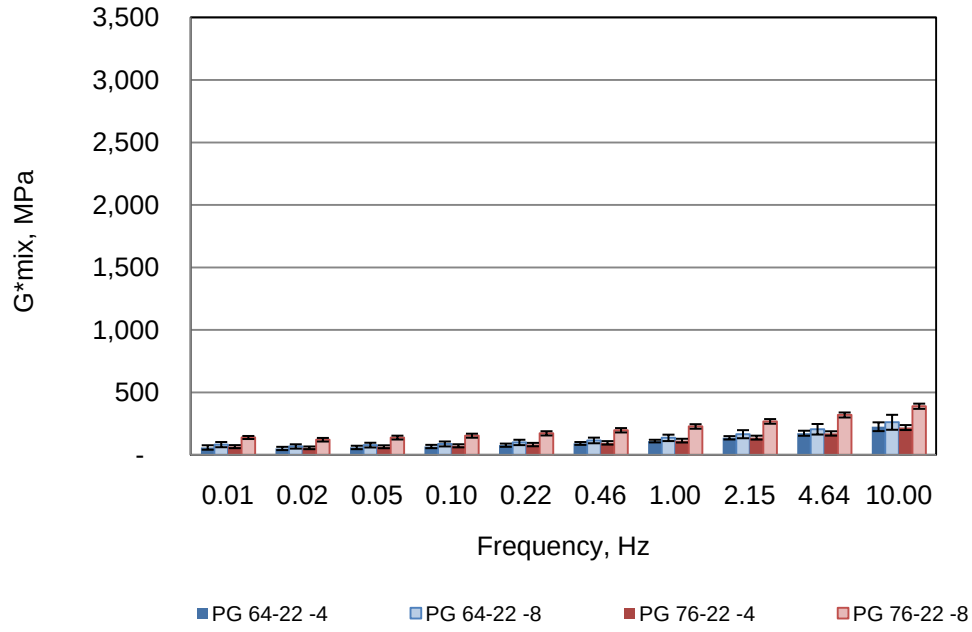

Figure C-4 Virgin Torsion G*$_{mix}$ Results @ 50°C

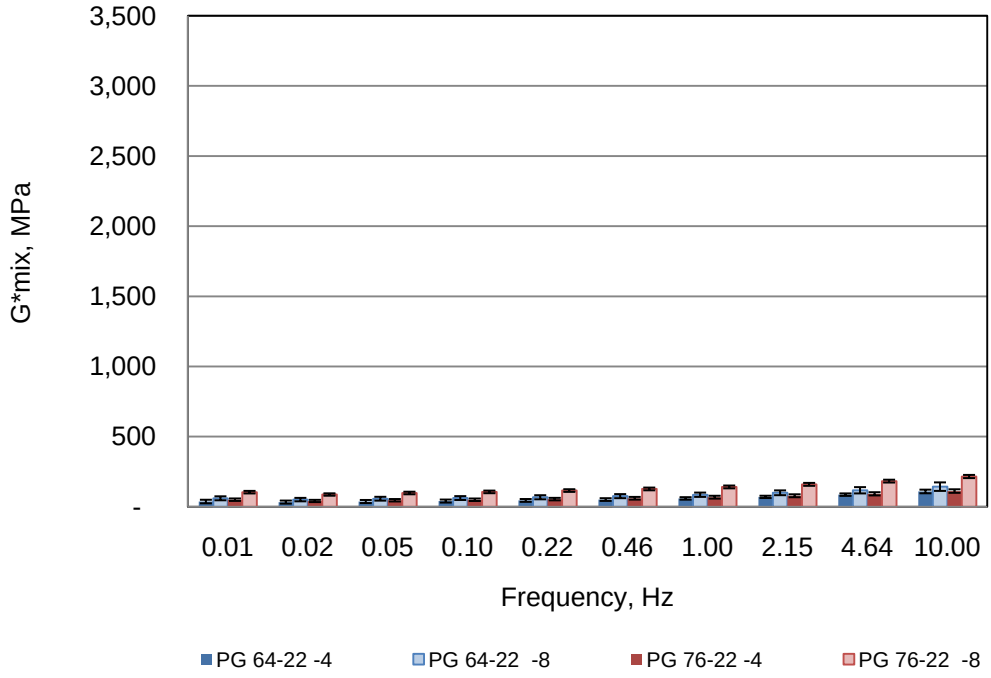

Figure C-5 Virgin Torsion G*$_{mix}$ Results @ 60°C

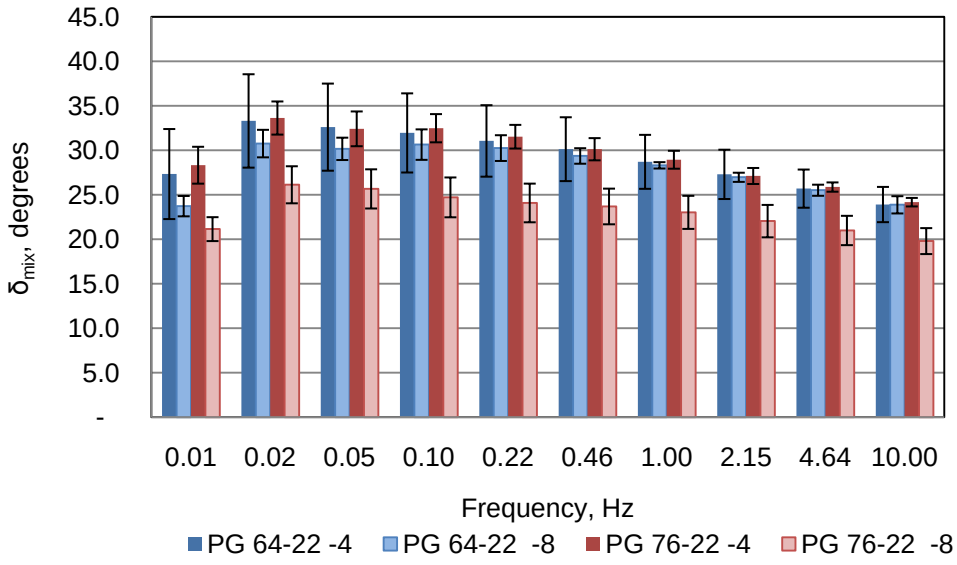

Figure C-6 Virgin Torsion δ$_{mix}$ Results @ 20°C

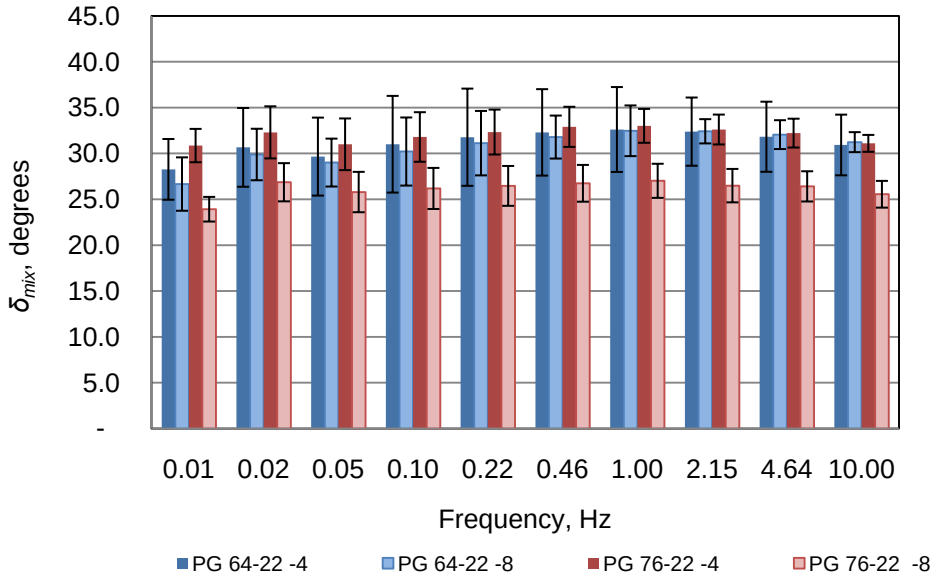

Figure C-7 Virgin Torsion δ_{mix} Results @ 30°C

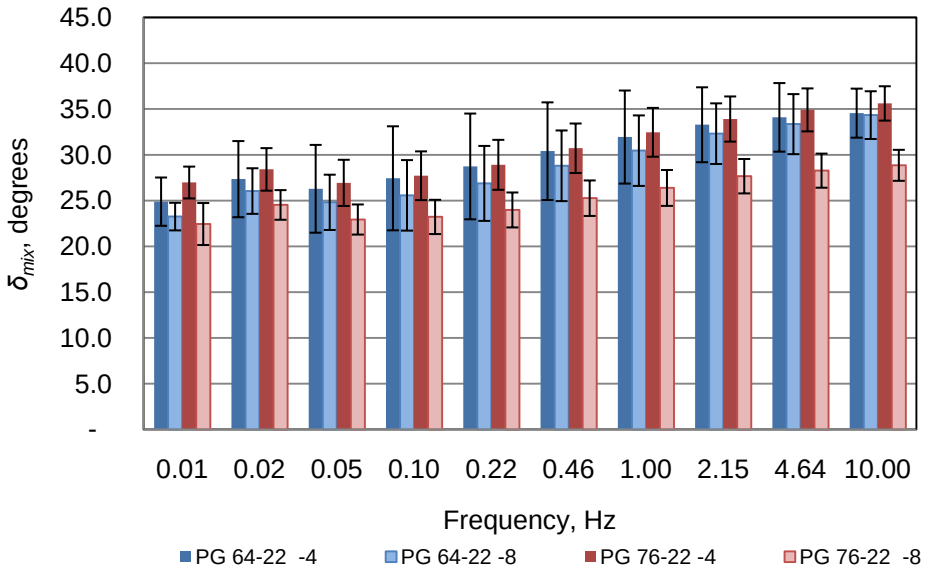

Figure C-8 Virgin Torsion δ_{mix} Results @ 40°C

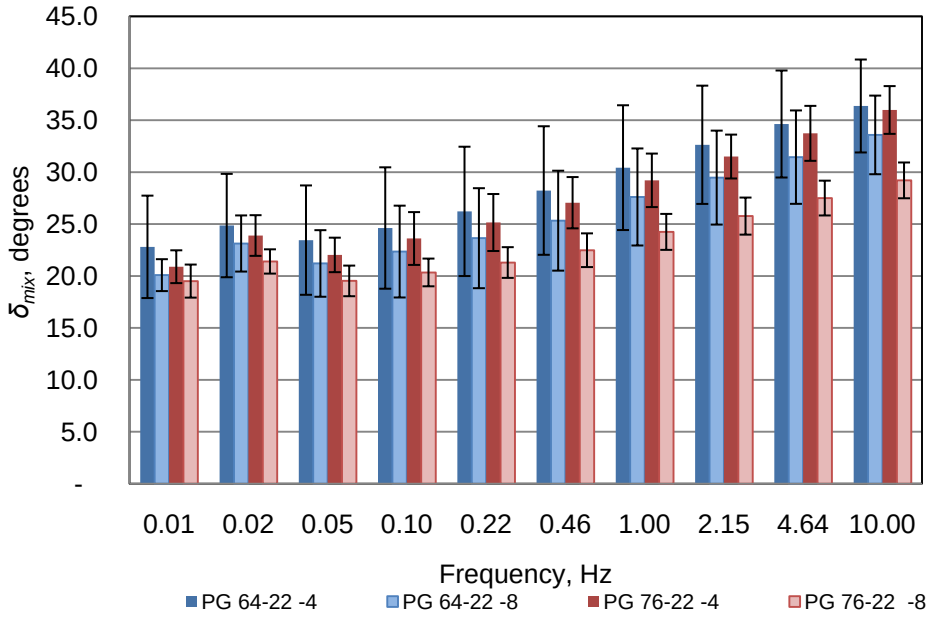

Figure C-9 Virgin Torsion δ_{mix} Results @ 50°C

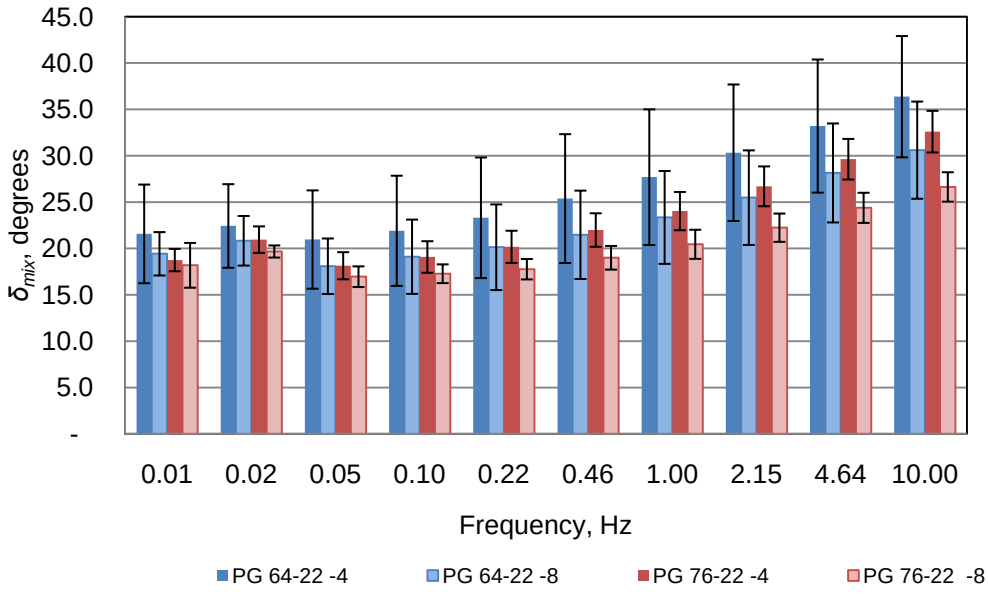

Figure C-10 Virgin Torsion δ_{mix} Results @ 60°C

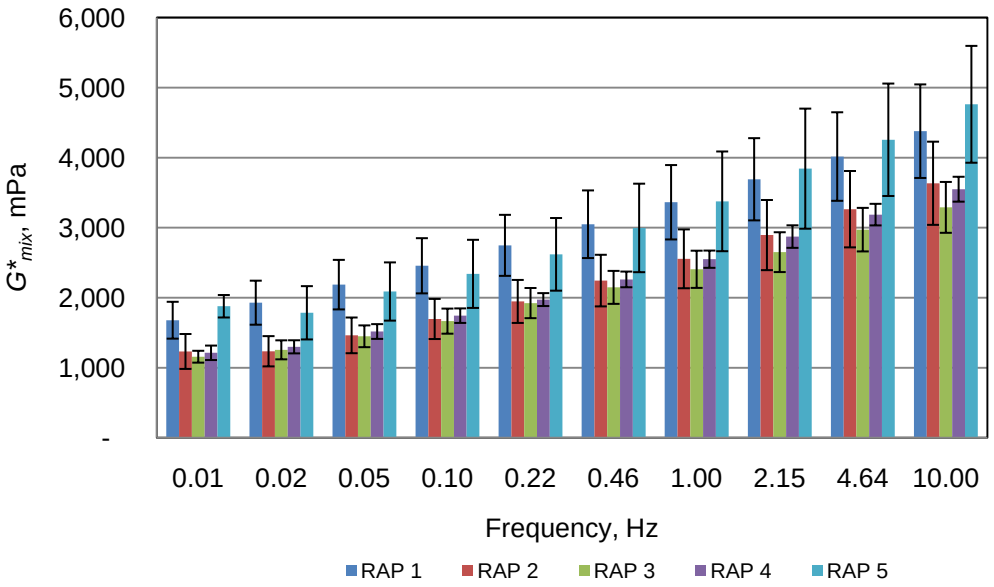

Figure C-11 RAP Torsion G^*_{mix} Results @ 20°C

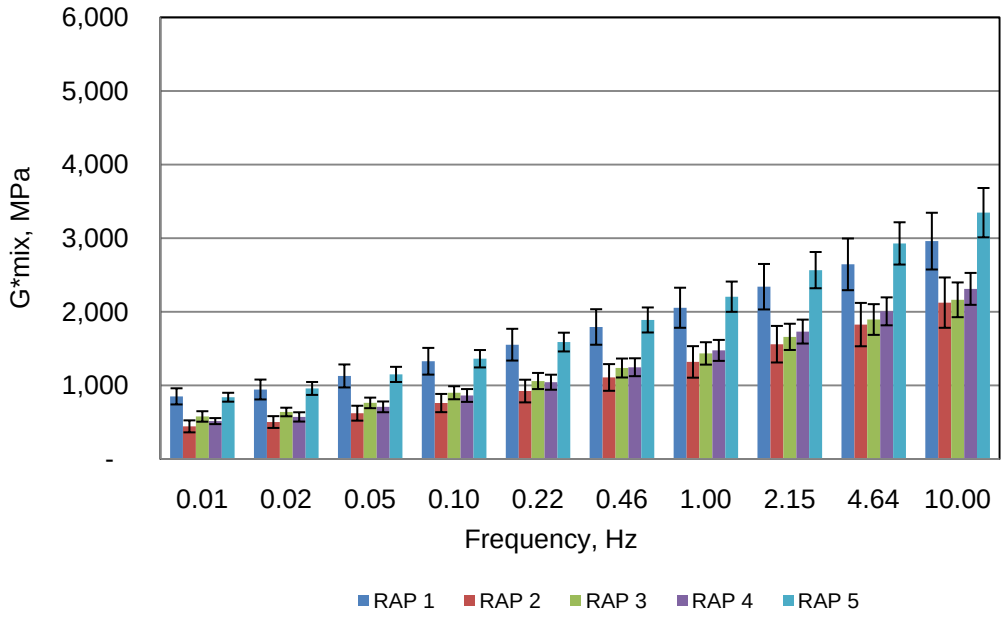

Figure C-12 RAP Torsion G^*_{mix} Results @ 30°C

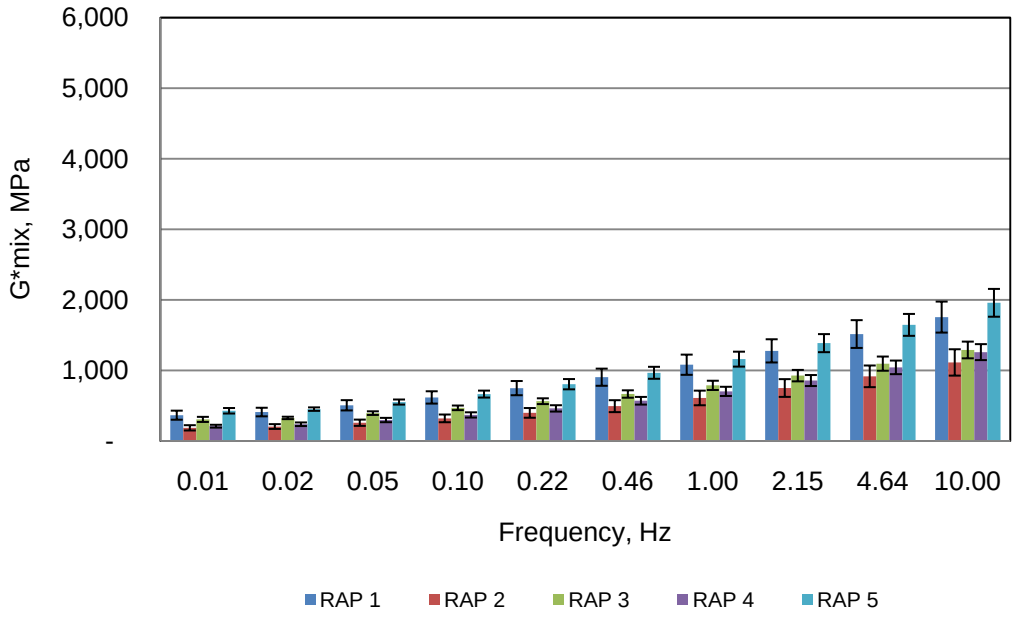

Figure C-13 RAP Torsion G^*_{mix} Results @ 40°C

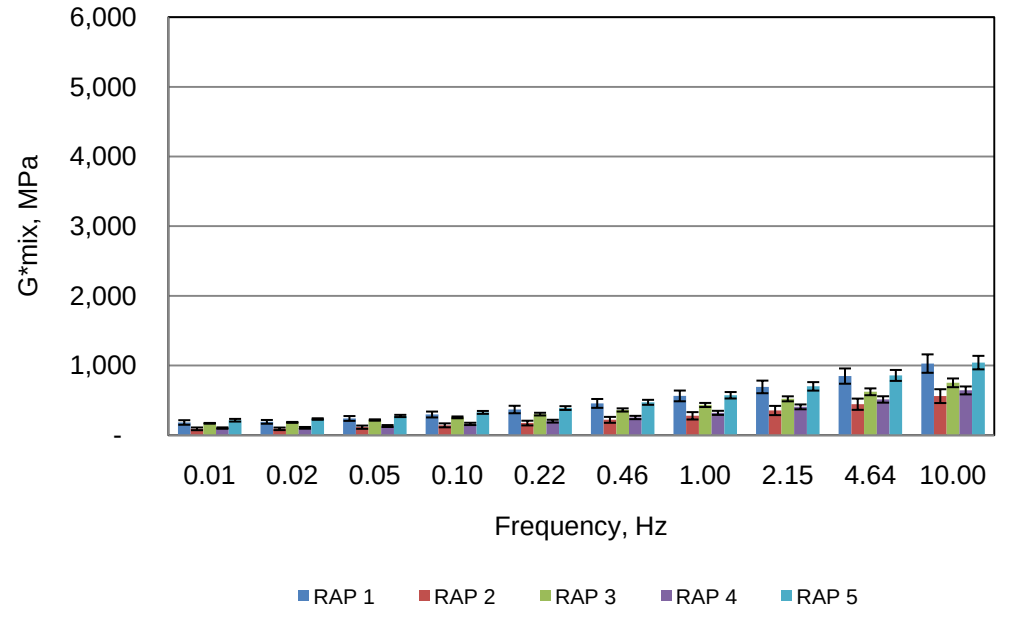

Figure C-14 RAP Torsion G^*_{mix} Results @ 50°C

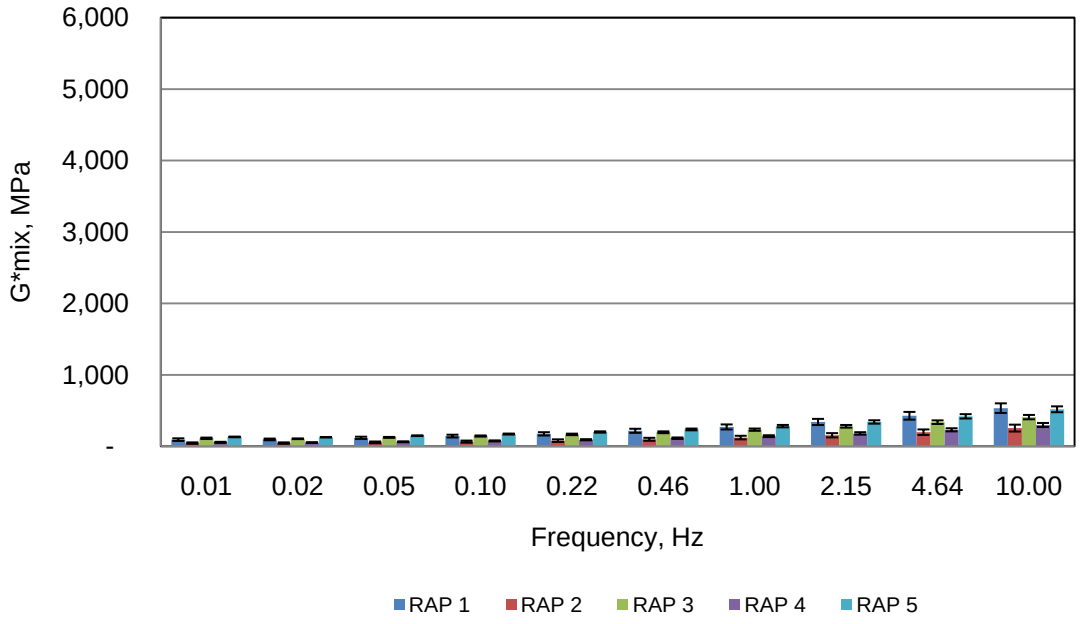

Figure C-15 RAP Torsion G^*_{mix} Results @ 60°C

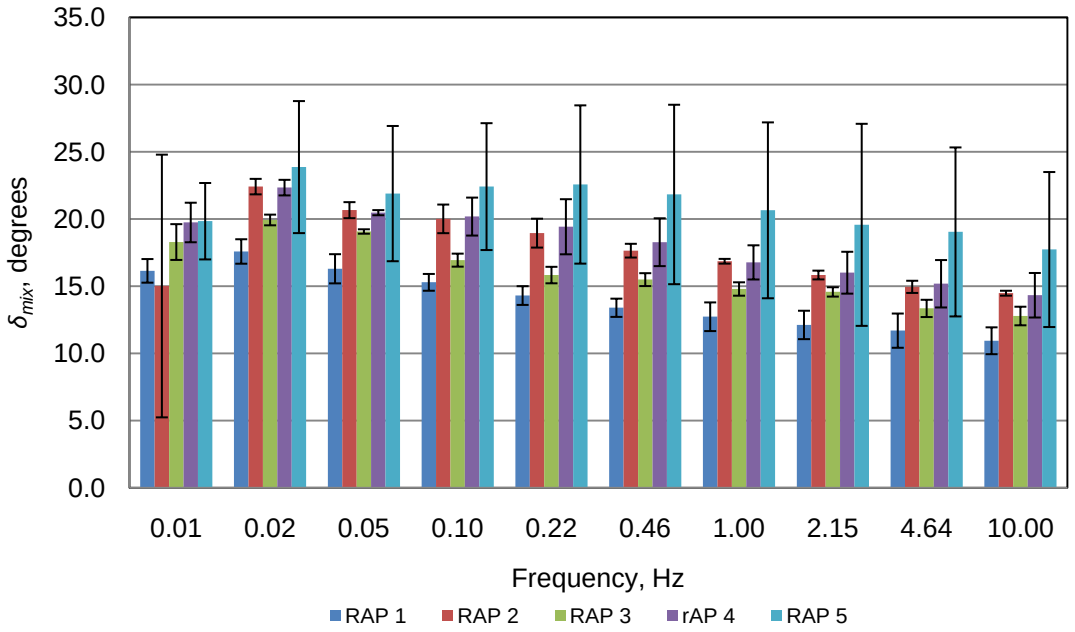

Figure C-16 RAP Torsion δ_{mix} Results @ 20°C

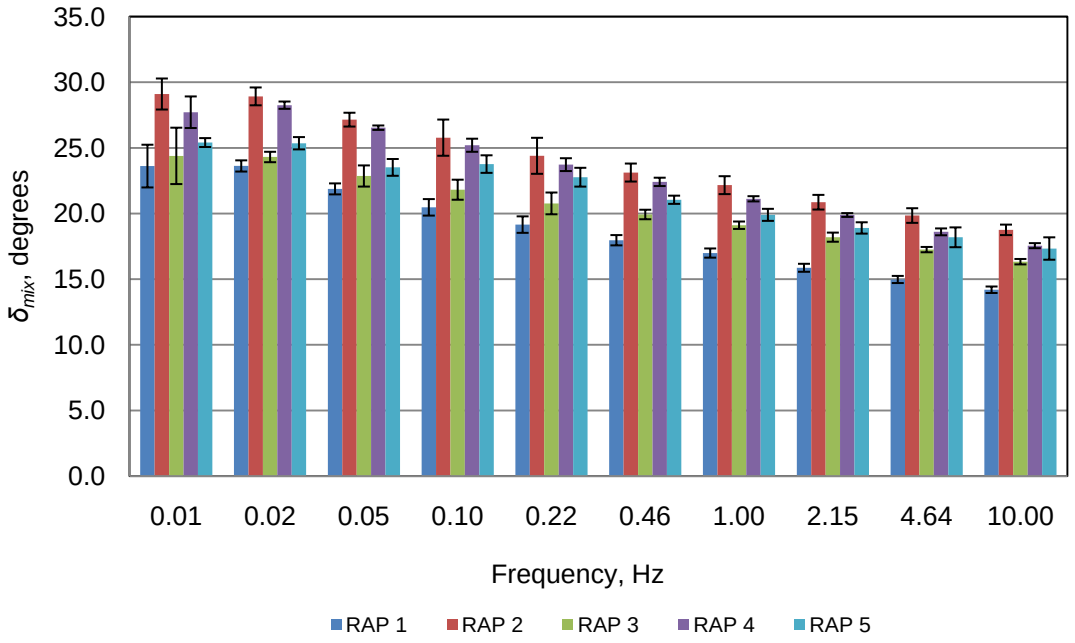

Figure C-17 RAP Torsion δ_{mix} Results @ 30°C

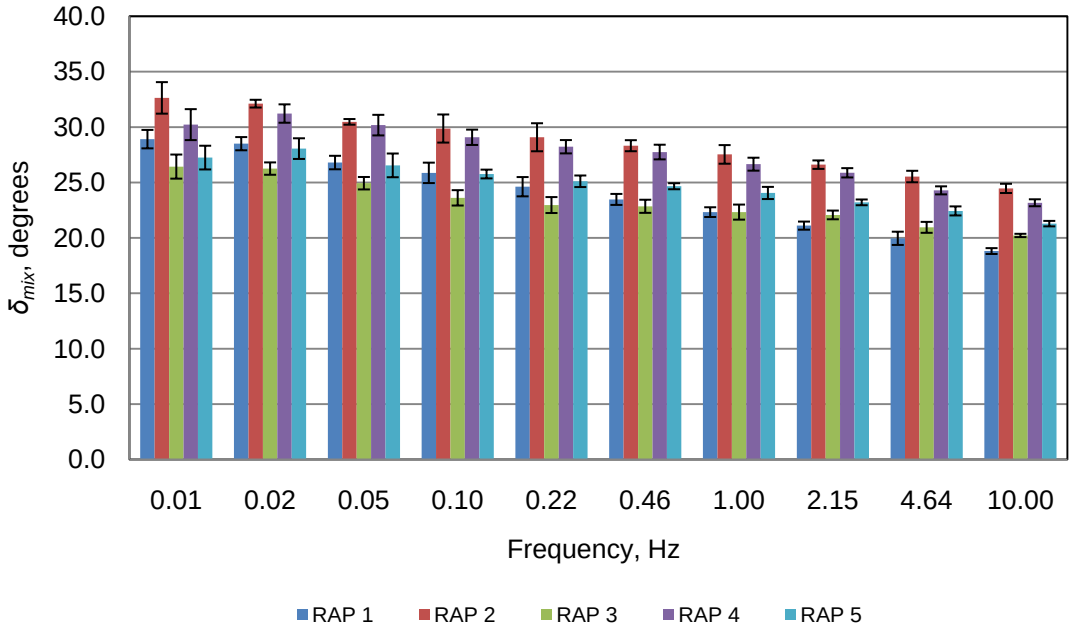

Figure C-18 RAP Torsion δ_{mix} Results @ 40°C

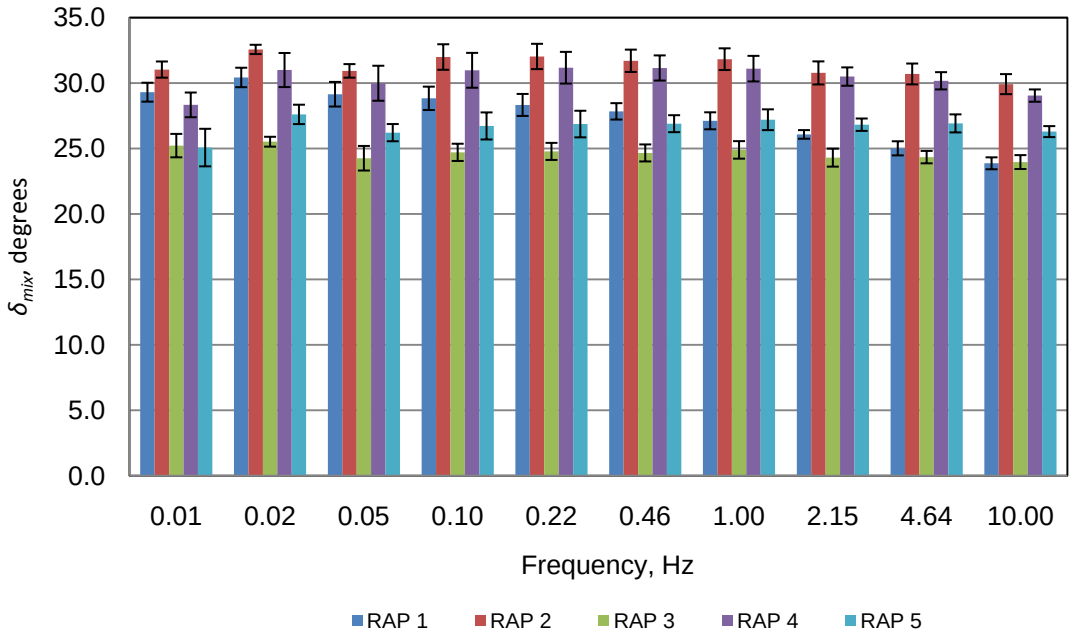

Figure C-19 RAPTorsion δ_{mix} Results @ 50°C

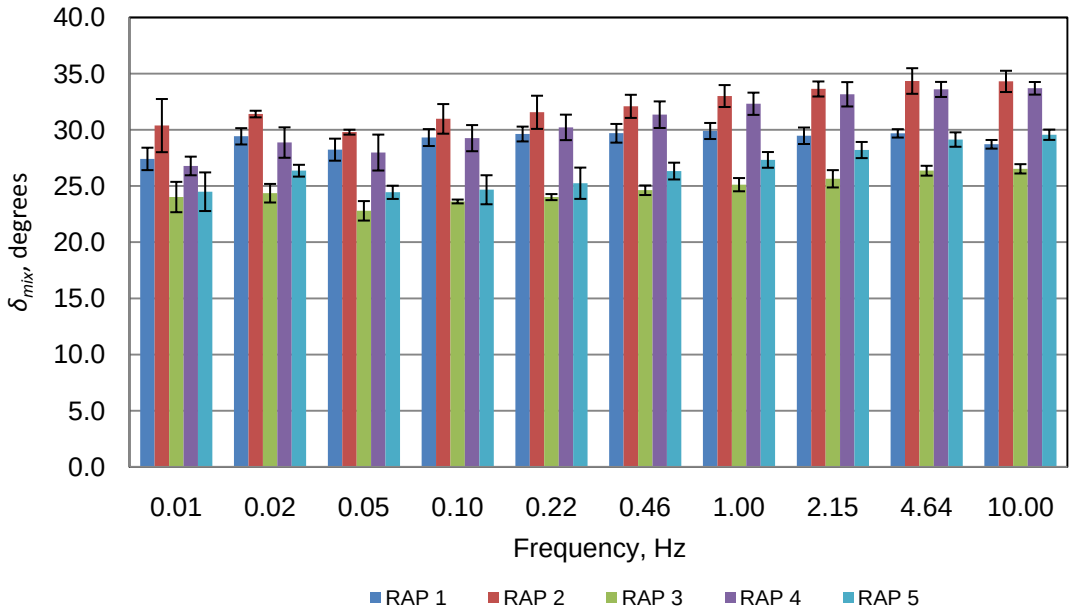

Figure C-20 RAP Torsion δ_{mix} Results @ 60°C

Appendix D

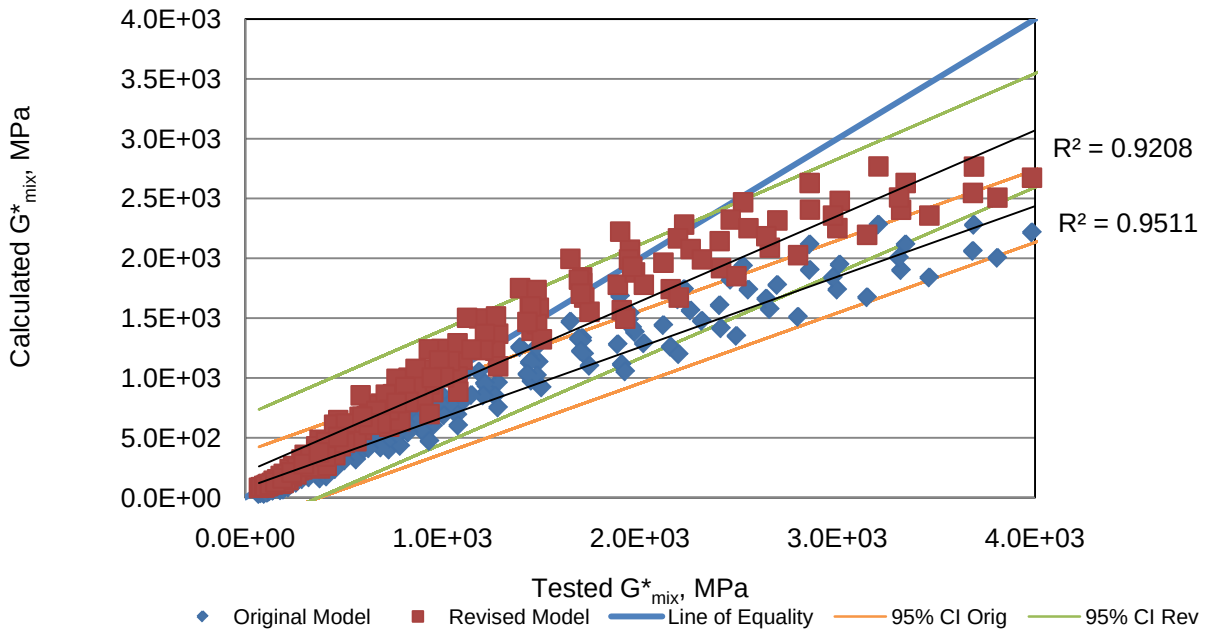

Figure D-1 RAP 1 Calculation Comparison for Original and Revised Hirsch

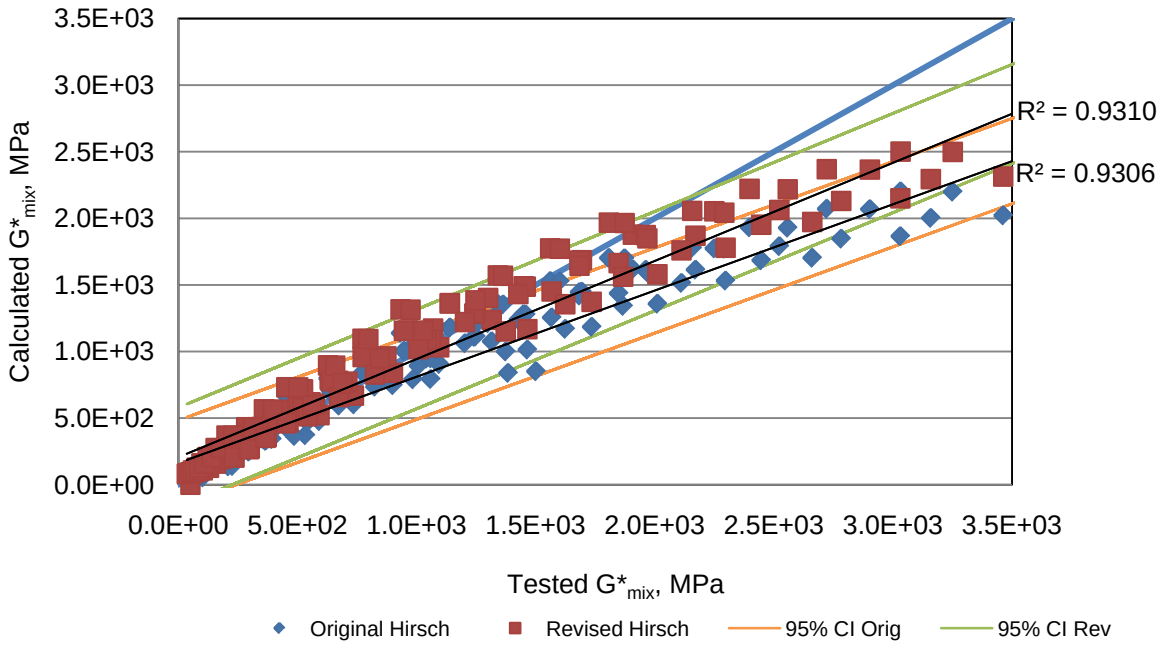

Figure D-2 RAP 2 Calculation Comparison for Original and Revised Hirsch

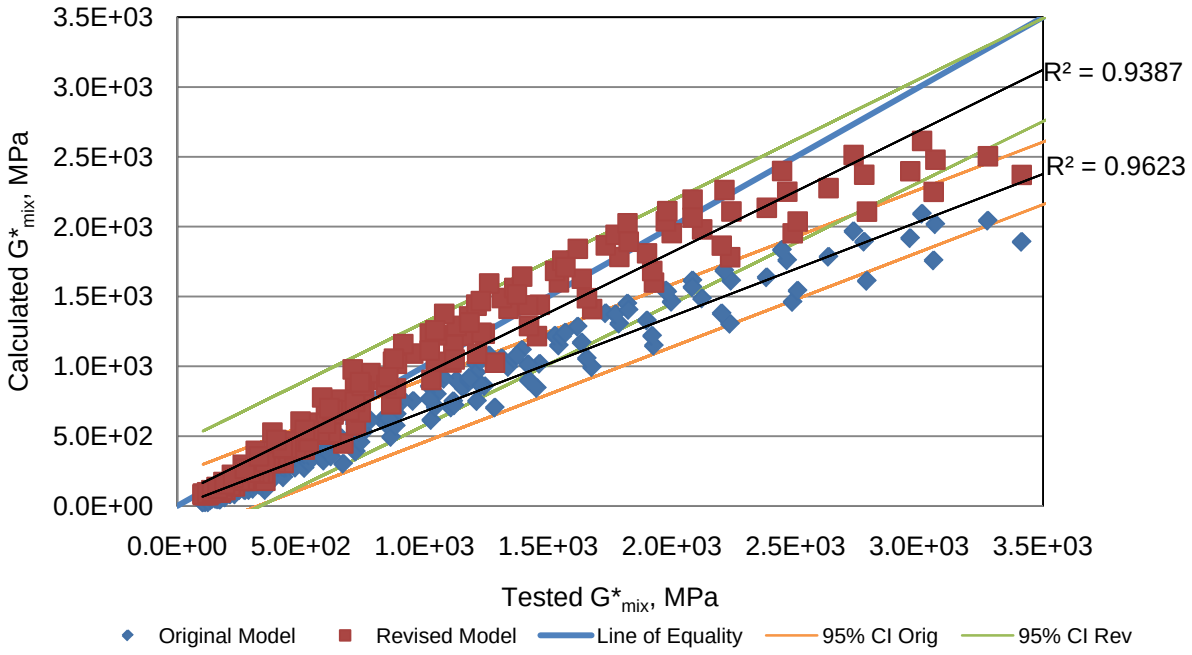

Figure D-3 RAP 3 Calculation Comparison for Original and Revised Hirsch

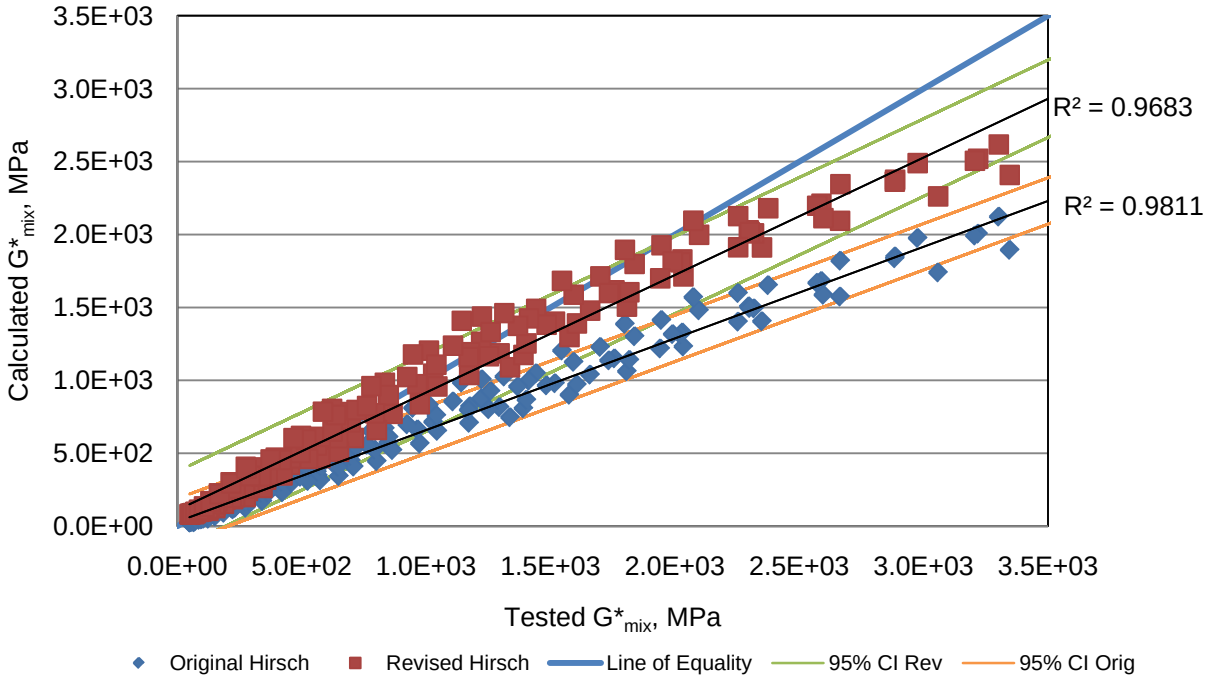

Figure D-4 RAP 4 Calculation Comparison for Original and Revised Hirsch

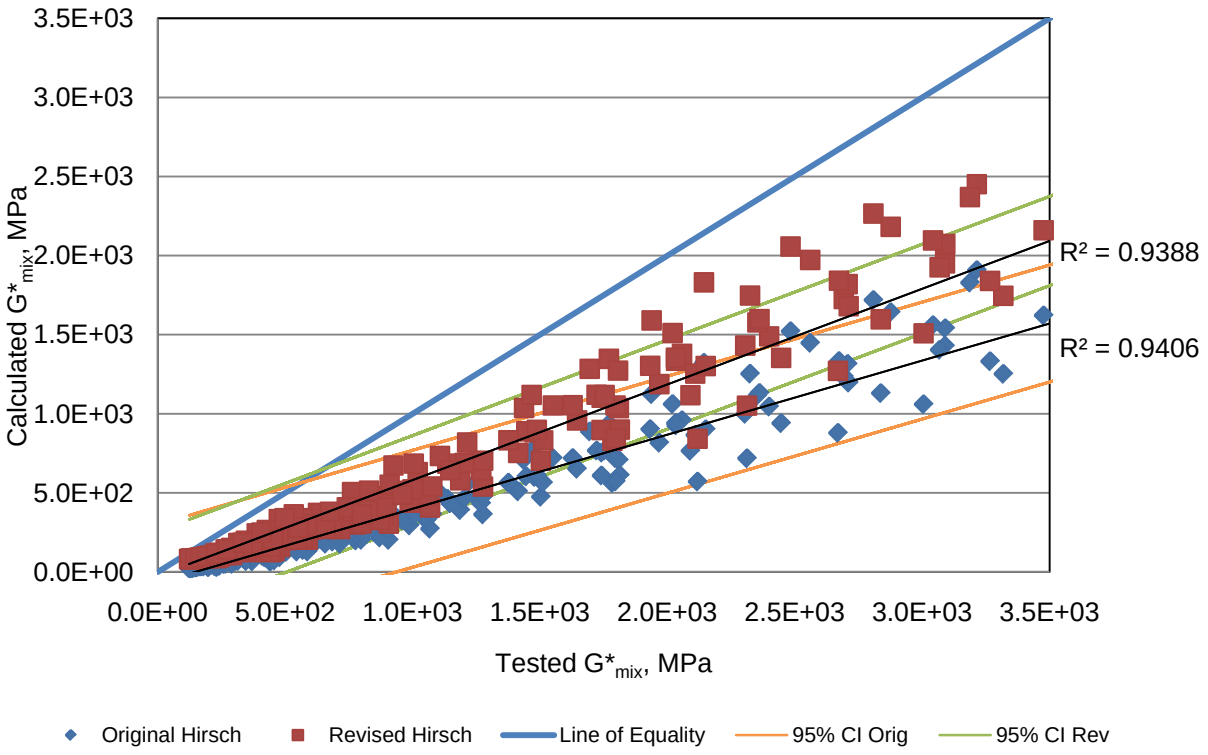

Figure D-5 RAP 5 Calculation Comparison for Original and Revised Hirsch

Appendix E

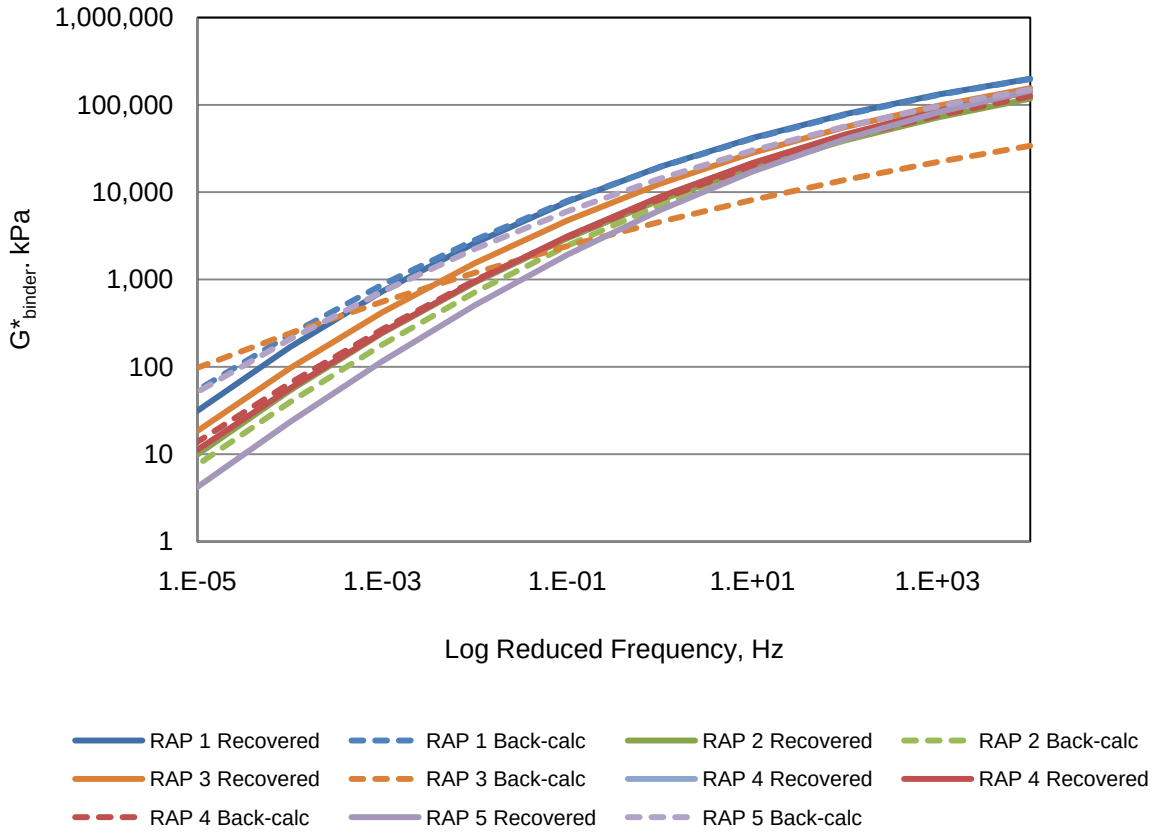

Figure E-1 RAP Binder Master Curves @ 25°C – Original Hirsch

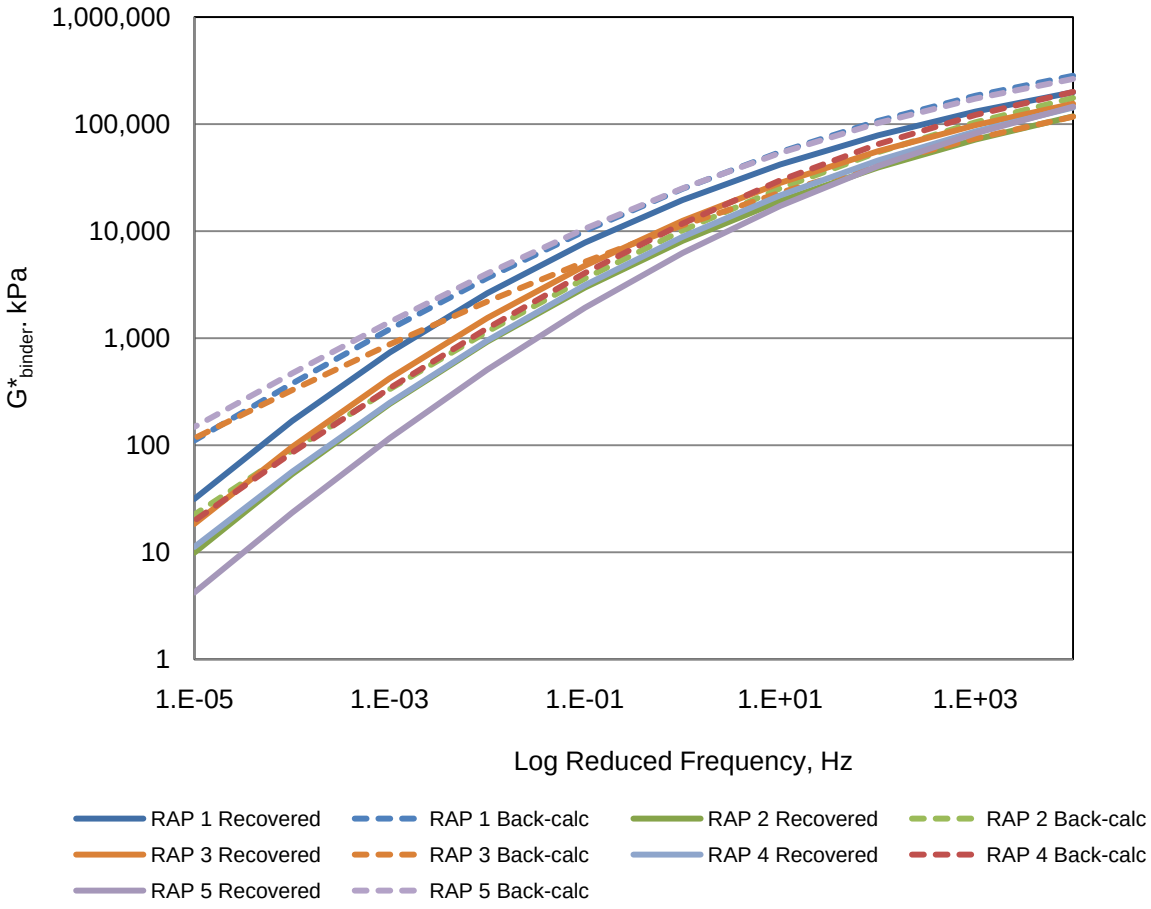

Figure E-2 RAP Binder Master Curves @ 25°C – Revised Hirsch

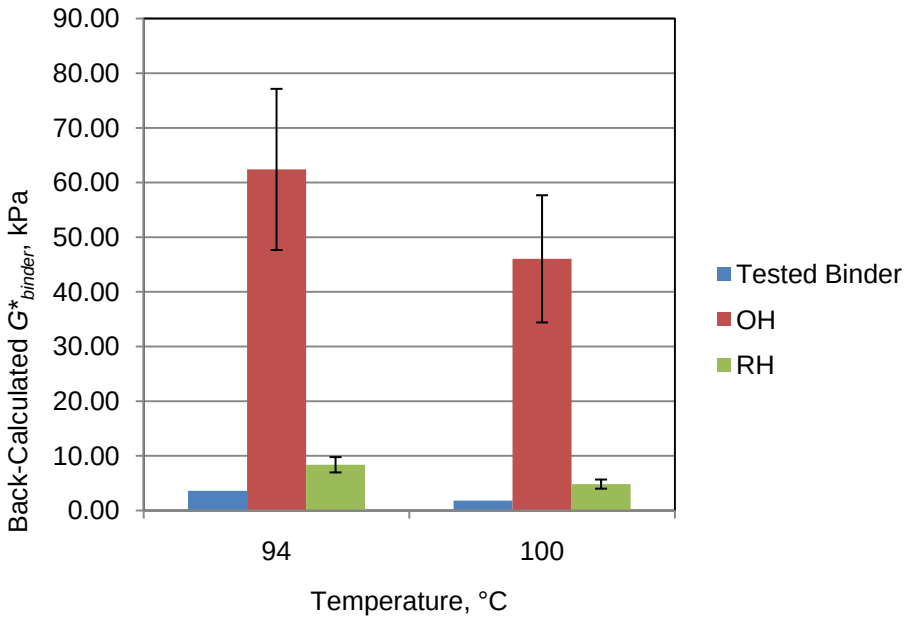

Figure E-3 High Temp Backcalculated G^*_{binder} Results- RAP 1

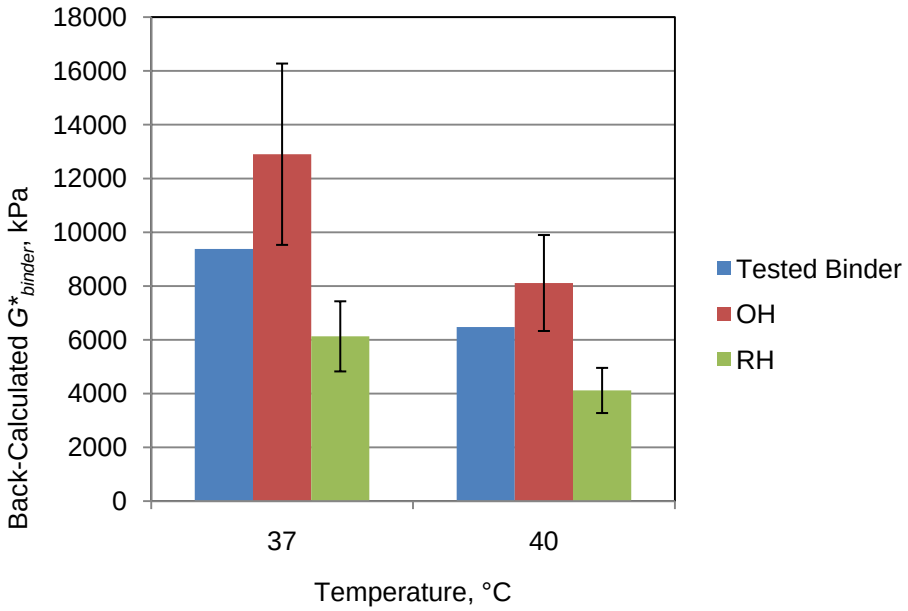

Figure E-4 Intermediate Temp Backcalculated G^*_{binder} Results- RAP 1

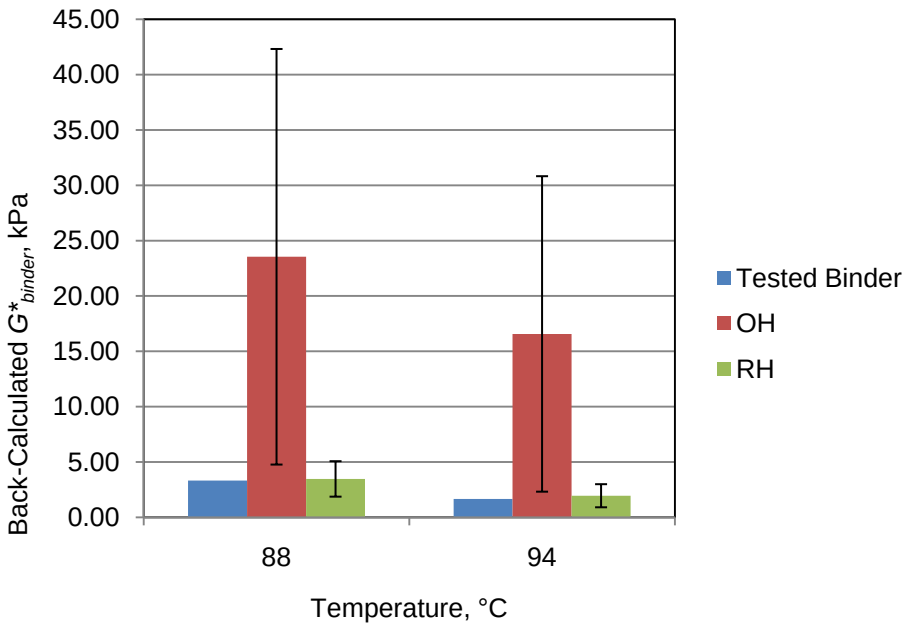

Figure E-5 High Temp Backcalculated G^*_{binder} Results-RAP 2

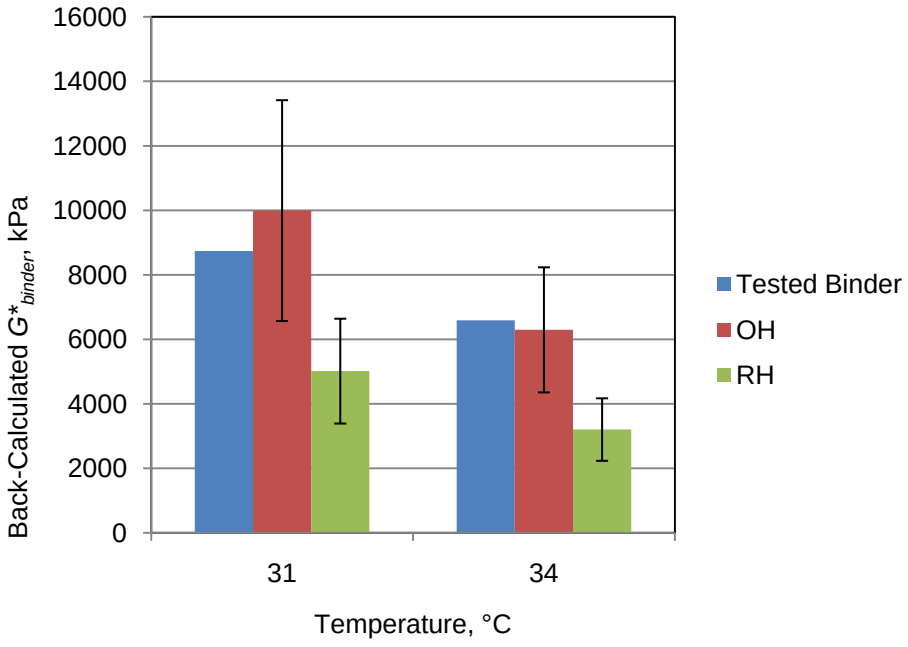

Figure E-6 Intermediate Temp Backcalculated G^*_{binder} Results-RAP 2

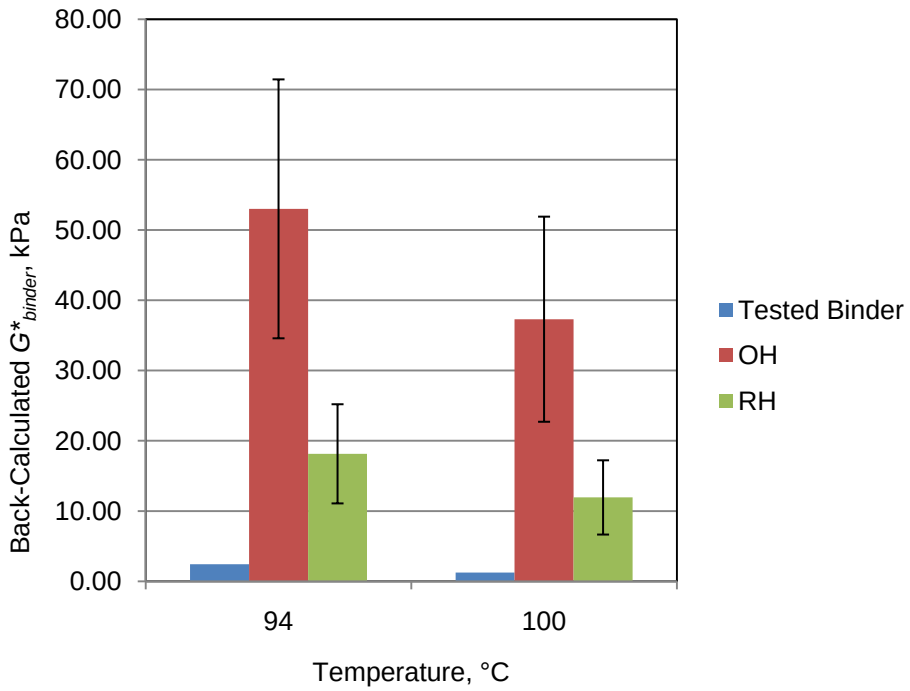

Figure E-7 High Temp Backcalculated G^*_{binder} Results-RAP 3

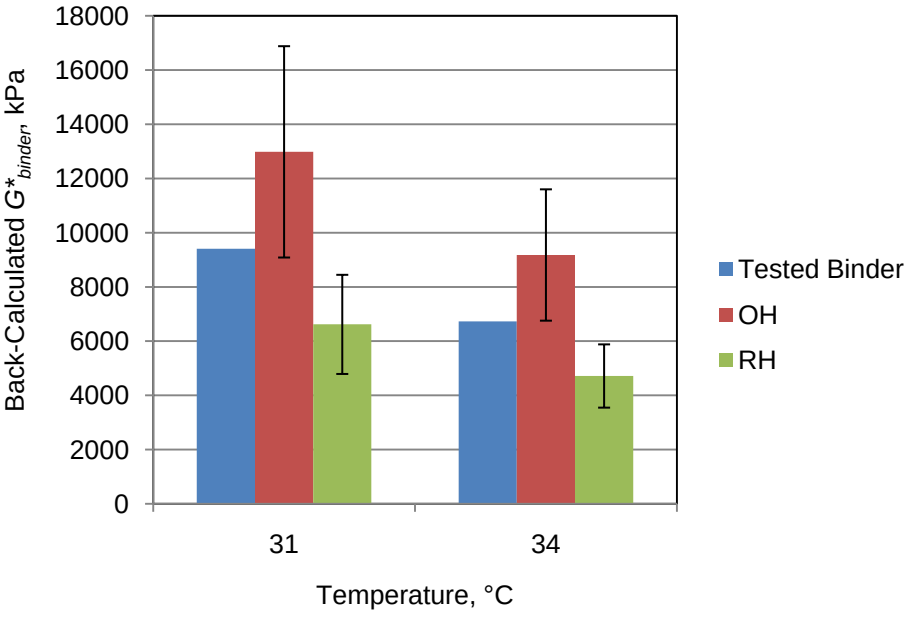

Figure E-8 Intermediate Temp Backcalculated G^*_{binder} Results- RAP 3

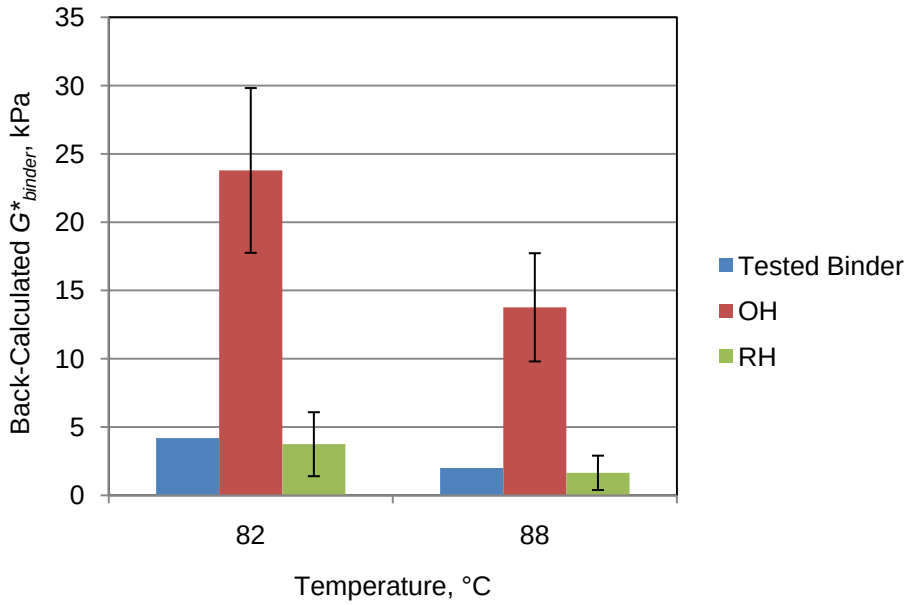

Figure E-9 High Temp Backcalculated G^*_{binder} Results-RAP 4

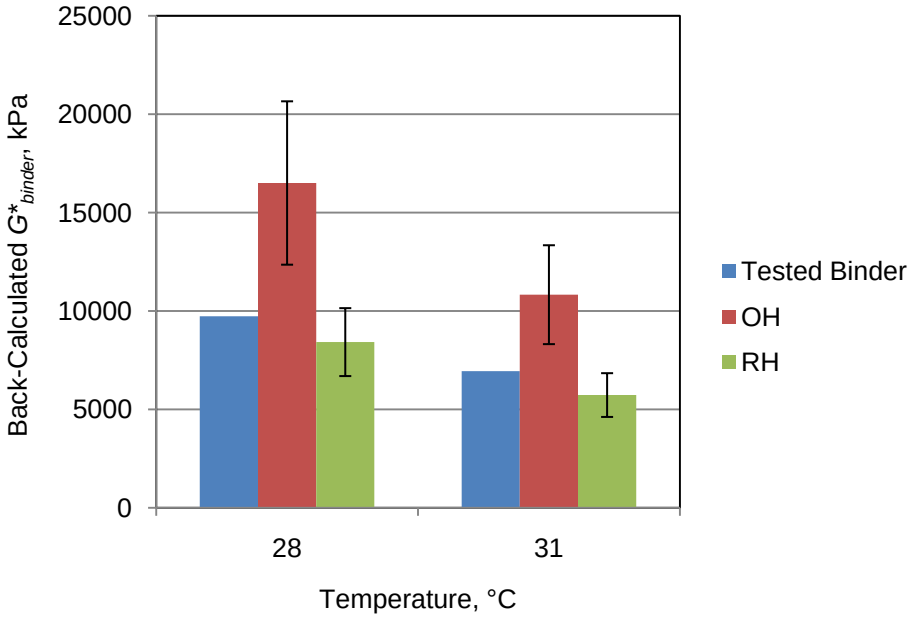

Figure E-10 Intermediate Temp Backcalculated G^*_{binder} Results-RAP 4

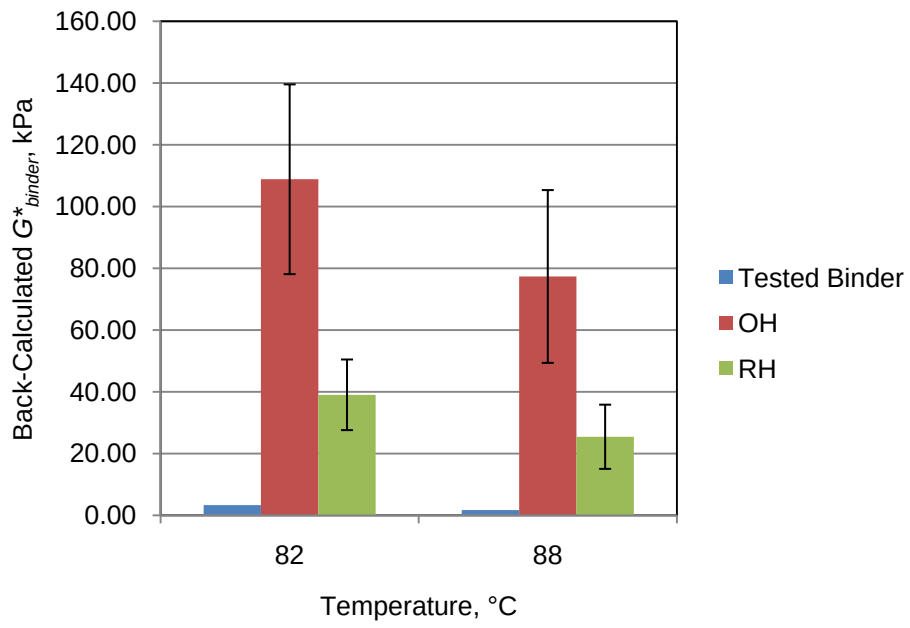

Figure E-11 High-temperature Backcalculated G^*_{binder} Results-RAP 5

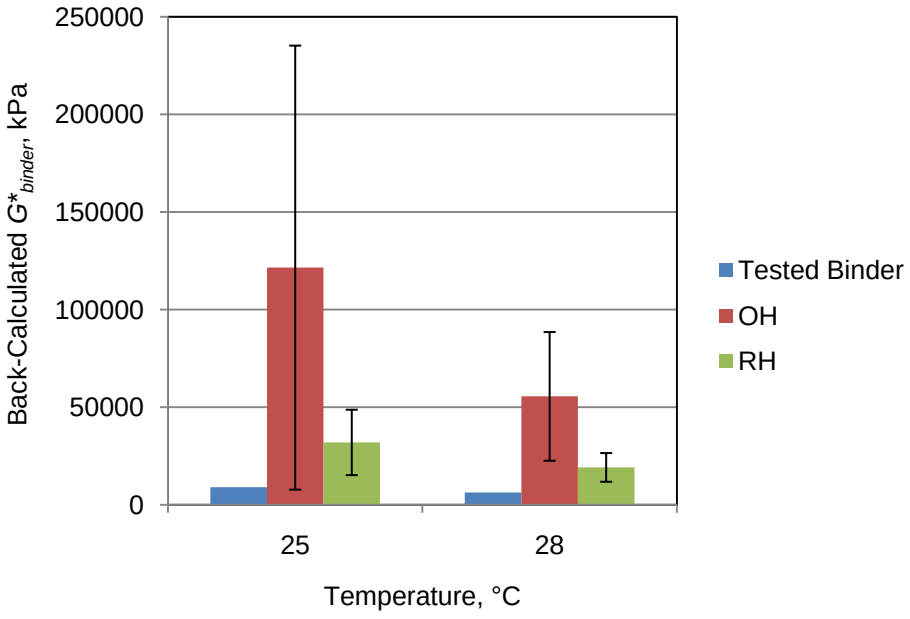

Figure E-12 Intermediate Temp Backcalculated G^*_{binder} Results- RAP 5

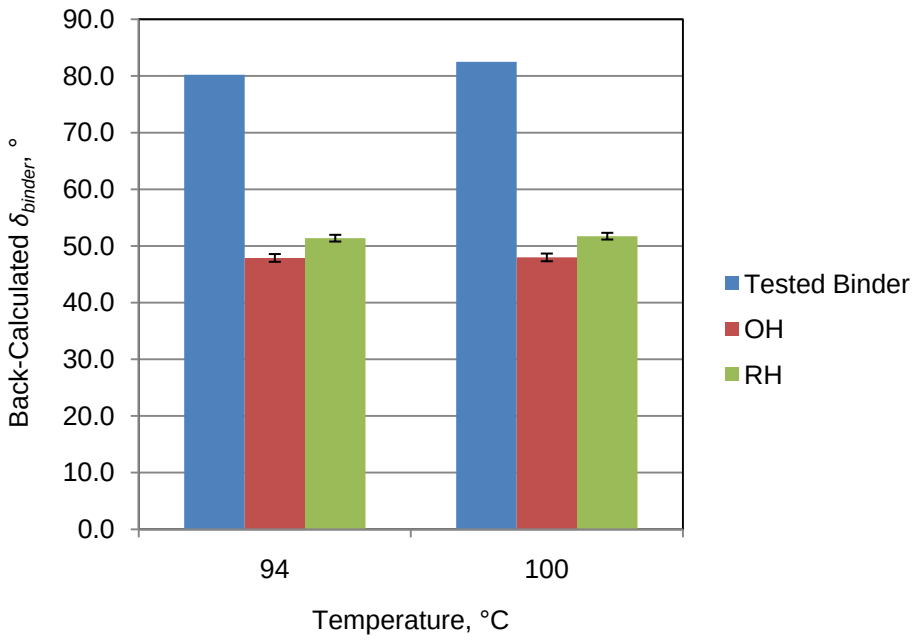

Figure E-13 High Temp Backcalculated δ_{binder} Results- RAP 1

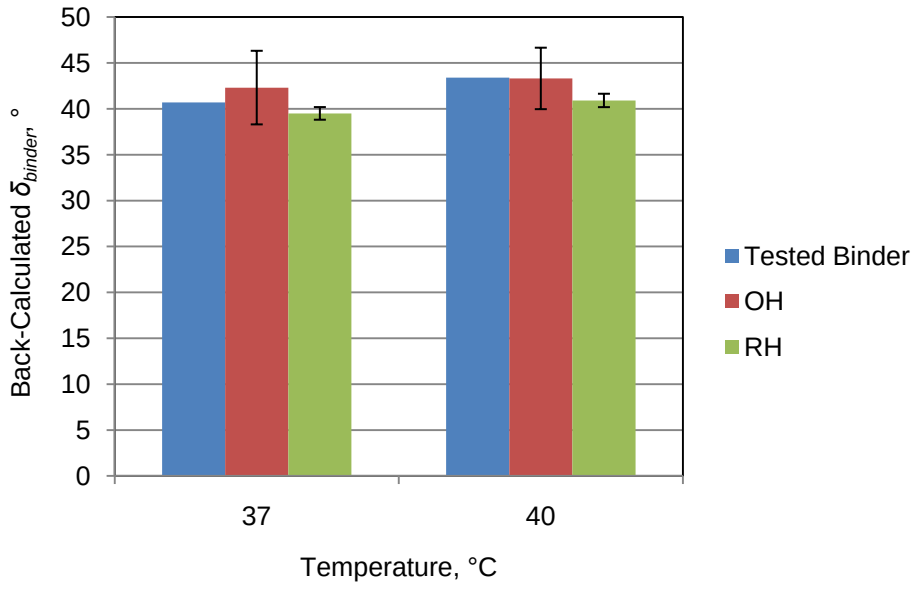

Figure E-14 Intermediate Temp Backcalculated δ_{binder} Results-RAP 1

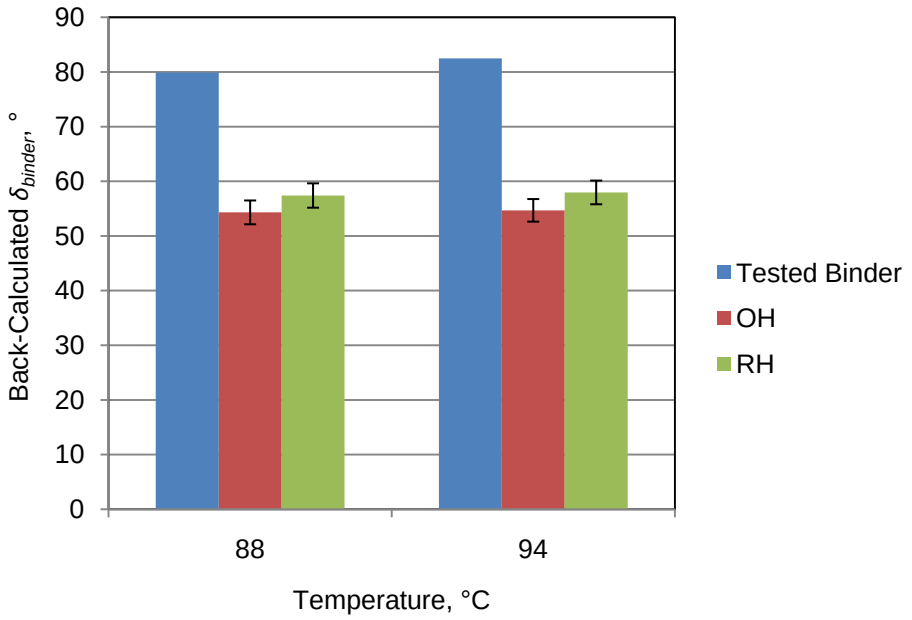

Figure E-15 High Temp Backcalculated δ_{binder} Results-RAP 2

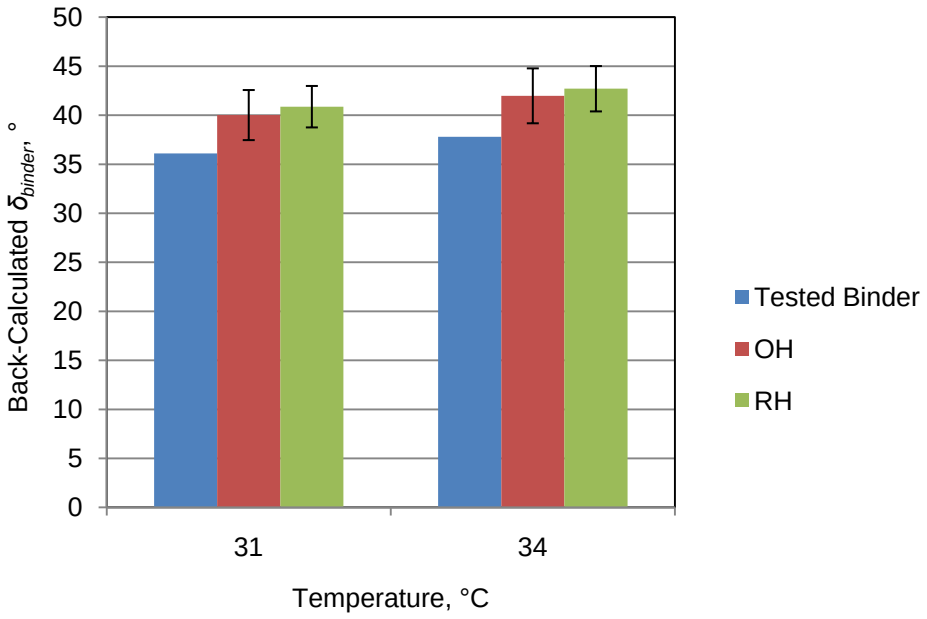

Figure E-16 Intermediate Temp Backcalculated δ_{binder} Results-RAP 2

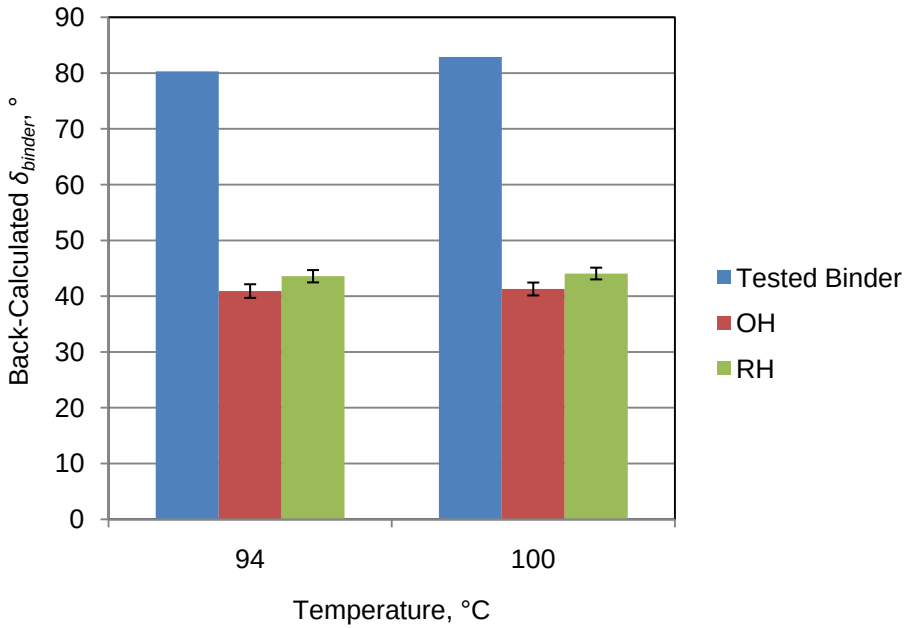

Figure E-17 High Temp Backcalculated δ_{binder} Results-RAP 3

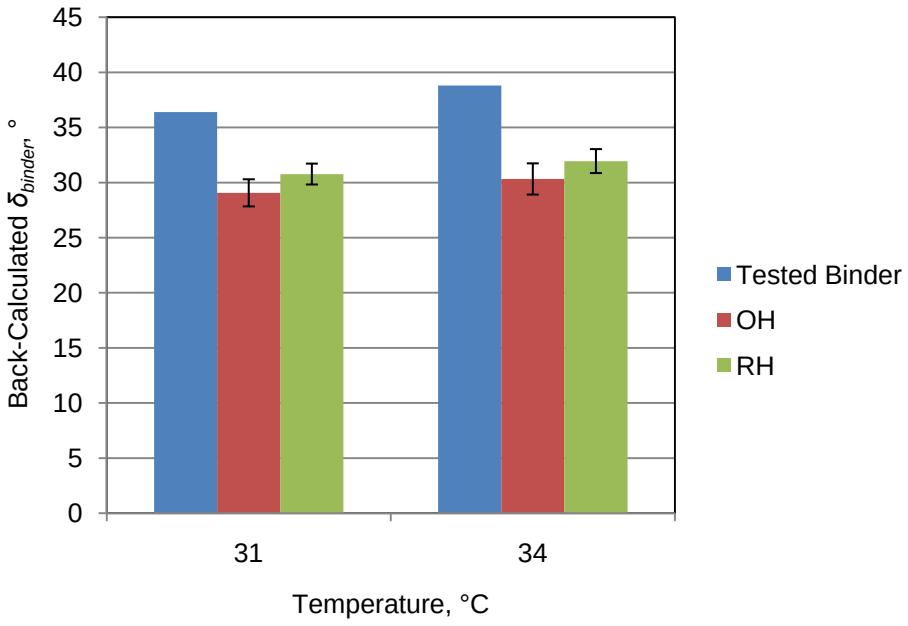

Figure E-18 Intermediate Temp Backcalculated δ_{binder} Results-RAP 3

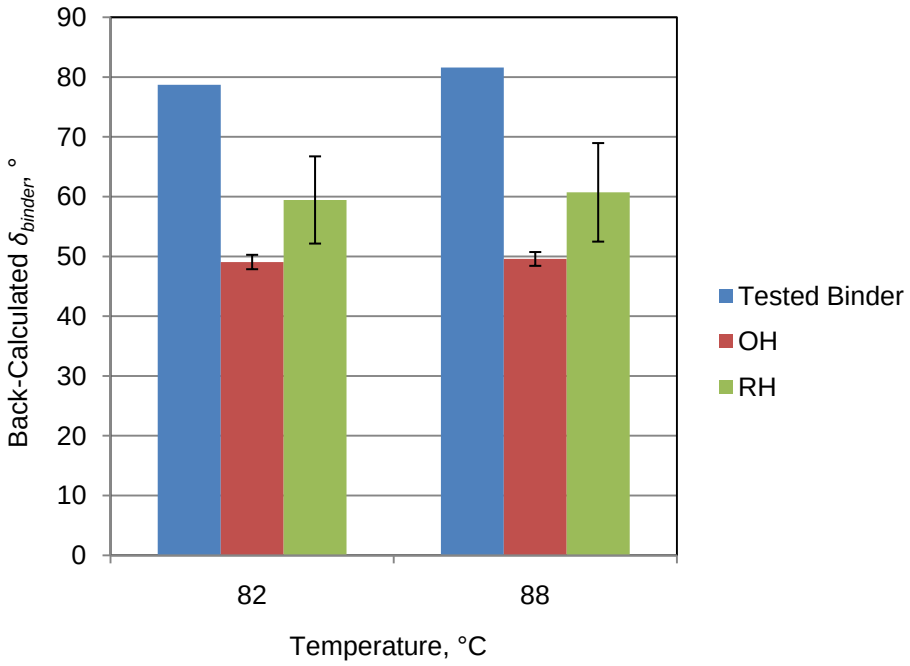

Figure E-19 High Temp Backcalculated δ_{binder} Result-RAP 4

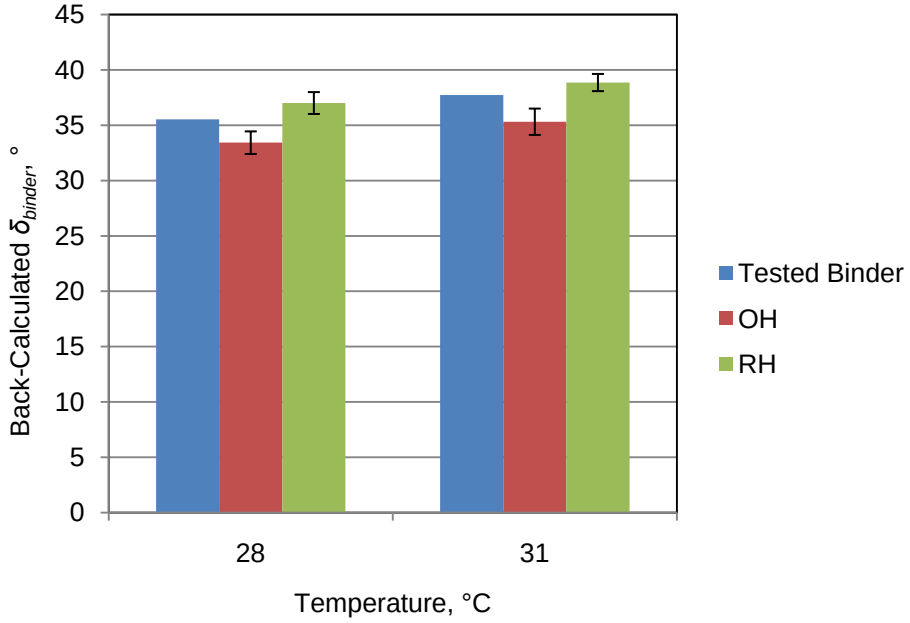

Figure E-20 Intermediate Temp Backcalculated δ_{binder} Results-RAP 4

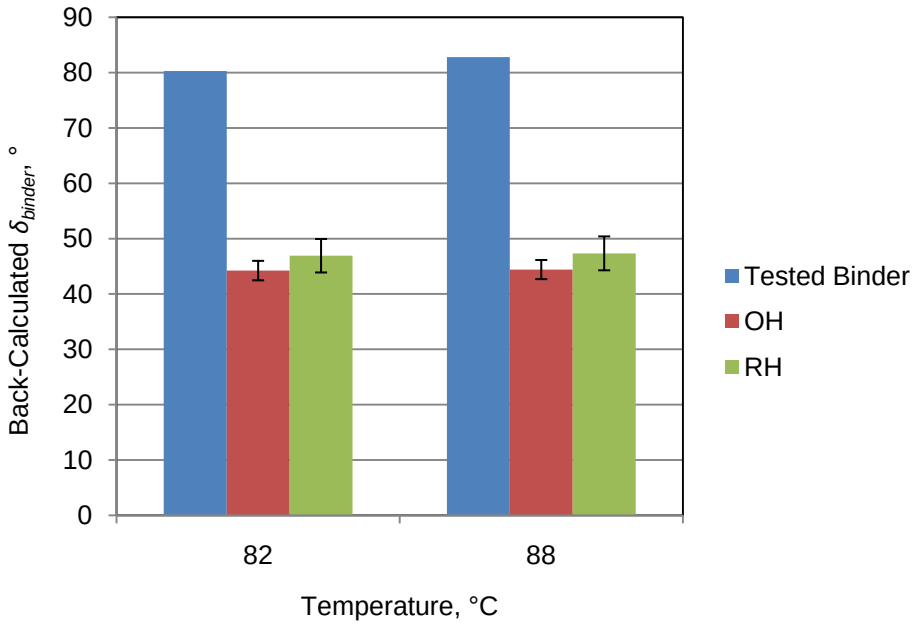

Figure E-21 High Temp Backcalculated δ_{binder} Results-RAP 5

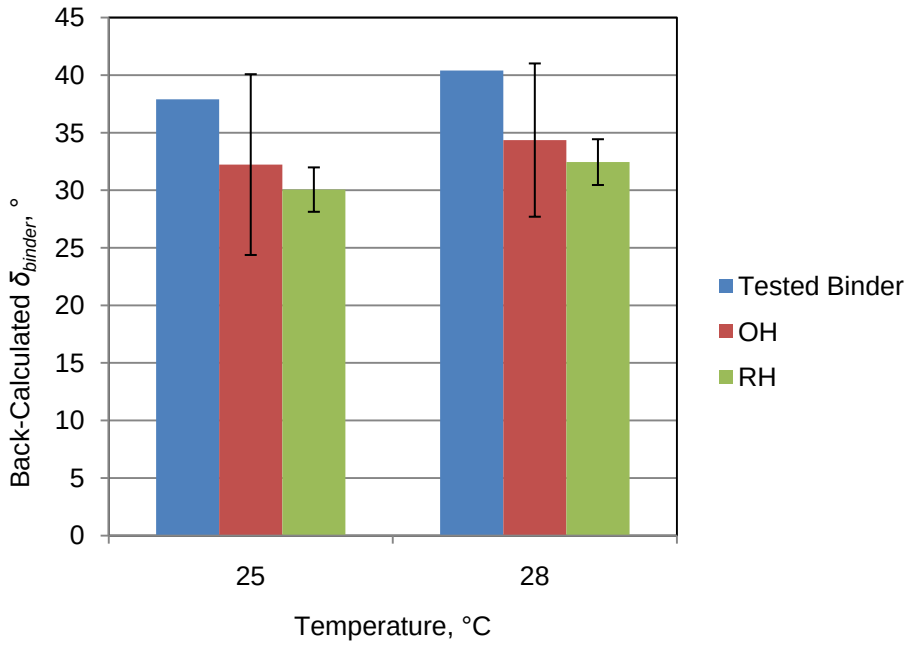

Figure E-22 Intermediate Temp Backcalculated δ_{binder} Results-RAP 5

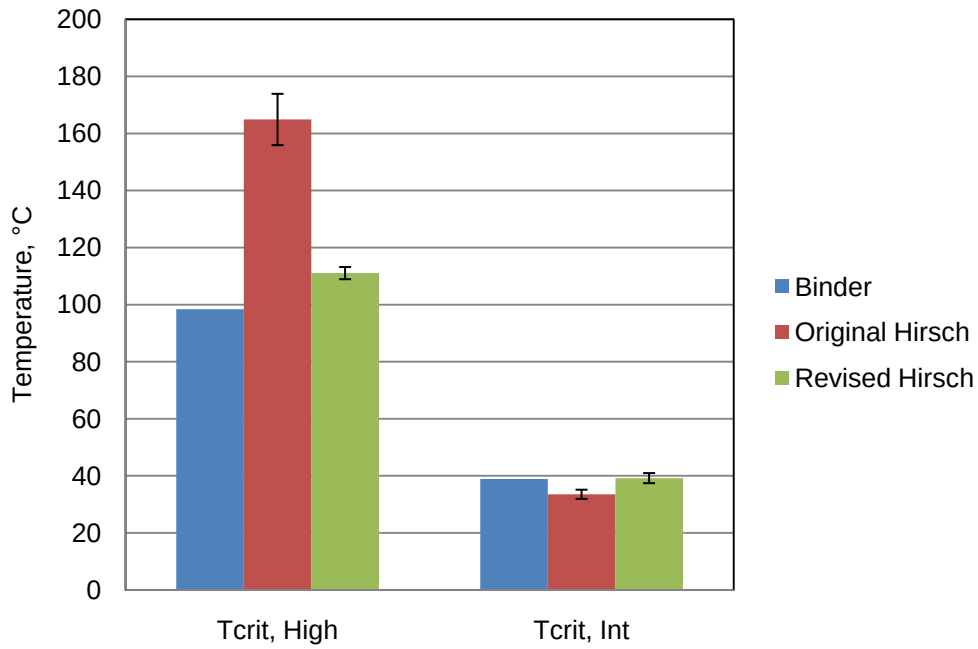

Figure E-23 Backcalculated T_{crit}-RAP 1

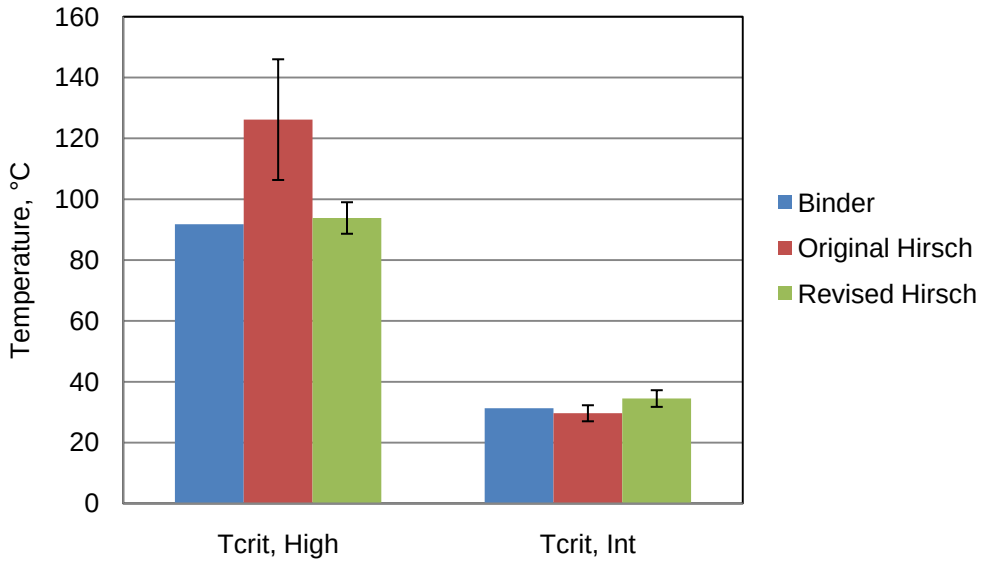

Figure E-24 Backcalculated T_{crit} -RAP 2

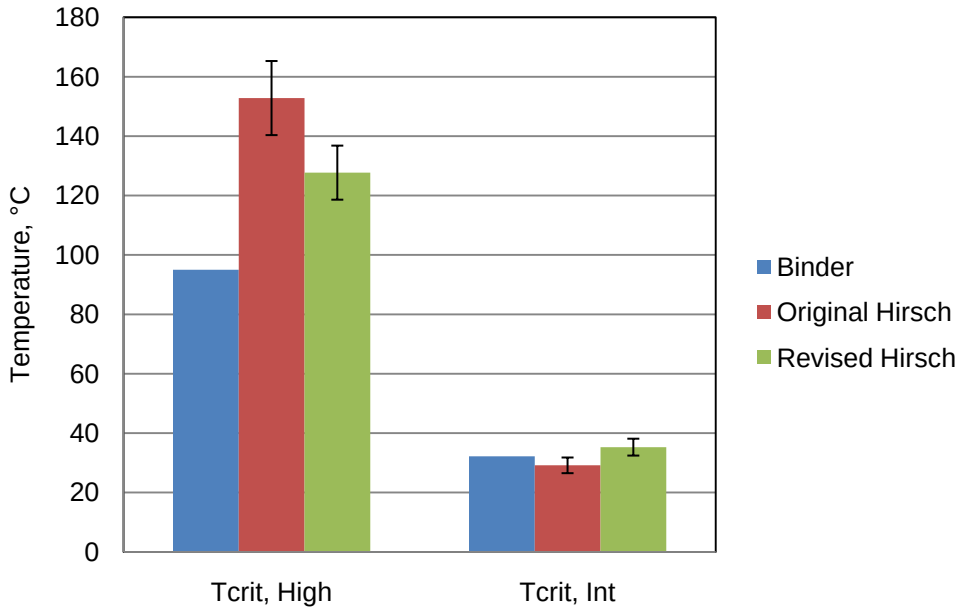

Figure E-25 Backcalculated T_{crit} -RAP 3

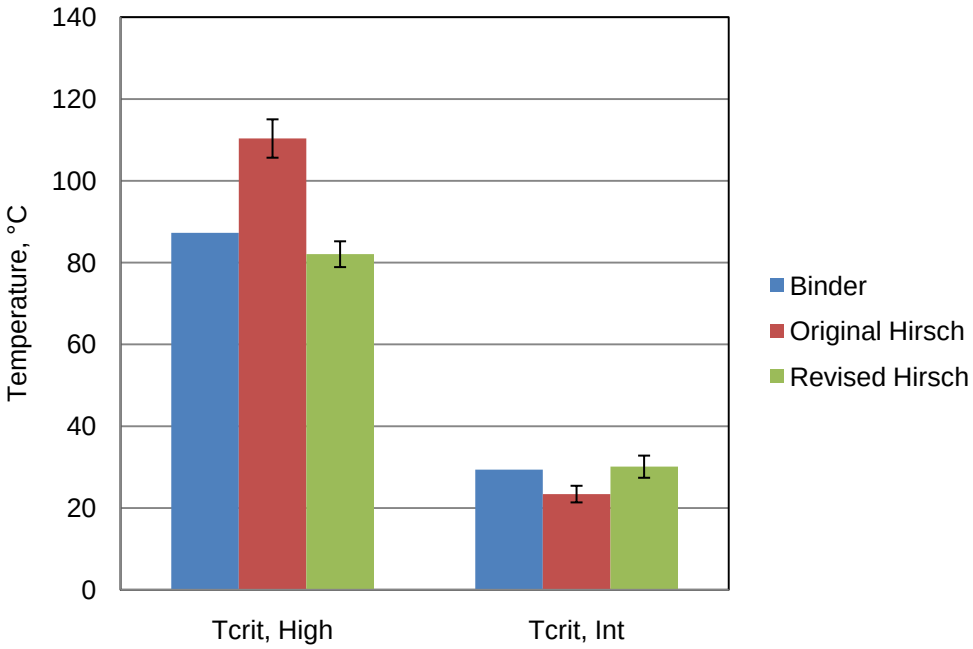

Figure E-26 Backcalculated T_{crit} -RAP 4

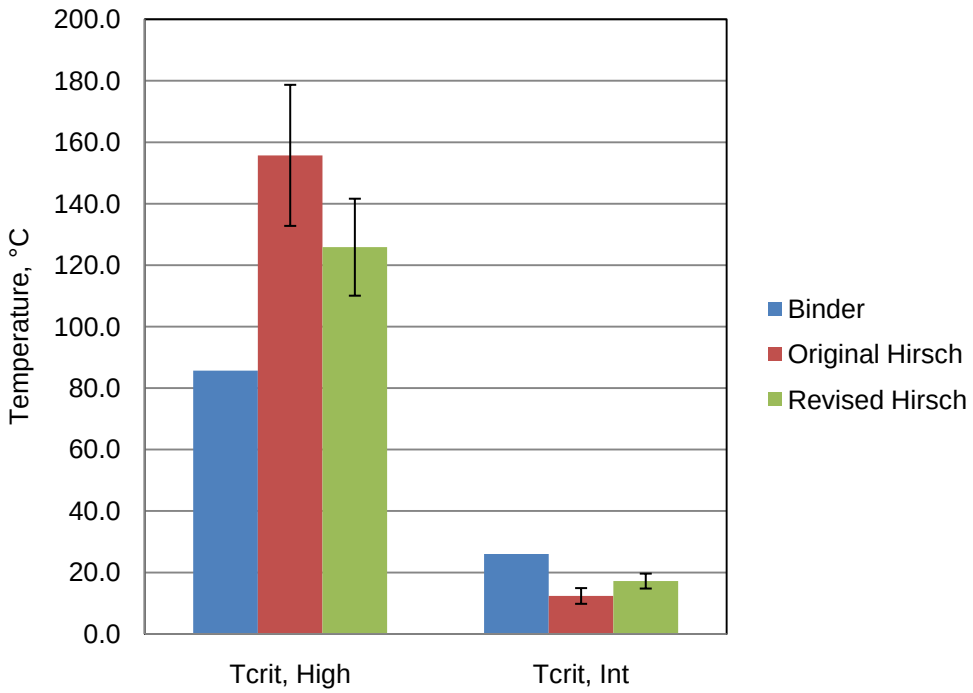

Figure E-27 Backcalculated T_{crit} -RAP 5

Appendix F

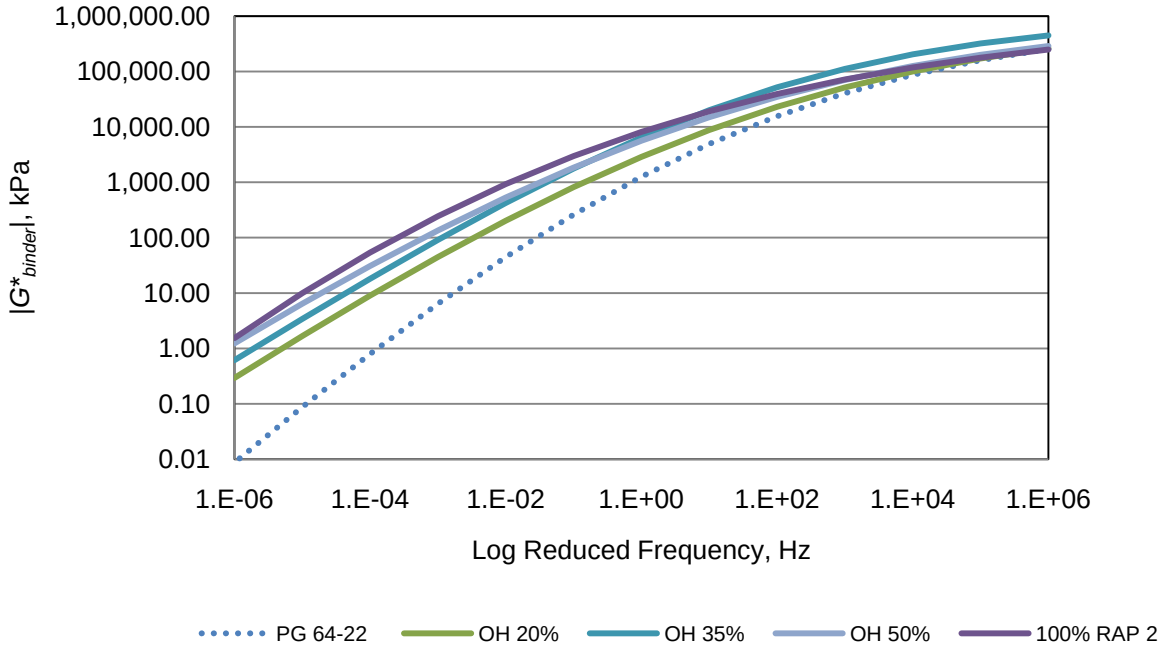

Figure F-1 PG 64-22 Laboratory Blend Master Curves for OH Model – RAP 2

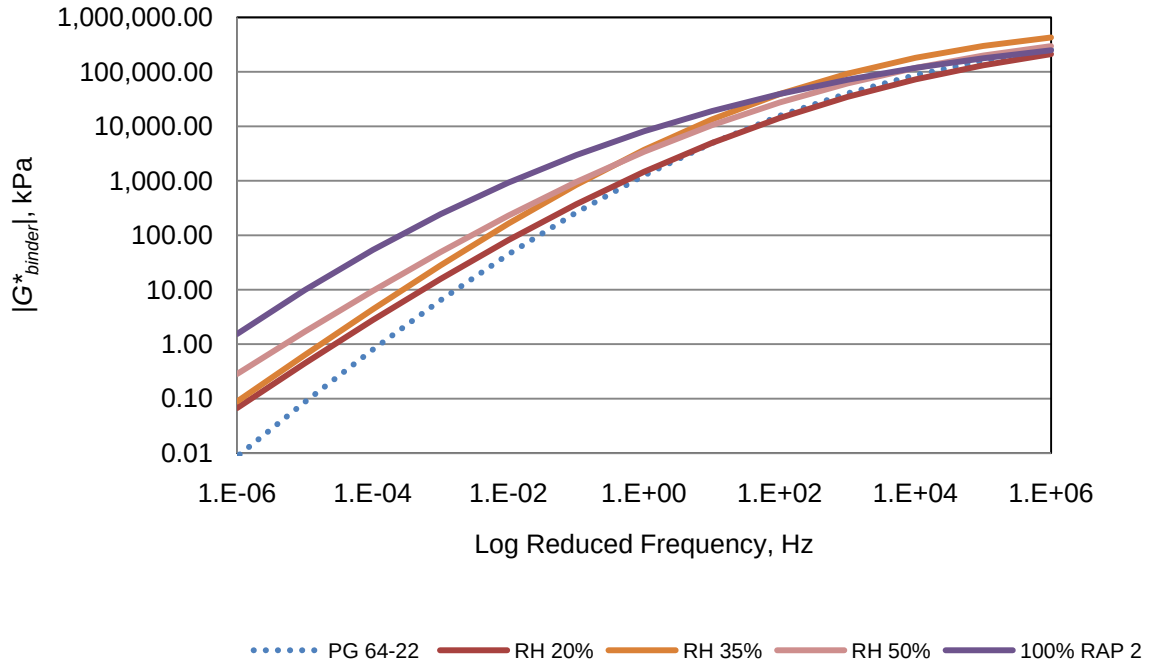

Figure F-2 PG 64-22 Laboratory Blend Master Curves for RH Model – RAP 2

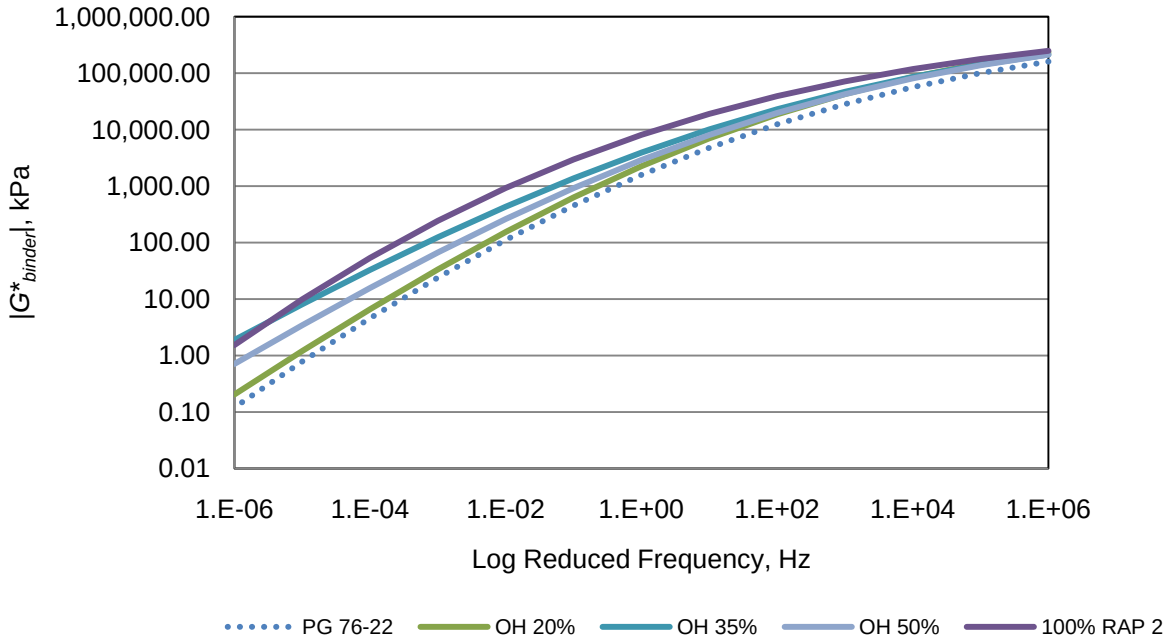

Figure F-3 PG 76-22 Laboratory Blend Master Curves for OH Model – RAP 2

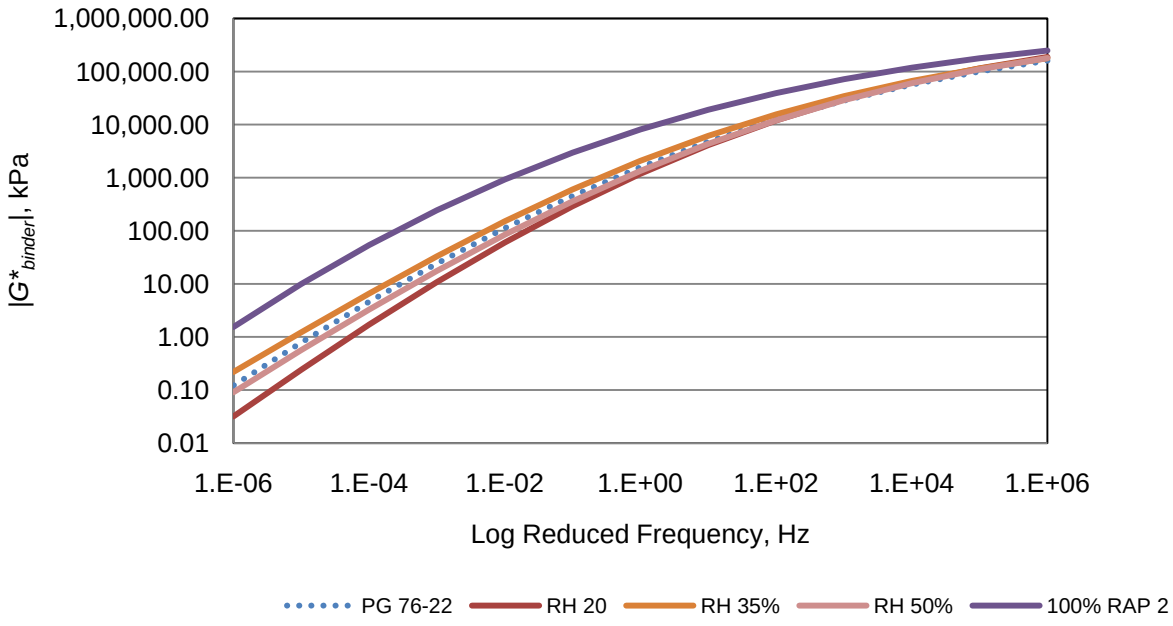

Figure F-4 PG 76-22 Laboratory Blend Master Curves for RH Model – RAP 2

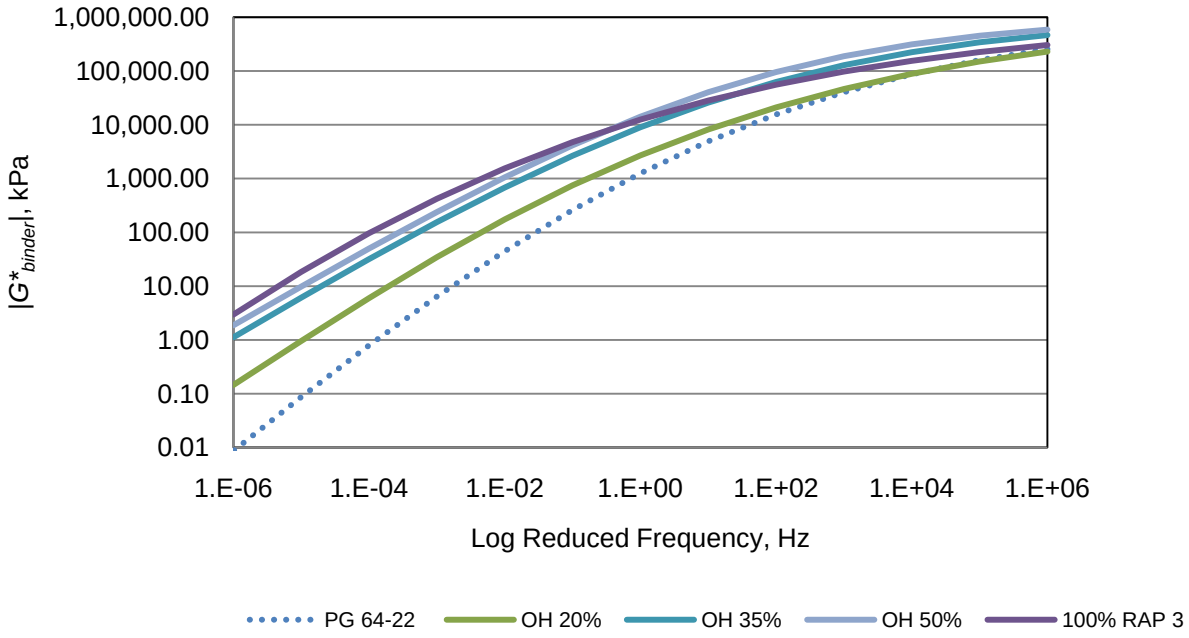

Figure F-5 PG 64-22 Laboratory Blend Master Curves for OH Model – RAP 3

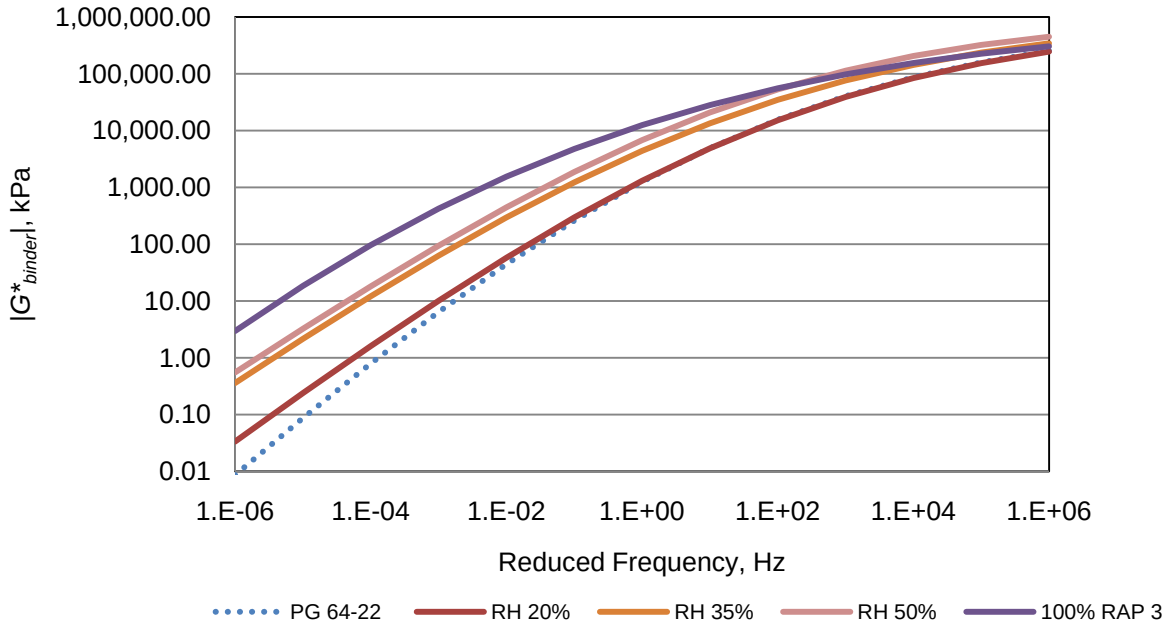

Figure F-6 PG 64-22 Laboratory Blend Master Curves for RH Model – RAP 3

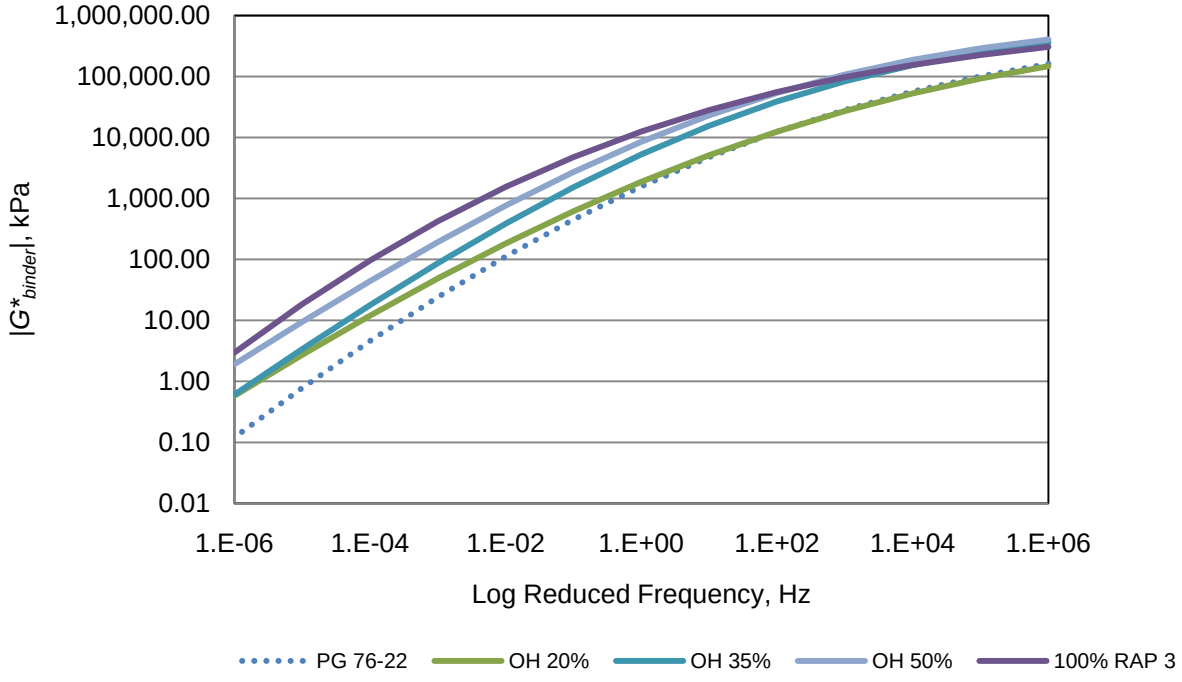

Figure F-7 PG 76-22 Laboratory Blend Master Curves for OH Model – RAP 3

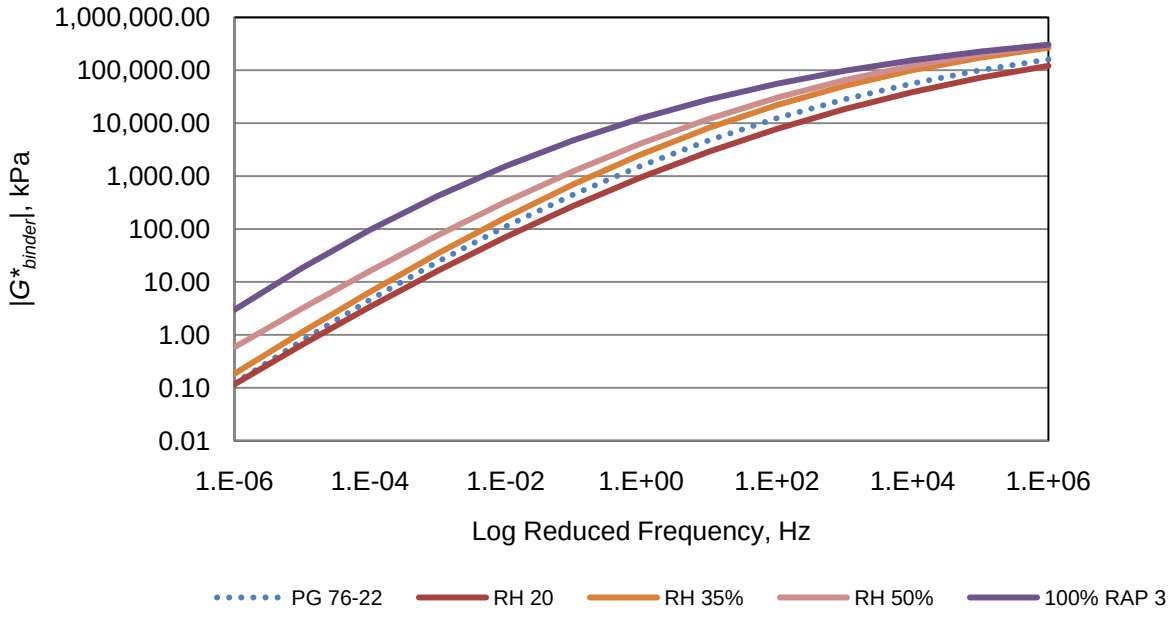

Figure F-8 PG 76-22 Laboratory Blend Master Curves for RH Model – RAP 3

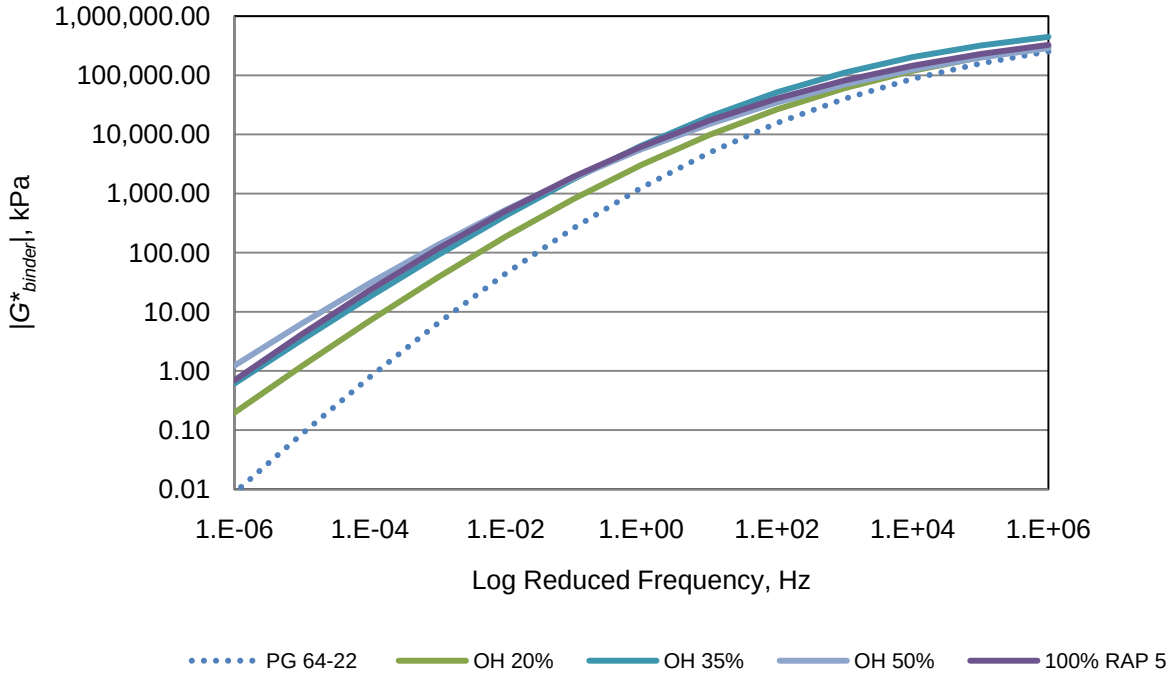

Figure F-9 PG 64-22 Laboratory Blend Master Curves for OH Model – RAP 5

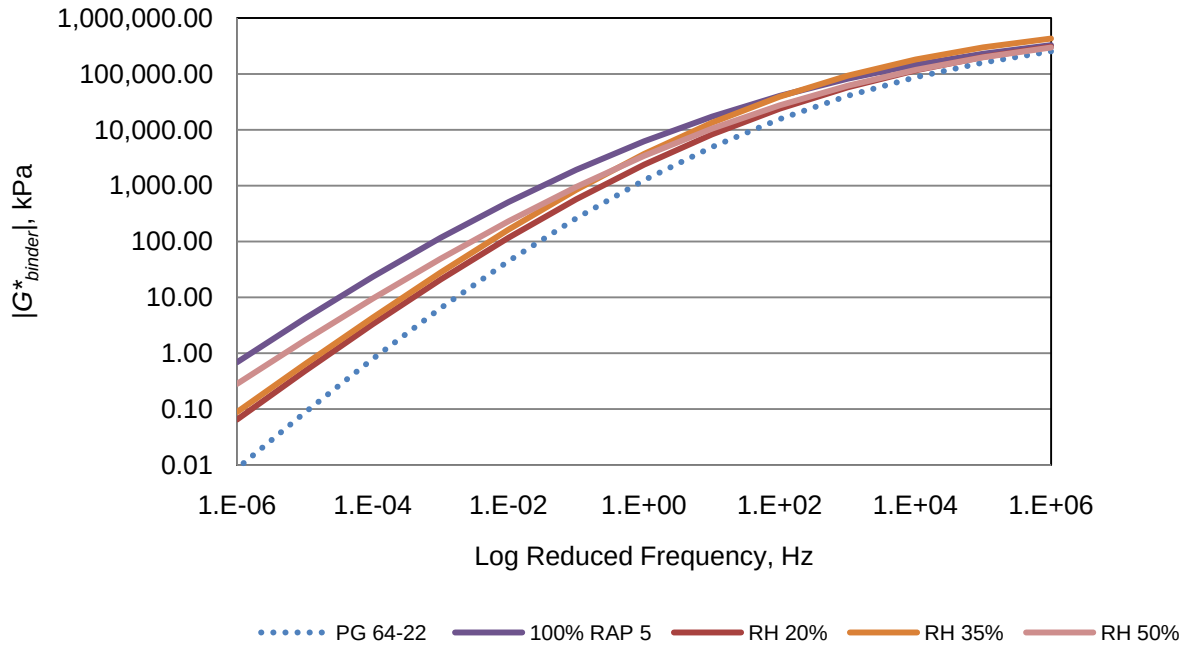

Figure F-10 PG 64-22 Laboratory Blend Master Curves for RH Model – RAP 5

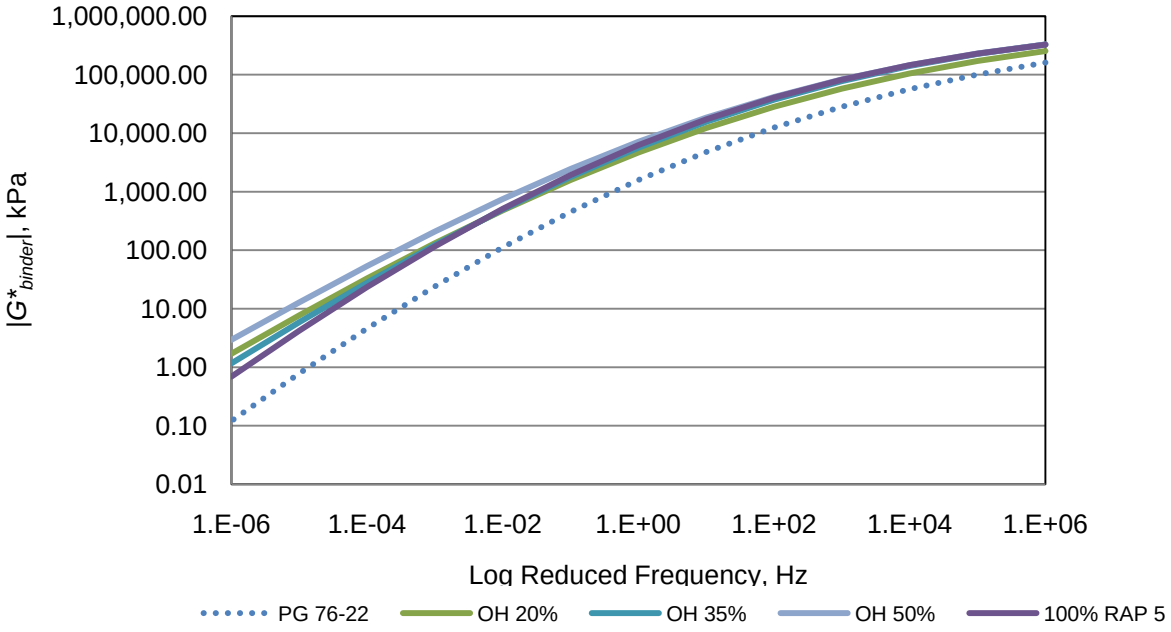

Figure F-11 PG 76-22 Laboratory Blend Master Curves for OH Model – RAP 5

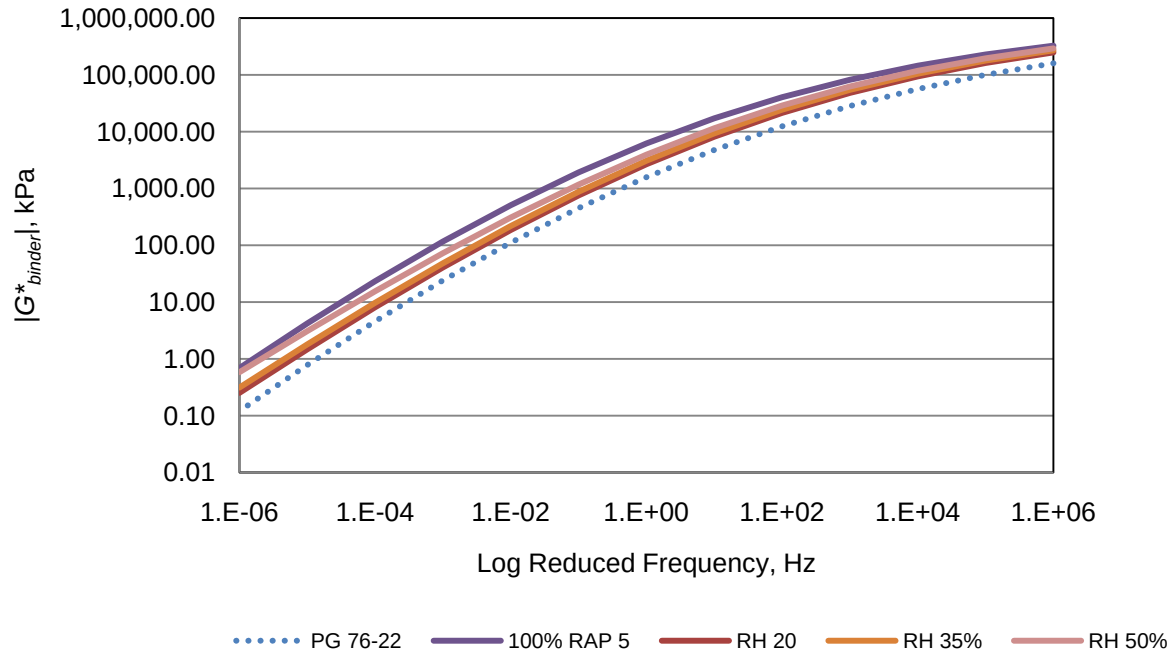

Figure F-12 PG 76-22 Laboratory Blend Master Curves for RH Model – RAP 5

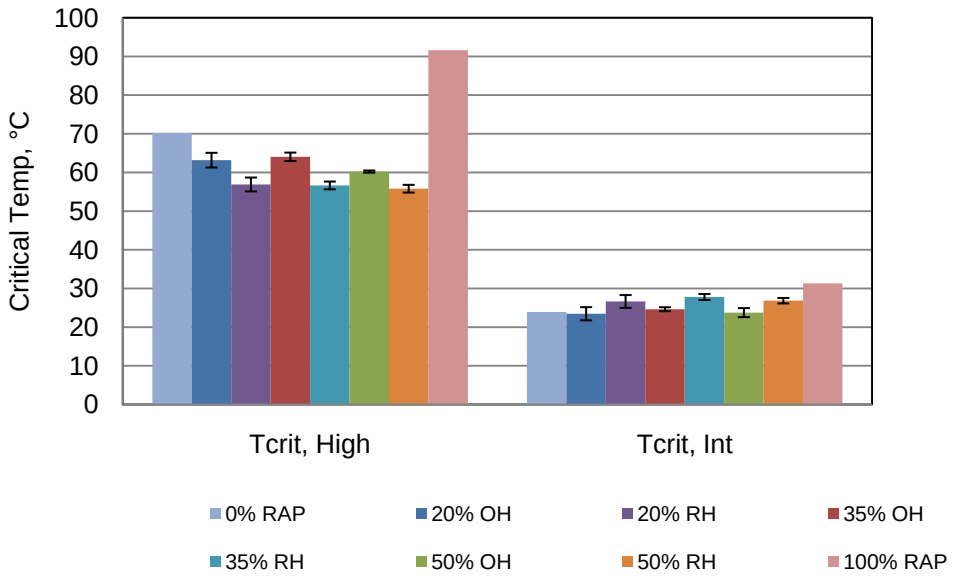

Figure F-13 RAP 2 Critical Temperatures, °C – PG 64-22

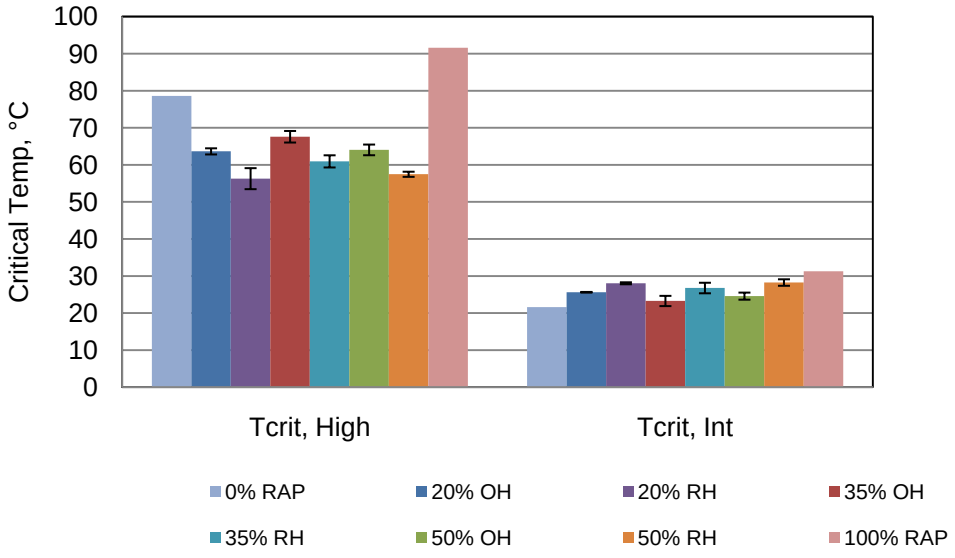

Figure F-14 RAP 2 Critical Temperatures, °C – PG 76-22

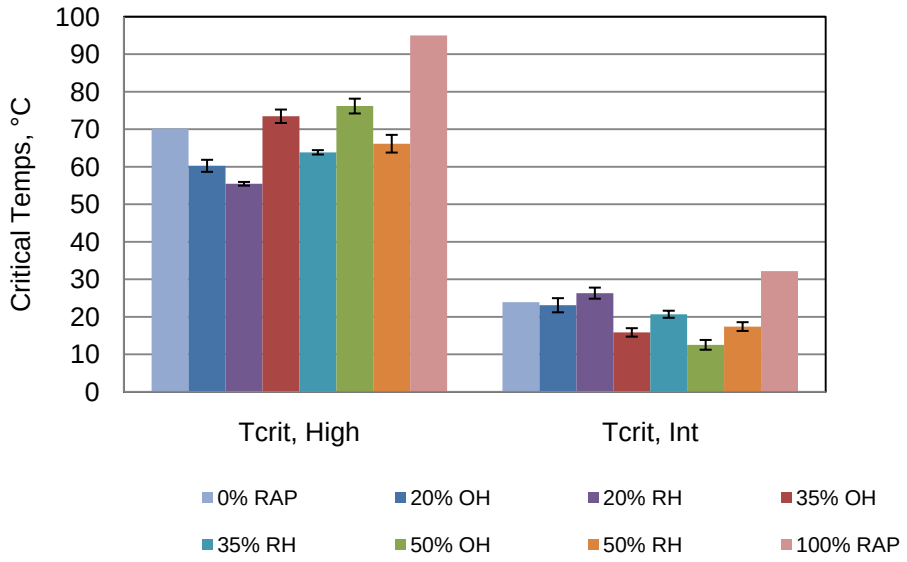

Figure F-15 RAP 3 Critical Temperatures, °C – PG 64-22

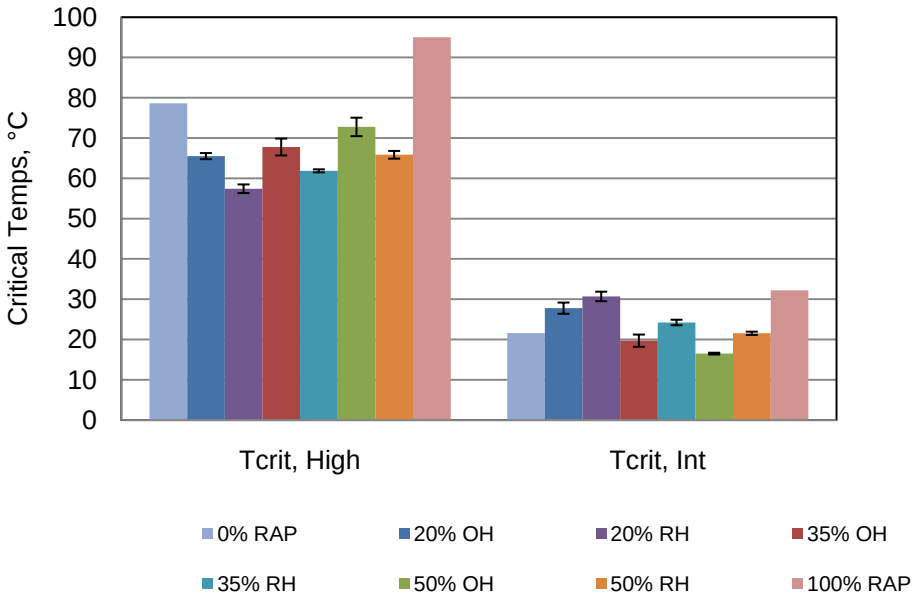

Figure F-16 RAP 3 Critical Temperatures, °C – PG 76-22

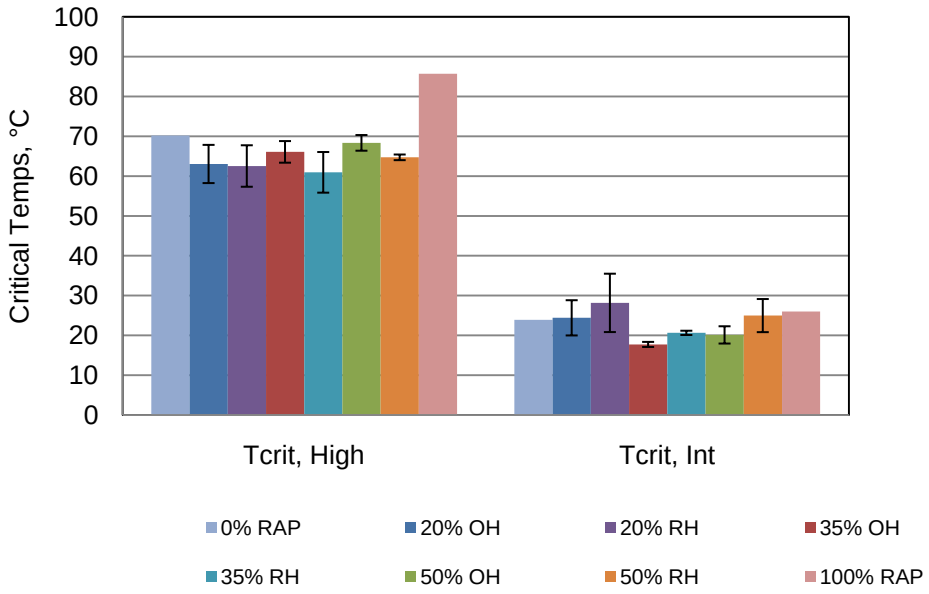

Figure F-17 RAP 5 Critical Temperatures, °C – PG 64-22

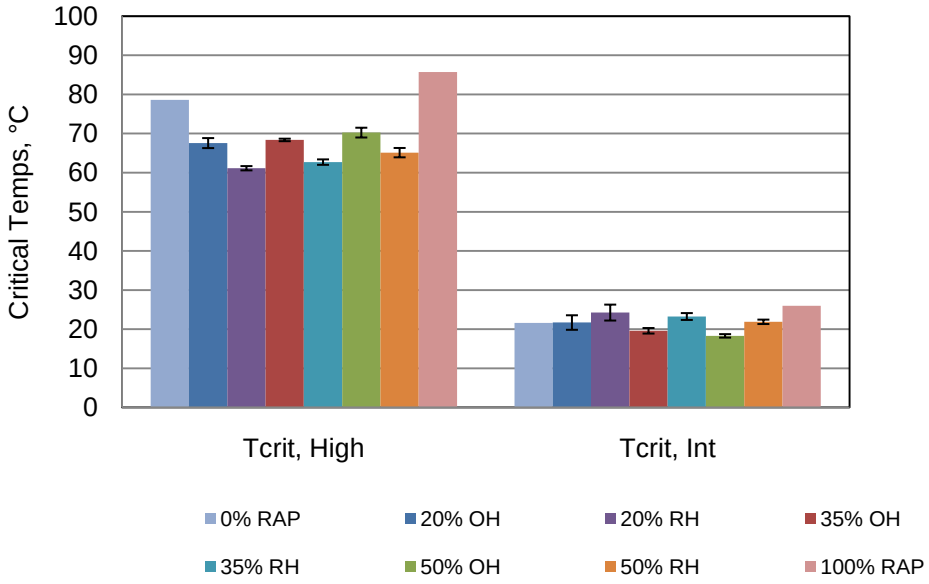

Figure F-18 RAP 5 Critical Temperatures, °C – PG 76-22

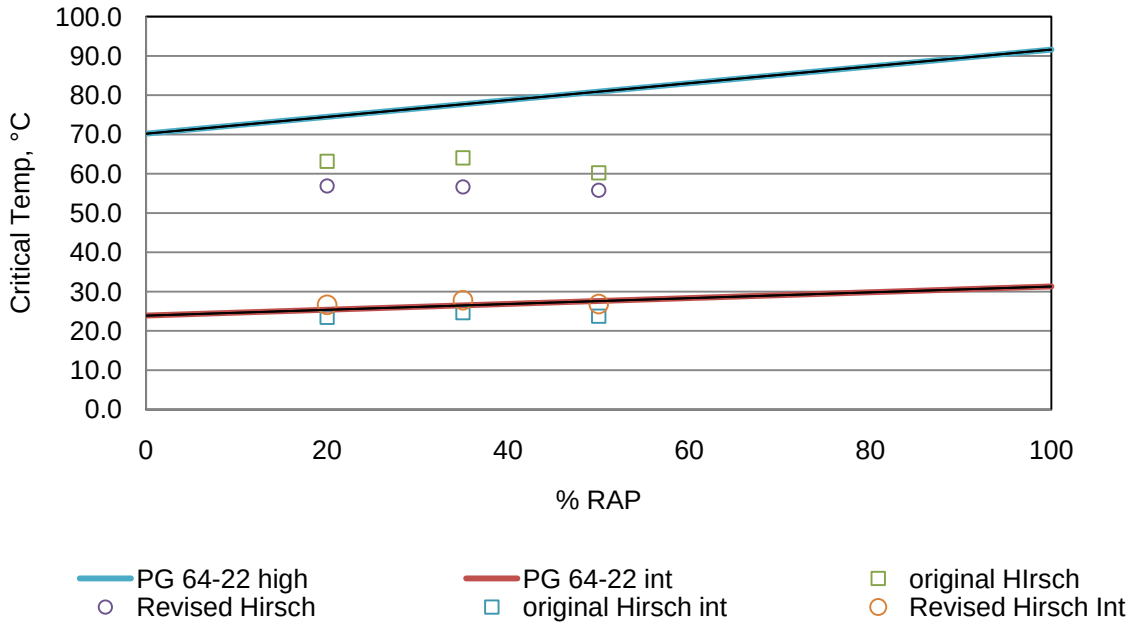

Figure F-19 PG 64-22 Blending Chart – RAP 2

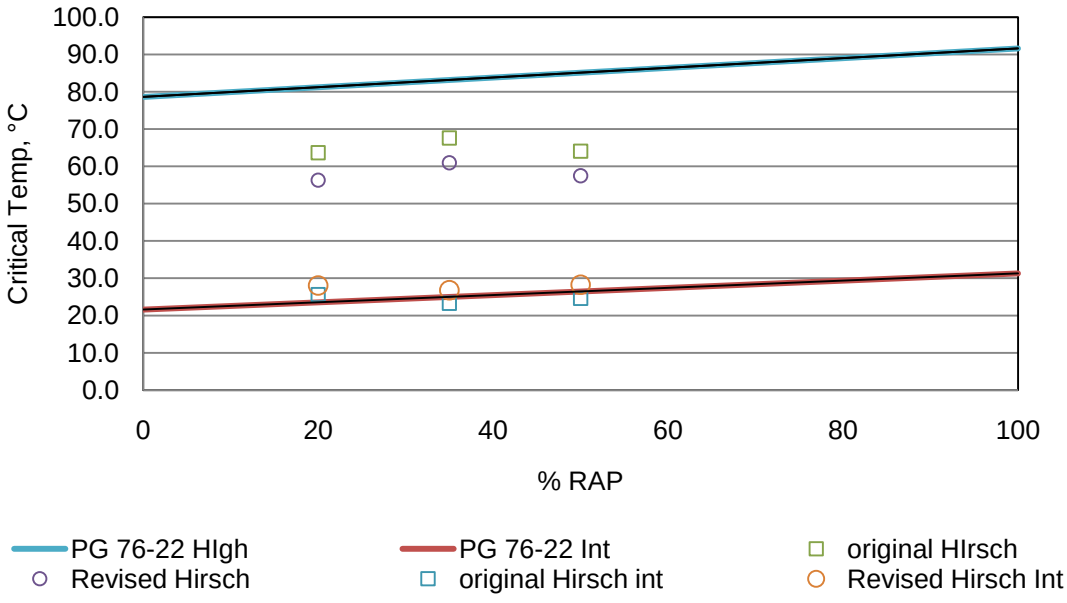

Figure F-20 PG 76-22 Blending Chart – RAP 2

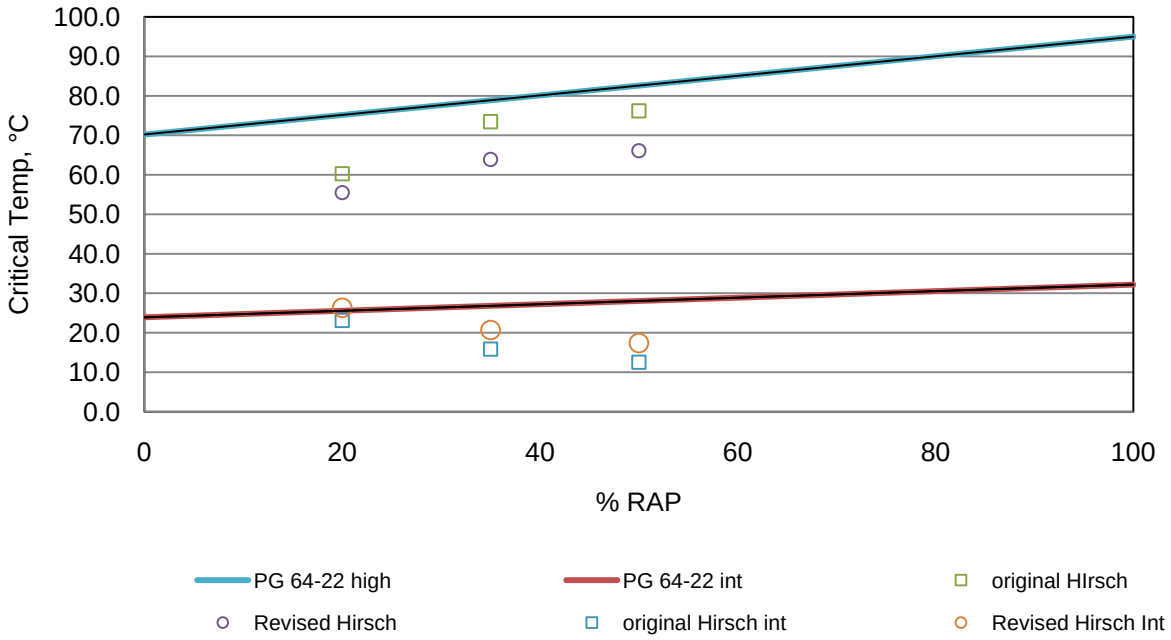

Figure F-21: PG 64-22 Blending Chart – RAP 3

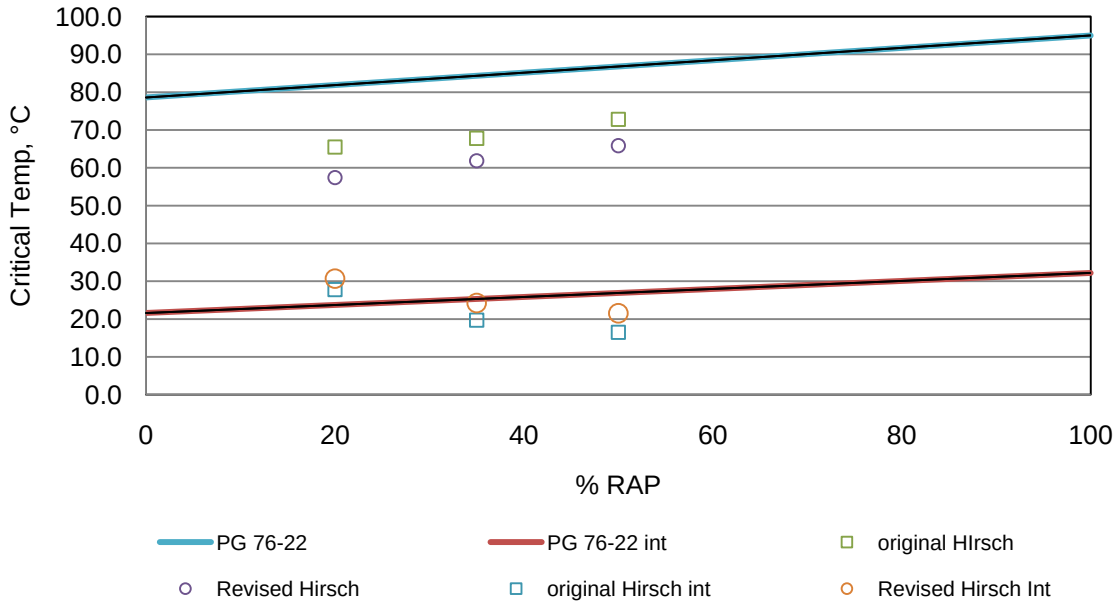

Figure F-22 PG 76-22 Blending Chart – RAP 3

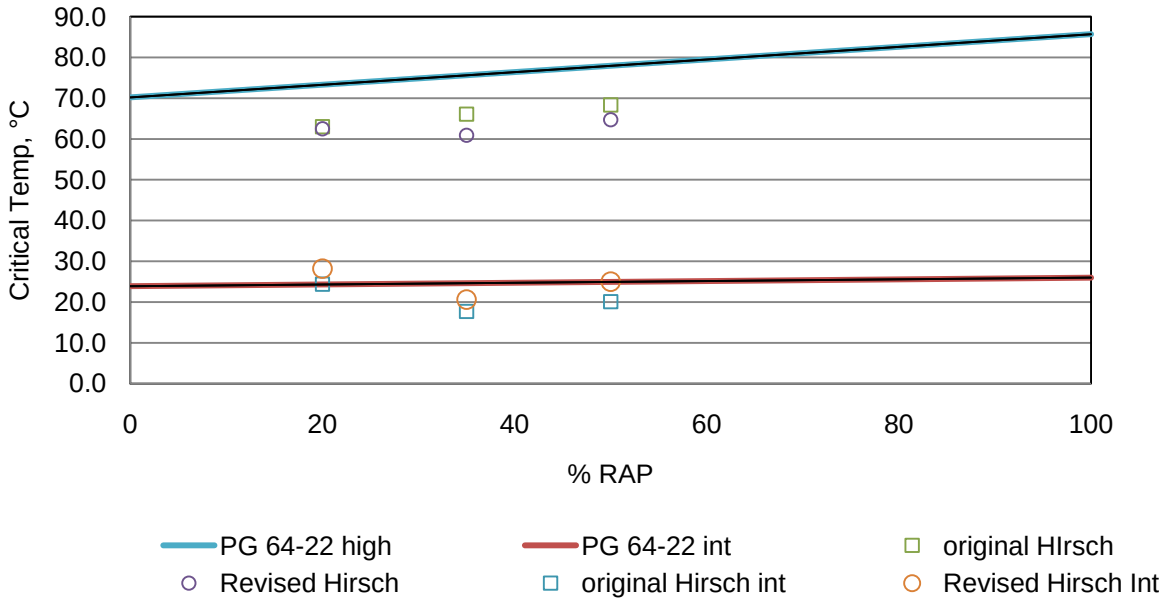

Figure F-23 PG 64-22 Blending Chart – RAP 5

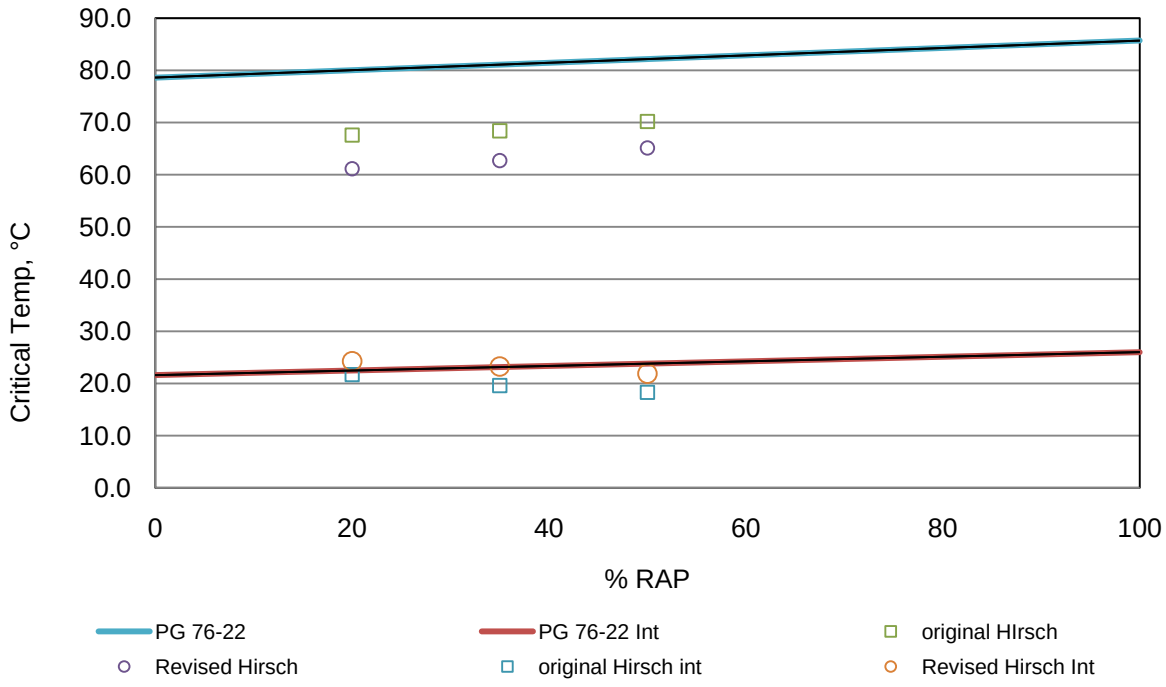

Figure F-24 PG 76-22 Blending Chart – RAP 5

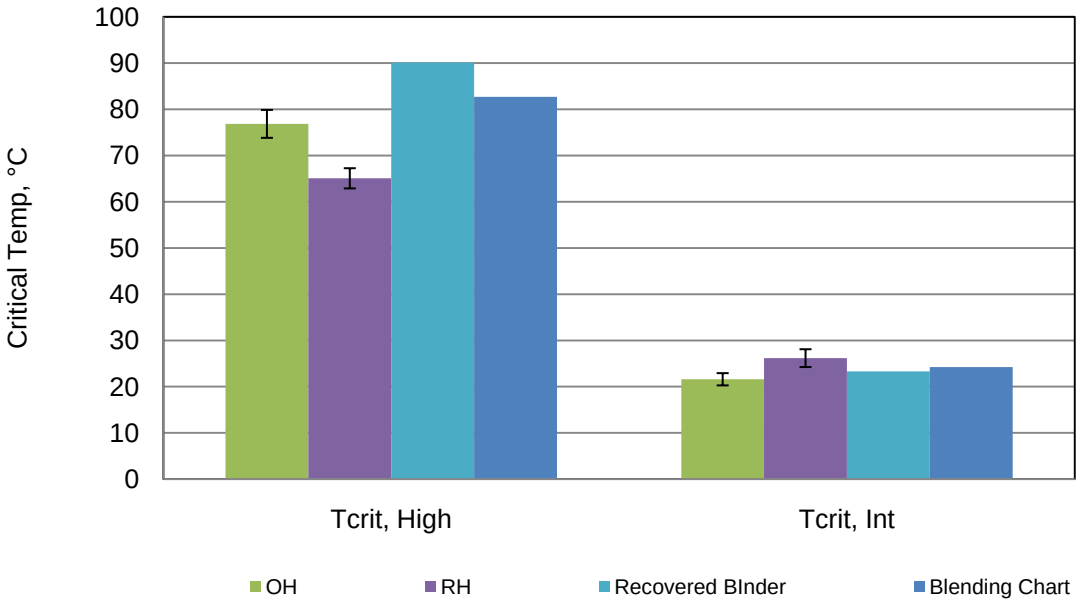

Figure F-25 Plant Mix A Critical Temperatures, °C

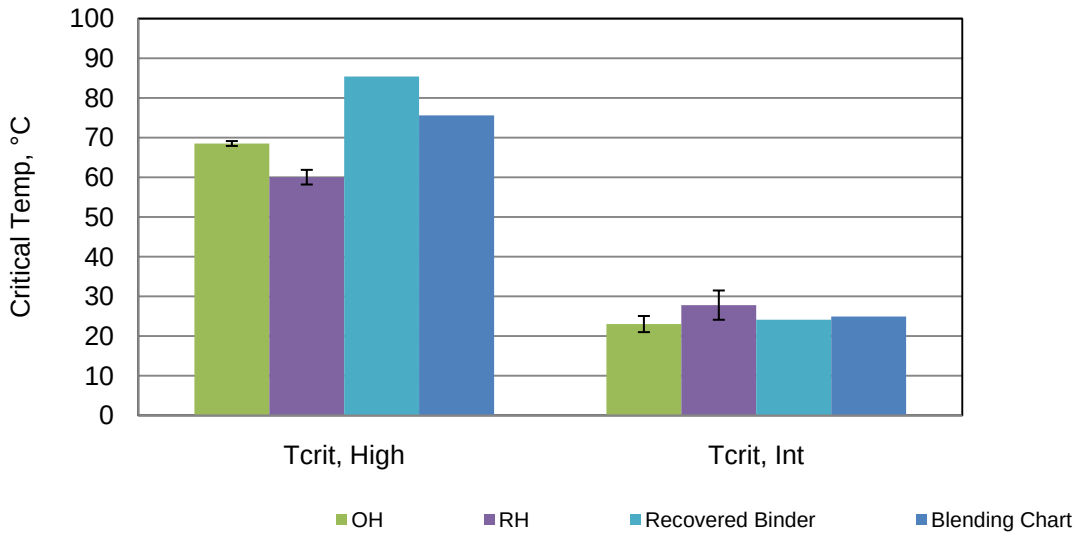

Figure F-26 Plant Mix B Critical Temperatures, °C

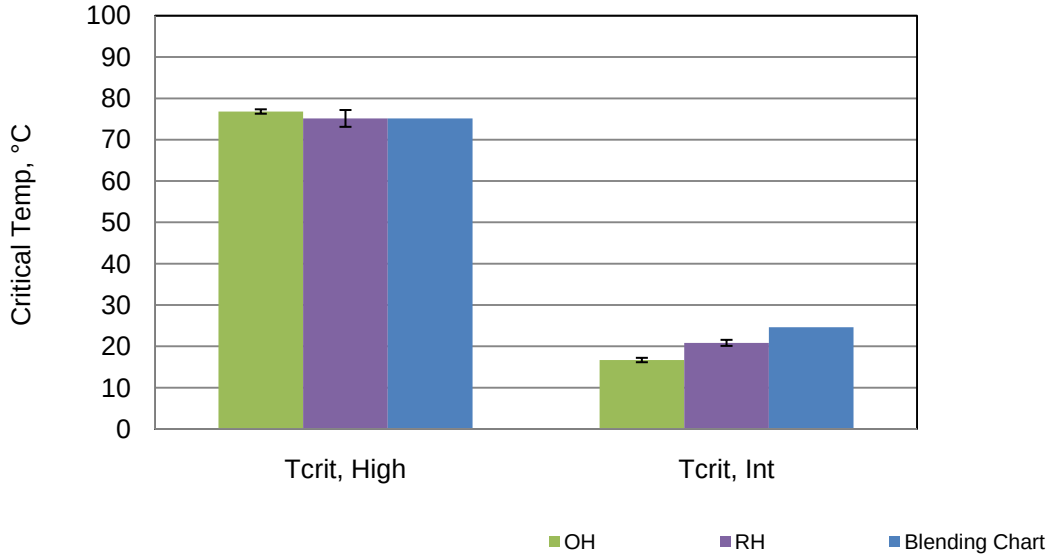

Figure F-27 Plant Mix C Critical Temperatures, °C

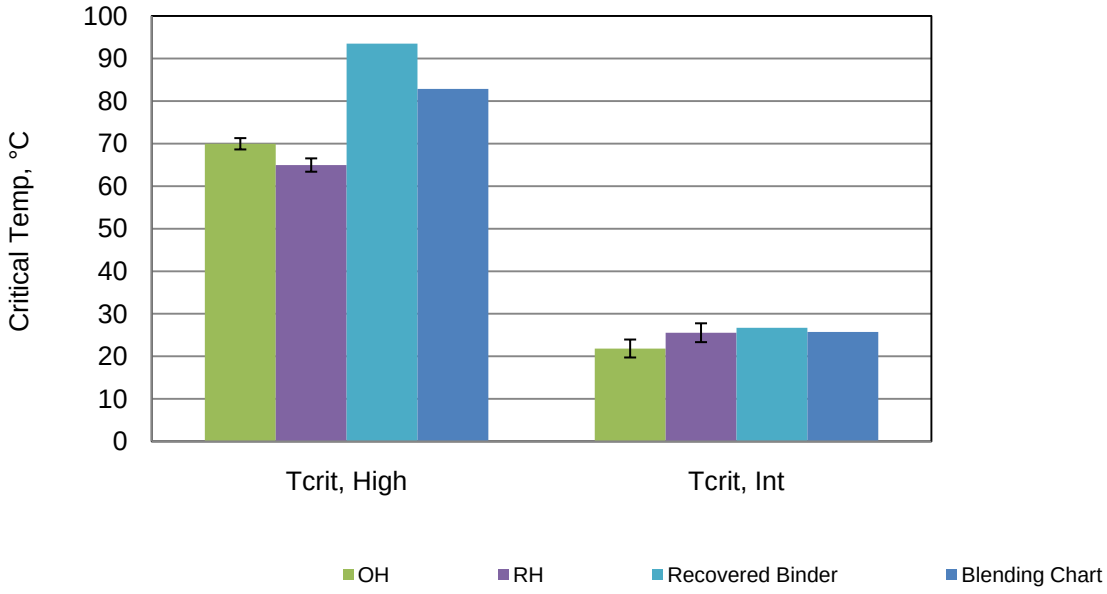

Figure F-28 Plant Mix D Critical Temperatures, °C

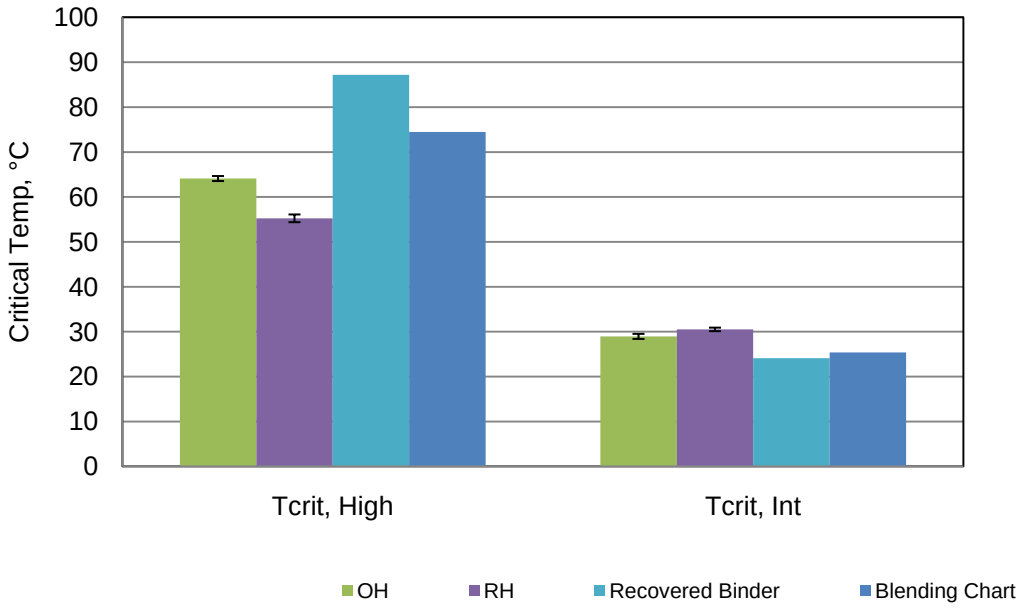

Figure F-29 Plant Mix E Critical Temperatures, °C